

Characterization of the *Popeye domain containing* gene family in zebrafish

Dissertation zur Erlangung des
naturwissenschaftlichen Doktorgrades
der Julius-Maximilians-Universität Würzburg

vorgelegt von
Bettina Carmen Kirchmaier
aus Frankfurt am Main

Würzburg, 2010

Eingereicht am:.....

Mitglieder der Promotionskommission:

Vorsitzender: Prof. Dr. Thomas Dandekar

1. Gutachter: Prof. Dr. Thomas Brand

2. Gutachter: Prof. Dr. Christoph Winkler

Tag des Promotionskolloquiums:.....

Doktorurkunde ausgehändigt am:.....

Für meine Familie, in Liebe

CONTENTS

Contents	4
Figures	9
Tables.....	10
1 Summary.....	11
2 Zusammenfassung.....	12
3 Introduction	13
3.1 The vertebrate heart.....	13
3.1.1 Formation of the heart field.....	13
3.1.2 Heart tube assembly and development of polarity.....	14
3.1.3 Chamber formation and cardiac conduction development.....	15
3.1.4 Heart remodeling	17
3.2 Electrical activity of the adult heart.....	17
3.2.1 The nodes and the fast conduction Purkinje fiber networks	19
3.2.2 Gap junctions.....	19
3.2.3 Cardiac currents involved in generation of myocardial action potentials	20
3.3 <i>Danio rerio</i>	23
3.3.1 The zebrafish as model system for cardiovascular research.....	23
3.3.2 Zebrafish heart development.....	24
3.3.3 Development of the cardiac conduction system in zebrafish	25
3.4 The <i>Popeye domain containing (Popdc)</i> gene family.....	27
3.4.1 Expression pattern.....	27
3.4.2 Protein structure and distribution	28
3.4.3 Interaction partners.....	29
3.4.4 Function.....	29
3.5 Aim of the study	31

4	Material	32
4.1	Biological material	32
4.1.1	Bacterial strains	32
4.1.2	Vectors	32
4.1.3	Fish lines	33
4.1.4	Primary and secondary antibodies	33
4.2	Molecularbiological material.....	33
4.2.1	DNA and protein ladders	33
4.2.2	Kits.....	34
4.3	Software.....	34
4.4	Equipment.....	35
4.5	Reagents.....	36
4.6	Enzymes	37
4.7	Primers.....	38
4.8	Morpholinos	38
5	Methods	39
5.1	Fish care	39
5.1.1	Setting up pair crosses	39
5.1.2	PTU treatment to prevent melanization of embryos.....	40
5.2	Genexpression manipulation in <i>Danio rerio</i>	40
5.2.1	Agarose plates for holding embryos	40
5.2.2	Microinjections	40
5.2.3	Morpholinos	41
5.2.4	Chemical treatment with cyclopamine	41
5.3	Physiological methods/Imaging methods.....	42
5.3.1	Recording of cardiac activity.....	42
5.3.2	Isolated calcium transient recordings by selective plane illumination microscopy (SPIM)	42
5.4	Microbiological methods.....	43
5.4.1	Ligation	43
5.4.2	Transformation.....	43

5.4.3	Cloning into plasmid vectors.....	45
5.4.4	Screening bacterial colonies using X-Gal and IPTG.....	45
5.4.5	Glycerol stocks	45
5.5	Molecularbiological methods.....	46
5.5.1	Preabsorption of antibody for whole mount <i>in situ</i> hybridization.....	46
5.5.2	Whole mount RNA <i>in situ</i> probe generation.....	46
5.5.3	Whole mount <i>in situ</i> hybridization using a single digoxigenin-labeled probe	47
5.5.4	RNA isolation using Trizol.....	50
5.5.5	<i>In vitro</i> transcription	51
5.5.6	<i>In vitro</i> synthesis of capped RNA.....	51
5.5.7	Preparation of plasmid DNA by alkaline lysis with SDS (Minipreparations 1-2 ml).....	51
5.5.8	Restriction analysis.....	53
5.5.9	Primer design.....	53
5.5.10	Endpoint PCR using Phusion™ DNA polymerase	53
5.5.11	Endpoint PCR using Taq polymerase.....	54
5.5.12	DEPC-treated water.....	54
5.6	Immunological methods	55
5.6.1	Phalloidin staining.....	55
5.6.2	Whole mount antibody staining with DAB.....	55
5.6.3	Whole mount immunocytochemistry (double staining MF20/S46)	56
5.7	Histological methods.....	57
5.7.1	Embedding using Epon 812.....	57
5.7.2	Embedding and sectioning using JB-4 resin.....	58
5.7.3	Cryosections.....	59
5.8	Proteinbiochemical methods	60
5.8.1	Western Blot.....	60
6	Results.....	61
6.1	The <i>Popdc</i> gene family in zebrafish	61
6.2	<i>Popdc2</i> is important for heart and skeletal muscle development in zebrafish.....	62
6.2.1	<i>Popdc2</i> is predominantly expressed in heart and skeletal muscle.....	62

6.2.2	Knockdown of <i>popdc2</i> leads to impaired musculature.....	65
6.2.3	<i>Popdc2</i> morphants develop cardiac conduction system abnormalities.....	72
6.2.4	Aberrant electrical activity is not caused by cellular changes within the AV canal of <i>popdc2</i> morphants.....	81
6.3	<i>Popdc3</i> might be important for cardiac conduction system development.....	85
6.3.1	<i>Popdc3</i> is expressed in distinct regions of the brain, heart and skeletal muscle.....	85
6.3.2	<i>Popdc3</i> morphants develop a complete heart block.....	88
6.4	Conserved amino acids within the <i>Popeye</i> domain are essential for <i>Popdc</i> function.....	91
6.4.1	Point mutations within the cyclic nucleotide binding domain of <i>Popdc1</i> lead to a different cardiac phenotype in zebrafish embryos.....	92
6.4.2	Point mutations within the cyclic nucleotide binding domain of <i>Popdc2</i> or overexpression of <i>Popdc2</i> results in no obvious phenotype in zebrafish.....	101
6.5	Expression analyses of genes linked to arrhythmia.....	103
6.5.1	<i>Shox2</i> is predominantly expressed in heart and brain in zebrafish development.....	103
6.5.2	The duplicated <i>hcn4</i> gene is expressed in distinct regions of the heart and in the diencephalon..	104
7	Discussion.....	106
7.1	Evolutionary conservation of <i>Popdc</i> gene family.....	106
7.1.1	Expression pattern.....	106
7.1.2	Function.....	107
7.1.3	Alternative splicing.....	108
7.2	<i>Popdc</i> gene family and its role in gastrulation.....	109
7.3	<i>Popdc</i> gene family and its role in muscle development and regeneration.....	109
7.3.1	Skeletal muscle development.....	109
7.3.2	Heart and craniofacial muscle development.....	111
7.4	<i>Popdc</i> gene family and its role in cell adhesion.....	112
7.5	<i>Popdc</i> gene family, genetic modifier of cardiac arrhythmias.....	113
7.5.1	<i>Popdc</i> genes, modulators of <i>Trek1</i>	114
7.6	<i>Popdc</i> gene family – a novel class of cAMP binding proteins.....	115
7.7	<i>Popdc</i> gene family and its role in inherited diseases.....	116
7.7.1	<i>Popdc</i> gene family and the sick sinus node syndrome.....	116

8	Literature.....	119
9	Appendix.....	125
9.1	Abbreviations.....	125
9.2	Genetic nomenclature.....	128
9.3	Supplemental videos.....	129
9.4	Eidesstattliche Erklärung.....	130
9.5	Curriculum vitae.....	131
9.6	Eigene Publikationen.....	133
9.7	Teilnahme an wissenschaftlichen Tagungen.....	134
9.8	Acknowledgements.....	135

FIGURES

Figure 1: Schematic overview of heart development in higher vertebrates (Christoffels et al., 2010).	15
Figure 2: Electrical activity of the myocardium (Nerbonne and Kass, 2005).	18
Figure 3: The relationship between cardiac ion fluxes and action potential (Cheng et al., 2003)	21
Figure 4: Heart development in zebrafish (Stainier, 2001).	25
Figure 5: Development of the cardiac conduction system in zebrafish and classification of zebrafish mutants (Chi et al., 2008).....	27
Figure 6: Comparison of secondary structure and tertiary structure predictions of cyclic nucleotide binding domains between PKA and Popdc1 (Breher, 2009).	29
Figure 7: Examples of the ECG curves of wild type and mutant heart in stress situations (Froese, 2008).	30
Figure 8: Protein sequence alignment of zebrafish Popdc1, Popdc2 and Popdc3.	61
Figure 9: Expression analysis of <i>popdc2</i> in the adult and embryonic zebrafish.	62
Figure 10: <i>Popdc2</i> is expressed in slow muscle precursors.	63
Figure 11: Inhibition of Hedgehog signaling pathway by cyclopamine results in a loss of <i>popdc2</i> expression in adaxial cells.	63
Figure 12: During somitogenesis <i>popdc2</i> is strongly expressed in heart and striated muscle.....	64
Figure 13: <i>Popdc2</i> is preferentially expressed in the developing heart and facial musculature during hatching period in zebrafish.	65
Figure 14: Knockdown strategy of <i>popdc2</i> in zebrafish.	66
Figure 15: MO1- <i>popdc2</i> and MO2- <i>popdc2</i> injected embryos displayed abnormal skeletal muscle development.	67
Figure 16: Characterization of the <i>popdc2</i> morphant phenotype in the skeletal muscle.....	68
Figure 17: Knockdown of <i>popdc2</i> leads to craniofacial muscle reduction.	69
Figure 18: <i>Popdc2</i> morphants display deformation of somites and intersegmental vessels.....	71
Figure 19: Knockdown of <i>popdc2</i> expression disrupts muscle fiber ultrastructure.	72
Figure 20: Knockdown of <i>popdc2</i> due to cardiac arrhythmia.....	73
Figure 21: Histological sections of <i>popdc2</i> morphants display no remarkable changes.....	74
Figure 22: <i>Popdc2</i> morphants display no change in chamber specification.	75
Figure 23: Myofibrillar arrays are evident in <i>popdc2</i> morphant's heart musculature.	76
Figure 24: <i>Popdc2</i> morphants develop cardiac conduction abnormalities and a diminished heart rate.	77
Figure 25: 5 dpf <i>popdc2</i> morphants exhibit an AV block.	80
Figure 26: 6 dpf <i>popdc2</i> morphants develop AV blocks as well as sinoatrial blocks.	81
Figure 27: Arrhythmic <i>popdc2</i> morphants show no alteration of the AV cardiomyocytes.	82
Figure 28: Arrhythmic <i>popdc2</i> morphants display alterations in cardiomyocyte shape	83
Figure 29: <i>Popdc2</i> morphants display no change in valve development.	84
Figure 30: <i>Popdc3</i> is expressed during heart development and is found in adult heart, muscle and brain.	85
Figure 31: At 24 hpf <i>popdc3</i> is expressed in distinct regions of the brain.....	86
Figure 32: 48 hpf embryos reveal <i>popdc3</i> expression in the outflow tract and distinct regions of the brain.	87

Figure 33: <i>Popdc3</i> expression in 72 hpf zebrafish embryos.....	88
Figure 34: Knockdown strategy of <i>popdc3</i> in zebrafish.....	88
Figure 35: <i>Popdc3</i> morphants display abnormal body curvature and pericardial edema.....	89
Figure 36: 3 dpf <i>popdc3</i> morphants do not exhibit any pathological alterations of cardiac conduction as revealed by SPIM analysis.....	90
Figure 37: The 4 dpf <i>popdc3</i> morphant develop a complete heart block as revealed by SPIM analysis.....	91
Figure 38: <i>Popdc1</i> ^{wt} overexpression induces a cardiac phenotype.....	93
Figure 39: Overexpression of <i>Popdc1</i> ^{D200A} or <i>Popdc1</i> ^{V217F} has no or only very mild effects on zebrafish embryogenesis.....	94
Figure 40: Injection of <i>Popdc1</i> ^{P202A} and <i>Popdc1</i> ^{E203A} resemble <i>Popdc1</i> ^{wt} overexpression phenotype.....	95
Figure 41: Overview of cardiovascular pathology after overexpression of <i>Popdc1</i>	96
Figure 42: Overexpression of <i>Popdc1</i> dues to a lengthening of the heart chambers.....	97
Figure 43: Point mutants <i>Popdc1</i> ^{D200A} and <i>Popdc1</i> ^{V217F} display no heart phenotype.....	98
Figure 44: Point mutations <i>Popdc1</i> ^{P202A} and <i>Popdc1</i> ^{E203A} intensify the observed <i>Popdc1</i> overexpression phenotype.....	99
Figure 45: Histology of the embryonic zebrafish heart after overexpression of <i>Popdc1</i> ^{wt} , <i>Popdc1</i> ^{D200A} and <i>Popdc1</i> ^{P202A}	100
Figure 46: <i>Popdc2</i> overexpression in zebrafish embryos resulted in no obvious phenotype.....	101
Figure 47: Overexpression of <i>Popdc2</i> ^{D2184A} or <i>Popdc1</i> ^{V201F} have only marginal effects on zebrafish development.....	102
Figure 48: <i>Shox2</i> expression in the developing zebrafish embryo.....	104
Figure 49: <i>Hcn4</i> expression is found in zebrafish brain and heart.....	105
Figure 50: Model for the distinct modulation of <i>myf5</i> and <i>myod</i> during craniofacial myogenesis of zebrafish.....	112

TABLES

Table 1: Genes encoding cardiac ion channel α and β subunits (Roden et al., 2002).....	22
Table 2: Commonly used antibiotic solutions adapted by Sambrook and Russel (Molecular Cloning: A Laboratory Manual (Third Edition)).....	44
Table 3: Generation of <i>in situ</i> probes.....	47
Table 4: Cycling instructions using Phusion™ DNA polymerase.....	53
Table 5: Cycling instructions using Taq Polymerase.....	54

1 SUMMARY

The *Popeye domain containing (Popdc)* gene family of membrane proteins is predominantly expressed in striated and smooth muscle tissues and has been shown to act as novel cAMP-binding proteins. In mice, loss of *Popdc1* and *Popdc2*, respectively, affects sinus node function in the postnatal heart in an age and stress-dependent manner. In this thesis, I examined gene expression pattern and function of the *Popdc* gene family during zebrafish development with an emphasis on *popdc2*. Expression of the zebrafish *popdc2* was exclusively present in cardiac and skeletal muscle during cardiac development, whereas *popdc3* was expressed in striated muscle tissue and in distinct regions of the brain. In order to study the function of these genes, an antisense morpholino-based knockdown approach was used. Knockdown of *popdc2* resulted in aberrant development of facial and tail musculature. In the heart, *popdc2* morphants displayed irregular ventricular contractions with 2:1 and 3:1 ventricular pauses. Recordings of calcium transients using a transgenic indicator line *Tg(cmlc2:gCaMP)^{s878}* and selective plane illumination microscopy (SPIM) revealed the presence of an atrioventricular (AV) block in *popdc2* morphants as well as a complete heart block. Interestingly, preliminary data revealed that *popdc3* morphants developed a similar phenotype. In order to find a morphological correlate for the observed AV conduction defect, I studied the structure of the AV canal in *popdc2* morphants using confocal analysis of hearts of the transgenic line *Tg(cmlc2:eGFP-ras)^{s883}*, which outlines individual cardiac myocytes with the help of membrane-localized GFP. However, no evidence for morphological alterations was obtained. To ensure that the observed arrhythmia phenotype in the *popdc2* morphant was based on a myocardial defect and not caused by defective valve development, live imaging was performed revealing properly formed valves. Thus, in agreement with the data obtained in knockout mice, *popdc2* and *popdc3* genes in zebrafish are involved in the regulation of cardiac electrical activity. However, both genes are not required for cardiac pacemaking, but they play essential roles in AV conduction. In order to elucidate the biological importance of cAMP-binding, wild type *Popdc1* as well as mutants with a significant reduction in binding affinity for cAMP *in vitro* were overexpressed in zebrafish embryos. Expression of wild type *Popdc1* led to a cardiac insufficiency phenotype characterized by pericardial edema and venous blood retention. Strikingly, the ability of the *Popdc1* mutants to induce a cardiac phenotype correlated with the binding affinity for cAMP. These data suggest that cAMP-binding represents an important biological property of the *Popdc* protein family.

2 ZUSAMMENFASSUNG

Die *Popeye domain containing (Popdc)* Gene kodieren für eine Familie von Membranproteinen, die vorwiegend in der gestreiften und glatten Muskulatur exprimiert werden und in der Lage sind cAMP zu binden. In Mäusen resultiert der Verlust von *Popdc1* oder *Popdc2* in einer stressinduzierten Sinusknotendysfunktion, die sich altersabhängig entwickelt. In meiner Dissertation habe ich das Expressionsmuster und die Funktion der *Popdc* Genfamilie mit Schwerpunkt auf dem *popdc2*-Gen im Zebrafisch untersucht. Das *popdc2*-Gen im Zebrafisch wurde ausschließlich in der Herz- und Skelettmuskulatur exprimiert, während *popdc3* sowohl in der quergestreiften Muskulatur, als auch im Gehirn exprimiert wurde. Um die Funktion dieser Gene zu untersuchen, wurde die Prozessierung der prä-mRNA mit Hilfe von Morpholinos unterdrückt, die gegen die Spleißdonor bzw. -akzeptorsequenzen von *popdc2* und *popdc3* gerichtet waren. Das Fehlen von *popdc2* im Zebrafisch resultierte in einer Fehlentwicklung der Gesichts- und Schwanzmuskulatur. Im Herzen der *popdc2*-Morphanten waren ventrikuläre Überleitungsstörungen mit einem 2:1 oder 3:1 Rhythmus zu beobachten. Analysen der Calciumfreisetzung mittels SPIM (selective plane illumination microscopy) in der transgenen Zebrafischlinie *Tg(cmlc2:gCaMP)^{s878}*, die einen fluoreszierenden Calciumindikator exprimiert, zeigten in den *popdc2*-Morphanten einen AV-Block bis hin zum kompletten Herzblock. Interessanterweise ergaben vorläufige Analysen in *popdc3*-Morphanten einen ähnlichen Phänotyp. Um eine mögliche morphologische Ursache der beobachteten AV-Überleitungsstörung zu finden, habe ich die Struktur des AV-Kanals von *popdc2*-Morphanten mit Hilfe der transgenen Zebrafischlinie *Tg(cmlc2:eGFP-ras^{s883})* und konfokaler Mikroskopie untersucht. Allerdings konnte ich kein Anzeichen für morphologische Veränderungen erkennen. Um sicherzugehen, dass der beobachtete Rhythmusphänotyp der *popdc2*-Morphanten nicht auf einer myokardialen Störung beruht oder auf einem Defekt bei der Klappenentwicklung, wurden zusätzlich Lebendaufnahmen angefertigt, die zeigten, dass die Klappen normal entwickelt waren. In Übereinstimmung mit den Daten aus den Knockout-Mäusen haben die *popdc2*- und *popdc3*-Gene auch im Zebrafisch eine wichtige Funktion bei der elektrischen Reizleitung im Herzen. Allerdings sind die beiden Gene für die Erregungsbildung im Sinusknoten nicht essentiell, sondern werden für die Signalübertragung im AV-Kanal benötigt. Um die biologische Signifikanz der cAMP-Bindung zu untersuchen, wurden Wildtyp-Popdc1 und Punktmutanten, die eine Reduktion in der cAMP-Bindung aufweisen, nach RNA-Injektion in Zebrafischembryonen überexprimiert. Die Injektion von Wildtyp-Popdc1 induzierte eine embryonale Herzinsuffizienz, die durch perikardiales Ödem und venösen Blutstau charakterisiert war. Die Fähigkeit der Popdc1-Punktmutanten, einen Herzphänotyp nach Überexpression zu induzieren, war direkt korreliert mit der Bindungsaffinität für cAMP. Diese Daten lassen den Schluss zu, dass die Fähigkeit der cAMP-Bindung eine wichtige biologische Eigenschaft der Popdc-Proteinfamilie darstellt.

3 INTRODUCTION

3.1 The vertebrate heart

3.1.1 Formation of the heart field

The heart is a muscular pump and is the first organ which starts to form and function during vertebrate embryogenesis. The embryonic origin of cardiac cell lineages is the bilateral heart field which is competent to respond to inductive signals and includes the precursors of myocardial and endocardial cells (Brand, 2003; Jacobson and Sater, 1988). In the mesoderm, the transiently expressed transcription factors *Mesp1* (mesoderm posterior 1) and *Mesp2* (mesoderm posterior 2) are the earliest molecular markers for cardiac progenitors (Buckingham et al., 2005). In mammals and birds, the bilateral heart field of the cardiogenic mesoderm merges at their anterior margins to form the so-called "cardiac crescent". Interestingly, recent studies have revealed that the heart is generated by two separate progenitor cell populations, the first and the second heart field, which segregate from a common progenitor at the stage of gastrulation (Cai et al., 2003; Kelly et al., 2001; Laugwitz et al., 2005). The first heart field originates in the anterior splanchnic mesoderm and builds the cardiac crescent, which later on gives rise to the left ventricle and atria. Within the first heart field, the myogenic differentiation in the lateral cells is limited by Notch signaling (Rones et al., 2000) while expression of *Serrate* which encodes for a Notch ligand is repressed through a negative feedback loop. The second heart field is derived from the pharyngeal mesoderm located medial to the cardiac crescent and trace-mapping experiments demonstrate that it contributes primarily to the right ventricle and outflow tract (Cai et al., 2003; Kelly and Buckingham, 2002; Laugwitz et al., 2005; Rones et al., 2000). Both heart fields seem to be regulated by complex positive and negative signaling networks, where members of Bmp, Shh, Fgf, Wnt and Notch are involved (Harvey, 2002).

Markers of the early stages of both heart fields are *Nkx2.5* (Harvey, 1996) and *Gata4* (Heikinheimo et al., 1994; Morrisey et al., 1996). *Nkx2.5* is the divergent homeodomain homolog of *Drosophila tinman* (Harvey, 1996) which is essential for heart formation. However, the *Nkx2.5* null mutant mouse does not inhibit heart formation, but heart development is blocked at the stage of looping morphogenesis indicating that there might be redundant pathways (Lyons et al., 1995). *Gata4* encodes for a zinc finger protein and is able to bind to consensus GATA sites found in several myofibrillar protein genes. In *Drosophila*, a single *Gata* gene, *pannier*, is required for cardiogenesis and works synergistically with *tinman* (Brand, 2003; Gajewski et al., 1999). Interestingly, both, *Gata4* knockout mice (Kuo et al., 1997), as well as zebrafish *gata5* mutants (Reiter et al., 1999) develop a cardia bifida phenotype (Brand, 2003). The first and the second heart field can be distinguished by the different expression of specific transcription factors and signaling molecules. Whereas the first heart field specifically expresses the T-box transcription factor *Tbx5* and the basic helix-loop-helix transcription factor *Hand1*, the second heart field is marked by *Isl1*, *Hand2* and *Fgf10* and others (Cai et al., 2003; Kelly et al., 2001; Olson, 2006).

Interestingly, there are similarities between the second heart field and the second myogenic field in the head (Grifone and Kelly, 2007; Tzahor, 2009). Recent experiments in chick and mouse models give evidence that cardiac and branchiomeric muscle developmental programs are tightly linked suggesting common evolutionary origins (Cai et al., 2003; Nathan et al., 2008). In chick and mouse, the cranial paraxial mesoderm and the splanchnic mesoderm contribute cells to the developing facial musculature in a temporal and spatial manner. In both animal models, the splanchnic mesoderm cells within the second myogenic field express *Isl1*. These *Isl1* positive cells migrate into the arterial pole of the heart and into the first branchial arch (Cai et al., 2003; Nathan et al., 2008). Not only the splanchnic mesoderm is linked to heart and craniofacial development, but also the cranial paraxial mesoderm has cardiogenic potential. Another study in chick revealed that a subset of cranial paraxial mesoderm cells contributes to both myocardial and endocardial cell populations within the cardiac outflow tract (Tirosh-Finkel et al., 2006). However, to date it is not clear whether branchiomeric and cardiac progenitor cells are distinct lineages with overlapping genetic programs or represent derivatives of the common mesoderm lineage.

3.1.2 Heart tube assembly and development of polarity

In the developing heart field and in the early heart tube exists a highly dynamic and species-specific pattern of contractile protein gene expression. Within the heart, the atrial and ventricular muscle cells differ in their electrophysiological, contractile, morphological and physiological phenotypes. Therefore these muscle lineages are separated early in development and studies in chick and zebrafish give evidence that the separation may start soon after gastrulation (Fishman and Chien, 1997; Stainier et al., 1993; Yutzey et al., 1994). At this point in time genes are expressed in a chamber-specific manner, e.g. *Amhc* which is limited to the preatrial region of the heart field and persists in the developing heart chamber (Yutzey et al., 1994). In addition, ventricular precursors in the cardiac crescent are verified by the expression of *Vmlc2* (O'Brien et al., 1993). *Vmlc2* is the earliest known marker for the ventricular muscle cells which maintains its expression in the ventricle throughout embryonic and postnatal development. The assembly of the linear heart tube is initiated by the convergence and fusion of the bilateral heart field along the midline. The linear heart tube is composed of an external myocardial and an internal endocardial layer and also displays a polarity along the anterior/posterior axis which orders the outflow tract, the right and left ventricle and atria and the inflow tract along the linear heart tube. This positional anterior/posterior identity is already seen in the cardiac crescent and is sensitive to perturbation by retinoic acid (Yutzey et al., 1994). The initial tubular heart has a caudal pacemaker activity which results in unidirectional peristaltic contractions and can be detected in form of a sinusoidal electrocardiogram (ECG) (Figure 1). Later on this caudal pacemaker activity shifts to the left side of the inflow tract. Formation of the sinus venosus (sinus horns and sinoatrial node (SAN) primordium) is accompanied by the addition of cardiomyocytes to the inflow tract. Similar to the mouse, the inflow pole of the zebrafish heart tube, which possesses pacemaker activity, is formed by differentiation of *Isl1* and *Tbx18* positive cells, indicating that the SAN precursors have features of both, the second heart field and sinus venosus precursors.

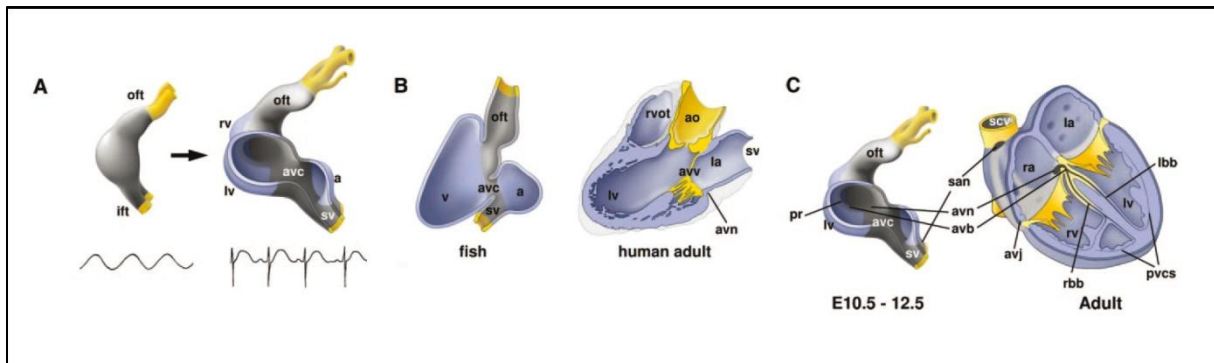


Figure 1: Schematic overview of heart development in higher vertebrates (Christoffels et al., 2010).

A) The early heart tube has a primitive phenotype (gray) and sinusoidal ECG. Chamber myocardium (blue) expands from the outer curvatures of the primary heart tube, whereas nonchamber myocardium (gray) of the sinus venosus (sv), AVC (avc), outflow tract (oft), and inner curvatures does not expand. The chamber heart has a mature type of ECG. B) The basic configuration of slow conducting pacemaker and fast conducting chamber components is found in the adult fish and human heart. C) The sinus node (san) forms in the sinus venosus, the AVN (avn), and atrioventricular junction (avj) in the atrioventricular canal. The ventricular septum crest part of the primary ring (pr) will form the AVB. a indicates atrium; ev, embryonic ventricle; ift, inflow tract; la, left atrium; lv, left ventricle; pvcs, peripheral ventricular conduction system; ra, right atrium; rv, right ventricle; scv, superior caval vein; rbb, right bundle branch.

Rightward looping of the heart occurs at a stage in which only the ventricular component and part of the atrioventricular canal has been formed. The morphogenetic steps needed to promote looping are guided by molecular asymmetries that are established by the left/right axis pathway which has its origin much earlier than the looping occurs (Brand, 2003). The looping heart tube expresses *Nkx2.5* and *Gata4* throughout the myocardium, whereas *Tbx5* and *Tbx20* are expressed in an anterior-posterior morphogen gradient with the highest expression seen in the inflow region. In addition, *Tbx20* displays an isolated expression domain within the outflow tract (Boogerd et al., 2009). Conduction patterns of imaged chick hearts at HH stage 17 reveal slower voltage transients within the atrioventricular canal (AVC) and along the outflow tract (Thompson et al., 2003). The embryonic AVC contains the precursors of the atrioventricular node (AVN) and the atrioventricular ring bundles and is largely a derivative of the first heart field.

3.1.3 Chamber formation and cardiac conduction development

During chamber development the heart starts to contract synchronously requiring higher conduction velocities of the depolarizing electrical impulse than in the tubular heart. Therefore genes for high conductance gap junctions, mitochondrial genes and genes for sarcomere components are upregulated in the chamber myocardium. Chamber-specific genes, which are involved, include *Connexin40* (*Cx40*) and *Connexin43* (*Cx43*), the transcription factors *Hand1*, *Irx4* and *Irx5* and the secreted factor *Anf* (Boogerd et al., 2009; Christoffels et al., 2000). The activation of the chamber-specific genes *Anf* and *Cx40* depends on protein-protein interactions between *Nkx2.5*, *Tbx5* and *Gata4*. Notably, *Tbx5* and *Nkx2.5* are not only expressed in the chamber myocardium but are also essential for the differentiation of the conduction system (Boogerd et al., 2009). Furthermore, gain-of-function mutations in *Nkx2.5* and *Tbx5* further cause AV conduction defects in mice (Moorman and Christoffels, 2003a). However, the sinus venosus, the AVC, inner curvatures, and the outflow tract do not differentiate into fast-conducting chamber myocardium, also called working myocardium, and retain their slow conduction properties. In amniotes, the working myocardium is initially detected in defined zones at the outer curvature of the

looping heart tube (Christoffels et al., 2010; Moorman and Christoffels, 2003a) and reveals the onset of chamber specification.

The sinus venosus, the pacemaker in the embryo and early fetus, expresses *Hcn4*, whereas chamber-specific genes like *Cx40*, *Cx43*, and *Scn5A* are repressed. At E 9.5 to E10 in the mouse embryo, a *Tbx3* expressing SAN primordium develops within the right side of the sinus venosus myocardium. Later on, at some as yet undefined prenatal stage, the actual SAN structure is confined and the rest of the sinus horn myocardium develops a working myocardium phenotype (Christoffels et al., 2010).

The AV conduction development is intertwined with the development of cardiac cushions, the primordia of the valves and membranous septae. The developing AVN and AV ring bundles always face the cushion mesenchyme and therefore it is proposed that signals from the cushion mesenchyme are able to mediate the maintenance and maturation of the pacemaker tissue (Christoffels et al., 2010). The cushions are first detected as localized swellings in the cardiac jelly, which are subsequently invaded by endothelial cells. The myocardium produces the signaling molecule *Bmp2* which induces *Tbx2* (and possibly *Tbx3*) transcription that in turn inhibits chamber-specific gene expression in the AVC and the outflow tract. In zebrafish, expression of *tbx2b* is restricted to the AVC and morpholino knockdown resulted in loss of the AVC and the AV conduction delay. Notch-Hey signaling in the chambers delimits the *Bmp2*-*Tbx2* pathway, hence AVC formation (Christoffels et al., 2010; Combs and Yutzey, 2009). *Bmp2* expression further increases hyaluronan and versican deposition in the cushion-forming regions and promotes endocardial cushion epithelial-mesenchymal transformation (EMT). During EMT, a subset of endothelial cells breaks connections with its neighbors and migrates into the cardiac jelly to populate the cushions with mesenchymal cells which has been well-studied *in vitro* and *in vivo* (Combs and Yutzey, 2009). Once the cushions are established, endocardial *Vegf* (vascular endothelial growth factor) expression maintains endothelial cell proliferation and inhibits EMT. After EMT, the cardiac cushions and subsequent valve primordial undergo growth via cell proliferation and continued extracellular matrix synthesis (Armstrong and Bischoff, 2004; Combs and Yutzey, 2009; Hinton et al., 2006).

One morphological feature of chamber formation is the appearance of trabecular myocardium. During chamber growth (at about HH stage 13 in chick), the ventricular myocardium thickens and trabeculae are built. The trabecular myocardium is the spongiform inner muscular layer that is less proliferative and more differentiated than the outer layer. With the help of retroviral lineage analyses, the development of trabeculae was observed (Christoffels et al., 2010; Mikawa and Hurtado, 2007). It was shown that the Neuregulin/ErbB signaling system is essential for the formation of trabeculae. Neuregulin1 is expressed in the endocardium, but it binds to membrane-bound tyrosine kinase co-receptors ErbB2 and ErbB4 in the myocardium (Harvey, 2002). Trabeculae are formed by proliferation of individual cardiomyocytes that build clusters. These myocyte clusters form trabeculae and in turn fuse. Due to a faster proliferation at the epicardial side than at the endocardial side of the trabeculae, cone-shaped structures are generated. It is thought that the bundle branches and the peripheral ventricular conduction system develop from the trabecular ventricular component (Moorman and Christoffels, 2003a; Moorman et al., 2005). The main function of the ventricular conduction system is to rapidly propagate and transmit impulses to the ventricular muscle. Purkinje fibers display a myocardial origin and are induced by coronary arterial beds which

recruit the differentiation of adjacent myocytes into conduction cells. *In vivo* experiments suggest that biomechanical forces created by the cardiovascular system and interactions between cardiac endothelial cells and myocytes play a crucial role in Purkinje fiber induction. Moreover, ET-1 (Endothelin-1) a shear-stress induced cytokine, can induce the expression of many Purkinje fiber marker genes *in vitro* and *in vivo* (Mikawa and Hurtado, 2007). The cells of the trabeculae and of the bundle branches have a poorly developed contractile apparatus and t tubuli, but display well-developed gap junctions, which are built from Cx40 and Cx43. Furthermore, during chamber expansion, expression of the genes *Anf*, *Cx40* and *Irx3* become restricted to the trabeculae and the ventricular conduction network (Christoffels et al., 2010; Mikawa and Hurtado, 2007).

3.1.4 Heart remodeling

During heart remodeling the septation of the heart is completed by fusion of the muscular inter-atrial and inter-ventricular septae with non-muscular atrioventricular septum so that left and right ventricles and left and right atria can be observed. The septal division of the chambers and formation of the valves involves endothelial cells and is necessary for the formation of a four-chambered heart with separate inflow and outflow poles. During heart growth, the cardiac neural crest cells populate the heart through the outflow tract and contribute to the formation of the great vessels and outflow septum (Harvey, 2002). Then, during the fetal stages of chick, mouse and human, the valve primordial elongate into thin valve leaflets.

While interventricular septation the unidirectional impulse propagates from the left ventricle via the ventricular apex (base-to-apex propagation). Close to the completion of septation, the fast ventricular conduction network is fully matured and the activation of the myocardium spreads from the apex toward the base of the ventricle (apex-to-base propagation) (Mikawa and Hurtado, 2007).

3.2 Electrical activity of the adult heart

The term arrhythmia defines aberrant electrical activity of the heart, which causes irregular cardiac contractions, loss of consciousness and in the most severe case, sudden cardiac death. Every year, about 450.000 individuals in the USA (Arnaout et al., 2007) and about 160.000 individuals in Germany (Statistisches Bundesamt, Deutschland) die from sudden cardiac death. Cardiovascular diseases are the leading cause of death in the Western world and in 2008 accounted for 43 % of deaths in Germany (Statistisches Bundesamt, Deutschland). Often the precise disease mechanism is not known. Even if the genetic basis for a particular heart disease has been recognized, the mechanism of how a mutation results in a particular disease phenotype is often not fully elucidated (Keating and Sanguinetti, 2001; Moorman and Christoffels, 2003b). Although mutations in ion channel genes were identified to play a role in long QT (LQT) syndrome, a disease that affects ventricular conduction (Keating and Sanguinetti, 2001), these mutations only account for less than 1 % of the total incidences of sudden cardiac death. Thus, we clearly lack knowledge on the genetic causes of sudden cardiac death and little to none causative therapeutic options are currently available. Therefore, currently, the only proven preventive therapy for sudden cardiac death is the automatic implantable cardioverter defibrillator (Priori et al., 2001). Extensive

research to identify and characterize inherited cardiac arrhythmias and the signaling pathways behind is needed to understand the cardiac conduction system.

Proper function of electrical activity is necessary for normal mechanical functioning of the heart. The heart, as a cardiac muscle, consists of two cell types: contractile cells and autorhythmic cells, which display pacemaker potentials for generating and conducting of the electrical impulse. The generation of myocardial action potentials reflects the sequential activation and inactivation of ion channels that conduct depolarizing inward, and repolarizing outward currents. In the center of the SAN, the electrical activity is initiated and propagates rapidly via the periphery through the atrial myocardium to the AVN, where the propagation of the depolarizing impulse is delayed. Then excitation spreads via the atrioventricular bundle into the His-Purkinje fibers towards the apex of the heart and from there into the working ventricular myocardium. The cardiac excitation spreading of the whole heart can be detected in surface electrocardiograms (ECG) (Christoffels et al., 2010; Mikawa and Hurtado, 2007; Nerbonne and Kass, 2005). The typical ECG tracing can be subdivided into the P wave, the QRS complex and the T wave. The P wave reflects atrial repolarization, the QRS complex represents the depolarization of all ventricular myocytes and the T wave corresponds to their repolarization marking at its end the beginning of ventricular relaxation. At the end of the T wave, the ECG tracing returns to its baseline. The interval from the beginning of the QRS complex to the end of the T wave (QT interval) resembles the duration of both the action potential and contraction of the ventricle (Figure 2).

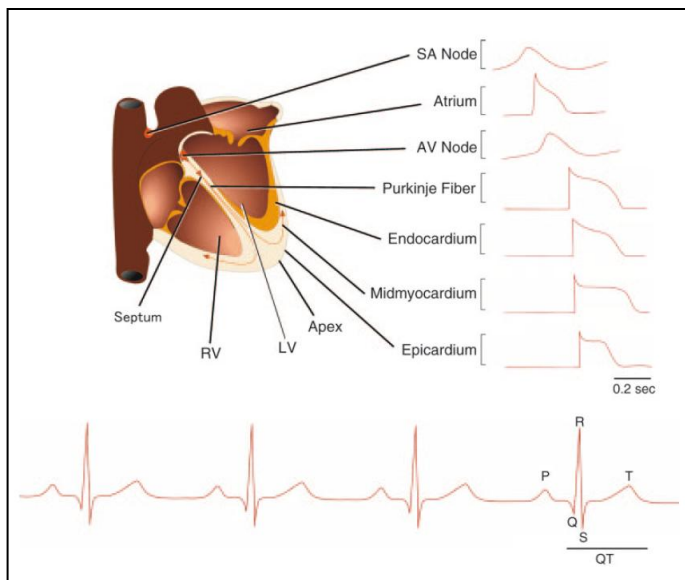


Figure 2: Electrical activity of the myocardium (Nerbonne and Kass, 2005).

The top represents a schematic human heart with illustration of typical action potential waveforms recorded in different regions. The bottom represents a surface electrocardiogram where three sequential beats are displayed. Each beat consists of a P wave, the QRS complex and the T wave. Abbreviations: AV Node = atrioventricular node; LV = left ventricle; RV = right ventricle; SA Node = sinoatrial node.

Changes in the length of the QT-interval of the ECG tracing characterize hereditary cardiac diseases like the short QT (SQT) syndrome and the long QT (LQT) syndrome. The SQT syndrome is defined by a shortened QT interval. The human SQT syndrome is a hereditary ion channelopathy which can cause sudden cardiac death and is associated with a high risk of arrhythmic events (atrial and ventricular fibrillation). The SQT is a channelopathy associated with gain-of-function mutations in the genes encoding repolarizing potassium channels (SQT1:

KCNH2, SQT2: *KCNQ1*, SQT3: *KCNJ2*). Moreover, loss-of function mutation in the alpha- and beta2 subunits of the $Ca_v1.2$ channel, which is responsible for conducting the long lasting calcium current (L-type calcium current) are also associated with SQT (SQT4: *CACNA1C*, SQT5: *CACNAB2*) (Hedley et al., 2009). The LQT syndrome is characterized by a prolonged QT interval and is the primary cause of the inheritable forms of sudden cardiac death and associated malignant ventricular arrhythmias (Cheng et al., 2003). LQT syndrome is caused by mutations in a total of 12 different disease-inducing loci. LQT syndrome has been shown to be a channelopathy associated with the loss-of-function in genes encoding repolarizing potassium ion channels, (LQT1: *KCNQ1*, LQT2: *KCNH2*, LQT7: *KCNJ2*) and their beta subunits (LQT5: *KCNE1*, LQT6: *KCNE2*). Moreover, LQT syndrome has been associated with mutations in genes that encode proteins that are involved in membrane targeting and/or clustering of ion channels: *Ankyrin B* (LQT4: *ANK2*), *Caveolin3* (LQT9: *CAV3*), *AKAP9* (LQT11), and *Syntrophin* (LQT12: *SNTA1*). Additionally, gain-of-function mutations in genes encoding the depolarizing sodium channel *SCN5A* (LQT3), the calcium channel $Ca_v1.2$ (LQT8) and the beta subunit *SCN4B* (LQT10) are associated with LQT (Hedley et al., 2009). Of note four of the mentioned genes (*KCNQ1*, *KCNH2*, *KCNJ2*, *CACNA1C*) have been associated with both LQT and SQT syndrome. All these mutations influence the timing of electrical excitation which is passed through the ventricle. In case of prolonged QT sodium channels remain open for a longer time than normal which in turn prolongs the time of refractoriness. This will also result in an enhancement of Na-Ca exchange current, which can trigger reactivation of the L-type calcium channel through which an early-after depolarization is triggered and this may trigger ventricular arrhythmia. A shorter than normal QT time shortens the time of refractoriness and due to heterogeneity of repolarizing ion channel expression, the likelihood of reentry arrhythmia in some areas of the ventricle becomes very high (Hedley et al., 2009).

3.2.1 The nodes and the fast conduction Purkinje fiber networks

The sinoatrial and atrioventricular nodal cells as well as the atrioventricular junction cells are smaller than working myocytes and lack t tubuli. They all share a poorly developed contractile and sarcoplasmic reticular apparatus, display high glycogen content, a lower mitochondrial content and are slow-conducting and poorly coupled (Boyett and Dobrzynski, 2007). The pacemaker of the heart, the “comma-shaped” sinus node, consists of a core and a periphery. In humans it is located adjacent to the terminal crest (crista terminalis). Its core is surrounded by an area that displays a myocardial phenotype which is further embedded in connective tissue and arteries. The slow impulse conduction component, the atrioventricular node, consists of loosely connected fibers in the superior and right margins, whereas in the inferior region the nodal cells are more confined (Dobrzynski et al., 2007). The fast-conducting His-Purkinje network in the ventricle is characterized by conduction cells scattered throughout the myocardium. It can be distinguished from ventricular muscle cells by the expression of *Cx40*, the predominant connexin of the His-Purkinje system in all higher vertebrates (Mikawa and Hurtado, 2007).

3.2.2 Gap junctions

The propagation of the electrical impulse and the coordination of the electromechanical functioning also depend on electrical coupling between cells, mediated by gap junctions. Gap junctions are present in all vertebrate tissues and are able to build gap junction channels, which span the two plasma membranes of neighboring cells

and therefore provide a connection between the cytoplasm of these cells. The channels consist of two connexons which are Connexin hexamers and the conductance is dependent on the Connexin type and the grade of modulation (Bruzzzone et al., 1996; Goodenough et al., 1996; Unger et al., 1999). Cx45, Cx30.2 and Cx30 subunits form gap junction channels with very low conductance expressed in the sinoatrial node, whereas Cx40 and Cx43 subunits assemble to high-conductance channels seen in the fast-conducting working myocardium (Miquerol et al., 2003).

3.2.3 Cardiac currents involved in generation of myocardial action potentials

The cardiac action potential consists of five phases (phases 0-4). In the fast responding cell (working myocardium, Purkinje fibers) inward rectifier K^+ channels are open at rest, whereas cardiac Na^+ channels are closed. When a propagated impulse leads to a change in the action potential across the cell, Na^+ channels in turn open. These voltage-gated cardiac Na^+ (Na_v) channels are mainly responsible for the rapid upstroke of action potential in the depolarization phase of the cardiomyocyte categorized as phase 0 (Figure 3) (Fozzard and Hanck, 1996; Roden et al., 2002). There are known and well-documented mutations within the cardiac $Na_v1.5$ channel encoded by the gene *Scn5a* which are linked to Brugada syndromes and to LQT3, as well as to conduction disorders revealing the impact of Na_v current (Table 1) (Nerbonne and Kass, 2005). Then, in the early phase of repolarization (the rapid phase 1), the sodium channels close and the transient outward K^+ currents (I_{to}) are activated. The characteristically plateau phase of the action potential, phase 2, reflects the balance between inward current and outward current (Figure 3). The inward current is largely produced by L-type Ca^{2+} channels. L-type Ca^{2+} channels are expressed in the working myocardium ($Ca_v1.2$), but also in the SAN and AVN cells, where they are involved in action potential generation, as well as in regulating automaticity ($Ca_v1.3$) and they are highly localized in the t tubuli near the storage sites for intracellular Ca^{2+} release. $Ca_v1.3$ knockout mice develop a bradycardia and sinus dysrhythmia due to the loss of the major component of the current: its activation at negative voltages (Dobrzynski et al., 2007). The outward current reflects the activated delayed rectifier K^+ channels. Delayed rectifier K_v currents are subdivided into I_{Kr} and I_{Ks} and are found in the atrium, the ventricle, the Purkinje fibers and the SAN, as well as in the AV node in the case of I_{Kr} . Expression of *Herg*, which encodes the pore-forming α subunit of the voltage-gated potassium channel, is responsible for the I_{Kr} current. Mutations within the gene *HERG* due to a reduction of I_{Kr} channel function and display the genetic cause of inheritable LQT2, as well as acquired forms of LQT syndrome (Cheng et al., 2003). I_{Ks} , which works in concert with I_{Kr} to terminate the plateau phase of the action potential, is mediated by the *KCNQ1* gene. Gain-of-function of *KCNQ1* leads to short QT syndrome whereas loss-of-function causes LQT1, the most common form of inherited LQT syndrome. In the final phase of repolarization, phase 3, several outward K^+ currents like I_{Kr} , I_{Ks} and I_{K1} are involved. Phase 4, in which the membrane potential returns to the baseline (Figure 3), is mediated by the current I_{K1} which represents expression of members of the Kir2 family (Nerbonne and Kass, 2005; Roden et al., 2002).

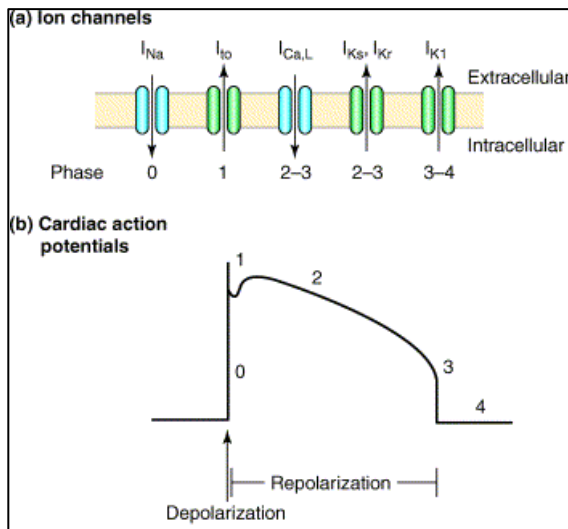


Figure 3: The relationship between cardiac ion fluxes and action potential (Cheng et al., 2003)

a) The sequence of ion fluxes across the cell membrane that mediates the action potential of a human ventricular muscle cell. The phase of the cardiac action potential that each ion current contributes to is indicated below the current. b) The action potential of a human ventricular myocyte. The cardiac action potential is composed of five phases (phases 0-4). The steep upstroke of phase 0 marks the beginning of an action potential. This upstroke is initiated by an influx of Na^+ currents (I_{Na}). The notch of phase 1 represents the early phase of repolarization, resulting from the closure of the sodium channels and the activation of transient outward K^+ currents (I_{to}). Phase 2 is the plateau phase of the action potential, and is generated primarily by inward Ca^{2+} currents ($I_{\text{Ca,L}}$), and the outward K^+ currents, I_{Kr} and I_{Ks} . Phase 3 represents the final phase of repolarization, and results from several outward K^+ currents, including I_{Kr} , I_{Ks} and I_{K1} . Phase 4, in which the membrane potential returns to the baseline, marks the end of a cardiac action potential, and it is mediated by I_{K1} .

In contrast to the fast responding working myocardium, slow response cells in the sinus node and the atrioventricular node display a slow, diastolic depolarization without a rapid upstroke in phase 1. This initial depolarization is accomplished by L-type and T-type Ca^{2+} channels and a sustained inward current (Roden et al., 2002). Cardiac T-type Ca_v channels are preferentially expressed in pacemaker and conducting cells ($\text{Ca}_v3.1$ and $\text{Ca}_v3.2$) and may have a role in pacemaking rather than regulating excitation-contraction coupling observed in L-Type Ca_v channels. The $\text{Ca}_v3.1$ knockout mouse supports this hypothesis showing bradycardia, a slowed heart rate and a prolonged sinus node recovery time (Dobrzynski et al., 2007). In the sinus node, the hyperpolarized-activated funny current (I_f) plays a major role in generating a pacemaking action potential. The funny current I_f is a cation current which is mainly generated by voltage-gated HCN channels. HCN channels provide an inward Na^+ current that slowly depolarizes the plasma membrane and closes upon depolarization. In sinoatrial cells, $Hcn4$ is the predominantly expressed HCN channel isoform (Biel et al., 2002). Targeted deletion of $Hcn4$ at the adult stage in mice leads to cardiac arrhythmia characterized by recurrent sinus pauses, but unexpectedly the $Hcn4$ null mutant mice display no impaired heart rate acceleration during sympathetic stimulation (Herrmann et al., 2007).

Table 1: Genes encoding cardiac ion channel α and β subunits (Roden et al., 2002)

Current	α Subunits		β Subunits	
	Gene	Human chromosomal location	Gene	Human chromosomal location
Inward currents				
I_{Na}	SCN5A	3p21	β_1 (SCN1B) β_2 (SCN2B)	19q13.1-q13.2 11q23
I_{Ca-L}	α_1C (CACNL1A1)	12pter-p13.2	β_1 (CACNB1) β_2 (CACNB2) $\alpha_2\delta$ (CACNA2D1)	17q21-q22 10p12 7q21-22
I_{Ca-T}	α_1H (CACNA1H)	16p13.3		
Outward currents				
I_{Ks}	<i>KvLQT1</i> (KCNQ1)	11p15.5	<i>minK/IsK</i> (KCNE1)	21q22.12
I_{Kr}	<i>HERG</i> (KCNH2)	7q36-q36	<i>minK/IsK</i> (KCNE1) <i>MiRP1</i> (KCNE2)	21q22.12 21q22.12
I_{Kur}	<i>Kv1.5</i> (KCNA5)		<i>Kvβ1</i> (KCNA1) <i>Kvβ2</i> (KCNA2 ??)	3q26.1 1p36.3
I_{K1}	<i>Kir2.1</i> (KCNJ2) <i>Kir2.2</i> (KCNJ12)	17q 17p11.1		
I_{K-Ach}	<i>GIRK1</i> , <i>Kir3.1</i> (KCNJ3) + <i>GIRK4</i> , <i>Kir3.4</i> (KCNJ5)	2q24.1 11q24		
I_{K-ATP}	<i>Kir6.2</i> , <i>BIR</i> (KCNJ11)	11p15.1	<i>SUR2</i> (ABCC9)	12p12.1
I_{TO}	<i>Kv4.3</i> (KCNB3) <i>Kv1.4</i> (KCNB4)	1p13.2 11p14		
I_f , I_h (pacemaker current)	<i>BCNG2</i> , <i>HCN2</i> <i>HCN4</i>	19p13.3 15q24-q25		
I_{Kp}	<i>TWIK1</i> (KCNK1) <i>CFTR</i> (ABCC7) <i>KvLQT1</i> (KCNQ1)	1q42-q43 7q31.2 11p15.5	<i>MiRP1</i> (KCNE2)	21q22.12

Recently, a new family of potassium channels has been discovered referred to as two pore domain K^+ (K_{2P}) channels. In contrast to K_v and K_{ir} channels, which assemble as tetramers, functional K_{2P} channels are homodimers consisting of four transmembrane domains and two pore-forming P loops arranged in tandem which contributes to the formation of the K^+ -selective pore. Interestingly, the K_{2P} channels have properties well suited to a role in mediating background K^+ conductance. For example the K_{2P} channels *Trek1* and *Task1* are expressed in the heart and heterologous expression of either of these subunits alone gives rise to instantaneous, noninactivating K^+ currents displaying little or no voltage-dependence (Goldstein et al., 2001; Lesage and Lazdunski, 2000). Furthermore, properties of the currents produced on expression of *Trek1* or *Task1* are similar to those of the current referred to as I_{KP} identified in guinea pig ventricular myocytes as well as I_{ss} in mouse ventricular myocytes. The subfamily of *Task* channels exhibit strong basal currents with very fast activation and inactivation kinetics. The other important subfamily, the *Trek* channels, display low basal activity, but are stimulated by stretch of the cell membrane, lysophospholipids and arachidonic acid and are inactivated by hypo-osmolarity and cAMP-dependent phosphorylation of Ser333 in the C-terminal domain (Lesage, 2003). *Trek1*

knockout mice display increased sensitivity to epilepsy and ischemia, however, it is not studied whether there is a cardiac phenotype. Because of the existence of various K_{2P} α -subunits, their ubiquitous expression, as well as the huge variety in K_{2P} channel regulation, these channels likely subserve a variety of important physiological functions which has to be experimentally demonstrated (Gurney and Manoury, 2009).

3.3 *Danio rerio*

3.3.1 The zebrafish as model system for cardiovascular research

Because unraveling the mechanisms of the cardiac conduction system development is essential to develop novel and safer therapeutic options for patients, vertebrate model systems are established for research. However, genetic manipulation of the conventional vertebrate model *Mus musculus* (mouse) is time-consuming and has a major limitation for arrhythmia research *in vivo*: the murine heart beats 7 to 10 times faster than the human and therefore leads to cardiac repolarization differences between mouse and human (Dahme et al., 2009; Milan and MacRae; Milan and MacRae, 2005). Beside the mouse, the zebrafish has emerged as a popular model organism for cardiovascular research. Its general features like external fertilization, rapid development and life cycle, as well as the ease of genetic manipulation are not the only advantages of this system. The earliest stages of cardiogenesis from heart specification to the formation of a two-chambered looped heart in zebrafish resemble the human heart during the first three weeks of gestation (Fishman and Chien, 1997) and the zebrafish allows us to monitor cardiac function in early heart development even without a functional circulatory system for several days (Pelster and Burggren, 1996). Moreover, the fundamental electrical properties of the zebrafish heart, the ion channel repertoire and its currents are remarkably similar to those of humans (Baker et al., 1997; Chi et al., 2008; Sedmera et al., 2003; Warren et al., 2001). Demonstrating the importance of the zebrafish model for arrhythmia research, Milan and colleagues revealed that drugs which cause repolarization abnormalities in humans also induce bradycardia and atrioventricular block in zebrafish (Milan et al., 2003). Recently they published a drug-sensitized zebrafish screen which identifies genes involved in repolarization (Milan et al., 2009). Also, the ease of genetic manipulation was used for several forward genetic screens in zebrafish and more than 100 genes required for heart formation and function were identified (Chen et al., 1996; Stainier et al., 1996; Stainier et al., 1995). Interestingly, these screens have revealed several mutations that perturb cardiac rhythm and contractility. For example the *reggae* zebrafish mutant has a pacemaker dysfunction similar to the human disorder known as sinus exit block and also zebrafish mutations which perturb impulse conduction (*island beat* and *polka* mutants) or atrioventricular nodal function (*ginger*, *breakdance* and *hiphop* mutants) were identified, as well as mutants with fibrillating hearts like *slip jig* and *tremblor* or zebrafish mutants with impaired contractility without affecting heart rate or rhythm (*weiches herz*, *low octane*, *dead beat*, *pie heart* and *tango* mutants) (Warren and Fishman, 1998). To date, not only forward genetic large-scale screens in zebrafish, but also reverse genetics are possible beside the gene knockdown using morpholino-modified antisense oligos. The establishment of TILLING (targeted induced local lesions in genomes) libraries by N-ethyl-N-nitrosourea-mutagenesis (ENU-mutagenesis) (Moens et al., 2008; Wienholds et al., 2002), viral insertional mutagenesis (Wang et al., 2007) and recently the targeted

inactivation of genes using zinc finger nucleases (Doyon et al., 2008; Meng et al., 2008) allows the knockout of every desired candidate gene. This spectrum of zebrafish mutants provides a system to study cardiac rhythm and contractility in an intact organism and helps to identify new genes with critical roles in cardiac conduction system. To characterize the amount of cardiovascular zebrafish mutants, an array of cellular, molecular, physiological and genetic techniques has been developed involving fate mapping (Warga et al., 2009), transgenes that express GFP in cardiomyocytes (Huang et al., 2003) or endothelial cells (Beis et al., 2005) and high-speed imaging (Huisken and Stainier, 2009; Schwerte and Fritsche, 2003; Schwerte and Pelster, 2000; Smyth et al., 2010). Furthermore, the complete sequence of the zebrafish genome is known and several marker-based physical maps are easy accessible (<http://www.zfin.org>).

3.3.2 Zebrafish heart development

By fluorescent dextran injection it was shown that the heart precursors in the zebrafish are found in the ventral marginal zone at the mid-late blastula stage (Lee et al., 1994; Stainier et al., 1993). These blastomeres are among the first to involute when gastrulation begins at 50 % epiboly. After involution they migrate towards the anterior-lateral regions and converge at the midline to generate the so-called “bilateral heart field” (Stainier et al., 1993). A migration defect of heart precursor cells towards the midline leads to two hearts, the so-called “cardia bifida”. Cardia bifida is seen for example in the zebrafish mutants *casanova* and *bonnie and clyde*, which have defective genes involved in endoderm control and formation, suggesting that proper migration is somehow endoderm dependent (Alexander et al., 1999; Kikuchi et al., 2000). The reported cardia bifida mutations and the affected genes in the zebrafish can be categorized into three groups: genes involved in endoderm control and formation (*casanova*, *bonnie and clyde*), genes involved in myocardial differentiation (*hands off*) and genes involved in myocardial migration (*miles apart*) (Stainier, 2001). After assessing the bilateral heart field, fate map studies revealed that at about 13-somite stage in zebrafish the ventricular and atrial precursors are physically separated with the ventricular precursors located at the medial and the atrial precursors in the more lateral part (Stainier et al., 1993). This diversification of ventricular and atrial precursors can be further proved by the expression of chamber specific markers, e.g. *vmhc* (ventricular myosin heavy chain), the earliest known marker for ventricular myocardium. At about 21-somite stage the bilateral heart field fuses to form an intermediate cone, which grows and rotates along the dorsoventral axis, thereafter building the linear heart tube at about 24 hours post fertilization (hpf) laying along the anterior/posterior axis (Figure 4). During this process, the myocardial cells start expression of genes involved in terminal differentiation like *tropoin T*, *tropomyosin* and *myosin*. At the same stage, the linear heart tube jogs to the left of the dorsal midline and *bmp4* expression is enhanced on the left side of the heart tube. This observed asymmetric pattern of cardiac *bmp4* seems to drive asymmetry in the zebrafish heart (Chen et al., 1997). The linear heart tube starts with peristaltic contraction and subsequently, after morphological differences between the cardiac chambers are detectable, the contraction is sequential (36 hpf). After the onset of chamber formation, the zebrafish heart undergoes rightward looping whereby the single ventricle is placed to the right of the single atrium (Ahmad et al., 2004). Interestingly, the zebrafish ventricle appears to be highly sensitive to genetic lesions in contrast to the atrium indicating that the atrial fate is more a

default state (Stainier, 2001). At 48 hpf, chamber separation is more defined by the formation of cardiac cushions at the atrioventricular boundary (Hu et al., 2000) and also the sinus venosus (inflow tract) and the bulbus arteriosus (outflow tract) are distinguishable. In higher vertebrates, the cardiac cushions are known to be remodeled into mature valve leaflets. However, in zebrafish, recent discoveries revealed that zebrafish valve leaflets are not formed through an intermediate stage as thought. Furthermore, they directly form by a process of invagination and the functional valve leaflets can be most clearly seen at 96 hpf (Scherz et al., 2008). Then, the ventricular myocardium thickens by concentric addition of myocardial cells between 48 hpf and 72 hpf and soon later trabeculation occurs.

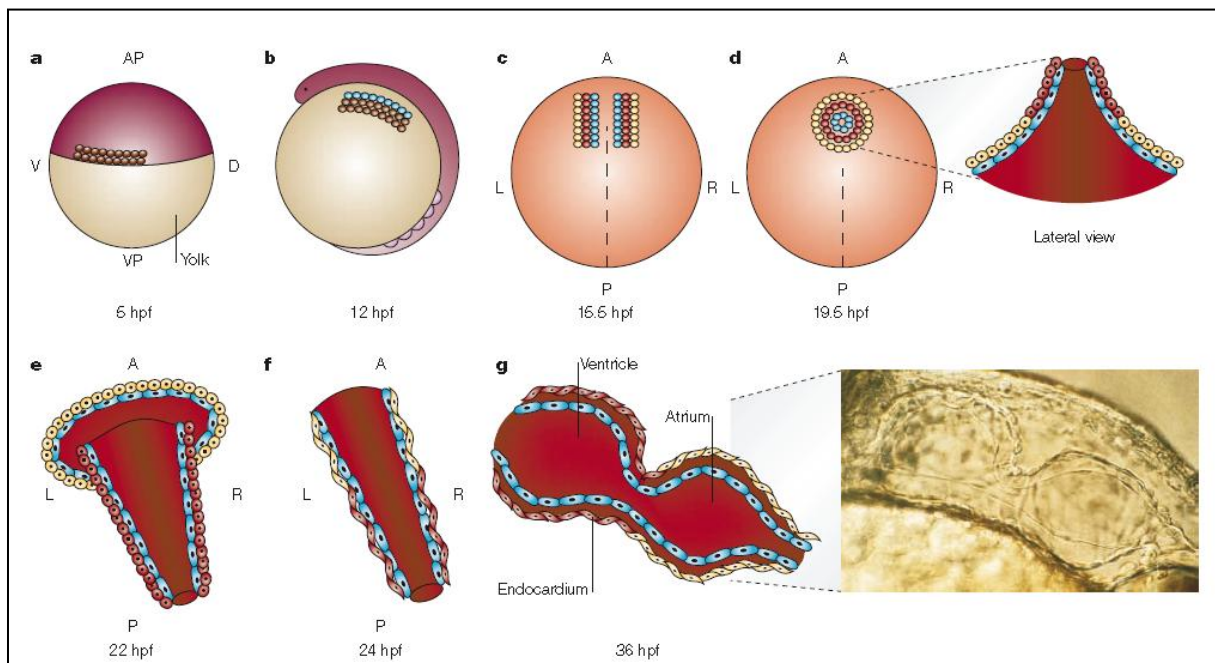


Figure 4: Heart development in zebrafish (Stainier, 2001).

a) At 5 hpf, the precardiac mesoderm is located throughout the ventral and lateral regions of the embryo. b) After involution (12 hpf), the cardiac precursor cells converge towards the embryonic axis. The cells indicated in blue are endocardial precursors. c) By the 13-somite stage (15.5 hpf), the myocardial precursors can be distinguished between preventricular (red) and preatrial (yellow) cells. d) By 19.5 hpf, the cardiac cone assembles. e) Next, the cone rearranges to form a linear heart tube. f) By 24 hpf, the linear heart tube assembles along the anteroposterior axis. g) By 36 hpf, distinct ventricular and atrial chambers form and the heart undergoes looping morphogenesis. Abbreviations: (A = anterior; AP = animal pole; D = dorsal; hpf = hours post fertilization; P = posterior; V = ventral; VP = vegetal pole; L = left; R = right).

3.3.3 Development of the cardiac conduction system in zebrafish

Although the zebrafish heart consists of only two heart chambers, the fundamental electrical properties of the zebrafish heart compared to those of humans are quite similar (Baker et al., 1997; Chi et al., 2008; Sedmera et al., 2003; Warren et al., 2001). Therefore, the zebrafish is emerging as a new animal model to identify molecules involved in cardiac conduction system development. By using the zebrafish system, Milan and colleagues demonstrated for the first time that *notch1b* and *neuregulin* induce AV conduction tissue further revealing flow-independency of this induction (Milan et al., 2006). Additionally, in the last five years, several genes involved in perturbing cardiac rhythm and contractility were identified with the help of zebrafish mutants, some of them could even be directly linked to known human diseases. This includes the SQT syndrome (Hassel et al., 2008) and the LQT syndrome (Arnaout et al., 2007). Both are hereditary cardiac diseases characterized by a change in the QT

interval in the ECG tracing which can cause sudden cardiac death. The zebrafish *reggae* mutant, which carries a gain-of-function mutation of *kcnh2*, is the first animal model of congenital SQT syndrome displaying a distinct phenotype of intermittent atrial fibrillation and accelerated cardiomyocyte repolarization (QT shortening) well-known of human SQT syndrome (Hassel et al., 2008). In contrast, the zebrafish mutant *breakdance*, which carries a loss-of-function mutation in *kcnh2*, is an appropriate animal model of inherited LQT syndrome demonstrating impaired Ca^{2+} release and/or reuptake in mutant ventricular myocytes due to the loss of I_{Kr} (Arnaout et al., 2007). Furthermore, it exists a zebrafish model consistent with “triggered arrhythmia” caused by early and delayed afterdepolarization (Langenbacher et al., 2005; Pogwizd and Bers, 2004). This zebrafish mutant called *tremblor* carries a mutation in the sodium-calcium exchanger 1 (Ncx1) and displays chaotic movements and impaired development of synchronized contractions in the heart similar to cardiac fibrillation (Langenbacher et al., 2005).

Despite the electrical properties of the cardiac conduction system in zebrafish are known (Sedmera et al., 2003), the development of the cardiac conduction system as well as the morphology and distribution of the pacemaker tissue was not well understood. Recently, Chi and colleagues described for the first time the development of the cardiac conduction system in zebrafish using an optical mapping system. They identified four distinct physiologic stages of the cardiac conduction system linked to cellular and anatomical changes of the zebrafish heart (Chi et al., 2008). First, optical mapping of the linear heart tube at 24 hpf reveals linear conduction without significant pauses from the sinus venosus to the outflow tract, suggesting the presence of a functional sinoatrial node pacemaker activity. Second, during chamber formation, the zebrafish heart has developed a distinct AV canal that separates the cardiac chambers and calcium transients revealed significant slowing at the AV canal and the outflow tract (Figure 5). The observed AV conduction delay correlates with cellular changes of the atrial, ventricular and AV myocardial cells. Atrial cardiomyocytes maintain their squamous cell morphology, whereas ventricular cardiomyocytes develop a cuboidal shape and the cardiomyocytes at the AV boundary have initiated apical membrane constriction, resulting in cells with a distinct trapezoidal shape. Furthermore, outer curvature cardiomyocytes elongate, whereas inner curvature cardiomyocytes remain rounded. Interestingly, also the cardiomyocytes at the AV boundary elongate and form a ring of cells around the AV canal. Third, at about 100 hpf, the rapid ventricular cardiac conduction system develops within the forming trabeculae and rapid proceeding of calcium transients from the trabeculae to the adjacent peripheral cardiomyocytes can be detected leading to conduction from the outer curvature to the base/inner curvature and is terminated at the outflow tract. Fourth, at 2-3 weeks of life, after ventricular apex formation, the fast conduction network is fully matured and the typical apex-to base activation pattern in the ventricle is seen (Chi et al., 2008).

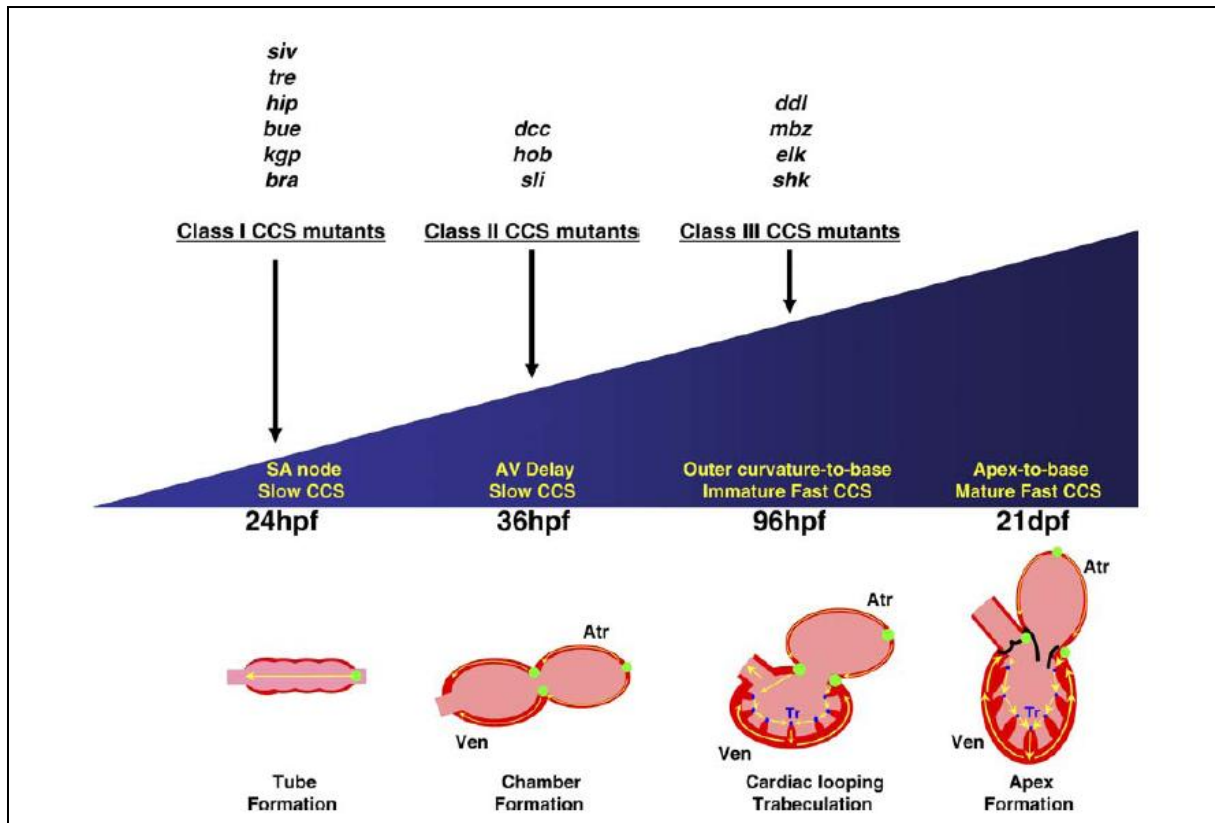


Figure 5: Development of the cardiac conduction system in zebrafish and classification of zebrafish mutants (Chi et al., 2008).

The diagram represents the four developmental stages of the cardiac conduction system. Mutations affecting each stage are listed above. Yellow arrows indicate the conduction flow. Green circles indicate slow conduction pathway/pacemaker and AV conduction delay. Blue circles indicate the fast conduction network. Abbreviations: Atr = atrium, Ven = ventricle, Tr = trabeculae., *siv* = silent ventricle, *tre* = tremblor, *hip* = hiphop, *bue* = bullseye, *kgp* = kingpin, *bra* = brady, *dcc* = dococ, *hob* = hobblobin, *sli* = slipjig, *ddl* = daredevil, *mbz* = mobitz, *elk* = elektra, *shk* = shocker.

3.4 The Popeye domain containing (*Popdc*) gene family

The *Popeye domain containing (Popdc)* genes have been isolated on the basis of their muscle-restricted expression pattern by two independent groups (Andree et al., 2000; Reese et al., 1999). In vertebrates (zebrafish, chick, mouse and human) three *Popdc* (*Popdc1-3*) genes have been identified (Andree et al., 2000; Reese et al., 1999). In all vertebrates examined *Popdc1* and *Popdc3* are located in close proximity on the same chromosome (chromosome 16 in zebrafish). In contrast, *Popdc2* is found on a different chromosome (chromosome 9 in zebrafish) and shows higher similarity to *Popdc3* than to *Popdc1*. The fact that in invertebrates one gene (*Drosophila*), and in basal chordates two genes (*Ciona intestinalis*) are found, might indicate that *Popdc* genes are evolved by tandem duplication and might be functionally redundant (Davidson and Levine, 2003). No known copies of *Popdc* genes are detected in either plants or single cell organisms suggesting that *Popdc* genes are limited to multicellular organisms.

3.4.1 Expression pattern

In vertebrates, all three *Popdc* genes are expressed in heart and skeletal muscle, with *Popdc2* being predominantly expressed in the myocardium whereas *Popdc1* and *Popdc3* display a broader tissue distribution (Andree et al., 2000; Breher et al., 2004; Froese and Brand, 2008; Torlopp et al., 2006). Additionally, Birgit

Andree revealed that in mouse and chick hearts one *Popdc* gene was partially expressed in the heart while another gene was expressed in the entire heart (Andree et al., 2000).

In *Popdc1^{-/-}* and *Popdc2^{-/-}* mice strong LacZ labeling was found in the cardiac crescent and maintained in the whole heart until adulthood (Andree et al., 2002; Froese and Brand, 2008). Interestingly, it was further shown that in adult heart tissue of transgenic *Popdc2^{-/-}* mice the cardiac conduction system like the sinoatrial node, the His bundle and the Purkinje fibers was first and strongly labeled (Froese, 2008). Consistently, analysis of *Popdc1^{-/-}* mice reveals elevation of LacZ expression in the ventricular conduction system compared to the ventricular working myocardium (Breher, 2009). Beside the strong heart expression, *Popdc1^{-/-}* and *Popdc2^{-/-}* mice display LacZ expression in the myotome and in the developing limb.

In *Xenopus* embryos the zygotic expression pattern is confined to the heart and appears to coincide with the onset of expression of α -MHC (myosin heavy chain alpha) (Hitz et al., 2002). However, in *Xenopus laevis*, as well as in *Drosophila melanogaster* *Popdc1* is also expressed in early stages of development. In *Xenopus*, maternal transcripts are detected in the blastula stages restricted to the animal pole cells (Ripley et al., 2006). In *Drosophila*, *Popdc1* is expressed in all epithelial follicle cells surrounding the oocyte (Lin et al., 2007).

3.4.2 Protein structure and distribution

The proteins encoded by the *Popdc* gene family lack any homology to other already known protein domains, however one typical signature of all *Popdc* proteins is a 70 amino acid long hydrophobic domain close to the N-terminus which by computer algorithms is predicted to form three consecutive transmembrane helices. In addition to these transmembrane domains, a conserved 150 amino acid long sequence is present in each *Popdc* protein and was termed *Popeye* domain (Pfam domain: pfam04831). Current consensus between the research groups is that the amino terminus is located extracellularly, while the carboxyl terminus is intracellular (Knight et al., 2003). Within the highly conserved *Popeye* domain exists an intracellular interaction domain thereby *Popdc* proteins can homodimerize (Kawaguchi et al., 2008).

Recently, by using secondary structure predictions, striking similarity of the *Popeye* domain with a cyclic nucleotide-binding domain was found (Figure 6) and binding of cAMP and cGMP by *Popdc* proteins was experimentally demonstrated (Breher, 2009, Froese et al., in preparation).

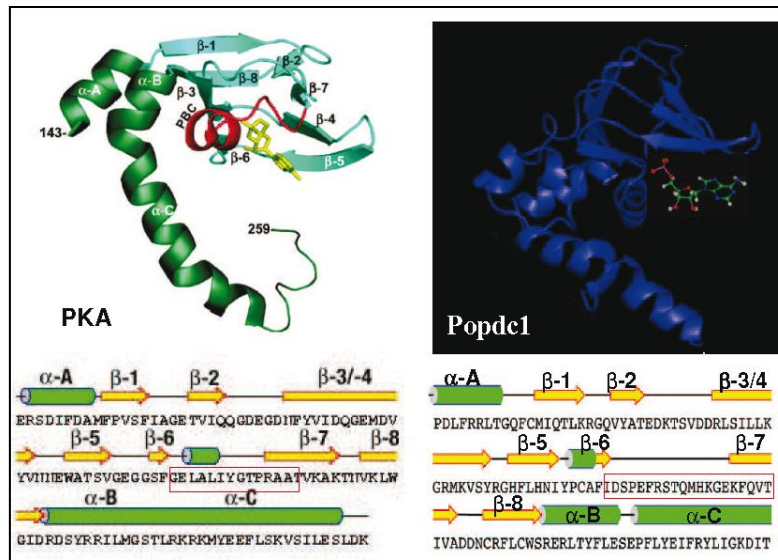


Figure 6: Comparison of secondary structure and tertiary structure predictions of cyclic nucleotide binding domains between PKA and Popdc1 (Breher, 2009).

Both secondary structures reveal similar sequence of α -Helices (green columns) and β - sheets (yellow arrows). The cyclic nucleotide binding domain is caged in red. The tertiary structure between PKA and Popdc1 resemble each other.

During epicardium formation in chick, Popdc1 is found in the cytoplasm of migrating mesenchymal cells and upon epithelialization it accumulates in cell-cell junctions (Reese et al., 1999; Vasavada et al., 2004; Wada et al., 2001). Popdc1 protein in the heart is predominantly localized to the intercalated discs, lateral membranes and the t tubuli. Within the t tubuli it co-localizes with Ca_v1.2, Caveolin3 and Ncx1. Popdc1 protein was increased in the ventricular conduction system compared to the ventricular working myocardium as already seen with the *Popdc1*-LacZ expression pattern (Breher, 2009).

3.4.3 Interaction partners

In epithelial cells, Popdc1 interacts specifically with ZO1 (zona occludens 1), although this interaction is not thought to be direct, and is involved in tight junction formation. Furthermore, Popdc1 disruption leads to mislocalization of junctional proteins (Osler et al., 2005). Also it is known, that Popdc1 co-localizes with Gefit in adult skeletal muscle and regulates Gefit activity, which in turn modulates downstream Rho GTPases involved in cell motility and adhesion (Smith et al., 2008). Recently, it has been demonstrated that Popdc1 regulates the vesicular transport by interacting with Vamp3 (Hager et al., 2010), a SNARE protein that promotes the fusion of membranes during vesicular transport (McMahon et al., 1993) and Popdc1 is identified as a caveolae protein that associates with costameres (Alcalay et al., submitted).

3.4.4 Function

The Bader group propose a role of *Popdc1* in early embryogenesis based on knockout and knockdown experiments in *Drosophila* and *Xenopus laevis* (Lin et al., 2007; Ripley et al., 2006). *Popdc1* reduction by antisense RNA leads to abnormal epithelial movement and failure of pole cell migration in *Drosophila* (Lin et al., 2007) and knockdown of *popdc1* in *Xenopus* causes an arrest in gastrulation (Ripley et al., 2006) suggesting that *Popdc1* plays an important role in rearrangement and movement in epithelial sheets during gastrulation.

However, *Popdc1* and *Popdc2* null mutant mice do not display an embryonic phenotype and demonstrate normal viability during postnatal life.

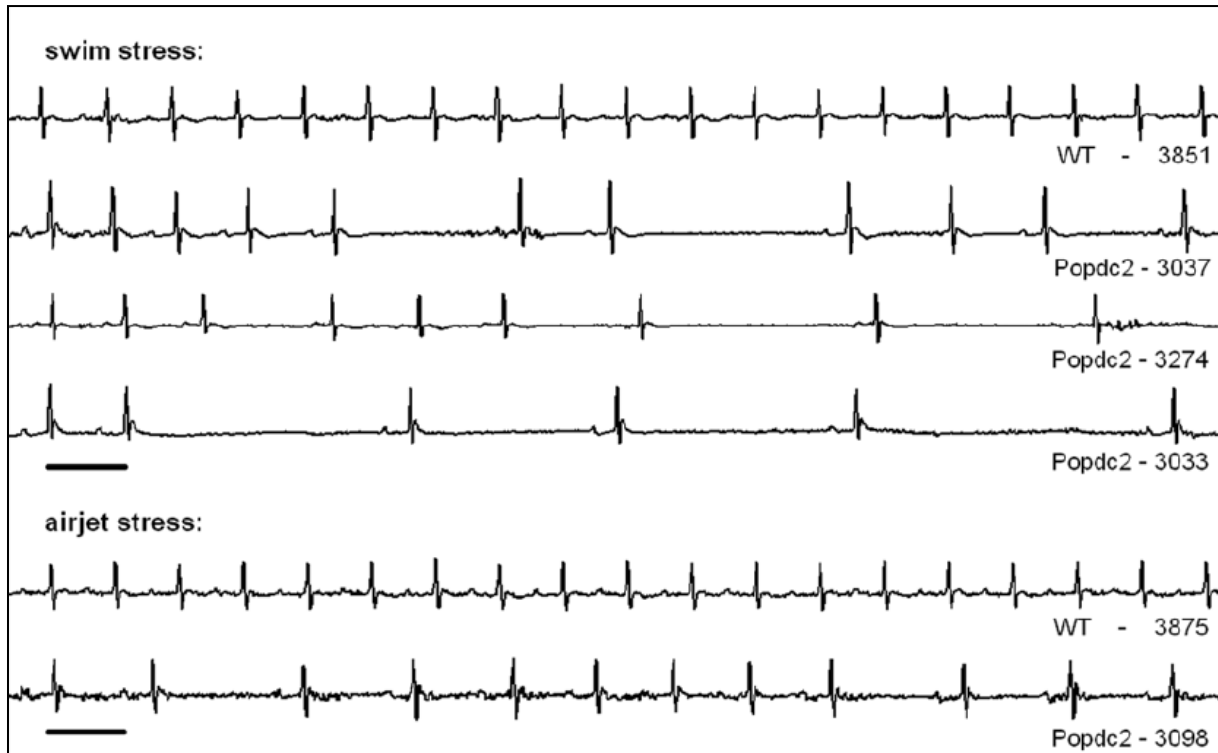


Figure 7: Examples of the ECG curves of wild type and mutant heart in stress situations (Froese, 2008).

ECG curves of wild type (3851, upper trace in swimming and 3875 in airjet stress) and mutant hearts (3037, 3274 and 3033, three lower traces in swimming and 3098, lower trace in airjet stress). Scale bar: 100ms.

Interestingly, both null mutant mice develop an age-dependent and stress-induced sinus bradycardia including periods of asystole (Figure 7) accompanied by degeneration of the sinoatrial node mainly in the inferior region which resembles a common disease in the elderly humans (Froese et al., in preparation, Breher et al., 2009). Furthermore, in *Popdc1* null mutant mice the ability to regenerate skeletal muscle is retarded. Similar is proposed for *Popdc2*^{-/-}, but has to be experimentally proved (Andree et al., 2002).

3.5 Aim of the study

The *Popdc* gene family was discovered one decade ago. The evolutionary conserved expression in striated muscle tissue suggests an essential role in heart and skeletal muscle. Recent studies revealed that *Popdc1* and *Popdc2* null mutant mice display an age-dependent stress-induced dysfunction of the sinus node, which is accompanied by a loss of tissue in the inferior part of the sinus node. One aim of this thesis was to characterize the *Popdc* gene family in zebrafish starting with an expression analysis followed by a functional characterization using a morpholino-based knockdown approach. By knockdown of *popdc2* we tested whether the requirement of *popdc2* for cardiac pacemaking is conserved during evolution. The proteins that are encoded by the *Popdc* gene family lack any homology to other known protein domains. Each of the *Popdc* proteins consists of an extracellular amino terminus, three transmembrane domains and a conserved domain within the intracellular carboxyl terminus termed the *Popeye* domain. Recently, the *Popeye* domain was recognized as a novel cAMP-binding protein. Point mutations within this phosphate binding cassette lead to impaired binding of cyclic AMP *in vitro*. Another aim of this thesis was to express these point mutants in zebrafish to study the role of cyclic nucleotide binding for *Popdc* function *in vivo*.

4 MATERIAL

4.1 Biological material

4.1.1 Bacterial strains

Name	Catalog number	Distributor
<i>E. coli</i> XL 1-Blue	#200249	Stratagene, Amsterdam, Netherlands
<i>E. coli</i> XL 10 Gold	#200314	Stratagene, Amsterdam, Netherlands

4.1.2 Vectors

Name	constructed/provided by
pBluescriptKS	Stratagene, Amsterdam, Netherlands
pGEM T easy	Promega, Mannheim, Germany
psGEM	(Michael Hollmann, 1994)
psGEM Popdc1, 2 & 3	Bettina Kirchmaier
psGEM zf-Popdc2eGFP	Bettina Kirchmaier
psGEM zf-Popdc2 2D-eGFP	Bettina Kirchmaier
psGEM Popdc1 [D200A]myc	Juliane Kuhtz
psGEM Popdc1 [P202A]myc	Juliane Kuhtz
psGEM Popdc1 [E203A]myc	Juliane Kuhtz
psGEM Popdc1 [V217F]myc	Juliane Kuhtz
psGEM Popdc1myc	Juliane Kuhtz
psGEM Popdc2 [D184A]myc	Patrick Meister
psGEM Popdc2 [V201F]myc	Patrick Meister
psGEM Popdc2 myc	Patrick Meister
pZL1-zf-Popdc3 (partial cDNA)	RZPD
pBluescriptKS zf-Popdc2	Kerstin Zander
pGEM T easy zf-bmp4 (partial cDNA)	Bettina Kirchmaier
pCMV Sport 6.1 shox2	RZPD
pGEM T easy zf-Hcn4 chr. 18 (partial cDNA)	Bettina Kirchmaier
pGEM T easy zf-Hcn4 chr. 25 (partial cDNA)	Bettina Kirchmaier
pGEM-T zf-cmlc2 (partial CDS)	(Yelon et al., 1999)
pBluescriptKS myoD	(Weinberg et al., 1996)
pGEM-T zf-vmhc (partial CDS)	(Yelon et al., 1999)

4.1.3 Fish lines

Name	Origin	Reference
TU	Nüsslein-Volhard Lab	
TL	Nüsslein-Volhard Lab	
ALB	Streisinger Lab	
<i>Tg(cmlc2:eGFP)</i>	Fishman Lab	(Huang et al., 2003)
<i>Tg(cmlc2:eGFP-ras)^{s883}</i>	Stainier Lab	(Beis et al., 2005; Chi et al., 2008)
<i>Tg(cmlc2:gCAMP x rasmCherry)</i>	Stainier Lab	
<i>Tg(cmlc2:gCaMP)^{s878} in sih</i>	Stainier Lab	(Arnaout et al., 2007)
<i>Tg(flk1:eGFP)^{s843}</i>	Stainier Lab	(Jin et al., 2005)
<i>Tg(gata1:dsRed)^{sd2}</i>	Zon Lab	(Traver et al., 2003)

4.1.4 Primary and secondary antibodies

Name	Catalog number	Distributor
anti-mouse TRITC	715-025-151	Dianova, Hamburg, Germany
anti-mouse Fab FITC	715-097-003	Dianova, Hamburg, Germany
peroxidase anti-mouse IgG (H + L)	PI-2000	Vector Laboratories, Servion, Switzerland
anti-myc	Clone 9E10, ab32	Abcam, Cambridge, UK
MF20		Developmental Studies Hybridoma Bank, Iowa City, USA
S46		Developmental Studies Hybridoma Bank, Iowa City, USA
Rhodamine phalloidin	R415	Molecular Probes
anti-popdc2	HPA024255/sc-66588	Sigma-Aldrich, Munich, Germany
anti-alpha tubulin		Sigma-Aldrich, Munich, Germany

4.2 Molecularbiological material

4.2.1 DNA and protein ladders

Name	Catalog number	Distributor
O'GeneRuler™ DNA Ladder Mix	#SM1173	Fermentas, St. Leon-Rot, Germany
100 bp DNA Ladder	T834.1	Roth, Karlsruhe, Germany
MagicMark™ XP Western Protein	LC5602	Invitrogen, Darmstadt, Germany

4.2.2 Kits

Name	Catalog number	Distributor
ABI Prism BigDye™ Terminator Cycle Sequencing Ready Reaction Kit		Applied Biosystems, Darmstadt, Germany
Amersham ECL™ Advance Western Blotting Detection Kit	RPN2135	GE Healthcare, Munich, Germany
mMESSAGE mMACHINE® T7 Kit (25 rxns)	AM1344	Applied Biosystems, Darmstadt, Germany
NucleoSpin® RNA Clean-up	740948.10	Macherey-Nagel, Düren, Germany
NucleoSpin® RNA Clean-up XS	740903.10	Macherey-Nagel, Düren, Germany
QIAEX II Gel Extraction Kit (150)	20021	Qiagen, Hilden, Germany
QIAGEN Plasmid Midi Kit (25)	12143	Qiagen, Hilden, Germany
QIAprep Spin Miniprep Kit (50)	27106	Qiagen, Hilden, Germany
QIAquick Nucleotide Removal Kit (50)	28304	Qiagen, Hilden, Germany

4.3 Software

Software	Source
Adobe Acrobat Pro Version 9.3.2.	Adobe Systems GmbH, Munich, Germany
Adobe Photoshop CS2	Adobe Systems GmbH, Munich, Germany
AxioVision Rel.4.7	Zeiss, Göttingen, Germany
ClustalW	European Bioinformatics Institute, Cambridge, UK
Endnote	Thomson Reuters, San Francisco, USA
Leica LCS Lite	Leica, Wetzlar, Germany
Matlab	The Mathworks, Inc., Natic, USA
Microsoft Office 2007	Microsoft, Unterschleißheim, Germany
Microsoft Word 2007	Microsoft, Unterschleißheim, Germany
Primer3 (http://frodo.wi.mit.edu/primer3/)	SourceForge.Net
Vector NTI	Invitrogen, Darmstadt, Germany
Video Savant	IO Industries Ontario, Canada
ZEN 2009 Light Edition	Zeiss, Göttingen, Germany

4.4 Equipment

Name	Distributor
Agarose electrophoresis system	PeqLab Biotechnologies, Erlangen, Germany
Binocular microscope MZFL III	Leica, Wetzlar, Germany
Breeding tanks	Tecniplast, Hohenpeißenberg, Germany
Bunsen burner	Hartenstein, Würzburg, Germany
Clean razor blades/scalpels	Bruno Bayha, Tuttlingen, Germany
Camera DFC320	Leica, Wetzlar, Germany
Camera AxioCam MRc5 or AxioCam Mrm	Zeiss, Göttingen, Germany
CLSM Leica TCS-SP2 AOBS	Leica, Wetzlar, Germany
CLSM Zeiss LSM 710	Zeiss, Göttingen, Germany
Cover slips	Menzel, Braunschweig, Germany
Cryostat Frigocut 2800	Reichert Jung, Wetzlar, Germany
Culture tubes	Hartenstein, Würzburg, Germany
Embedding moulds	Polysciences, Warrington, USA
Falcon tubes	Sarstedt, Nümbrecht, Germany
Heat block	Hartenstein, Würzburg, Germany
High speed video camera Basler A504k	Basler Ahrensburg, Germany
Incubator	Memmert, Schwabach, Germany
Magnet stirrer IKAMAG RCT	IKA Werke, Staufen, Germany
Microcentrifuge (Mikro200)	Hettich, Tuttlingen, Germany
Microinjection needles	BioMedical Instruments, Zollnitz, Germany
Microinjector IM 300	Narishige, London, UK
Micromanipulator	World Precision Instruments
Microscope Axiovert 25	Zeiss, Göttingen, Germany
Microscope Axiovert 200M	Zeiss, Göttingen, Germany
Microscope slides	Menzel, Braunschweig, Germany
Microtome for plastic sectioning	Leitz, Wetzlar, Germany
Microwave oven Privileg	Quelle, Fürth, Germany
Pellet pestle	Hartenstein, Würzburg, Germany
Petri dishes	Sarstedt, Nümbrecht, Germany
pH meter pH 523	WTW, Weilheim, Germany
Pipettes	Eppendorf, Hamburg, Germany
Plastic tanks	Aqua Schwarz, Göttingen, Germany
Shaker	Bühler, Düsseldorf, Germany
Stirring water bath	Braun, Berlin, Germany
Tape	Tesa, Hamburg, Germany
Thermocycler (Primus-25 or Primus-96)	PeqLab Biotechnologies, Erlangen, Germany
Ultramicrotome Microm HM500	Zeiss, Göttingen, Germany
Vortex apparatus L46 GLW	Hartenstein, Würzburg, Germany
Watchmaker forceps	Hartenstein, Würzburg, Germany

4.5 Reagents

If not otherwise stated standard reagents used in this thesis were supplied by the companies AppliChem, (Darmstadt, Germany); Gibco (Darmstadt, Germany); Merck (Darmstadt, Germany); Roth (Karlsruhe, Germany) and Sigma-Aldrich (Munich, Germany). Reagents and suppliers considered of specific interest to this thesis are listed below.

Name	Distributor
2,3 BDM (Butanedione monoxime)	Fluka, Munich, Germany
2-Dodecenylsuccinic acid anhydride	Serva, Heidelberg, Germany
Acetone	Applichem, Darmstadt, Germany
Agar Agar	Roth, Karlsruhe, Germany
Agarose NEEO	Roth, Karlsruhe, Germany
Ammonium acetate	Applichem, Darmstadt, Germany
Ampicillin sodium salt	Applichem, Darmstadt, Germany
Bacto agar	Becton, Dickinson and Company
Bacto tryptone	Becton, Dickinson and Company
Bacto yeast extract	Becton, Dickinson and Company
BCIP (5-Bromo-4-chloro-3-indolyl-phosphate)	Boehringer, Mannheim, Germany
BigDye (Hidi)	Applied Biosystems, Darmstadt, Germany
Boric acid	Applichem, Darmstadt, Germany
Calcium sulfate dyhydrate p.A.	Applichem, Darmstadt, Germany
DAB (Diaminobenzidine)	Sigma-Aldrich, Munich, Germany
DAPI (4', 6-Diamidino-2-phenylindol)	Roche, Mannheim, Germany
Dextranblue	Fluka, Munich, Germany
Dinatriumcarbonat (di-sodium carbonate?)	Applichem, Darmstadt, Germany
Di-potassium hydrogen phosphate anhydrous	Merck, Darmstadt, Germany
Di-sodium hydrogen phosphate dihydrate	Applichem, Darmstadt, Germany
Di-Sodium tetraborate decahydrate	Roth, Karlsruhe, Germany
DMSO (Dimethyl sulfoxide)	Applichem, Darmstadt, Germany
EDTA (ethylenediaminetetraacetic acid)	Applichem, Darmstadt, Germany
Entellan	Sigma-Aldrich, Munich, Germany
Epon 812 (Glycidether)	Serva, Heidelberg, Germany
Ethanol, p.A.	Applichem, Darmstadt, Germany
Ethidium bromide solution 1%	Applichem, Darmstadt, Germany
FCS (Fetal Calf Serum)	PAA, Cölbe, Germany
Formamide	Merck, Darmstadt, Germany
Glucose	Roth, Karlsruhe, Germany
Glutaraldehyde	Merck, Darmstadt, Germany
Glycerol anhydrous	Applichem, Darmstadt, Germany
Glycine, p.A.	Roth, Karlsruhe, Germany
Haematoxylin	Sigma-Aldrich, Munich, Germany
Heparin sodium salt	Sigma-Aldrich, Munich, Germany
HEPES	Applichem, Darmstadt, Germany
Hydrogen peroxide, 30 %	Applichem, Darmstadt, Germany
IPTG	Roth, Karlsruhe, Germany
Isopropanol, p.A.	Applichem, Darmstadt, Germany
JB-4	Polysciences, Warrington, USA
Sea Plaque agarose	Cambrex, Wokingham, UK
Magnesium chloride hexahydrate p.A.	Merck, Darmstadt, Germany
Magnesium sulfate heptahydrate p.A.	Roth, Karlsruhe, Germany
Methanol	Applichem, Darmstadt, Germany

Name	Distributor
Methyl cellulose	Sigma-Aldrich, Munich, Germany
Methylene blue	Merck, Darmstadt, Germany
Methylnadic anhydride	Serva, Heidelberg, Germany
Mowiol 4-88	Merck, Darmstadt, Germany
NBT (4-nitroblue tetrazolium chloride)	Boehringer, Mannheim, Germany
N-Phenylthiourea, Grade II, approx. 90%	Sigma-Aldrich, Munich, Germany
Nuclear Fast Red	Vector Laboratories, Servion, Switzerland
Osmium tetroxide microscopy grade	Roth, Karlsruhe, Germany
Paraformaldehyde	Applichem, Darmstadt, Germany
Phenol red	Sigma-Aldrich, Munich, Germany
Polyfreeze Tissue Freezing Medium	Polysciences, Warrington, USA
Potassium chloride	Applichem, Darmstadt, Germany
propylenoxid	Fluka, Munich, Germany
SDS (sodium dodecylsulfat)	Roth, Karlsruhe, Germany
Red sea sea salt	Aqua Schwarz, Göttingen, Germany
Sodium bicarbonate	Applichem, Darmstadt, Germany
Sodium chloride	Applichem, Darmstadt, Germany
β-Mercaptoethanol	Fluka, Munich, Germany
Sucrose	Applichem, Darmstadt, Germany
Tricaine (3-aminobenzoic acid ethyl ester)	Sigma-Aldrich, Munich, Germany
Tris	Roth, Karlsruhe, Germany
Tris-borate	Applichem, Darmstadt, Germany
Triton x-100	Roth, Karlsruhe, Germany
Trizol	Invitrogen, Darmstadt, Germany
Tween-20	Applichem, Darmstadt, Germany
Uranylacetat	Electrical microscope sciences
X-Gal	Roth, Karlsruhe, Germany
Xylene	Applichem, Darmstadt, Germany
Yeast tRNA	Roche, Mannheim, Germany

4.6 Enzymes

Name	Distributor
AMV reverse Transcriptase	Promega, Mannheim, Germany
Phusion Polymerase F-530S or F-530L	Finnzymes, Frankfurt am Main, Germany
Pronase	Roche, Mannheim, Germany
Protease	Sigma-Aldrich, Munich, Germany
Proteinase K	Roth, Karlsruhe, Germany
Restriction endonucleases	Neb, Frankfurt am Main, Germany
RNasin	Promega, Mannheim, Germany
RQ1 DNase	Promega, Mannheim, Germany
SP6 RNA Polymerase	Promega, Mannheim, Germany
T3 RNA Polymerase	Promega, Mannheim, Germany
T4 Ligase	Promega, Mannheim, Germany
T7 RNA Polymerase	Promega, Mannheim, Germany
Takara Taq Polymerase	TaKaRa, Saint-Germain-en-Laye, France

4.7 Primers

Primer	Sequence
Primer for RT-PCR	
Zf- β -Actin-fw	5'-ctt gcg gta tcc ac gaga c-3'
Zf- β -Actin-rev	5' gcg cca tac aga gca gaa-3'
Zf-popdc2-fw	5'-gac ggg gaa cag aag cac aga ca-3'
Zf-popdc2-rev	5'-acc gcc cat ata gcc cag aaa aa-3'
Zf-popdc3-fw	5'-ggc gtg gcg gag gaa gaa-3'
Zf-popdc3-rev	5'-gcc cgg ccc gtt aca gaa-3'
Primer for RT-PCR (Morpholino Analysis)	
MO-popdc2-fw3	5'-ctg ctg atg ctg cag tgt tt-3'
MO-popdc2-rev3	5'-ggc acg tcc tct ttg gta tc-3'
Zfpopdc2intron1fw	5'-tgc agc tga aat ctg aat gg-3'
Zfpopdc2intron1rev	5'-ggt taa agc agg cc acct ga-3'
Zfpopdc3-144bp-fw	5'-ccc gaa gga tcg gta ttt ca-3'
Zfpopdc3-870bp-rev	5'-agc tcg gta acc gga gat ca-3'
Primer for cloning of <i>in situ</i> probes	
Zf_Hcn4-chr25-2578bp-rev	5'-ctg gtg gtt gtg gtc ctc tt-3'
Zf-Hcn4-chr25-1758bp-fw	5'-aca ttt ggt ggc tcc tca tc-3'
Zf_Hcn4-chr18-1746bp-fw	5'-tcc cca tca aag ctt cat tc-3'
Zf_Hcn4-chr18-2555bp-rev	5'-cta cag ggt ttg ggc gtt ag-3'
Anf-fw	5'-aca cgt tga gca gac aca gc-3'
Anf-rev	5'-tgt taa caa att aag ccg tat tgt-3'
Amhc-fw	5'-agc cac tac cgc ctc tct acg g-3'
Amhc-rev	5'-ggt gga att gga cg acct tgc c-3'
Primer for cloning of GFP-fusion constructs	
EcoRI-2dgfp-start-fw	5'-nnn nnn gaa ttc atg gtg agc aag ggc ga-3'
XhoI-2dgfp-stop-rev	5'-nnn nnn ctc gag cta cac att gat cct agc aga agc ac-3'
BamHI-zfpopdc2-282bp-fw	5'-nn nnn gga tcc gac agc aga ggc tca aac atg-3'
EcoRI-zfpopdc2-1409bp-rev	5'-nnn nnn gaa ttc ctt caa ata ttc cct ctc atg ccc-3'
BamHI-zfpopdc2-275bp-fw	5'-nnn nnn gga tcc aat tgg aga cag cag agg ct-3'
BamHI-zfpopdc2-1409bp-rev	5'-nnn nnn gga tccc ctt caa ata ttc cct ctc atg cc-3'
Primer for cloning of full-length CDS in psGEM	
XbaI-mpopdc1-111-fw	5'-nnn nnn tct aga gac gcg caa gga ctt ttc-3'
HindIII-mpopdc1-1384-rev	5'-nnn nnn aag ctt agg ctt ggc taa cac aag ga-3'
Mpop3not1-fw	5'-nnn ngc ggc cgc atg gga aag cga agg act ct-3'
Mpop3xhoI-rev	5'-nnn ctc gag ggc aat ggc atc ttg att ct-3'
Mpop2-not1-fw	5'-nnn ngc ggc cgc agg ctt tca agc ttc cat ga-3'
Mpop2-EcoRV-rev	5'-nnn gat atc gtc ctg caa ccc ata aag ga-3'

4.8 Morpholinos

Morpholino	Sequence
Zf-popdc2-1donor	5'-ggt caa ttg ttt ctc acc tgc cag a-3'
Zf-popdc2-1acc	5'-cta atc ctg tga aag cag aag atc c-3'
Popdc3-ex2-acc	5'-cac tcg tat cct gtt tta gtg ata a-3'
Gene tools standard control	5'-cct cct acc tca gtt aca att tat a-3'

5 METHODS

5.1 Fish care

5.1.1 Setting up pair crosses

Method:

Mating crosses were best set up in the afternoon using the same conditions under which the fish are otherwise maintained. The mating containers were checked for successful matings the next day before noon. Eggs were collected and transferred into a Petri dish in E3 Medium.

Reagents:

Embryo media E3 (for standard work with embryos)

(5 mM NaCl, 0.17 mM KCl, 0.33 mM CaCl₂, 0.33 mM MgSO₄)

E3 can be made up as a 60x stock.

Danieaus:

(58 mM NaCl, 0.7 mM KCl, 0.4 mM MgSO₄, 0.6 mM Ca (NO₃)₂, 5.0 mM HEPES pH 7.1-7.3).

Methylcellulose:

3% Methylcellulose was made in either water or E3 medium. It was dissolved by mixing over several hours.

MESAB (also called Tricaine or MS322):

4 mg/ml ethyl-m-aminobenzoate methanesulphonate was solved in E3. The stock solution should be reffridgerated. For the working solution MESAB was diluted 1:20 to 1:100.

Artemia nauplia:

To 14 l of tap water 100 ml sea salt were added and aerated vigorously. 65 ml of shrimp eggs were added keeping the temperature at 28 °C. After 24 hours most of the *Artemia* should be hatched.

5.1.2 PTU treatment to prevent melanization of embryos

Method:

The embryos were placed in E3 medium containing PTU at a final concentration of 0.2 mM no later than 24 hpf to prevent melanization.

Reagent:

100x PTU (= 20 mM) (1-Phenyl-2-thiourea M = 152.2 g/mol)

3.04 g were added in 1 l double distilled water and were heated to 65 °C to reach full solvation grade. The stock solution was stored at room temperature. The working concentration was obtained by 1:100 dilution.

5.2 Genexpression manipulation in *Danio rerio*

5.2.1 Agarose plates for holding embryos

Method:

- Liquefied 1.5 % agarose in E3 was poured into a plastic Petri dish to a depth of about 5 mm. A plastic mould was floated carefully into the agarose to avoid trapping air bubbles below the mould.
- When the agarose was completely solidified, the mould was lifted using coarse forceps.

5.2.2 Microinjections

Method:

- 1-to 4-cell embryos were transferred to a microinjection plate which was covered with E3-Medium.
- A clean microinjection needle was loaded with 2-4 µl of injection solution using a pipette with a gel-loader tip. Phenol Red was used as a non-toxic injection tracer when added at 0.05%.
- The injection pressure and injection time were adjusted and the Morpholino or *in vitro* transcribed mRNA was injected into the yolk.
- Once all embryos in the plate were injected, the eggs were transferred to a sterile Petri dish filled with prewarmed E3 medium.
- Dead and unfertilized embryos were removed 4-5 hours later.

Reagents:

Phenol Red 0.5 % (Sigma)

5.2.3 Morpholinos

Method:

- Lyophilized morpholinos were dissolved in ddH₂O to give a final concentration of 1 mM and were diluted with 1 x Danieau injection buffer plus 0.05% Phenol Red.
- The morpholinos were injected as described above. Stock and working solutions were stored at -20 °C.

5.2.4 Chemical treatment with cyclopamine

At shield stage, about 6 hpf, zebrafish embryos in their chorions were treated with 50 µM cyclopamine dissolved in embryo medium and 1 % ethanol. Control embryos were only treated with 1 % ethanol in embryo medium.

5.3 Physiological methods/Imaging methods

5.3.1 Recording of cardiac activity

Method:

The imaging system consisted of an inverted microscope (Zeiss Axiovert 25) equipped with a digital high speed video camera (Basler A504k, Basler Ahrensburg, Germany), which in turn was connected to a personal computer. As camera configuration tools VLL Toolbox and CCT+software (Basler Ahrensburg, Germany) were used and the recording of sequences of single digital pictures was managed by Video Savant 4.0 (IO Industries Ontario, Canada).

- MO1-*popdc2* morphants and MO-*control* morphants were recorded between 5 dpf and 7 dpf.
- For measurements the embryos were anesthetized with 0.1 g l⁻¹ tricaine, embedded in 2.5 % LMP Agarose/0.1g l⁻¹ tricaine and transferred to the incubation chamber (temperature 28.0 °C).
- Video images were recorded from the heart (20000 images, 50 frames per second, fps) and analyzed.

5.3.2 Isolated calcium transient recordings by selective plane illumination microscopy (SPIM)

Method:

Pretreatment and embedding procedure:

The zebrafish embryos were embedded in 1.5% low melting agarose in E3 in plastic syringes. It was necessary that the contraction of the heart was uncoupled to record the cardiac conduction wave. Therefore *sih* mutant embryos younger than 4 dpf were used and were anesthetized by adding 10 µl Tricaine to 1 ml of LMW agarose. For recordings of older embryos, they were transferred to a 40 mM BDM-solution in E3 for 1-2 minutes and then embedded in 1.5% low melting agarose in E3 with a 20 mM BDM concentration. The embryos in their imaging chamber were also incubated with 20 mM BDM in E3.

Imaging:

Videos of the calcium transient were recorded with SPIM. The attenuated 488 nm laser line was focused to a 6 µm thick light sheet. The sample was oriented such that a thin slice of atrium, AV canal, and ventricle was illuminated.

Analysis:

For each sample, 3000 pictures with a framerate of 54.4 frames per second were recorded. The obtained video sequences were analyzed with Matlab (The Mathworks, Natick, MA). Six areas within the video sequence were selected and fluorescence intensity in these areas was plotted over time in a semilogarithmic way.

5.4 Microbiological methods

5.4.1 Ligation

Calculation

A 1:1 or 1:3 molar ratio of vector : insert DNA were used when cloning a fragment into a plasmid vector. The amount of insert DNA was calculated with the help of the following formula:

$$\frac{\text{ng of vector} \times \text{kb size of insert} \times \text{molar ratio of insert/vector}}{\text{kb size of vector}} = \text{ng of insert}$$

Ligation reaction

In a typical ligation reaction 100-200 ng of vector DNA were used. The following reaction was assembled in a sterile microcentrifuge tube: 100 ng vector DNA, calculated ng insert DNA, 1 μ l ligase 10x buffer, 1 μ l T4 ligase and nuclease-free water were added to a final volume of 10 μ l. The ligation reaction was mixed and was incubated at room temperature for 3 hours or at 4 °C overnight.

Reagents:

T4 DNA ligase (# 217017, Promega)

5.4.2 Transformation

Method:

- The competent cells (XL1-Blue) were thawed on ice and 5 μ l of the ligation reaction was added.
- The reaction was mixed by gently flicking against the microcentrifuge tube and was incubated on ice for about 15 to 30 minutes.
- The competent cells were heat shocked at 42 °C for 50-60 seconds without shaking the microcentrifuge tube. The tube was rapidly transferred to an ice bath and the competent cells were allowed to chill for 1 minute.
- 200 μ l prewarmed SOC medium was added to each microcentrifuge tube and the solution was incubated at 37 °C and 220 rpm for 1 hour to allow the bacteria to recover and to express the antibiotic resistance marker encoded by the plasmid.
- An appropriate volume of transformed competent cells were plated onto LB agar plates containing the appropriate antibiotic and the plates were inverted and were incubated overnight at 37 °C. The transformed colonies should appear in 12-16 hours.

Reagents:

SOC-medium (100 ml):

2.0 g bacto-tryptone, 0.5 g bacto-yeast extract, 1 ml 1 M NaCl, 0.25 ml 1 M KCl, 1 ml 2 M Mg²⁺ stock (filter-sterilized), 1 ml 2 M glucose (filter-sterilized).

Bacto-tryptone, bacto-yeast extract, NaCl and KCl were added to 97 ml distilled water. The solution was stirred to dissolve and was autoclaved. After it was cooled to room temperature 2 M Mg²⁺ stock and 2 M glucose were added each giving a final concentration of 20 mM. The medium was filled up to 100 ml with sterile distilled water. The pH should be 7.0.

LB-agar/LB-plates:

10 g bacto-tryptone, 5 g bacto-yeast extract, 5 g NaCl and 15 g bacto-agar were weighed and filled up to 1 liter with distilled water. The pH was adjusted to 7.4 with NaOH and HCl. The LB-agar was autoclaved and was cooled to about 50 °C before adding the appropriate antibiotic. 30-35 ml of medium was poured into petri dishes. The hardened plates were stored at 4 °C up to one month.

LB-medium (Luria-Bertani Medium) (1 l) :

10 g tryptone, 5 g yeast extract and 10 g NaCl were weighed and filled up with distilled water to 1 liter. The pH was adjusted to 7.4 with NaOH and HCl. The LB-medium was autoclaved and stored either by room temperature or at 4 °C.

Table 2: Commonly used antibiotic solutions adapted by Sambrook and Russel (Molecular Cloning: A Laboratory Manual (Third Edition))

	Stock solution		Working concentration	
	Concentration	Storage	Stringent plasmids	Relaxed plasmids
Ampicillin	50 mg/ml in H ₂ O	-20 °C	20 µg/ml	50 µg/ml
Carbenicillin	50 mg/ml in H ₂ O	-20 °C	20 µg/ml	60 µg/ml
Chloramphenicol	34 mg/ml in ethanol	-20 °C	25 µg/ml	170 µg/ml
Kanamycin	10 mg/ml in H ₂ O	-20 °C	10 µg/ml	50 µg/ml
Streptomycin	10 mg/ml in H ₂ O	-20 °C	10 µg/ml	50 µg/ml
Tetracyclin	5 mg/ml in ethanol	-20 °C	10 µg/ml	50 µg/ml

5.4.3 Cloning into plasmid vectors

5.4.3.1 Directional cloning

- -Restriction sites within the vector which do not cut the desired insert were chosen.
- Primers containing the insert sequence and sequence of the chosen restriction site were designed.
- The insert was amplified with these primers.
- The circular plasmid vector and the PCR-product (the desired insert) were digested with the chosen enzymes.
- The PCR-product and the plasmid vector were purified by using isopropanol precipitation.
- A certain amount of insert was ligated into the target vector.
- An appropriate strain of E.coli was transformed.
- The resulting transformed colonies were screened by digestion with restriction enzymes.

5.4.3.2 Cloning PCR products into T vectors (e.g. pGEM-T and pGEM-T easy vector systems, Promega)

For cloning PCR products into T vectors, the pGEM-T Easy Vector system from Promega was used by following the manufacturer's instructions. The obtained bacterial colonies were screened using X-Gal and IPTG for blue-white selection.

5.4.4 Screening bacterial colonies using X-Gal and IPTG

Method:

- Direct application of X-Gal and IPTG to agar plates
100 µl of 100 mM IPTG and 50 µl of 2 % X-Gal solution were pipetted onto the center of a premade agar plate containing the appropriate antibiotic. A sterile spreader was used to spread the solution over the entire surface of the plate. The plate was incubated at 37 °C until all of the fluid had disappeared.
- Identifying colonies carrying recombinant plasmids
Colonies carrying wild type plasmids were pale blue or dense blue whereas colonies carrying recombinant plasmids were white. The plates were viewed against a white background and the recombinant white colored colonies were picked with a fresh pipette tip.

5.4.5 Glycerol stocks

Bacteria growing on plates, or in liquid culture, can be stored at – 80 °C in aliquots of LB medium containing 30 % (v/v) sterile glycerol. Aliquots were prepared of 1 ml of LB with glycerol and were vortexed to ensure that the glycerol is completely dispersed.

5.5 Molecularbiological methods

5.5.1 Preabsorption of antibody for whole mount *in situ* hybridization

Method:

- Different stages of zebrafish embryos were collected and were fixed overnight at 4 °C in 4 % PFA/PBS.
- The embryos were washed 4 times for 5 minutes each time in PBT and were stored in 100 % Methanol at -20 °C. The embryos should not be dechorionated.
- The embryos were rehydrated by rinsing 3 times for 5 minutes in PBT and were transferred to a 2 ml Eppendorf tube.
- The embryos were homogenized using a pestle and were adjusted to 1 ml PBT.
- 10 µl of antibody were added and the antibody solution was shaken at least overnight at 4 °C.
- The probe was centrifuged and was filtered to remove the homogenized embryos.
- Before use the probe was filled up with blocking buffer to a final 1:2000 antibody dilution and was stored at 4 °C.

5.5.2 Whole mount RNA *in situ* probe generation

Method:

All steps were carried out at room temperature, unless stated otherwise.

- Plasmid linearization
1-5 µg of plasmid-DNA was digested for 3 hours or overnight at 37 °C with 1 µl restriction enzyme, 3 µl 10x restriction buffer, 3 µl 10x BSA and ddH₂O (final volume 30 µl). Removal of the buffer was obtained by the qiagen nucleotide removal kit by following the manufacturer's instructions (Qiagen). The pure linearized plasmid DNA was dissolved in 14.5 µl ddH₂O.
- In vitro transcription
6 µl 5x transcription buffer, 3 µl 100 mM DTT, 1 µl 40 u/µl RNAsin, 3 µl 10x RNA labeling mix and 2,5 µl T7, T3 or SP6 Polymerase were added to the linearized plasmid and the probe was incubated for 2 hours at 37 °C. After the incubation the DNA was removed by adding 3 µl DNase for 15 minutes at 37 °C.
- RNA retrieval and purification
For RNA retrieval and purification the Rneasy Cleanup Kit was used following the manufacturer's instructions (Macherey Nagel). The pure *in situ* probe was stored at -80 °C. 1 µl of the probe was used to measure the concentration of the synthesized probe. Before usage the probe was dissolved in hybridization solution and was stored at -20 °C.

Reagents and Kits:

10x digoxigenin RNA labeling Kit (Roche)
 5x transcription buffer (Promega)
 100 mM DTT (Promega)
 T3/T7/SP6-Polymerases (Promega)
 RNAsin (Promega)
 Qiagen Nucleotide Removal Kit (Qiagen)
 Rneasy Cleanup Kit (Macherey Nagel)
 Restriction endonucleases (NEB)

Table 3: Generation of *in situ* probes

Gene	Plasmid	Digestion	Polymerase	Resistance
Zf-popdc2	pKS Bluescript	BamHI	T3 polymerase	Ampicillin
Zf-popdc3	pZIPLOX	Sal I	SP6 polymerase	Ampicillin
Zf-vmhc	pGEM-T	Not I	T7 polymerase	Ampicillin
Zf-cmlc2	pGEM-T	Not I	T7 polymerase	Ampicillin
Zf-myod	PCRII	BamHI	T7 polymerase	Ampicillin
Zf-Hcn4 Chr. 18	pGEM-T easy	Nde I	T7 polymerase	Ampicillin
Zf-Hcn4 Chr. 25	pGEM-T easy	Spe I	T7 polymerase	Ampicillin
Zf-shox2	pCMV-Sport6.1	EcoRV	T7 polymerase	Ampicillin
Zf-bmp4	pGEM T easy	Spe I	T7 polymerase	Ampicillin

5.5.3 Whole mount *in situ* hybridization using a single digoxigenin-labeled probe

Method:

All steps were carried out at room temperature, unless stated otherwise.

- Fixation and storage

The embryos were fixed with 4 % paraformaldehyde in PBS overnight at 4 °C. The embryos were washed twice in PBS, 5 minutes each and were incubated three times with 100% methanol for 5 minutes each. The methanol was replaced with fresh 100 % methanol and the embryos were stored at – 20 °C.

- Rehydration

The embryos were rehydrated by soaking in 75 % methanol/PBS, 50 % methanol/PBS 25 % methanol/PBS and 100 % PBS for 5 minutes each.

- Proteinase K digestion and postfixation

The embryos were digested with proteinase K (10 µg/ml in PBST) depending on their stage of development. After proteinase K treatment the embryos were rinsed at least 5 times with PBT to dilute the proteinase K

and were washed twice with PBT. The embryos were fixed for 20 minutes with 4% paraformaldehyde in PBT and were washed with PBT at least 5 times as described above.

- Prehybridization

The embryos were prehybridized at 70 °C with hybridization solution between 1-4 hours.

- Hybridization

The embryos were incubated at 70 °C overnight with hybridization solution plus labeled probe (The hybridization temperature depends on the required stringency).

- Posthybridization washes

The embryos were washed once at 70 °C in 75% Hyb/25% 2x SSC, 50% Hyb/50% 2x SSC, 25% Hyb/75% 2x SSC, 100 % 2x SSC at least 10 minutes each step and were then washed twice at 70 °C 0.2 x SSC for 30 minutes. All solutions should be pre-warmed, in order to ensure that the required temperatures are reached quickly during the washing procedure. After that the embryos were rinsed in 75% 0.2x SSC/25% PBT, 50% 0.2x SSC/50% PBT, 25% 0.2x SSC/75% PBT, 100 % PBT for 5 minutes each step.

- Blocking and antibody incubation

The embryos were blocked for at least 1 hour at room temperature (better overnight at 4 °C). They were incubated with anti-digoxigenin Fab-alkaline phosphatase at a 2000-fold dilution in blocking solution and were rocked gently for 2 hours at room temperature or overnight at 4 °C.

- Wash steps and detection

The embryos were rinsed several times with PBT plus 2 mg/ml BSA and were incubated overnight at 4 °C in this solution. The next day the embryos were washed 4 times (25 min each) with PBT plus 2 mg/ml BSA and were equilibrated 3 times (5 min each) in staining buffer. The staining buffer was mixed with 4.5 µl NBT and 3.5 µl BCIP per ml and the embryos were incubated in this staining solution. The embryos were stained for 30 minutes to overnight in the dark, until staining intensity increased no further or until background staining started to develop. The staining procedure was stopped by washing extensively in PBST.

- Clearing and storage

The samples were incubated twice with 0.1 M glycine/0,1 % Tween-20 5 minutes each. The embryos were rinsed in PBT and were cleared twice in 100 % ethanol for 5 minutes. Afterwards they were washed twice with PBT. At this point, embryos could be stored in the dark, preferably in 4 % paraformaldehyde in PBST at 4 °C.

Reagents:

Staining buffer:

100 mM Tris pH 9.5, 50 mM MgCl₂, 100 mM NaCl, 0.1 % Tween-20

4 % Paraformaldehyde/PBS:

4 g of paraformaldehyde (PFA) were mixed with 100 ml PBS and heated at 68 °C until it was dissolved. A few drops of NaOH were added to adjust the pH at 7.4. The solution was stored at – 20 °C.

NBT (4-nitroblue tetrazolium chloride):

75 mg/ml in 70 % dimethylformamide

BCIP (5-bromo-4-chloro-3-indolyl-phosphate):

50 mg/ml in dimethylformamide

10x Dig-labelling Kit (Roche)

20x SSC:

For 1 liter 175.3 g NaCl and 88.2 g sodiumcitrate were solved. The pH should be around 7.0.

0.1 M glycine pH 2.2 (M = 238.31 g/mol)

10x PBS Stock solution (1.37 M NaCl, 85 mM Na₂HPO₄ x 2 H₂O, 27 mM KCl, 15 mM KH₂PO₄)

80.1 g NaCl, 2.01 g Na₂HPO₄, 15.13 g KCl, 2.04 g KH₂PO₄ were dissolved in 800 ml dH₂O and the pH was adjusted with HCl to 7.4. Then the stock solution was filled to 1000 ml and autoclaved. The stock solution was stored at room temperature.

1 x PBS:

The working solution was produced by 1:10 dilution of the 10x PBS stock solution in ddH₂O.

PBT:

PBS plus 0.1 % Tween-20

Hybridization solution:

(50 % formamide, 5 x SSC, 5 mg/ml torula (yeast) RNA, 50 µl/ml heparin, 0.1 % Tween-20). Should be kept at -20 °C

Blocking solution:

(5 % sheep serum, 2 mg/ml BSA in PBT)

5.5.4 RNA isolation using Trizol

Method:

All steps were carried out at room temperature, unless stated otherwise.

- Homogenization

The living zebrafish embryos at the desired stage were collected and transferred into a 1.5 µl microcentrifuge tube. Remaining liquid was withdrawn and the embryos were either frozen and stored at – 80 °C or were directly weighed. Per 50-100 mg zebrafish embryo 1 ml Trizol was used for homogenization of the tissue. For tissue of less than 10 mg of tissue only 0.8 ml Trizol was needed. After the correct amount of Trizol was added, the embryos were homogenized with a syringe.

- Phase separation

The homogenized embryos were incubated for 5 minutes. Afterwards 0.2 ml chloroform per ml Trizol was added and the microcentrifuge tube was shaken vigorously for about 15 seconds. The probe was incubated again for 2-3 minutes and was centrifuged at 11200 rpm for 15 minutes at 4 °C. After the centrifugation step the colorless aqueous phase was transferred to a fresh microcentrifuge tube.

- RNA precipitation

0.5 ml isopropanol per ml Trizol were added and after vortexing the probe was incubated for 10 minutes. To precipitate the RNA, the probe was centrifuged at 11200 rpm for 10 minutes at 4 °C. The supernatant was removed and 1 ml 75 % ethanol/H₂O_{DEPC} per 1 ml Trizol was used to wash the RNA pellet. Therefore the probe was vortexed and was centrifuged at 9000 rpm for 15 minutes at 4 °C. The liquid was withdrawn and the RNA was dried for about 10 minutes. The dry RNA was dissolved in 40 µl H₂O_{DEPC}.

- DNA removal

The dissolved RNA was mixed with 10 µl 5x transcription buffer, 2 µl RQ1 DNase and 1 µl RNasin and the solution was incubated for 1 hour at 37 °C.

- RNA precipitation

1 volume of phenol/chloroform was added and the mixture was vortexed and centrifuged for 2 minutes at full speed. The upper aqueous phase was transferred to a fresh microcentrifuge tube and 10 µl 2 M sodium acetate pH 4.5 and 150 µl ice cold ethanol were added. After vortexing, the solution was incubated for at least one hour or overnight at -80 °C. The probe was vortexed and was centrifuged at 9000 rpm for 15 minutes at 4 °C. The liquid was withdrawn and the RNA was dried for about 10 minutes. The dry RNA was dissolved in 40 µl H₂O_{DEPC}, 1 µl of the probe was used to measure the RNA concentration and the rest was stored at – 80 °C.

Reagents:

2 M NaOAc pH 4.5

5.5.5 *In vitro* transcription

5.5.6 *In vitro* synthesis of capped RNA

Method:

All steps were carried out at room temperature, unless stated otherwise.

- Plasmid generation
For capped RNA synthesis psGEM plasmids containing full-length cDNA were generated.
- Linearization
The plasmids were linearized by enzymatic digestion with NheI and the T7 RNA polymerase promoter site were used for *in vitro* transcription. The enzymatic digestion was purified with the help of the qiagen nucleotide removal kit by following the manufacturer's instructions (Qiagen). The pure linearized plasmid DNA was dissolved in RNase-free water and the template concentration was adjusted to a concentration of 0.5 µg/µl.
- *In vitro* transcription
For *in vitro* transcription T7 mMESSAGE mMACHINE kit from Ambion was used by following the manufacturer's protocol. Approximately 20-30 µg RNA were obtained by each reaction.
- RNA purification
The capped RNA was purified with the RNA XS Cleanup Kit from Macherey-Nagel and was dissolved in 20 µl of RNase-free water. The RNA yield was determined by reading the $A_{260\text{nm}}$ of a 1:100 diluted aliquot. Additionally one aliquot was controlled by gel electrophoresis. The capped RNA was stored at -80 °C.

5.5.7 Preparation of plasmid DNA by alkaline lysis with SDS (Minipreparations 1-2 ml)

For preparation of Plasmid DNA the Qiagen Mini prep kit following the manufacturer's instructions (Qiagen) was used or the protocol below.

(This protocol, contributed by D. Ish-Horowicz is a modification of the method of (Birboim and Doly, 1979).

Method:

All steps were carried out at room temperature, unless stated otherwise.

- 3-5 ml of LB-medium containing the appropriate antibiotic was inoculated with a single colony of transformed bacteria. The culture was incubated overnight at 37 °C and 220 rpm.

- A 1.5 – 2 ml of the culture was poured into a microfuge tube and was centrifuged for 2 minutes at 4000 rpm. When centrifugation was complete, the medium was removed and the bacterial pellet was left as dry as possible. This step was repeated twice.
- The bacterial pellet was resuspended in 100 µl ice-cold GET plus RNase solution by vortexing.
- 200 µl of 0.2 N NaOH + 1 % SDS was added to the bacterial suspension. The content was mixed by inverting the tube rapidly 3-5 times. Do not vortex.
- 150 µl of an ice-cold alkaline lysis solution III was added. The tube was inverted several times and was stored on ice for 3-5 minutes.
- The probe was centrifuged at least for 8 minutes with full speed. The supernatant was transferred to a fresh tube.
- Two volumes of isopropanol were added to the probe and were mixed by vortexing.
- The sample was centrifuged for 8 minutes at maximum speed.
- The supernatant was removed and 1 ml of 70 % ethanol was added. The probe was vortexed briefly and was then recentrifuged.
- All supernatant was removed and the pellet was dried until the ethanol had evaporated and no fluid was visible in the tube (5-10 minutes).
- The nucleic acids were dissolved in 50 µl TE-buffer or ddH₂O and the DNA solution was stored at -20 °C.

Reagents:

LB-Medium (per liter):

10 g bacto-tryptone, 5 g bacto-yeast extract and 5 g NaCl were weighed and filled up to 1 liter with distilled water. The pH was adjusted to 7.4 with NaOH and HCl. The LB-medium was autoclaved and was stored at 4 °C.

GET + RNase solution (Alkaline Solution I):

(50 mM glucose, 10 mM EDTA, 25 ml TrisHCl (pH 8.0)). The stock solution was stored at room temperature. For the working solution RNase (final concentration 10 µg/ml) was added and it was stored at 4 °C.

Alkaline solution II:

(0.2 N NaOH, 1 % SDS). The solution was stored at room temperature.

Alkaline solution III:

To 60 ml of 5 M potassium acetate 11.5 ml of glacial acetic acid and 28.5 ml of H₂O were added. The resulting solution is 3 M with respect to potassium and 5 M with respect to acetate.

10 x TE-buffer (pH 8.0):

(100 mM Tris-HCl (pH 7.4), 10 mM EDTA (pH 8.0)). Sterilize solutions by autoclaving for 20 min and store the buffer at room temperature.

5.5.8 Restriction analysis

1 μ l of enzyme was added to 1 μ g of purified DNA in a final volume of 50 μ l of the appropriate 1x buffer followed by incubation for 3 hours or overnight at the recommended temperature. To keep glycerol concentration at less than 5% in a reaction, the restriction enzyme, which is supplied in 50% glycerol, should not exceed 10% of the total reaction volume.

5.5.9 Primer design

Primers were designed with the help of the software primer 3 (<http://frodo.wi.mit.edu/primer3/>) and ordered from Thermo Hybaid.

5.5.10 Endpoint PCR using Phusion™ DNA polymerase

Method:

For a 50 μ l reaction 10 μ l 5 x Phusion HF buffer, 1 μ l 10 mM dNTPs (final concentration 200 μ M each), x μ l forward Primer, x μ l reverse Primer, 1.5 μ l DMSO (final concentration 3 %) and about 50-250 ng of template DNA were mixed and ddH₂O was added to a final volume of 50 μ l.

The PCR was performed like shown in the table below. The optimal primer annealing temperature was calculated according to the nearest-neighbor method using the offered calculator provided on Finnzymes website (www.finnzymes.com).

Table 4: Cycling instructions using Phusion™ DNA polymerase

Cycle step	Temperature	Time	Cycles
Initial denaturation	98 °C	30 s	1
Denaturation	98 °C	10 s	25-40
Annealing	Depending on primer pair	30 s	
Extension	72 °C	30s/1 kb	
Final extension	72 °C	10 min	1
	4 °C	hold	

5.5.11 Endpoint PCR using Taq polymerase

Method:

For a PCR-reaction 2.5 µl 10x PCR buffer, 2 µl dNTP-Mix (2.5 mM each) 0.5 µl template (about 250 ng), 2 µl forward and 2 µl reverse primer with a stock concentration of 10 pM and 0.2 µl Taq-Polymerase were mixed and ddH₂O was added to a final volume of 25 µl.

The PCR was performed like shown in the table below. The optimal primer annealing temperature was calculated according to Primer3, an open source computer program.

Table 5: Cycling instructions using Taq Polymerase

Cycle step	Temperature	Time	Cycles
Initial denaturation	94 °C	5 min	1
Denaturation	94 °C	30 s	25-40
Annealing	Depending on primer pair	30 s	
Extension	72 °C	1 min/1 kb	
Final extension	72 °C	10 min	1
	4 °C	hold	

5.5.12 DEPC-treated water

Method:

0.1 ml DEPC was added to 100 ml of double distilled water and was shaken vigorously to bring the DEPC into solution. The solution was incubated for at least 12 hours at 37 °C and was autoclaved to reduce any trace of DEPC.

5.6 Immunological methods

5.6.1 Phalloidin staining

Note: Methanol can disrupt actin during fixation process. Therefore it is best to avoid any methanol containing fixatives. The preferred fixative is methanol-free formaldehyde.

Method:

All steps were carried out at room temperature, unless stated otherwise.

- Fixation

The embryos were fixed overnight with 4 % PFA/PBS at 4 °C or at 2-3 hours at room temperature. Then they were equilibrated at least for 30 minutes in 0.2% TritonX-100 in PBS or PBDT.

- Staining

The embryos were incubated for 15 minutes with rhodamine-phalloidin 1:150 diluted in 0.2% TritonX-100 in PBS or PBDT. Finally they were washed 3 times for 5 minutes each step with 0.2% TritonX-100 in PBS or PBDT.

5.6.2 Whole mount antibody staining with DAB

Method:

All steps were carried out at room temperature, unless stated otherwise.

- Blocking and primary antibody incubation

The embryos were blocked with 10 % FCS in PBDT for at least 1 ½ hours on a rocking platform at 4 °C. After the blocking step they were incubated with the primary antibody in 5 % FCS/PBDT overnight at 4 °C.

- Washing steps and secondary antibody incubation

The embryos were washed 4 times for 30 minutes with 1.5 % FCS in PBDT. After the washing steps the embryos were incubated with the secondary antibody coupled with horseradish peroxidase (1:200 dilution) either overnight at 4 °C or for at least 3 hours at room temperature. The embryos were rinsed again 4 times with 1.5 % FCS in PBDT each step took 30 minutes.

- Equilibration and DAB staining

The embryos were equilibrated two times for 5 minutes with 50 mM Tris-HCl pH 7.6. Later they were incubated in DAB solution in the dark. Then 2 µl of 0.3 % H₂O₂ to 1 ml DAB-solution was added. The colour reaction was stopped by adding PBS several times.

Reagents:

Diaminobenzidine (DAB):

DAB was prepared by dissolving the contents of one DAB tablet (10 mg) in 15 ml 50 mM Tris pH 7.6 and filtering with a disposable unit attached to a disposable syringe.

50 mM Tris pH 7.6

5.6.3 Whole mount immunocytochemistry (double staining MF20/S46)

Method:

All steps were carried out at room temperature, unless stated otherwise.

- Fixation and storage

The embryos were fixed overnight with Dent's Fixative. The next day they were bleached overnight with Dent's bleach. The embryos were stored in 100 % methanol.

- Rehydration

The embryos were rehydrated in 75% methanol/25 % PBT, 50% methanol/50 % PBT, 25% methanol/75 % PBT for 20 minutes in each solution. Then they were rinsed 2-3 times for 2 minutes in PBBDT.

- Blocking and antibody staining

The embryos were blocked with 10 % FCS in PBBDT for at least 1 ½ hours on a rocking platform at 4 °C. After the blocking step they were incubated with MF20 antibody (1:100 dilution) in 5 % FCS/PBBDT overnight at 4 °C. The next day the embryos were washed 4 times for 30 minutes each with 1.5 % FCS in PBBDT. After the washing steps the embryos were incubated with a secondary antibody (Fab-Fitc anti-mouse 1:50 dilution) either overnight at 4 °C or for at least 3 hours at room temperature. The embryos were rinsed again 4 times with 1.5 % FCS in PBBDT each step last 30 minutes. The embryos were incubated with S46 antibody (1:100) in 5 % FCS/PBBDT overnight at 4 °C. The next day the washing steps were repeated like already described above. Finally the embryos were incubated with the secondary antibody TRITC anti-mouse for at least 3 hours at room temperature or overnight at 4°C. The embryos were washed once in PBSBT and were then analyzed.

Reagents:

Dent's Fixative:

80 % methanol, 20 % DMSO

Dent's Bleach:

20 % DMSO in methanol, 10 % H₂O₂

PBDT:

1x PBS plus 0.1 % Tween-20 plus 1 % DMSO

PBSBT:

1x PBS plus 0.1 % Tween-20 plus 0,3 % BSA

5.7 Histological methods

5.7.1 Embedding using Epon 812

Method:

- Fixation:
Embryos were transferred into the fixative I at room temperature for several hours. Then they were fixed at 4 °C for 18 hours in the same solution. The embryos were washed for 30 min at 4 °C with 0.066 M phosphate buffer and then contrasted for 2 hours with solution II.
- Washing steps:
The embryos were washed 3 times each for 5 minutes with ddH₂O, and incubated overnight with 0.5 % uranyl acetate (in H₂O) and then washed 3 times each for 5 min with ddH₂O.
- Dehydration:
The embryos were dehydrated for 5 min each step in 50 %, 70 %, 90 %, 96 % ethanol and again washed for 10 min in 100 % ethanol and then transferred into 100 % propylenoxide.
- Embedding:
The embryos were incubated for 4 hours into 50 % propylenoxide/50 % Epon 812 and then transferred overnight into pure Epon 812. The embedded embryos were hardened by 60 °C for two days.

Reagents:

Fixative I:

6.25 % glutaraldehyde buffered with 0.066 M phosphate buffer; (pH 7.4).

Solution II:

2 % OsO₄ in 50mM cacodylate buffer (pH 7.2).

0.2 M Cacodylat stock solution

48.2 g cacodylat were dissolved in 1 liter distilled water. The solution was stored at 4 °C.

Epon 812:

(12 g Epon 812, 24.7 g Dodecyl succinic anhydride)

The components were weighed into a 50 ml plastic beaker and covered with parafilm and were stirred on a magnetic stirrer for about 15 minutes. 0.5 ml DMP-30 was added. The stirring was continued for another 15 minutes.

5.7.2 Embedding and sectioning using JB-4 resin

Method:

- Fixation

The embryos were fixed with 4 % paraformaldehyde in PBS overnight at 4 °C and were washed twice in PBS.

- Dehydration

The embryos were dehydrated with 50 %, 70 %, 80 %, 90 % and 100 % ethanol (1 hour to 4 hours depending on size).

- Infiltration

The fishes were transferred to 25 % ethanol/75 % JB-4, 50 % ethanol/50 % JB-4, and 10 % ethanol/ 90 % JB-4 (1 hour each step). At last they were incubated overnight in 100 % JB-4. 100 % JB-4 solution was changed at least three times.

- Embedding

1.5 ml infiltration solution and 60 µl Solution B (Accelerator) were mixed and embedding procedure was started immediately. The embryos were transferred into the embedding mould and were oriented while the solution started to harden (about 30 minutes).

- Sectioning

2-10 µm sections were cut using a glass or tungsten knife on a rotary microtome and were transferred into a water bath. The sections were collected on a polylysine-coated glass microscope slides and were dried on a hot plate at 70 °C. Sections were counterstained with Fast Red or haematoxylin and eosin.

Reagents:

20 ml infiltration solution:

(20 ml JB-4 solution A (monomer A), 0,25 g benzoyl peroxide, plasticized (catalyst))

0.25 g of the Catalyst was added to Monomer A and was dissolved for 10-20 min. The infiltration solution can be stored for up to 2 weeks in the fridge at 4 °C (keep it dark).

5.7.3 Cryosections

Method:

- Fixation
Embryos were fixed with 4 % paraformaldehyde in PBS overnight at 4 °C and were washed twice in PBS, 5 minutes each step.
- Infiltration
The embryos were incubated at 4 °C in 10 % sucrose/PBS and 20 % sucrose/PBS each step for at least for 4 hours (embryos should sink to the bottom). The embryos were infiltrated at 4 °C overnight in 30 % sucrose/PBS.
- Embedding
The embryos were rinsed in 50 % OCT/50 % PBS for 10 min. This step was repeated with 100 % OCT. The embedding mould was filled with OCT and the embryos were placed into the mould. The embedding mould was placed on dry ice and the embryos were oriented until the mould was frozen.
- Sectioning
The frozen sample was placed in the cryostat and was frozen onto the holder with some additional fresh OCT. 10-14 µm sections were cut and collected on Superfrost microscope slides. The slides were air dried for several hours or were stored at – 80 °C. Sections were counterstained with different histological stains.

5.8 Proteinbiochemical methods

5.8.1 Western Blot

Method:

To one zebrafish embryo 25 µl lysis-buffer + 2x SDS sample buffer were added. The samples were heated at 95 °C for 5 min and then frozen in liquid nitrogen or processed directly for Western blotting. One embryo per lane was separated on 12 % SDS-gel, and semi-dry blotted onto PVDF-membrane. The membrane was stained with Ponceau S solution and blocked in 5 % nonfat dry milk in 1x TBT (0.5 % Tween in TBS). The PVDF membrane was incubated over night at 4°C with primary antibody in blocking buffer, washed 30 min with 4 changes of TBT. Identical antibody incubation step and washing steps were done for the secondary horseradish peroxidase conjugated antibody. Proteins were detected using a chemiluminescence protein detection method.

Reagents:

Lysis buffer:

0.05 M Tris (pH 7), 8 M urea, 1 % SDS, 1 % β-mercaptoethanol.

TBS:

8 g of NaCl, 0.2 g of KCl and 3 g of Tris base were dissolved in 800 ml H₂O. Then the pH was adjusted to 7.4 with HCl and the solution was filled with H₂O to 1 liter.

2 x SDS buffer:

125 mM Tris (pH 6.8); 4 % (w/v) SDS, 20 % glycerol, one spatle tip of bromo phenolblue.

Despite the different amino acid sequence of Popdc1, Popdc2, and Popdc3, the overall domain prediction revealed a high degree of similarity: the amino terminus of the protein harbored at least one N-glycosylation motif and the *Popeye* domain was present. Additionally, two invariant sequence motifs (DSPE and FQVT), which belong to a presumptive phosphate-binding cassette within the *Popeye* domain, were found. However, only two transmembrane domains instead of three were predicted for the *popdc* genes in zebrafish (Figure 8).

6.2 *Popdc2* is important for heart and skeletal muscle development in zebrafish

6.2.1 *Popdc2* is predominantly expressed in heart and skeletal muscle

To examine the role of *popdc2* in zebrafish development, I started with expression analyses using RT-PCR and whole mount *in situ* hybridization. In the adult zebrafish, *popdc2* expression was mainly detectable in the heart and weaker in muscle tissue, the brain and the ovary. Interestingly, the RT-PCR transcript, which was found in the ovary tissue, was about 100 bp smaller than predicted (Figure 9A). *Popdc2* expression in the embryo was first observed by whole mount *in situ* hybridization in the medial part of the somites with the start of somitogenesis (Figure 10A, A'), whereas expression at 18-somite stage was close to the limit of detection via RT-PCR (Figure 9B). As revealed by RT-PCR, the expression level reached its maximum at 24 hpf and decreased at 48 hpf and 72 hpf.

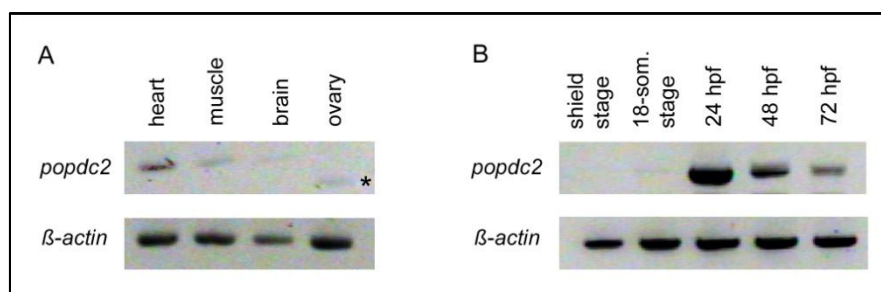


Figure 9: Expression analysis of *popdc2* in the adult and embryonic zebrafish.

RT-PCR was performed using total RNA isolated from (A) selected adult tissues or (B) embryos. In the adult zebrafish the strongest expression was observed in the heart whereas in muscle, brain and in ovary only weak expression was detected. Note that the expressed transcript in the ovary is lower (asterisk). During zebrafish embryogenesis, *popdc2* expression started at the somite stage and increased after tubular heart formation (24 hpf). Abbreviations: hpf = hours post fertilization.

To analyze the expression pattern of *popdc2* during somitogenesis, I compared the expression of *popdc2* in the early embryo with that of *myod*, a transcription factor, which is found in all muscle precursor cells (Figure 10B, B'). In comparison to *popdc2*, *myod* had a broader expression pattern. It is known that *myod* is expressed in the adaxial slow muscle precursor cells and in the dermomyotome. It seemed that at least at 16-somite stage *popdc2* was only expressed in the adaxial slow muscle precursor cells (Figure 10A, A'). To verify this finding, I inhibited the Hedgehog signaling pathway with cyclopamine, a plant-derived alkaloid that binds to Smoothened, the receptor protein of Hedgehog and which was added to the embryos after the shield stage. It is further known that

Hedgehog signaling is required for the commitment of slow muscle precursors. Slow and fast muscle precursors become committed to their respective fates during a 5h period between shield and early somite stages (Hirsinger et al., 2004). At the shield stage, only the slow muscle precursor cells are Hedgehog sensitive. Thus, after administration of cyclopamine, only these cells should be absent, whereas the fast muscle precursors were expected to be largely unaffected. After the cyclopamine treatment, the embryos were fixed and *popdc2* as well as *myod* expression as internal control were analyzed by whole mount *in situ* hybridization. As expected, cyclopamine treated embryos did not show any expression of *myod* in the inner part of the somites, only the paraxial somites were stained (Figure 11B) and *popdc2* expression in cyclopamine treated embryos was absent (Figure 11D). No change in the expression pattern was observed in control embryos. Therefore, I conclude that at somite stage only the slow muscle precursor cells express *popdc2*.



Figure 10: *Popdc2* is expressed in slow muscle precursors.

Shown are whole mount *in situ* hybridization results for (A, A') *popdc2* and (B, B') the skeletal muscle-specific marker *myod* at 16-somite stage in zebrafish. *Popdc2* expression was only present in adaxial slow muscle precursor cells (A, A') in comparison to *myod* which was detected in adaxial slow muscle precursor cells and in the paraxial somites. Abbreviations: wt = wild type, 16-som. = 16-somite stage.

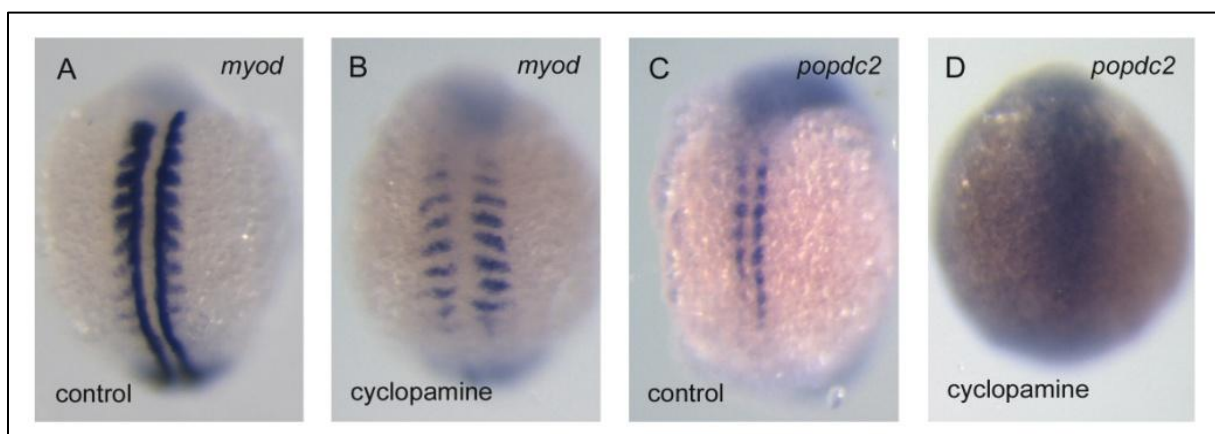


Figure 11: Inhibition of Hedgehog signaling pathway by cyclopamine results in a loss of *popdc2* expression in adaxial cells.

Embryos were treated after shield stage with 50 μ M cyclopamine to interfere with Hedgehog signaling while (A, C) control embryos were only exposed to 1 % ethanol. Embryos were fixed at 10-12-somite stage and subjected to whole mount *in situ* hybridization with (A, B) *myod* and (C, D) *popdc2* probes, respectively. Cyclopamine treated embryos displayed a loss of adaxial cells (slow muscle precursors) which are present in the medial part of the somites. This resulted in a loss of the medial expression domain of *myod*, whereas in the paraxial expression domain the somites harboring fast muscle precursor cells remained intact. On the other hand *popdc2* expression was completely lost in cyclopamine treated embryos.

To characterize the expression pattern of *popdc2* in detail, I further used whole mount *in situ* hybridization and *in situ* sections. I chose developmental stages throughout the period of heart formation in the zebrafish, i.e. 24 hpf (linear heart tube formation), 48 hpf (chamber formation), and 72 hpf (chamber maturation). As described before, the first expression was observed at somite stage in the slow muscle precursor (adaxial) cells. However, at this time in the bilateral heart field no *popdc2* expression was detected (Figure 10A). *Popdc2* expression in the heart started only after fusion of the bilateral heart field with the cardiac cone (Figure 12C) and expression was maintained in the linear heart tube at 24 hpf (Figure 12F, G). Additionally, at 24 hpf *popdc2* was strongly expressed in the myotomes (Figure 12A, D, E) and transversal sections through the tail revealed that slow and fast muscles were stained (Figure 12H).

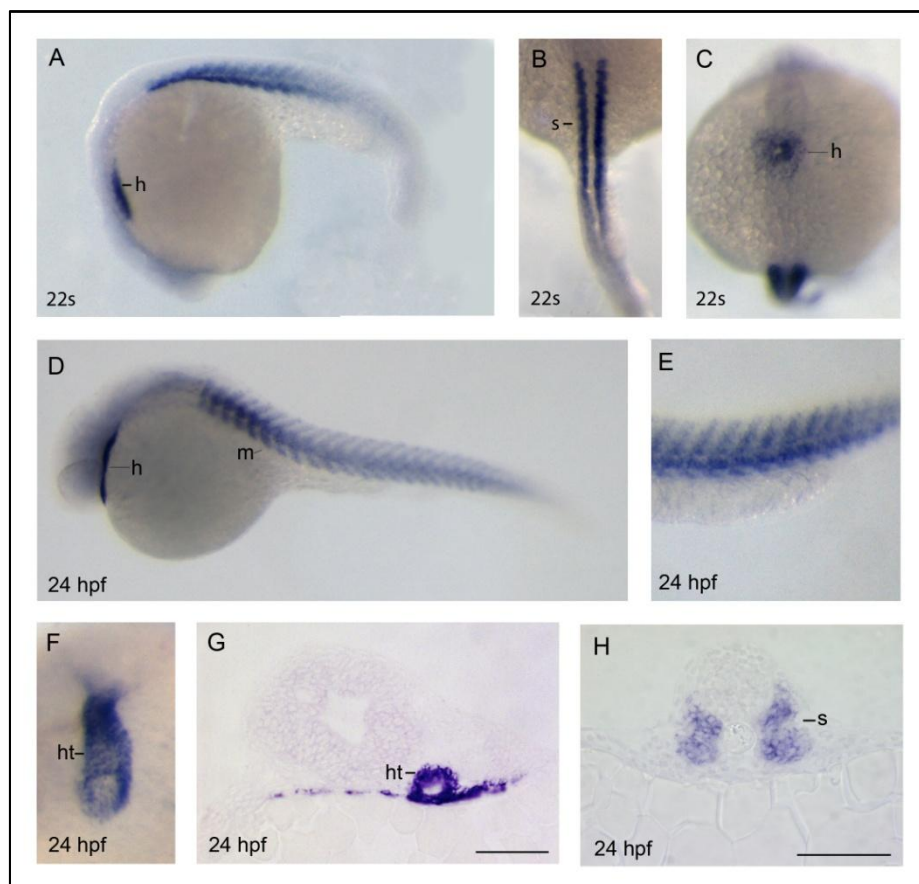


Figure 12: During somitogenesis *popdc2* is strongly expressed in heart and striated muscle.
Expression analysis of *popdc2* in zebrafish embryos at 22 hpf and 24 hpf by whole mount *in situ* hybridization. (A, D, E) Lateral, (B) dorsal, and (C, F) ventral view. The hybridized embryos were subsequently sectioned (G, H). Abbreviations: h = heart; hpf = hours post fertilization; ht = heart tube; m = muscle, s = somite. Scale bar = 100 μ m.

Popdc2 was expressed in both, the ventricle and atrium, at 48 hpf (Figure 13C-F) and 72 hpf (Figure 13G-J). In contrast to the heart, where high levels of expression were maintained, expression in the somites and in the forming tail musculature was reduced at 72 hpf (Figure 13B). Interestingly, at 72 hpf expression of *popdc2* in the facial muscles was observed (Figure 13G, H, J). To further analyze whether *popdc2* expression displays chamber-specific differences between ventricle and atrium, the hybridized embryos were sectioned. The myocardial staining of *popdc2* appeared to be identical in the ventricle and in the atrium.

Taken together, during embryogenesis *popdc2* is a strong, striated muscle-specific marker, which is expressed in differentiating cardiac and skeletal muscle. The expression begins at the somite-stage and is maintained at least during the first three days of development.

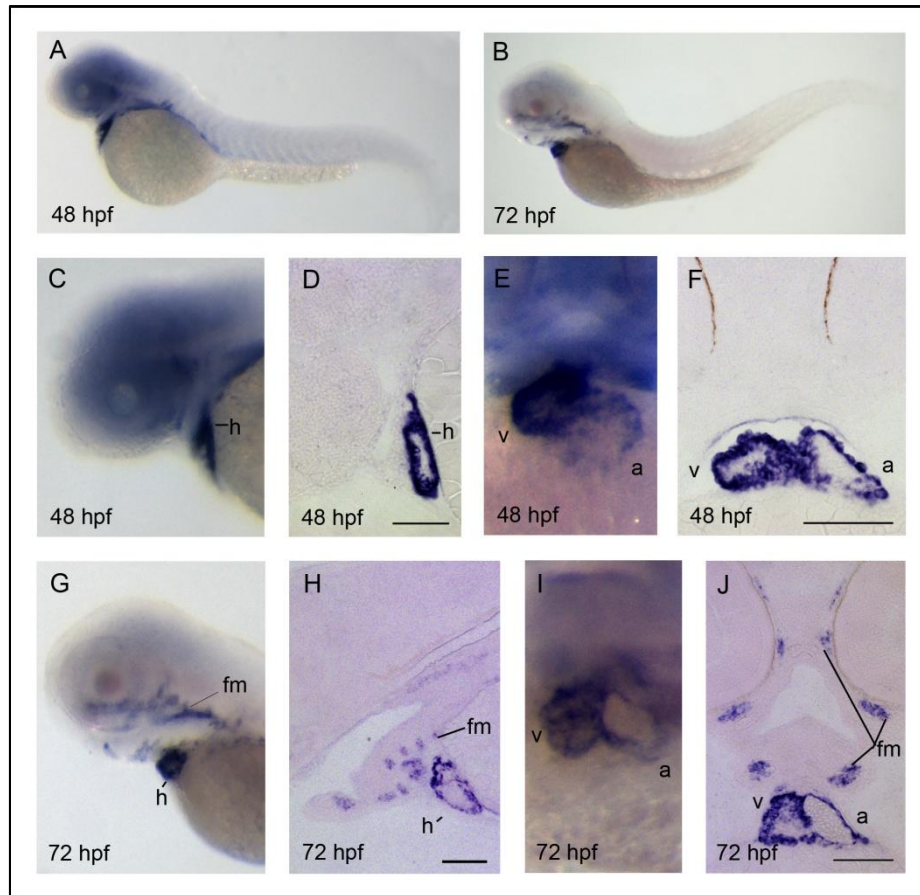


Figure 13: *Popdc2* is preferentially expressed in the developing heart and facial musculature during hatching period in zebrafish.

(A-J) Zebrafish embryos were subjected to whole mount *in situ* hybridization using a *popdc2* probe and (D, F, H, J) subsequently transversally sectioned. *Popdc2* was strongly expressed in the myocardium (A-J) of both heart chambers, and was further expressed in the facial musculature at 72 hpf (G, H, J). Abbreviations: a = atrium; fm = facial musculature; h = heart; hpf = hours post fertilization; v = ventricle. Scale bar = 100 μ m.

6.2.2 Knockdown of *popdc2* leads to impaired musculature

The strong expression of *popdc2* during cardiac and skeletal muscle development prompted us to test the function of this gene using a reverse genetic approach in the developing zebrafish embryo. The *popdc2* gene in zebrafish consists of 3 coding and 1 non-coding exon (Figure 14). To perturb *popdc2* function, I used antisense morpholino oligos directed against the splice donor (MO1) and acceptor site of exon 2 (MO2) in the *popdc2* gene (Figure 14A). To test the efficiency of the two injected morpholinos, RT-PCR analysis was employed (Figure 14B, C). RT-PCR from MO1-*popdc2* and MO2-*popdc2* injected embryos displayed a severe reduction of properly spliced *popdc2* transcripts at least until 72 hpf in the case of MO2-*popdc2* injected embryos and 96 hpf in the case of MO1-*popdc2* injected embryos (Figure 14B), as well as an increase of the *popdc2* transcript by an insertion of intron 1 (Figure 14C).

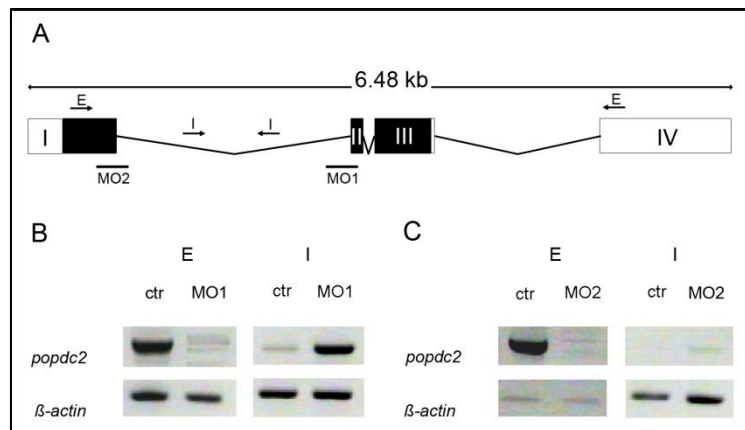


Figure 14: Knockdown strategy of *popdc2* in zebrafish.

A) *Popdc2* consists of 4 exons. Exon 1 to exon 3 are coding, while exon 4 remains untranslated. The morpholino-modified oligonucleotides were directed against the splice donor site of exon1 (MO2) and splice acceptor site of exon2 (MO1). Arrows depict the primers for the RT-PCR analysis. (B) RT-PCR analysis of 4 dpf control-injected and MO1-*popdc2* injected embryos. MO1-*popdc2* morphants displayed a decrease of properly spliced *popdc2* in MO1-*popdc2* morphants, but an increase of intron 1 insertion; β -actin served as control. (C) RT-PCR analysis of 72 hpf control-injected or MO2-*popdc2* injected embryos showed only a faint expression of *popdc2* in MO2-*popdc2* morphants and insertion of intron 1 while the expression of β -actin was similar between the control embryos and the morphants. Abbreviations: ctr = MO-control injected embryos, MO1= embryos injected with a morpholino directed against the splice-acceptor site of Exon 2 in *popdc2*, MO2 = embryos injected with a morpholino directed against the splice-donor site of exon2 in *popdc2*.

Injection of the same amount of MO1-*popdc2* and MO2-*popdc2* morpholino resulted in a similar phenotype with aberrant tail musculature at 24 hpf and slight pericardial edema and blood retention at 48 hpf (Figure 15). However, RT-PCR analysis of the morpholino-injected embryos might indicate that the *popdc2* morpholino MO1 is more effective because of the higher increase of the *popdc2* transcript with intron 1 insertion (Figure 14B, C). The data presented are therefore mostly of MO1-*popdc2* injected embryos.

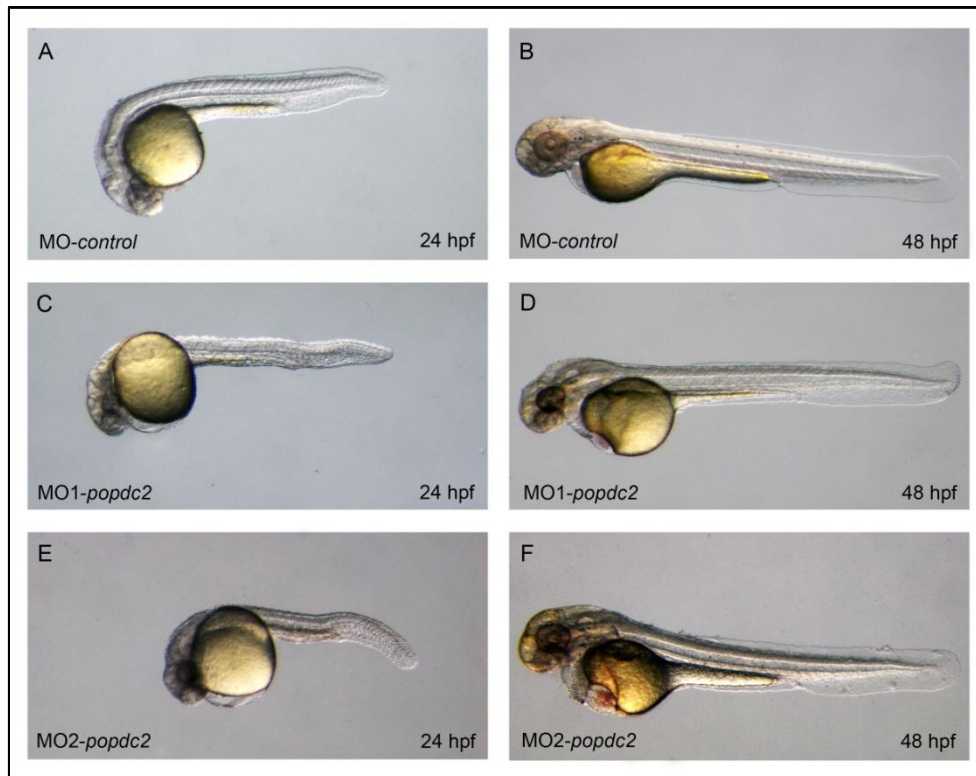


Figure 15: MO1-*popdc2* and MO2-*popdc2* injected embryos displayed abnormal skeletal muscle development

Lateral view of (A, B) control injected embryos and (C-F) *popdc2* morphants at 24 hpf (A, C, E) and 48 hpf (B, D, F). Abbreviations: hpf = hours post fertilization.

Injection of MO1 morpholino of an amount of 0.5 ng to 1.6 ng resulted in a disorganized tail musculature at 24 hpf and a dismorphic heart developing a pericardial edema at 48 hpf (Figure 15C, D). According to their phenotype the morphants monitored at 24 hpf could be subdivided into a sub-population with disorganized tail, categorized as class I (Figure 16B, D), and another with posterior shortening in addition to a disorganized tail, categorized as class II, (Figure 16C, D). Due to the growing pericardial edema, the atrium was stretched and the ventricle collapsed during cardiogenesis. Thus, a detailed analysis of the heart morphology was not possible. I therefore focused on facial and tail musculature.

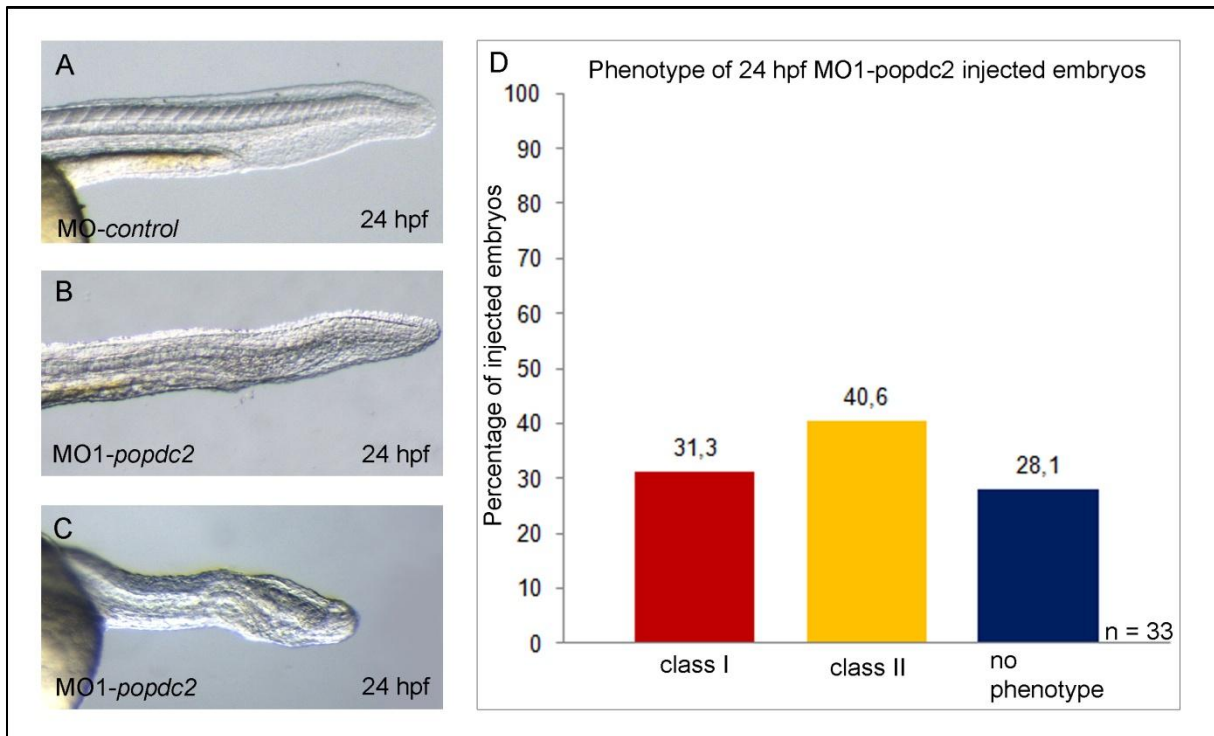


Figure 16: Characterization of the *popdc2* morphant phenotype in the skeletal muscle.

(A-C): Lateral view of the tail of (A) control injected embryo, (B) *popdc2* morphant with aberrant tail musculature (class I) and (C) *popdc2* morphant with posterior shortened and disorganized tail musculature (class II) at 24 hpf. (D) Diagram of MO1-*popdc2* injected embryos. *Popdc2* morphants displayed an aberrant tail musculature at 24 hpf, which can be subdivided into a mild phenotype with aberrant tail musculature (class I) and a severe phenotype with posterior shortened and disorganized tail (class II).

To visualize aberrant craniofacial muscle development in *popdc2* morphants, the MF20 antibody directed against myosin heavy chain, was used. In whole mount stained embryos a reduction of the craniofacial muscle formation was seen in *popdc2* morphants in contrast to the control. In all control morpholino injected embryos extraocular muscles were visible, whereas in the *popdc2* morphants only the inferior rectus, the superior oblique and the superior rectus were identified tentatively (Figure 17B, B'). Furthermore, *popdc2* morphants exhibited rudimentary forms of the pharyngeal muscles adductor mandibulae, adductor opercula, dilator opercula, and levator arcus palatine (Figure 17D, D'). Furthermore, the sternohyoideus, a muscle, which is the teleost equivalent of the amniotes tongue, was shortened (Figure 17D, D').

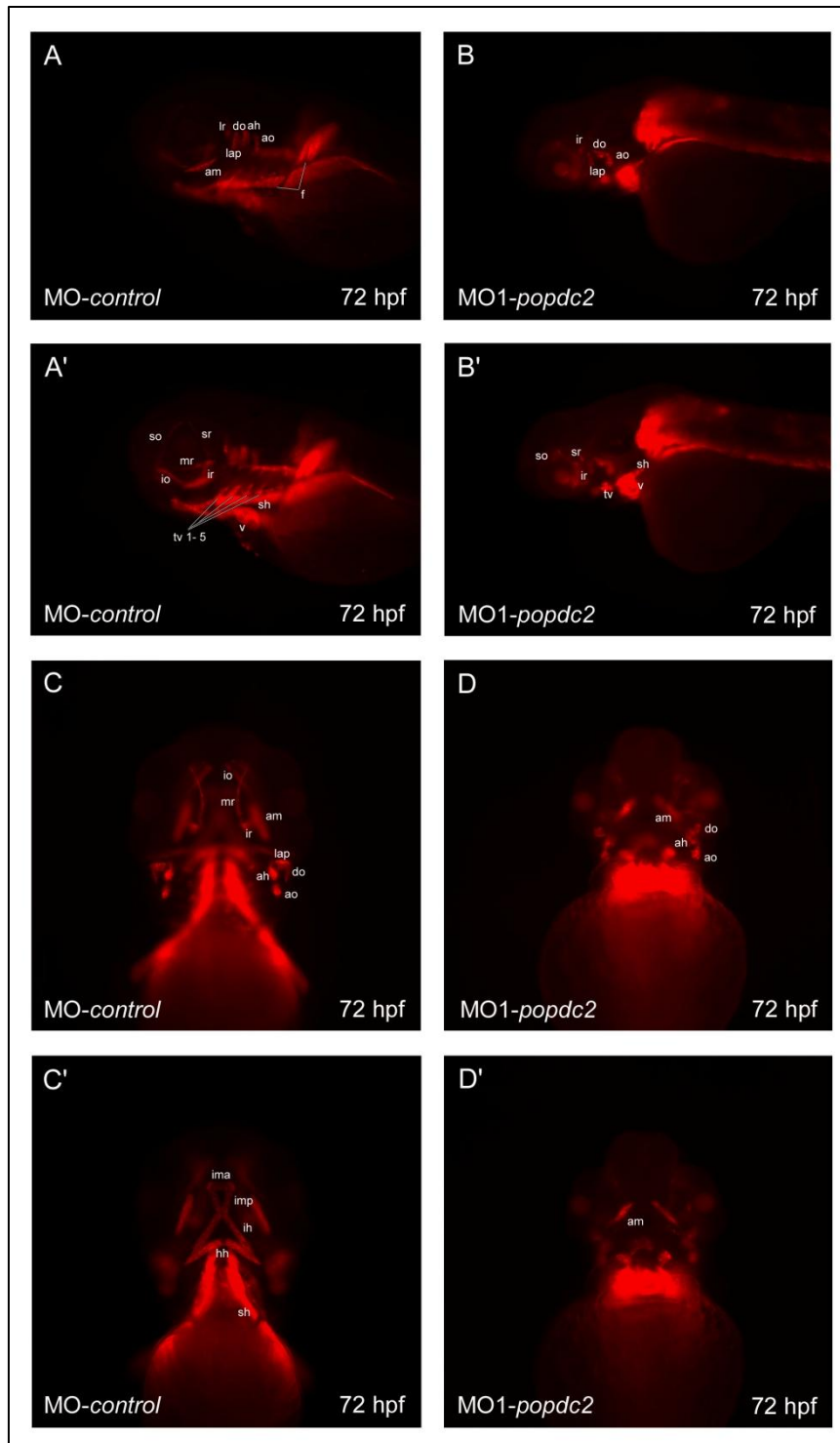


Figure 17: Knockdown of *popdc2* leads to craniofacial muscle reduction.

Craniofacial muscle differentiation of 72 hpf MO-control injected embryos (A, A', C, C') and MO1-*popdc2* injected embryos (B, B', D, D') as revealed by whole mount staining using MF20 antibody. (A-B') Lateral view, (C-D') ventral view. In the MO-control injected embryos the extraocular muscles inferior oblique (io), interior rectus (ir), lateral rectus (lr), medial rectus (mr), superior oblique (so), and superior rectus (sr) were stained (A, A', C), whereas in MO1-*popdc2* injected embryos only interior rectus (ir), superior oblique (so) and superior rectus (sr) could be detected (B, B', D). While the pharyngeal muscles adductor hyoideus (ah), adductor mandibulae (am), adductor operculi (ao), dilator operculi (do), hyohyoideus (hh), interhyoideus (ih), intermandibularis anterior (ima), intermandibularis posterior (imp), levator arcus palatine (lap), and the trunk migrate muscles sternohyoideus (sh) were present in the control, only diminished forms of adductor hyoideus (ah), adductor mandibulae (am), adductor operculi (ao), dilator operculi (do), levator arcus palatine (lap), and sternohyoideus (sh) were found in the *popdc2* morphants. Abbreviations: hpf = hours post fertilization, tv1-5: transverses ventralis 1-5.

Next, I examined the aberrant tail muscle development of the *popdc2* morphants at 24 hpf and 72 hpf. At about 24 hpf, the segmentation period is finished and the fast muscle fibers are found in the inner part of the myotome, whereas slow muscle fibers form a superficial monolayer on the surface of the myotome (Stickney et al., 2000). To detect F-actin, which is abundantly present in muscle cells, whole mount red phalloidin staining and confocal laser scanning microscopy (CLSM) were employed. In contrast to wild type embryos, which displayed a chevron-shaped somite structure at 24 hpf, MO1-*popdc2* injected embryos showed compressed somites and a posterior shortened tail (Figure 18A, B). This phenotype was enhanced by double injection of MO1 and MO2 morpholino which resulted in severe deformed somites (Figure 18C). At 72 hpf, the tail of the *popdc2* morphants exhibited a more u-shaped than chevron-shaped structure. Additionally, the myofibrils within the myosepta of the *popdc2* morphants seemed disorganized, loosely packed and not that dense like the wild type ones (Figure 18D-F). With digital motion analysis (Schwerte and Pelster, 2000) I imaged in cooperation with Dr. Thorsten Schwerte, University of Innsbruck, Austria, the intersegmental vessel development. Probably due to the aberrant tail musculature, intersegmental vessels of the *popdc2* morphants were missing or malformed. Usually, intersegmental vessels are found in every myoseptum of the zebrafish tail at 4 dpf (Figure 18G). However, in 4 dpf MO1-*popdc2* injected embryos intersegmental vessels at the posterior end were missing and irregular loops could be observed (Figure 18H).

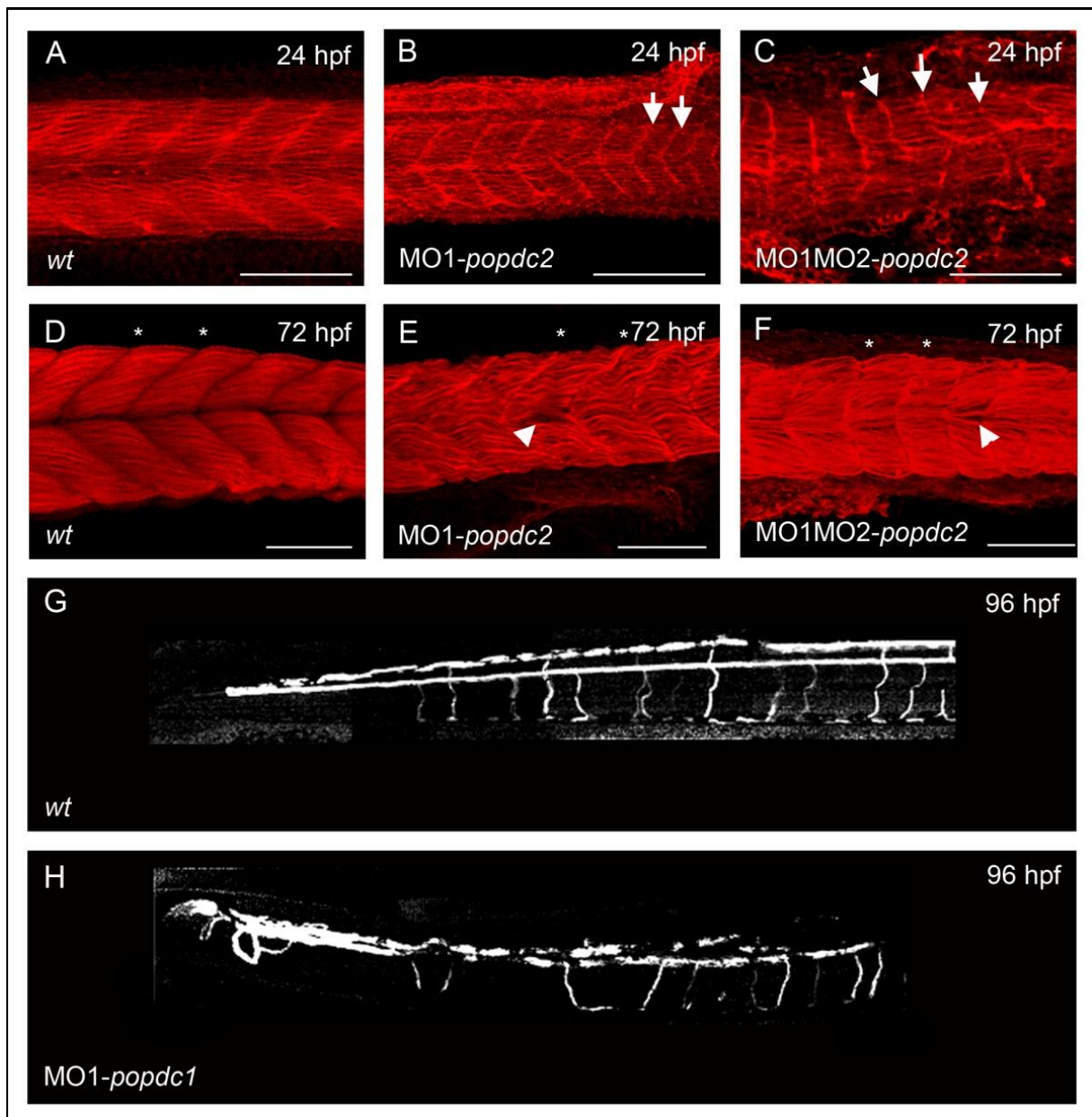


Figure 18: *Popdc2* morphants display deformation of somites and intersegmental vessels.

(A-F) Phalloidin rhodamine staining of (A, D) wild type embryos, (B, E) MO1-*popdc2* injected embryos and (C, F) MO1 + MO2-*popdc2* injected embryos representing the severe phenotype at 24 hpf and 72 hpf. (B, C) At 24 hpf the morphants had a remarkable deformation and compression of somites (arrows) or their derivatives with an increasing effect on the more posterior segments in comparison to the wild type (A). (E, F) At 72 hpf the typical v-shape was altered and the morphant's tail seemed unorganized and not that dense like the control (C) (asterisks, arrowhead). (G, H) Due to changes in tail musculature, intersegmental vessels at 96 hpf were missing or malformed. Abbreviations: hpf = hours post fertilization, wt = wild type.

To display the observed malformed and thin myofibril structure of the MO1-*popdc2* morphant's tail in detail, I used transversal semi-thin sections counterstained with methylene blue. The disrupted organization of the fast muscle fibers was already visible in the semi-thin sections of the 72 hpf *popdc2* morphant. The muscle field appeared reduced in volume and individual borders of muscle fibers were not clearly discernible (Figure 19B). Therefore, I decided to look at the ultrastructure of slow and fast muscle fibers of the tail. The electron micrograph of the outer region of the tail revealed that in wild type embryos (Figure 19A') the outer epithelial layer was thicker and more restricted than in the *popdc2* morphant (Figure 19B'). The ultrastructure of the fast muscle fibers displayed a compact flower-like organization of myofibrils subdivided in quadrants by the sarcoplasmic reticulum. Higher

magnification exhibited the arrangement of thick and thin myofibrils (Figure 19A''). Although the fast muscle fibers of the *popdc2* morphant were disrupted and not organized in the same compact form seen in the wild type, the arrangement of thick and thin myofibrils was not obviously changed. Interestingly, in the MO1-*popdc2* injected embryo more mitochondria were found around the unorganized fast muscle fibers. Furthermore, the observed mitochondria seemed more condense than normal and were scattered throughout the probe.

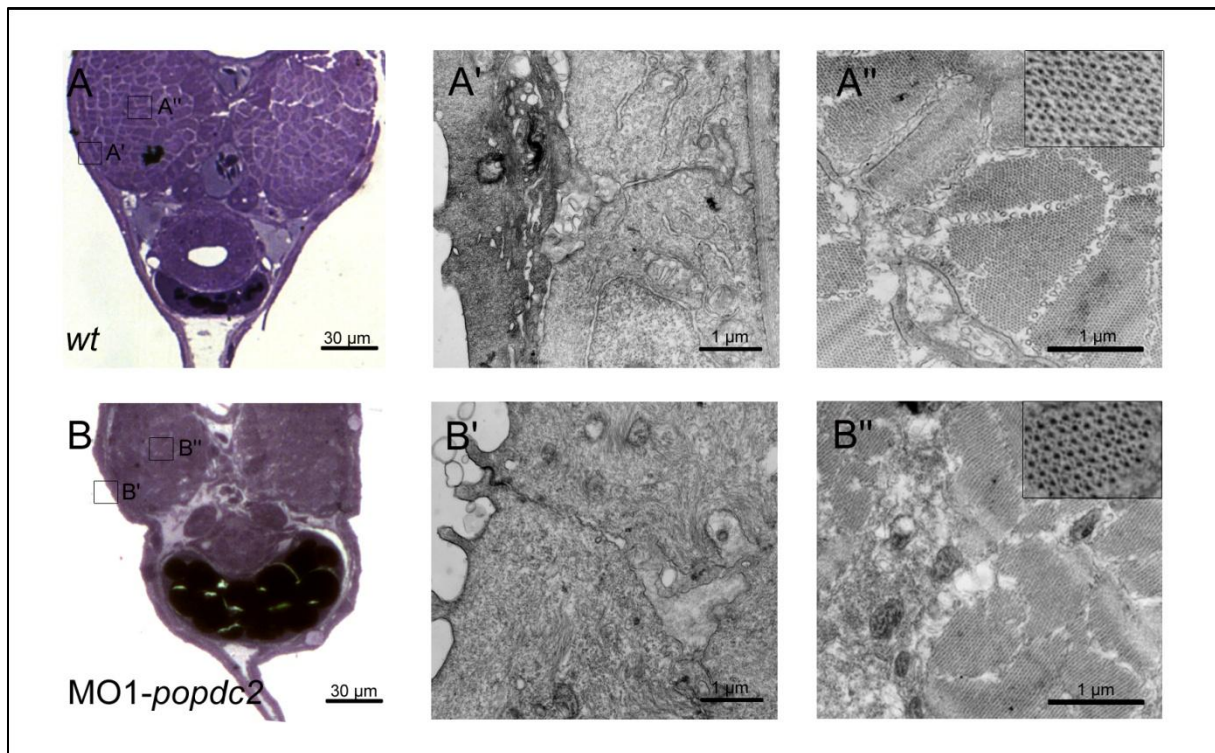
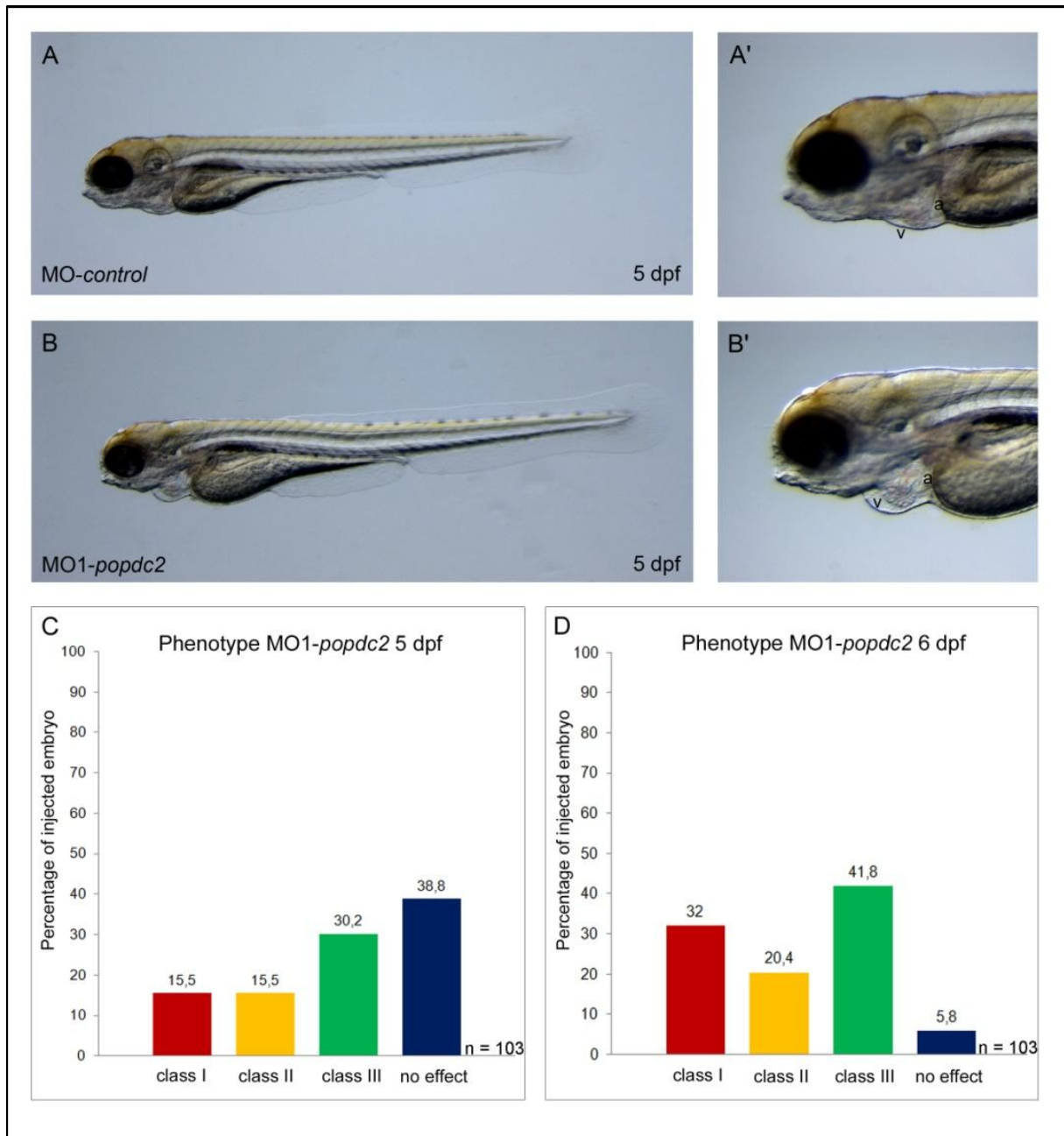


Figure 19: Knockdown of *popdc2* expression disrupts muscle fiber ultrastructure.

(A, B) Transversal semi-thin sections and (A', A'', B', B'') transmission electron microscopy of 72 hpf wild type or MO1-*popdc2* injected embryonic tails. (A'') The wild type embryo demonstrated clearly the well-organized and densely packed muscle fibers of the fast muscles. The inset in A'' showed a higher magnification of the electron micrograph and revealed that thick and thin filaments are present. (B) The MO1-*popdc2* injected embryos displayed an aberrant musculature, (B'') the fast muscles were not organized in a flower-like structure like the wild type but thick and thin filaments could be detected.

6.2.3 *Popdc2* morphants develop cardiac conduction system abnormalities

When using very low amounts of morpholinos (0.27 ng – 0.8 ng), the morphological aberrations that have been described above were negligible. However, in many cases the heart still displayed a mild form of pericardial edema. Some morphants developed a cardiac arrhythmia which was first observed between 3 dpf and 4 dpf at 28.5° C. Initially, at 3 dpf and 4 dpf, some hearts displayed pericardial edema and irregular heart beat or cardiac arrest after 3 to 5 minutes of visual inspection. At about 5 dpf, the incidence of cardiac arrhythmia increased and in many morphants several episodes of irregular heart rhythm or even heart stops were detected during an observation period of 1 minute. Additionally, not only cardiac arrhythmia, but also a weakly contracting ventricle was seen (Figure 20C). At 6 dpf, about 94 percent of the MO1-*popdc2* injected embryos displayed pericardial edema, irregular heart rhythm or a weakly contracting ventricle (Figure 20D).



After *in vivo* analyses of *popdc2* morphants, which did not show any aberration that would explain the observed phenotype, I performed histological and ultrastructural analysis of the MO1-*popdc2* injected embryos displaying cardiac arrhythmia.

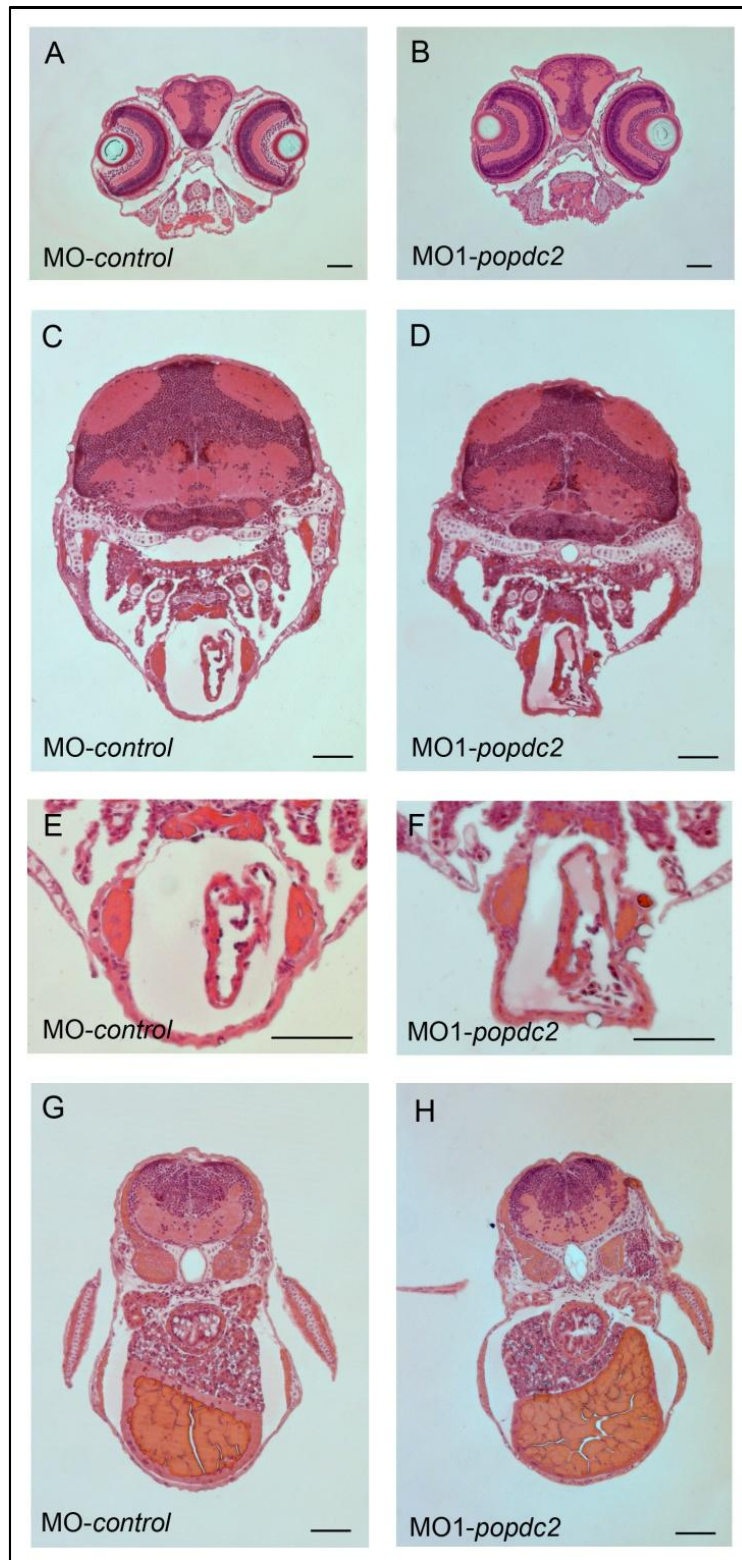


Figure 21: Histological sections of *popdc2* morphants display no remarkable changes. Transversal hematoxylin and eosin stained sections of (A, C, E, G) 5 dpf control and (B, D, F, H) *popdc2* morphants. No changes or missing structures in head (A, B, C, D) and tail (G, H) region between the *control* morphants and the *popdc2* morphants were detected. (F) Focusing on the heart, neither change in the thickness of the ventricle nor malformed cushions was observed in *popdc2* morphants, although they showed a distinct arrhythmia phenotype. Scale bar = 100 μ m.

5 μm thick transversal sections through 5 dpf *popdc2* morphants with rhythm defects, counterstained with hematoxylin/eosin, did not display any aberrations. The head of the control injected embryos (Figure 21A) was similar to the *popdc2* morphant head (Figure 21B), no huge edemas within the head region of the *popdc2* morphant were detected and the brain and the different layers of the eye seemed to be not altered. Comparing the control morphant heart with the *popdc2* morphant heart, I could not detect any obvious difference; both had a well developed multi-layered ventricle, an atrium and valves (between the ventricle and atrium) (Figure 21C-F). Transversal sections behind the heart demonstrated that *popdc2* morphants have developed pectoral fins, the esophagus, the liver and nephros just as seen in the control (Figure 21G, H).

Additionally, as expected, *popdc2* morphants revealed no change in chamber specification proved by whole mount *in situ* hybridization probing the genes *cardiac myosin light chain 2 (cmlc2)* and *ventricular myosin heavy chain (vmhc)* (Figure 22).

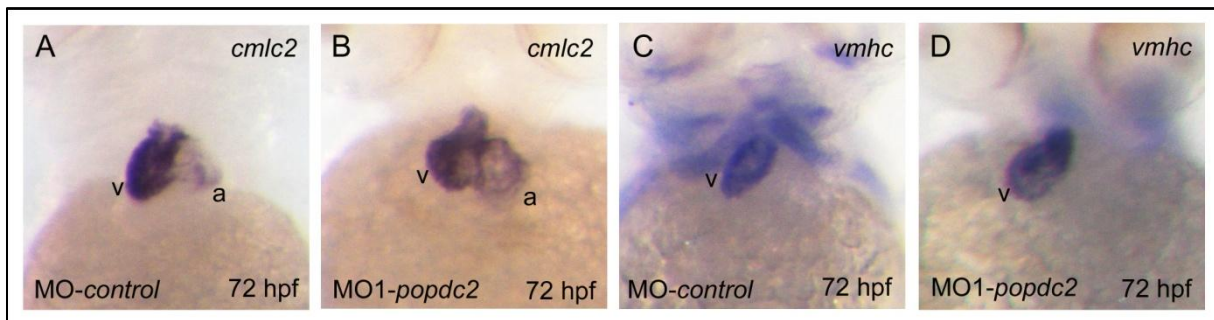


Figure 22: *Popdc2* morphants display no change in chamber specification.

Whole mount *in situ* hybridization of 72 hpf (A, C) control injected embryos and (B, D) *popdc2* morphants. Consistent with the control, *popdc2* morphants display (B) *cmlc2* expression in both heart chambers and (D) *vmhc* expression in the ventricle.

Electron micrographs of the ventricular wall of 72 hpf wild type or MO1-*popdc2* injected embryos should give further insight into the muscular ultrastructure of the heart. In Figure 23 myofibrillar arrays were evident and bundled into consecutive units in both, wild type and morphant cardiomyocytes. The electron micrographs showed the typical sarcomeres, which extend between Z-bands and surrounding mitochondria.

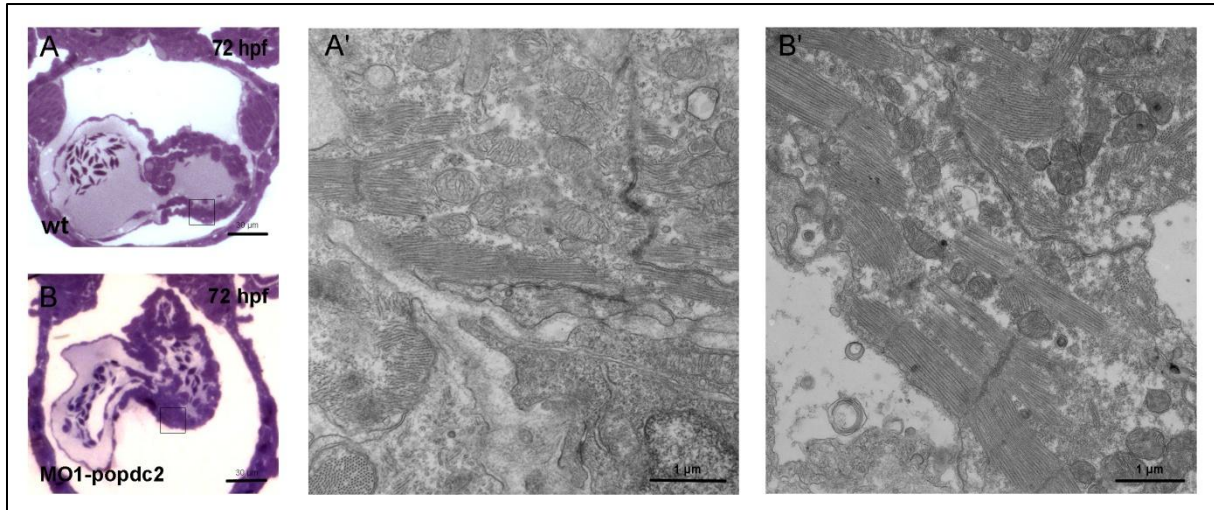


Figure 23: Myofibrillar arrays are evident in *popdc2* morphant's heart musculature.

(A, B) Transversal semi-thin sections and (A', B') transmission electron microscopy of 72 hpf wild type or MO1-*popdc2* injected embryonic hearts. Myofibrillar arrays were evident in (A') wild type and in (B') *popdc2* morphants.

To further characterize the cardiac phenotype, I collaborated with the laboratory of Dr. Thorsten Schwerte at the Institute for Zoology and Limnology, Innsbruck University, Austria. There, I used high speed video microscopy to record MO1-*popdc2* injected and MO-control injected embryos between 4 dpf and 7 dpf *in vivo*. The single images of the obtained videos were further analyzed as follows. The heart rate of the *popdc2* morphants with stable rhythm were determined by measuring the time interval necessary for 30 heart beats and evaluated statistically. *Popdc2* morphants with arrhythmia and the corresponding control were analyzed with software programmed by Dr. Thorsten Schwerte which detects heart rate changes by beat-to-beat analysis. Cardiac muscle performance was illustrated as luminance periodograms (Schwerte and Fritsche, 2003). Furthermore, the valve motion and the correct blood flow of 4 dpf embryos were surveyed.

In comparison to the control (supplemental video S1), the beating frequencies of *popdc2* morphants were diminished, and the differences reached statistical significance ($p \leq 0.05$) at 5 dpf and 7 dpf (Figure 24B). Luminance periodograms of 5 dpf *popdc2* morphants (supplemental video S2) revealed irregular ventricular contraction with 2:1 and 3:1 ventricular pauses while sinus rhythm and atrial contractility was normal (Figure 24A) suggesting a first-degree and second-degree atrioventricular block, respectively. Consistent data were obtained at 6 dpf and 7 dpf. At 5 dpf, the 2:1 atrioventricular block occurred with high frequency ($30 \pm 6/\text{min}$ ($n = 4$)). In addition, a 3:1 conduction block (3 ± 1) was observed. Interestingly, at 7 dpf, *popdc2* morphant hearts displayed extensive pauses of atrial and ventricular contraction each with a duration of approximately $9.8 \text{ s} \pm 1.8 \text{ s}$ per minute. This is probably due to abnormal excitation and defective sinoatrial node function. Finally, the inspection of the valve motion and the blood flow of 4 dpf *popdc2* morphants demonstrated no alteration indicating that the atrioventricular block is not caused by malformed valves. These data validate the aforementioned observation made in Würzburg.

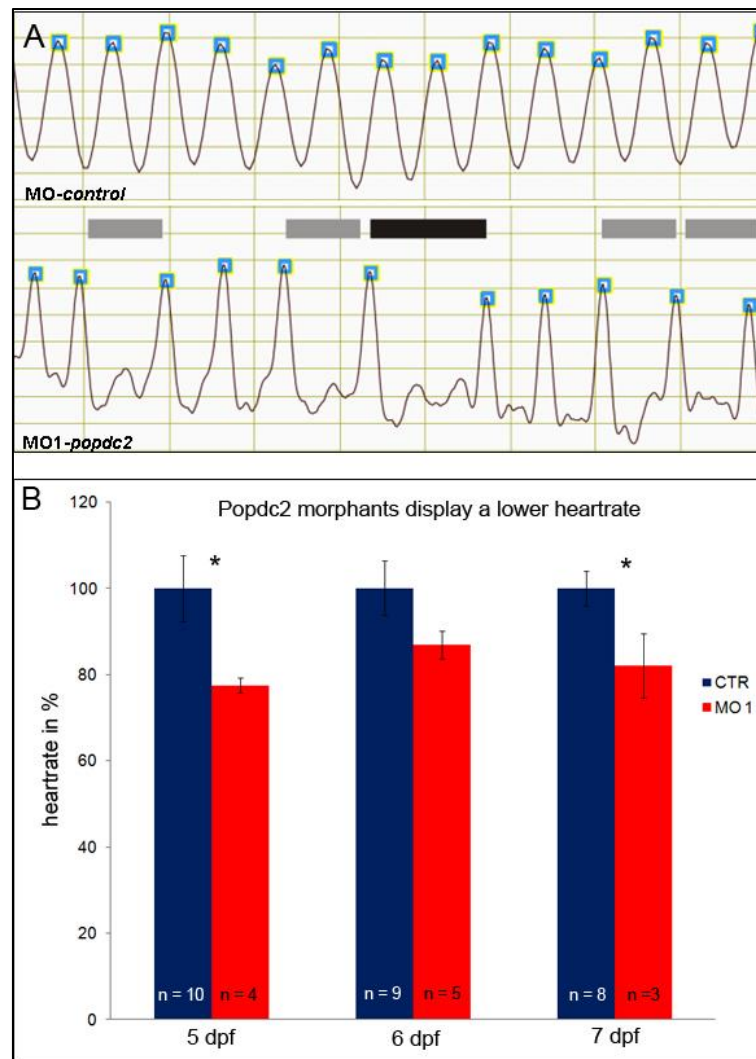


Figure 24: *Popdc2* morphants develop cardiac conduction abnormalities and a diminished heart rate.

A) Comparison of luminance periodograms of a 5 dpf heart from a control and a *popdc2* morphant. The *popdc2* morphant revealed 2:1 (light grey bar) and 3:1 (black bar) atrioventricular rhythm. In contrast to 5 dpf, 6 dpf and 7 dpf wild type embryos, *popdc2* morphants develop a lower heart rate (B). The difference in beating frequency of wild type and *popdc2* morphants reached statistical significance ($p \leq 0.05$) indicated by an asterisk at 5 dpf and 7 dpf. Abbreviations: n = number of analyzed animals at each stage, CTR = control injected embryos, MO1 = MO1 morpholino injected embryos.

Because *Popdc2* knockout mice displayed an age-dependent development of chronotropic incompetence during swimming exercise, mental stress (airjet), and after β -adrenergic stimulation with isoproterenol (Froese, 2008), I decided to also treat the *popdc2* morphants with isoproterenol. Isoproterenol has got a chronotropic and inotropic effect on the heart and there are known functional adrenergic receptors at 3 dpf in zebrafish (Hsieh and Liao, 2002). Together with Dr. Thorsten Schwerte and Franziska Guentner, 5 dpf *popdc2* morphants were analyzed before and 10 minutes after the treatment with isoproterenol using high speed video microscopy. Before isoproterenol application, the *popdc2* morphants displayed only 76.7 % of the heart rate compared to the control embryos. These data are consistent with the measured heart frequency in the assay before (Figure 24B). 10 minutes after isoproterenol application both, the MO-control injected embryos and the MO1-*popdc2* injected embryos, showed a similar increase in heart rate (about 7 %). In some *popdc2* morphants an increase of 2:1

ventricular pauses after isoproterenol treatment was observed, however, this effect was statistically not significant.

To exclude that the cardiac conduction phenotype of *popdc2* morphants is only caused by impaired cardiac muscle, I analyzed the electrical activity of the zebrafish heart by displaying the calcium transients of both, the *popdc2* morphants and control embryos, using multiple selective plane illumination microscopy (mSPIM) (Huisken and Stainier, 2009; Huisken et al., 2004). Therefore, I collaborated with Prof. Didier Stainier, University of California, San Francisco, USA, under direct guidance of Dr. Jan Huisken. Didier Stainier's laboratory has developed a cardiac-specific fluorescent calcium indicator zebrafish line to analyze the formation of the cardiac conduction system (Arnaout et al., 2007). This transgenic zebrafish line called *Tg(cmlc2:gCaMP)^{s878}* specifically expresses gCaMP, a genetically engineered calcium reporter based on a circular permutation of green fluorescent protein (GFP) (Nakai et al., 2001) at all developmental stages in the heart, using the cardiac-specific promoter *cmlc2*. MO1-*popdc2* injected and MO-control injected embryos were imaged at 5 dpf and 6 dpf. To visualize the calcium transients, the zebrafish hearts had to be silent. Therefore, the hearts were mechanically uncoupled with the help of 2,3-butanedione monoxime (BDM). 2,3-BDM is a well-characterized, low-affinity, non-competitive inhibitor of skeletal muscle myosin-II. Mapping the electrical activity of the control morphants at 5 dpf exhibited that the calcium activation pattern started in the sinus node and propagated along the atrium. At the AV boundary the calcium transient was slowed and proceeded from the AV boundary across the ventricle to the outflow tract where the calcium transient decelerated (supplemental video S3). With the help of a software tool programmed with Matlab, an optical section from the recorded video was chosen and from these optical section regions within the atrium, the AV boundary and the ventricle were determined. Then, the fluorescence intensity of a single pixel from each region was recorded and plotted over time. The plot of the 5 dpf control embryo depicted the periodic variation of the fluorescence intensity over time in atrium, AV-boundary, and ventricle and represented the excitation wave which propagates throughout the heart (Figure 25A, D). Recordings of 5 dpf *popdc2* morphants revealed an atrioventricular block. At the beginning, the calcium transients started and propagated regularly through the atrium, but sometimes the calcium transients stopped at the AV boundary so that no excitation could be seen in the ventricle (supplemental video S4). Figure 25 shows representative plots of two *popdc2* morphants with the first morphant displaying a 4:1 ventricular pause while the atrium paced continuously (Figure 25E). The second morphant exhibited five 2:1 ventricular pauses within the analyzed 15 seconds (supplemental video S5). Although the fluorescence intensity varied regularly in the atrium of the second morphant, it seemed that the distance between the peaks was sometimes shortened, particularly before or after the ventricular pause (Figure 25F). This is a sign for an uncoupled atrium and ventricle and is characteristic for a third grade AV nodal block. I can therefore conclude that both analyzed *popdc2* morphants developed an atrioventricular block already recorded using high speed video microscopy in Innsbruck. Next, I imaged the 6 dpf MO-control injected or MO-*popdc2* injected embryos. Visually the excitation pattern of the 6 dpf control embryos resembled the recorded video of the 5 dpf controls, but unexpectedly, the according plot showed sometimes a retardation of fluorescence variety in atrium and ventricle. This is probably due to the treatment with 2,3-BDM. 2,3-BDM is known to cause proarrhythmic effects. However, this retardation of fluorescence variety in atrium and

ventricle was never seen in the *popdc2* morphants and had no similarity with the observed *popdc2* morphant phenotype. Interestingly, the *popdc2* morphants were extremely resistant against the 2,3-BDM treatment in contrast to the control embryos. Recordings of 6 dpf *popdc2* morphants displayed atrioventricular blocks and sinoatrial blocks as well and in 7 dpf *popdc2* morphants a complete heart block could be also visualized in comparison to the control (supplemental videos S8 and S9). Recorded videos of *popdc2* morphants developing an atrioventricular block started with a regular calcium excitation pattern from the sinus node through the atrium, but the calcium wave was sometimes blocked in the AV boundary (supplemental video S6). Videos of *popdc2* morphants developing a sinoatrial block revealed that beneath regular calcium excitation pattern propagated through the whole heart, calcium transients were missing in atrium and the ventricle as well (supplemental video S7). The fluorescence intensity of a 6 dpf *popdc2* morphant with atrioventricular block and one with a sinoatrial block were plotted over time (Figure 26E, F). The plot of the first *popdc2* morphant depicted 2:1 and 3:1 ventricular pauses, while the fluorescence intensity in the atrium varied normally (Figure 26E). The second *popdc2* morphant displayed a loss of calcium transients in atrium and in ventricle (Figure 26F). Reflecting all the analyzed calcium alterations I confirmed that the observed arrhythmia in *popdc2* morphants is caused by aberrant electrical activity of the heart.

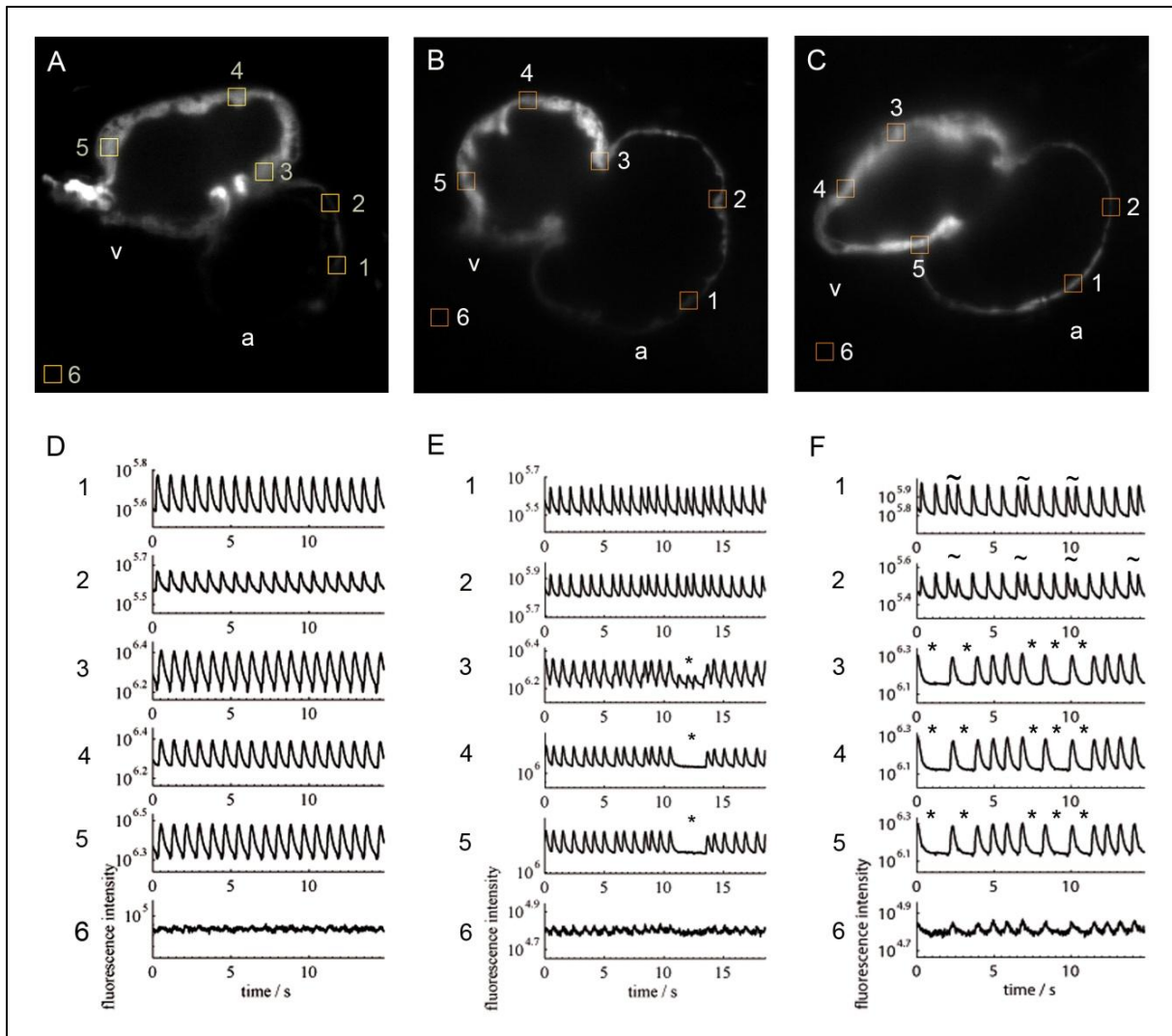


Figure 25: 5 dpf *popdc2* morphants exhibit an AV block.

Optical sections of 5 dpf *Tg(cmlc2:gCaMP)^{s978}* hearts from (A) a control morphant and (B, C) *popdc2* morphants. The numbered squares represent areas where calcium transients from the atrium, AV-canal, ventricle and background were recorded. (D, E, F) Fluorescence intensity of a single pixel from each region was measured to obtain calcium transients and plotted over time in seconds. All plots are semi-logarithmic. (A, D) In the control heart varied fluorescence intensity with time in atrial and ventricular regions of the heart as the wave of depolarization propagated through the heart. This wave represents the electrical activity of a wild type heart. (B, E) In the first *popdc2* morphant, fluorescence intensity varied in the atrium (1, 2) whereas in the ventricle (4, 5) between 10 and 15 seconds a constant low-level intensity was observed (asterisk). (C, F) In the second *popdc2* morphant, fluorescence intensity varied in the atrium (1, 2) whereas in the ventricle several times fluorescence intensity peaks were missing (asterisks), furthermore before the low level fluorescence intensity in the ventricle is observed, the calcium transients passed the atrium faster (-). Both *popdc2* morphants lacked ventricular conduction waves. Abbreviations: dpf = days post fertilization, a = atrium, v = ventricle.

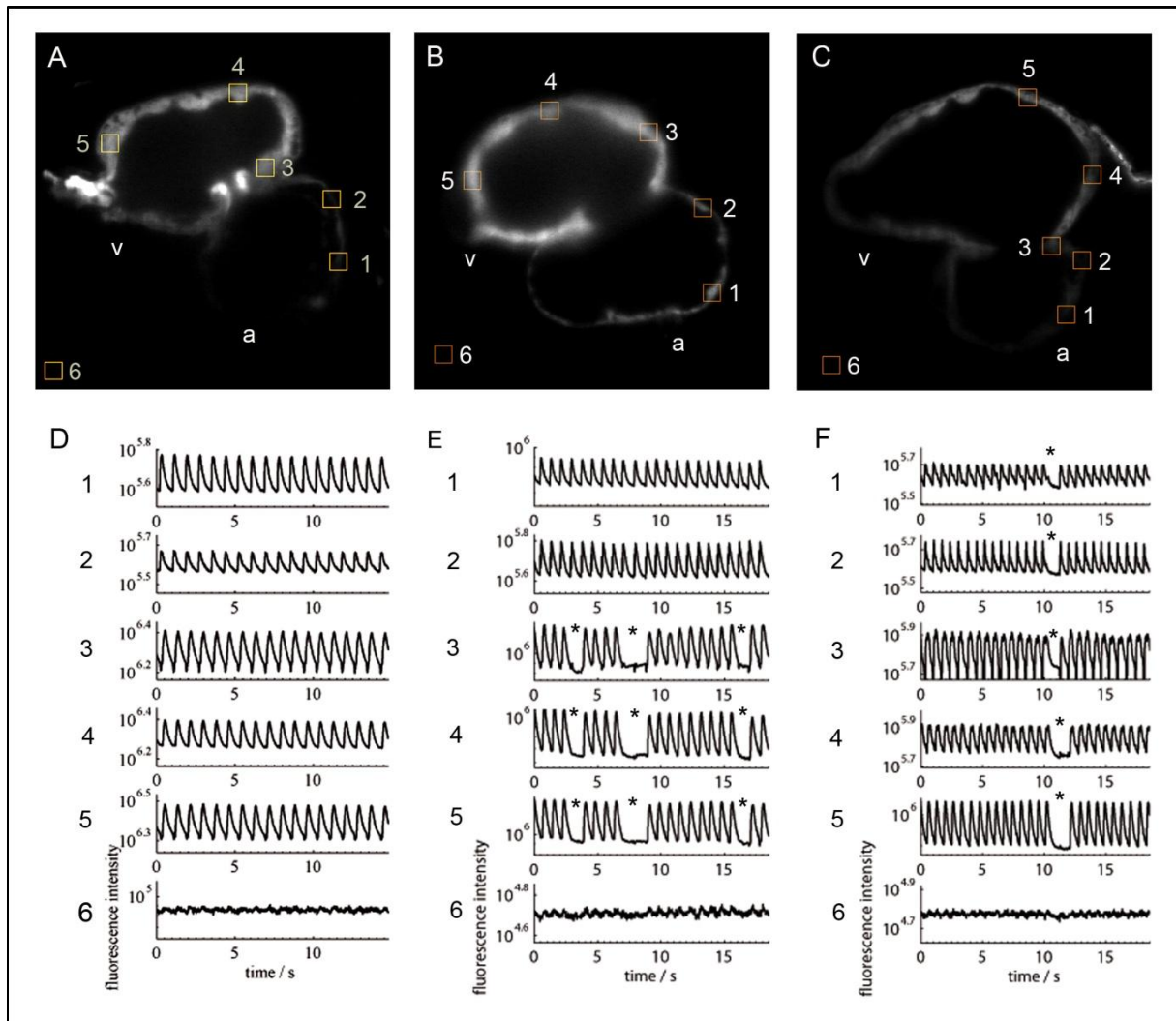


Figure 26: 6 dpf *popdc2* morphants develop AV blocks as well as sinoatrial blocks.

Optical sections of *Tg(cmlc2:gCaMP)^{s878}* hearts from (A) a 5 dpf control morphant (identical to Figure 25A, D) and (B, C) 6 dpf *popdc2* morphants. (D, E, F) SPIM videos were processed to determine the fluorescence intensity of selected regions represented by numbered squares over time. selected region has a corresponding number in the semilogarithmic plot aside. (A, D) in the control heart, the fluorescence intensity changed over time in atrial and ventricular regions of the heart as the wave of depolarization propagated through the heart. (B, E) In the first *popdc2* morphant, fluorescence intensity varied in the atrium (1, 2) whereas in the ventricle a block of calcium transients (marked with asterisks) was detected representing an AV block. (C, F) In the second *popdc2* morphant a block of electrical activity in atrium and ventricle (here indicated with asterisks) was observed reflecting a sinoatrial block. Abbreviations: dpf = days post fertilization, a = atrium, v = ventricle.

6.2.4 Aberrant electrical activity is not caused by cellular changes within the AV canal of *popdc2* morphants

Aberrant electrical activity could be caused by morphological alterations. In the *popdc2* morphants, we particularly paid attention to cardiac myocytes of the AV canal which are proposed to have pacemaker potential. To clarify the morphology of the cardiomyocytes especially within the AV canal of *popdc2* morphants, I imaged five 5 dpf *popdc2* morphants displaying cardiac arrhythmia and the corresponding controls *in vivo*, utilizing confocal microscopy and the transgenic zebrafish line *Tg(cmlc2:eGFP-ras)^{s883}* (Jungblut et al., unpublished data) which outlines individual cardiomyocytes with membrane-bound GFP. The following analyses were done with the help

of Dr. Benno Jungblut, MPI Bad Nauheim. Regarding the 3D reconstruction of *popdc2* morphant and control hearts, no obvious differences were detected (Figure 27A, B). Furthermore, because the development of the trabeculae is important for the fast conducting system, I ensured that the ventricle of *popdc2* morphants (Figure 27B''') displayed the same level of trabeculation as the control (Figure 27A'''). Although all analyzed *popdc2* morphants (Figure 27B', B'') exhibited no difference in the typical cardiomyocyte morphology in the AV canal when compared to the control injected embryos (Figure 27A', A''), all *popdc2* morphants developed an elongation of cardiomyocytes behind the AV canal at about the height of the developing valves.

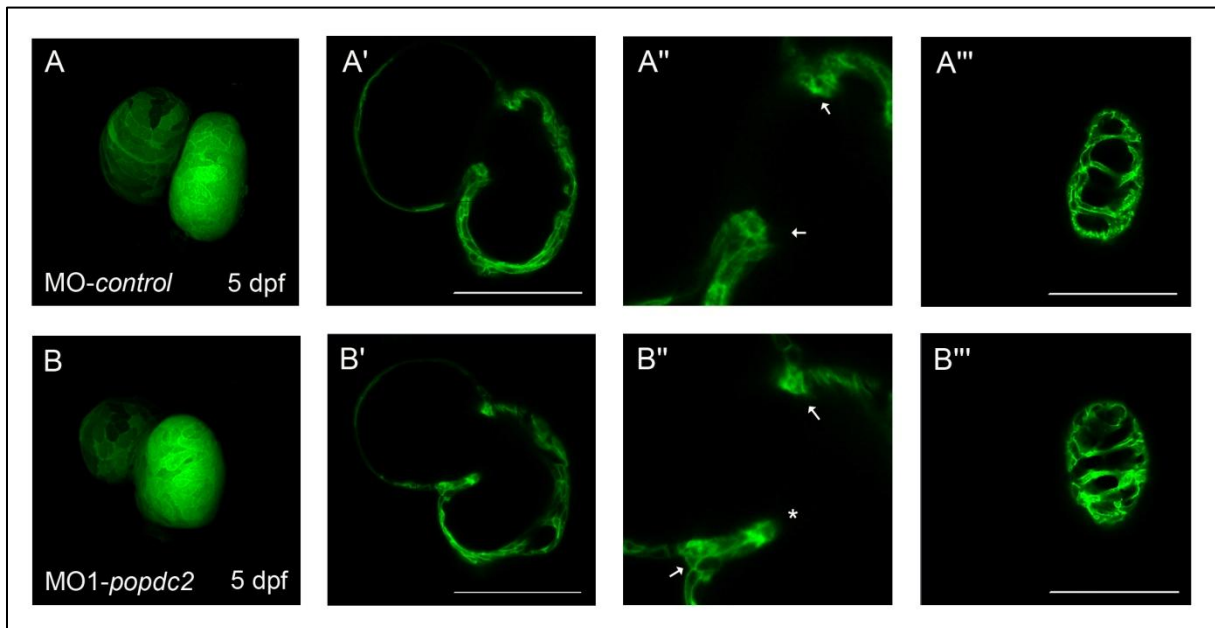


Figure 27: Arrhythmic *popdc2* morphants show no alteration of the AV cardiomyocytes.

(A, B) 3D image of 5 dpf *Tg(cmlc2:eGFP-ras)^{s883}* hearts constructed by using confocal stacks. Single images through the heart of *popdc2* morphants with arrhythmia demonstrated that the ventricle was trabeculated (B''') and the AV cardiomyocytes indicated with arrows were not altered (B'') and resembled the control heart (A', A''). Interestingly, behind the AV boundary an extension of cardiomyocytes (asterisk) in the ventricle was found in all examined *popdc2* morphants. Abbreviations: dpf = days post fertilization. Scale bar = 100 μ m.

Detailed observation of the morphology of single cardiomyocytes within the ventricle revealed that *popdc2* morphants displayed also circular cardiomyocytes in addition to only cuboidal cardiomyocytes seen in the control embryos (Figure 28C, D). Unexpectedly, one of the five imaged *popdc2* morphants showed a cardiomyocyte tissue bridge (Figure 28B).

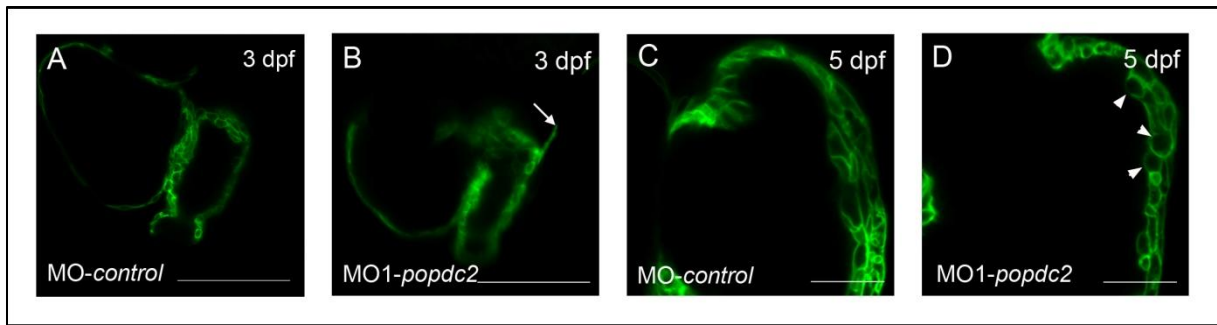


Figure 28: Arrhythmic *popdc2* morphants display alterations in cardiomyocyte shape

(A-D) Single images through (A, B) 3 dpf and (C, D) 5 dpf *Tg(cmlc2:eGFP-ras)^{s883}* hearts. In contrast to the 3 dpf control (A), the *popdc2* morphant developed a myocardial tissue bridge indicated with an arrow (B). In comparison to the 5 dpf ventricle of the control heart (C) the *popdc2* morphant displayed circular myocytes indicated with arrowheads. Abbreviations: dpf = days post fertilization. Scale bar figure A, B = 100 μ m, scale bar figure C, D = 25 μ m.

Because the observed elongation of cardiomyocytes was detected near the valves, I also analyzed valve formation in *popdc2* morphants using the transgenic zebrafish line *Tg(flk1:eGFP)^{s843}* which labels the endocardium by expressing GFP. In this assay, I analyzed 5 dpf *popdc2* morphants without cardiac arrhythmia as well as *popdc2* morphants with rhythm defects and the corresponding controls *in vivo*. Ventral confocal sections of a control injected embryos (Figure 29A'), the *popdc2* morphants without (Figure 29B') and with cardiac arrhythmia, respectively (Figure 29C') demonstrated clearly that the valves are present in all cases.

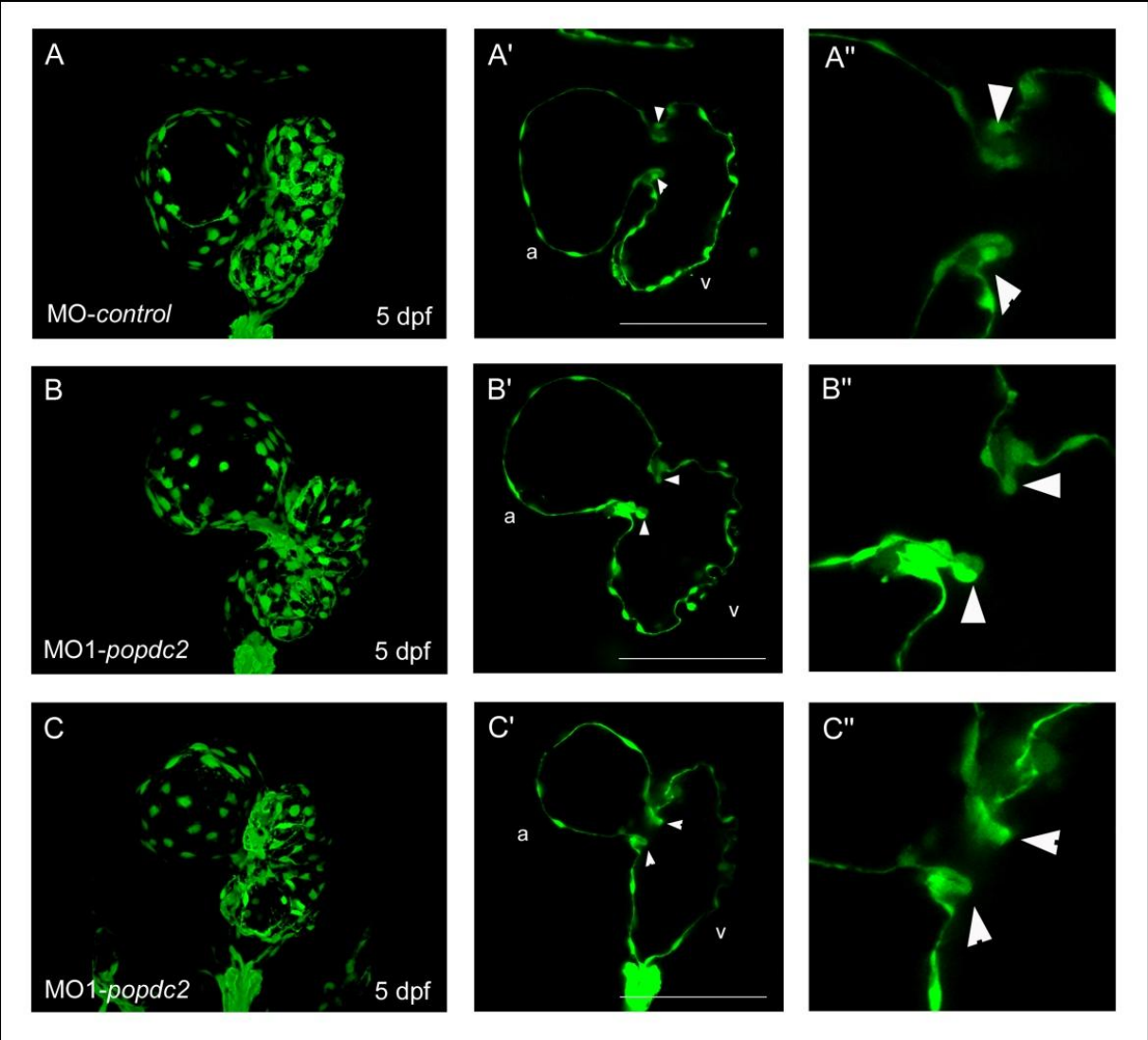


Figure 29: *Popdc2* morphants display no change in valve development.
(A, B, C) 3D image of 5 dpf *Tg(flk1:eGFP)^{s843}* zebrafish hearts constructed by using confocal stacks. Ventral sections through the hearts of (A') the control injected embryo and (B') *popdc2* morphants without arrhythmia and (C') developed arrhythmia exhibited the presence of valves in all cases (arrowhead). Abbreviations: a = atrium, dpf = days post fertilization, v = ventricle. Scale bar = 100 μ m.

6.3 *Popdc3* might be important for cardiac conduction system development

6.3.1 *Popdc3* is expressed in distinct regions of the brain, heart and skeletal muscle

To further investigate the expression of *popdc* genes in zebrafish development, I additionally examined the expression pattern of *popdc3*. In contrast to the expression pattern of *popdc2* in the adult zebrafish, where the strongest expression was found in heart tissue, RT-PCR analyses of *popdc3* expression revealed high expression in brain and skeletal muscle and only weak expression in the heart (Figure 30A). During embryogenesis, *popdc3* expression was faintly expressed at 18 somite stage, robust expression was seen at 24 hpf and 48 hpf and expression declined at 72 hpf (Figure 30B).

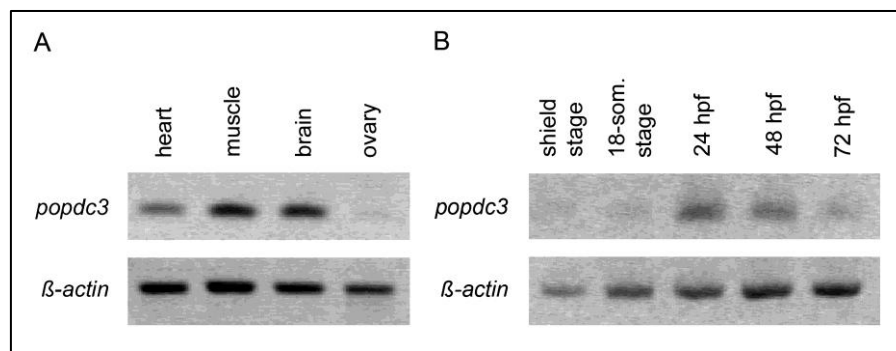


Figure 30: *Popdc3* is expressed during heart development and is found in adult heart, muscle and brain. *Popdc3* RT-PCR analysis of total RNA isolated from (A) adult tissues or (B) total embryos of the indicated age. For control purpose expression of β -actin was monitored. (A) In the adult, the strongest *popdc3* expression was observed in the skeletal muscle and brain whereas in the heart weak expression was detected. (B) During embryogenesis, *popdc3* expression started at 18 somite stage, robust expression was seen at 24 hpf while expression level declined at 72 hpf. Abbreviations: hpf = hours post fertilization.

To analyze the expression pattern of *popdc3* in further detail, zebrafish embryos at 24 hpf, 48 hpf and 72 hpf were subjected to whole mount *in situ* hybridization with a *popdc3* probe. At 24 hpf, no expression in the linear heart tube was detected (Figure 31B), but in distinct regions of the brain like the ventral diencephalon, the ventral mesencephalon, the brain ventricular zone, and the midbrain/hindbrain boundary (Figure 31A, C), *popdc3* expression was observed. Furthermore, *popdc3* was expressed in the otic vesicles. In the outflow tract region of the heart, two expression domains were detected (Figure 31B). These domains appeared as a stream of cells and tentatively were identified as neural crest cells that migrate into the outflow tract. This interpretation, however, needs to be corroborated using double labeling experiments employing neural crest marker genes.

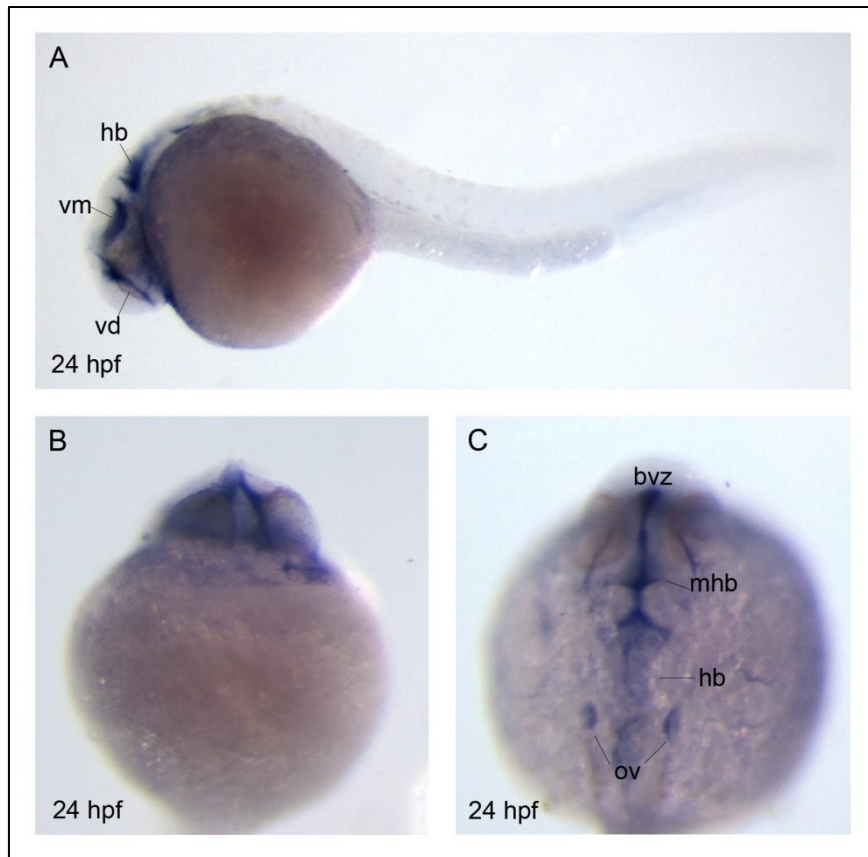


Figure 31: At 24 hpf *popdc3* is expressed in distinct regions of the brain.

Expression analysis of *popdc3* in zebrafish embryos at 24 hpf by whole mount *in situ* hybridization. (A) Lateral, (B) ventral, and (C) dorsal view. Expression was detected in areas of the brain like the ventral diencephalon (vd), the ventral mesencephalon (vm) as well as the hindbrain (hb). Also in addition the brain ventricular zone (bvz), the midbrain-hindbrain boundary (mhb) and the otic vesicles (ov) expressed *popdc3*. Although the linear heart tube was not stained, it appeared that tissues around the heart express *popdc3*. Abbreviations: bvz = brain ventricular zone, hb = hindbrain, hpf = hours post fertilization, mhb = midbrain hindbrain boundary, ov = otic vesicle, vd = ventral diencephalon, vm = ventral mesencephalon.

After heart chamber specification, i.e. at 48 hpf, *popdc3* expression is maintained in the otic vesicles and in the lateral hindbrain. Furthermore, the fin buds and an undefined region above the heart expressed *popdc3* as well. In addition to *in situ* hybridization, muscle tissue was stained with a MF20 antibody to display the muscular *popdc3* expression pattern. It was observed that only the anterior part of the fin buds showed *popdc3* expression. Furthermore, it appeared that cardiac myocytes in the heart chambers did not express *popdc3*, however possibly neural crest cells and/or great vessels developing from the outflow tract were labeled by the *popdc3* probe (Figure 32).

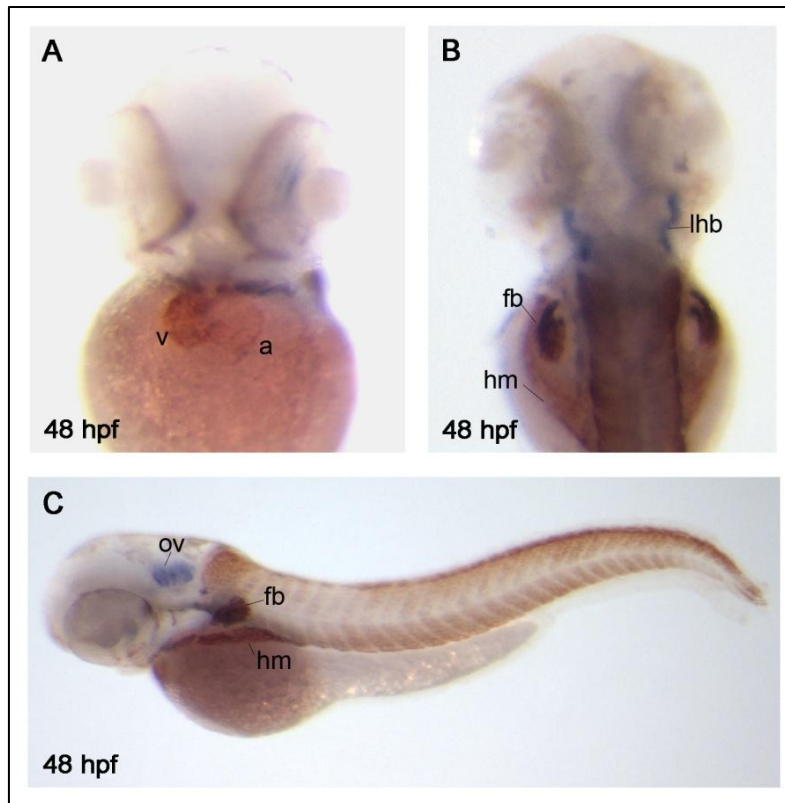


Figure 32: 48 hpf embryos reveal *popdc3* expression in the outflow tract and distinct regions of the brain.

Whole mount *in situ* hybridization of *popdc3* and counterstaining with MF20 antibody. (A) ventral, (B) dorsal, and (C) lateral view of stained embryos. At 48 hpf *popdc3* was expressed in the outflow tract region, putative neural crest cells, the anterior parts of the fin buds, the lateral hindbrain and in the otic vesicles. Abbreviations: a = atrium, fb = fin bud, hm = hypaxial muscles, lhb = lateral hindbrain, ov = otic vesicle.

At 72 hpf, *popdc3* expression was observed in the outflow tract of the heart (Figure 33A and B). 7 μ m sections from stained embryos revealed expression in the diencephalon and in particular layers of the eye (Figure 33C and D). Comparing the expression data of *popdc3* with that of *popdc2* it can be concluded that the expression pattern of *popdc2* and *popdc3* do not fully overlap, although both genes are expressed during the same developmental stages. While *popdc2* was strongly expressed in the whole heart, *popdc3* showed only expression in the outflow tract. Furthermore, *popdc3* displayed unique expression domains in the brain.

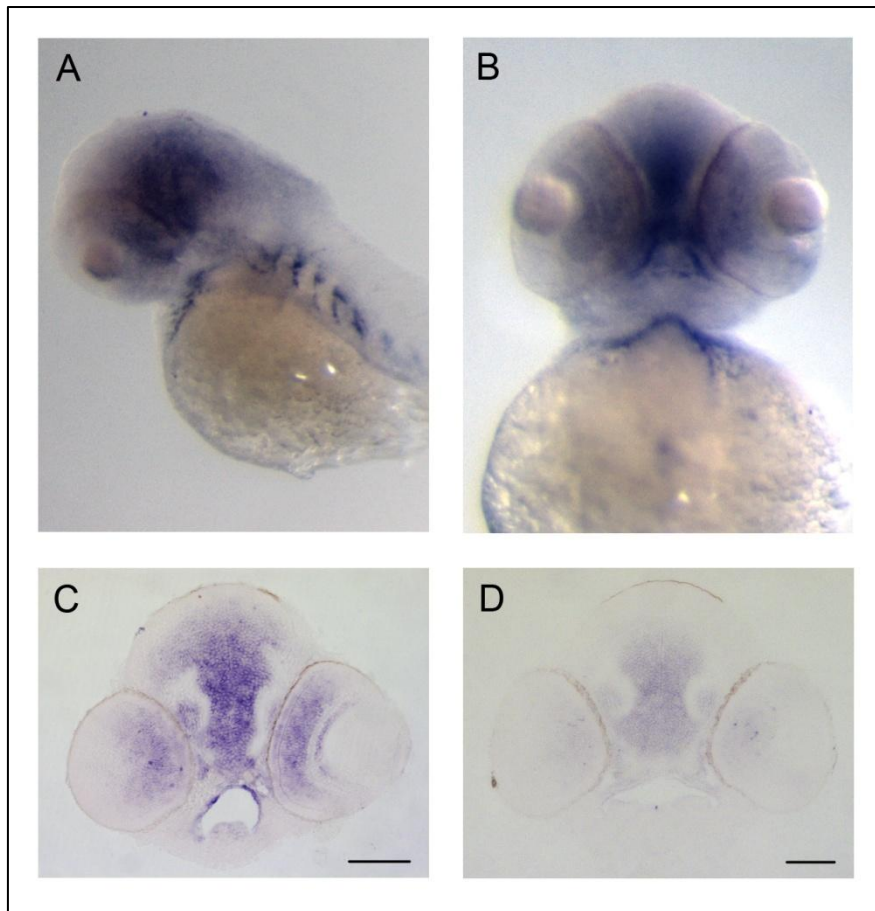


Figure 33: *Popdc3* expression in 72 hpf zebrafish embryos.

(A, B) Zebrafish embryos (72 hpf) were subjected to whole mount *in situ* hybridization using a *popdc3* probe and (C, D) subsequently sectioned through the head region. (A) *Popdc3* was expressed in the outflow tract region and the outer part of the heart chambers. (B) The ventral region of the embryo highlighted the staining in the outflow tract and the eye. (C, D) Transversal sections through the stained head exhibited *popdc3* expression in the diencephalon and in the inner nuclear layer, the outer nuclear layer and the ganglion cell layer of the eye. Scale bar = 100 μ m.

6.3.2 *Popdc3* morphants develop a complete heart block

Because *popdc3* expression differs from that of *popdc2*, I was interested whether the loss of *popdc3* also affects cardiac conduction system development like *popdc2* does or whether it possibly plays an unknown role in the nervous system. Therefore, I began to examine the electrical activity of *popdc3* morphants employing the injection of 1.6 ng of a splice acceptor morpholino in zebrafish embryos. Splicing blockade of this particular splice site prevented the inclusion of exon 2 which harbours the Popeye domain (Figure 34).

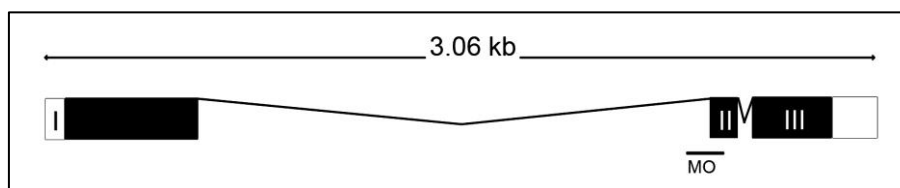


Figure 34: Knockdown strategy of *popdc3* in zebrafish.

(A) *Popdc3* consists of 3 exons. The morpholino-modified oligo was directed against the splice site of intron 1 (MO). Abbreviations: MO = Morpholino directed against the splice-acceptor site of Exon 2 in *popdc3*.

59 % of the *popdc3* morpholino-injected embryos (n = 97) displayed an obvious phenotype in the tail, which is possibly due to a muscle defect (Figure 35). Furthermore, the *popdc3* morphants developed a pericardial edema, which is an indicator for cardiac dysfunction. No other phenotypic alterations were observed.

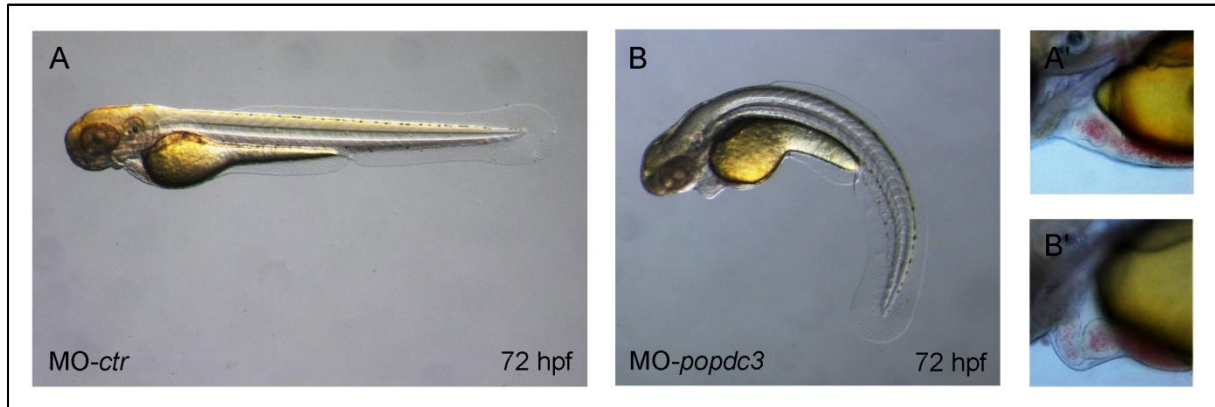


Figure 35: *Popdc3* morphants display abnormal body curvature and pericardial edema

Lateral view of (A) control and (B) MO-*popdc3* injected embryos at 72 hpf. The majority of the *popdc3* morphants had developed a curved tail (A, B). High magnification view of the heart region of (A') control and (B') *popdc3* morphant's heart. The morphant displayed pericardial edema, blood retention, as well as slight dilatation of the cardiac chambers. Abbreviations: ctr = control, hpf = hours post fertilization.

In order to further study the cardiac phenotype, the electrical activity of the *popdc3* morphant heart was monitored. For this purpose, the mSPIM technique and the zebrafish transgenic line *Tg(cmlc2:gCaMP)^{s878}* were again utilized. Because 2,3 BDM can cause pro-arrhythmic effects, the *popdc3* morpholino and the control morpholino were injected into the transgenic line *Tg(cmlc2:gCaMP)^{s878}* which also harbors the *silent heart* mutation. The heart of the *silent heart* mutant fails to contract because of a null mutation in the *cardiac troponin T* (*tnnt2*) gene. However, over time this mutant develops a pericardial edema and a lengthened heart. Therefore, it is possible to image the electrical activity of the heart only until day 4, because after this point the heart starts to collapse. Moreover, the phenotype induced by *silent heart* mutation, may also mask the morphologic cardiac phenotype that is induced by loss of *popdc3*. I first analyzed *popdc3* morphants and control morpholino-injected embryos at 3 dpf. At this stage, no difference between the morphants and controls was observed. In both cases the recorded movies demonstrated regular calcium transients traveling from the atrium to the AV canal where the calcium transients were slowed and were further propagated over the ventricle to the outflow tract (supplemental videos S10 and S11). The plotted fluorescence intensity over time of both movies revealed that no cardiac conduction phenotype could be observed at 3 dpf (Figure 36).

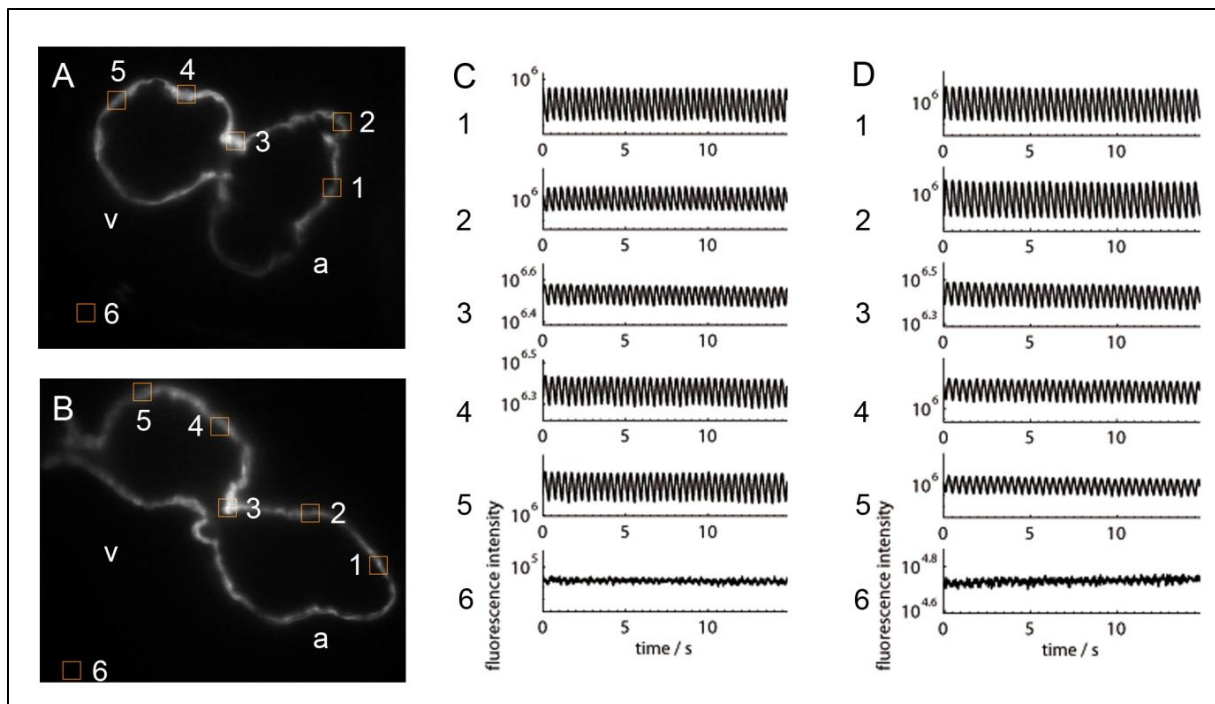


Figure 36: 3 dpf *popdc3* morphants do not exhibit any pathological alterations of cardiac conduction as revealed by SPIM analysis.

Optical sections of 3 dpf *Tg(cmlc2:gCaMP)^{s87b} × silent heart* zebrafish hearts from (A) a control and (B) a *popdc3* morphant. The numbered squares represent areas where calcium transients for the atrium, AV-canal, ventricle, and background were recorded. (C, D) Fluorescence intensity of a single pixel from each region was measured to obtain calcium transients and plotted over time in seconds. All plots are semi-logarithmic. (C) In the control heart fluorescence intensity varied with time in atrial and ventricular regions of the heart as the wave of depolarization propagated through the heart. (D) In the *popdc3* morphant heart identical fluorescence intensity variation was observed. Abbreviations: dpf = days post fertilization, a = atrium, v = ventricle.

Additionally, *popdc3* morphants and control injected embryos were imaged at 4 dpf. In the control injected embryo the calcium transients started at the inflow region of the atrium and proceeded after the AV conduction delay through the ventricle to the outflow tract (supplemental video 12). In contrast, the *popdc3* morphant displayed aberrant cardiac conduction. Initially, the calcium transients traveled normally through the atrium to the AV canal. In the AV canal and in the ventricle, however, the calcium transients progressed slower and seemed uncoupled to the calcium transients observed in the atrium (supplemental video 13). Thus, *popdc3* morphants develop a complete heart block, which is reminiscent to a third degree atrioventricular block, starting at 4 dpf similar to the *popdc2* morphants (Figure 37D). However, further work is required to study functional deficit in the *popdc3* morphants and to further delineate the defect observed in *popdc3* morphants.

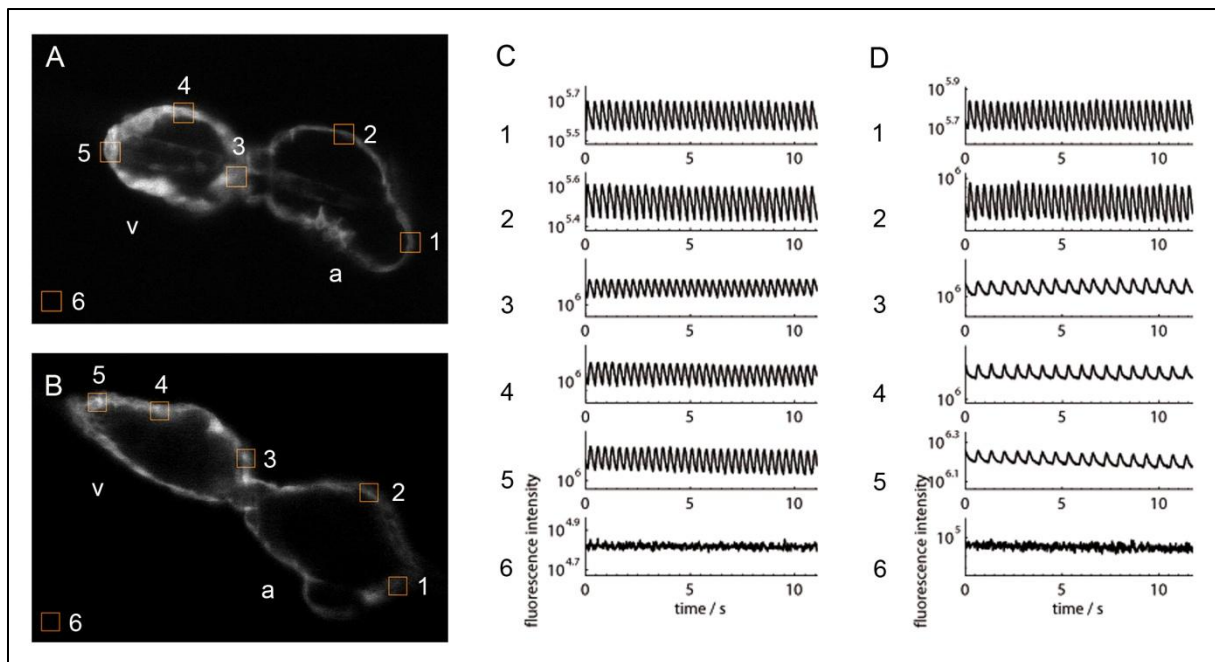


Figure 37: The 4 dpf *popdc3* morphant develop a complete heart block as revealed by SPIM analysis.

Optical sections of a 4 dpf *Tg(cmlc2:gCaMP)^{s878} x silent heart* zebrafish hearts from (A) a control morphant and (B) a *popdc3* morphant. SPIM videos were processed to determine the fluorescence intensity of selected regions represented by numbered squares over time. Each selected region has a corresponding number in the semilogarithmic plot aside (C, D). (A, C) in the control heart, the fluorescence intensity changed over time in atrial and ventricular regions of the heart as the wave of depolarization propagates through the heart. (B, D) In the *popdc3* morphant, fluorescence intensity varied in the atrium (1, 2) whereas in the ventricle a block of calcium transients was detected, representing a complete heart block (4, 5). Abbreviations: dpf = days post fertilization, a = atrium, v = ventricle.

6.4 Conserved amino acids within the *Popeye* domain are essential for *Popdc* function

Based on the observed results that *Popdc* genes in mice and zebrafish are important for cardiac conduction, my colleagues and I tested the hypothesis whether *Popdc* proteins are a novel family of channel proteins themselves or able to interact with ion channels. Therefore, I cloned the full coding sequence of murine *Popdc1*, *Popdc2* and *Popdc3* in the psGEM vector for the synthesis of capped mRNA, which is required for injection into frog or zebrafish oocytes. In collaboration with Prof. Erhard Wischmeyer, Institute of Physiology II, University of Würzburg, Germany, and Dr. Stephanie Breher, capped mRNA (cRNA) was injected into *Xenopus laevis* oocytes and the injected eggs were analyzed by voltage clamp technique in order to study single cell currents. Surprisingly, no current was measured when *Popdc1*, *Popdc2* or *Popdc3* mRNA was injected. However, co-injection of *Trek1* cRNA, a two-pore domain potassium channel, resulted in a significant increase of *Trek1* current. This findings demonstrate that *Popdc* proteins are not channel proteins for themselves but are capable to modulate channel activity such as that of *Trek1* (Breher, 2009).

Next, we tried to find out how *Popdc* proteins are able to modulate ion channel conductivity. Secondary structure predictions using Psipred (<http://bioinf.cs.ucl.ac.uk/psipred/psiform.html>) revealed similarity of the *Popeye* domain with a cyclic nucleotide-binding domain. Therefore, Dr. Stephanie Breher tested the ability of *Popdc* proteins to interact with cyclic nucleotides by binding of native *Popdc1* protein to cAMP agarose. She confirmed that *Popdc1*, 2 and 3 as well as the carboxy-terminus of *POPDC1* alone harboring the *Popeye* domain can bind to cAMP

agarose. The interaction of Popdc1 with cyclic nucleotides is specific hence competition of binding was successful only with cyclic AMP, but not with ATP (Breher, 2009). Within the putative PBC of the cAMP binding domain there are two highly conserved sequence motifs (DSPE and FQVT) which we hypothesized to be directly involved in cyclic nucleotide binding. To clarify this, Juliane Kultz generated point mutations in Popdc1 by substituting residues D200, P202 and E203 to alanine and residue V217 to phenylalanine. Her biochemical results revealed a reduced binding of Popdc1^{D200A}, Popdc1^{E203A} and Popdc1^{V217F} to cAMP agarose whereas Popdc1^{P202A} showed an increased affinity. The cAMP-binding efficiency can be described as follow: Popdc1^{P202A} > wt > Popdc1^{E203A} > Popdc1^{V217F} > Popdc1^{D200A} and highlights the importance of the conserved amino acids for cyclic nucleotide binding (Kultz, 2008).

6.4.1 Point mutations within the cyclic nucleotide binding domain of Popdc1 lead to a different cardiac phenotype in zebrafish embryos

To further elucidate the functional effect of these point mutations in Popdc1 *in vivo*, myc tagged Popdc1^{P202A}, Popdc1^{E203A}, Popdc1^{V217} and Popdc1^{D200A} constructs, which have been sub-cloned into the psGEM-Vector by Juliane Kultz, were transcribed to cRNA and injected into zebrafish embryos. The developing embryos were analyzed for the first 3 days of development to cover the time of cardiogenesis until chamber specification.

Injection of 100 pg wild type *Popdc1* (*Popdc1^{wt}*) capped RNA in 171 zebrafish embryos resulted in a cardiac overexpression phenotype. At 24 hpf, 7 percent of the injected embryos displayed signs of a slight pericardial edema and skeletal muscle defects. At 48 hpf the phenotype was more pronounced, 38 percent of the injected zebrafish embryos showed a slowed blood circulation, blood retention under the yolk and a faint pericardial edema (categorized as class I). In addition to the observed effects of class I categorized zebrafish embryos, 28 percent of the injected embryos had slight skeletal muscle defects (categorized as class II) (Figure 38). At 72 hpf, the blood retention declined in class I and class II categorized embryos while the pericardial edema increased (Figure 38B, D).

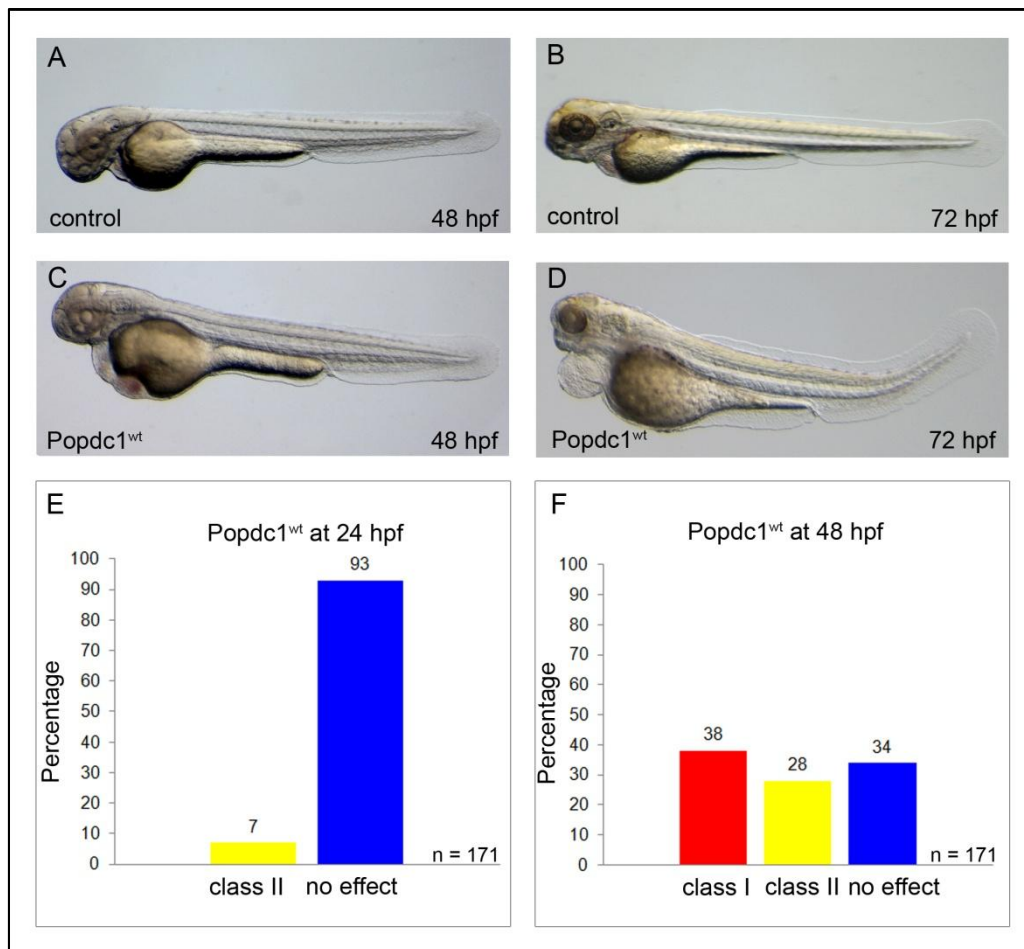


Figure 38: *Popdc1*^{wt} overexpression induces a cardiac phenotype.

Lateral views of (A, B) uninjected control embryos and (C, D) embryos injected with mouse *Popdc1*^{wt} cRNA at 48 hpf and 72 hpf. (E, F) Diagram of the relative number of embryos with pathological phenotype. The diagrams display the first sign of an overexpression phenotype at 24 hpf (E) and the fully developed cardiac phenotype at 48 hpf (F). (C) At 48 hpf the mean percentage of the embryos developed a pericardial edema, slowed blood circulation and blood retention. (D) At 72 hpf, the blood retention declined while the pericardial edema increased. Abbreviations: class I = embryos displaying pericardial edema, blood retention and slowed circulation, class II = embryos displaying the observed phenotype categorized in class I plus a slight skeletal muscle defect in the tail, hpf = hours post fertilization.

In contrast to the pathological phenotype in embryos injected with *Popdc1*^{wt} cRNA, *Popdc1*^{D200A} cRNA induced only in 8 percent out of 149 injected embryos a pathological phenotype in the heart. This phenotype was similar to that observed in embryos receiving *Popdc1*^{wt} cRNA. When the amount of cRNA was increased from 100 to 240 pg no further increase in the amount of embryos with an aberrant morphology was observed (Figure 39). Therefore, the conserved amino acid aspartate on position 200 is not only necessary for efficient cAMP binding but also essential to induce an overexpression phenotype in zebrafish. Thus, cAMP-binding is essential for the biological function of *Popdc1* *in vivo*.

Additionally, injection of either 100 pg or 240 pg of *Popdc1*^{V217F} cRNA resulted in a decreased number of embryos with pericardial edema compared to *Popdc1*^{wt} cRNA. Only 23 percent (n = 103) showed any pathology, whereas the majority of *Popdc1*^{V217F} expressing embryos had a wild type like appearance as the uninjected control embryos (Figure 39G to H). Similar to point mutation *Popdc1*^{D200A}, *Popdc1*^{V217F} had only a minor effect after being overexpressed.

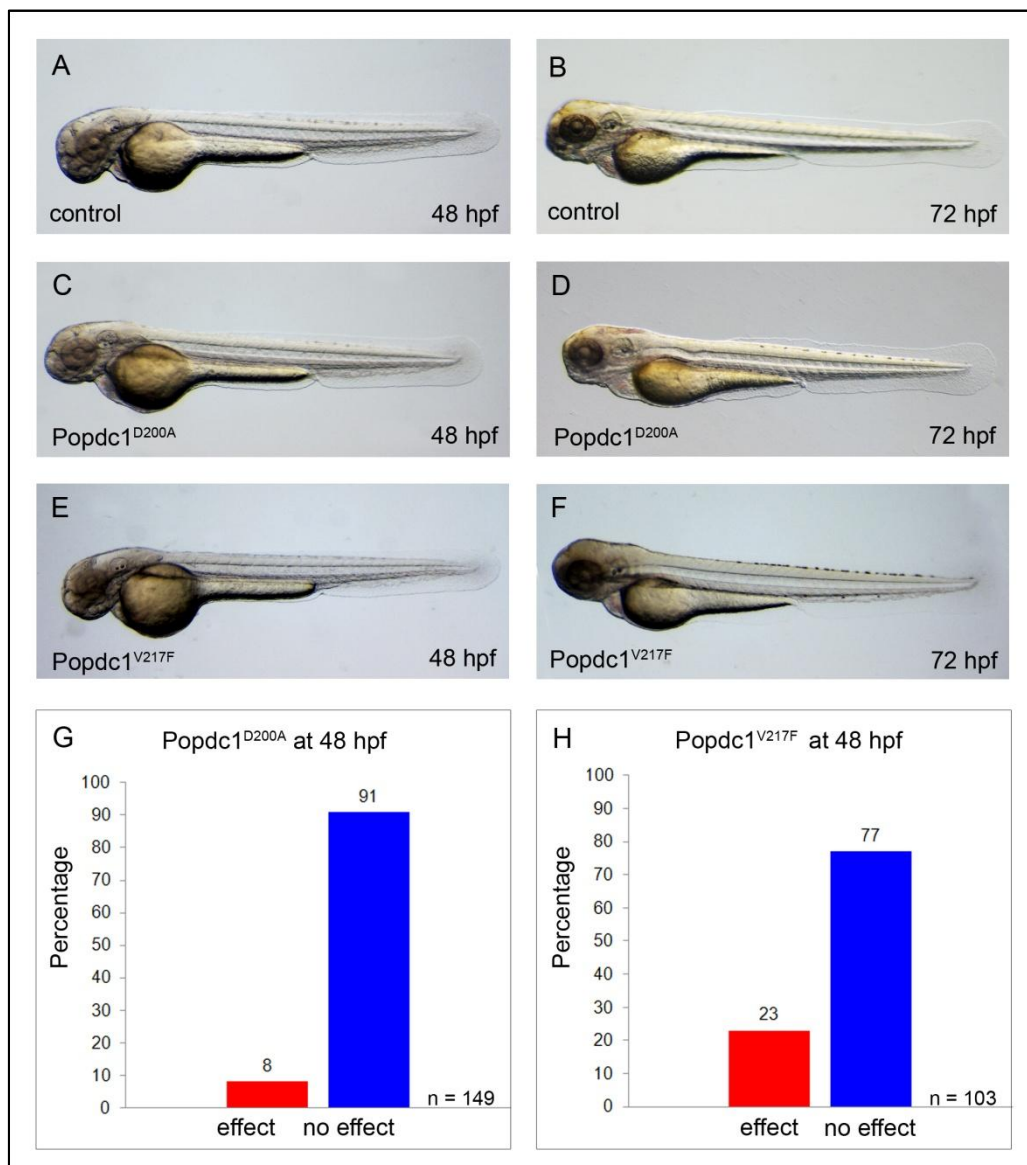


Figure 39: Overexpression of *Popdc1^{D200A}* or *Popdc1^{V217F}* has no or only very mild effects on zebrafish embryogenesis. (A, B) Lateral view of uninjected control embryos (These are the same as the one shown in Figure 38). Representative zebrafish embryos injected with either (C, D) *Popdc1^{D200A}* or (E, F) *Popdc1^{V217F}* at 48 hpf and 72 hpf displayed no difference to control embryos. The diagram of (G) *Popdc1^{D200A}* injected embryos or (H) *Popdc1^{V217F}* injected embryos demonstrate the faint effect on zebrafish heart function. Abbreviations: hpf = hours post fertilization.

Overexpression of *Popdc1^{P202A}* and *Popdc1^{E203A}* in contrast affected cardiac development and induced cardiac pathology in a frequency which was more extensive than that of *Popdc1^{V217F}*, but less than that of *Popdc1^{wt}* (Figure 40).

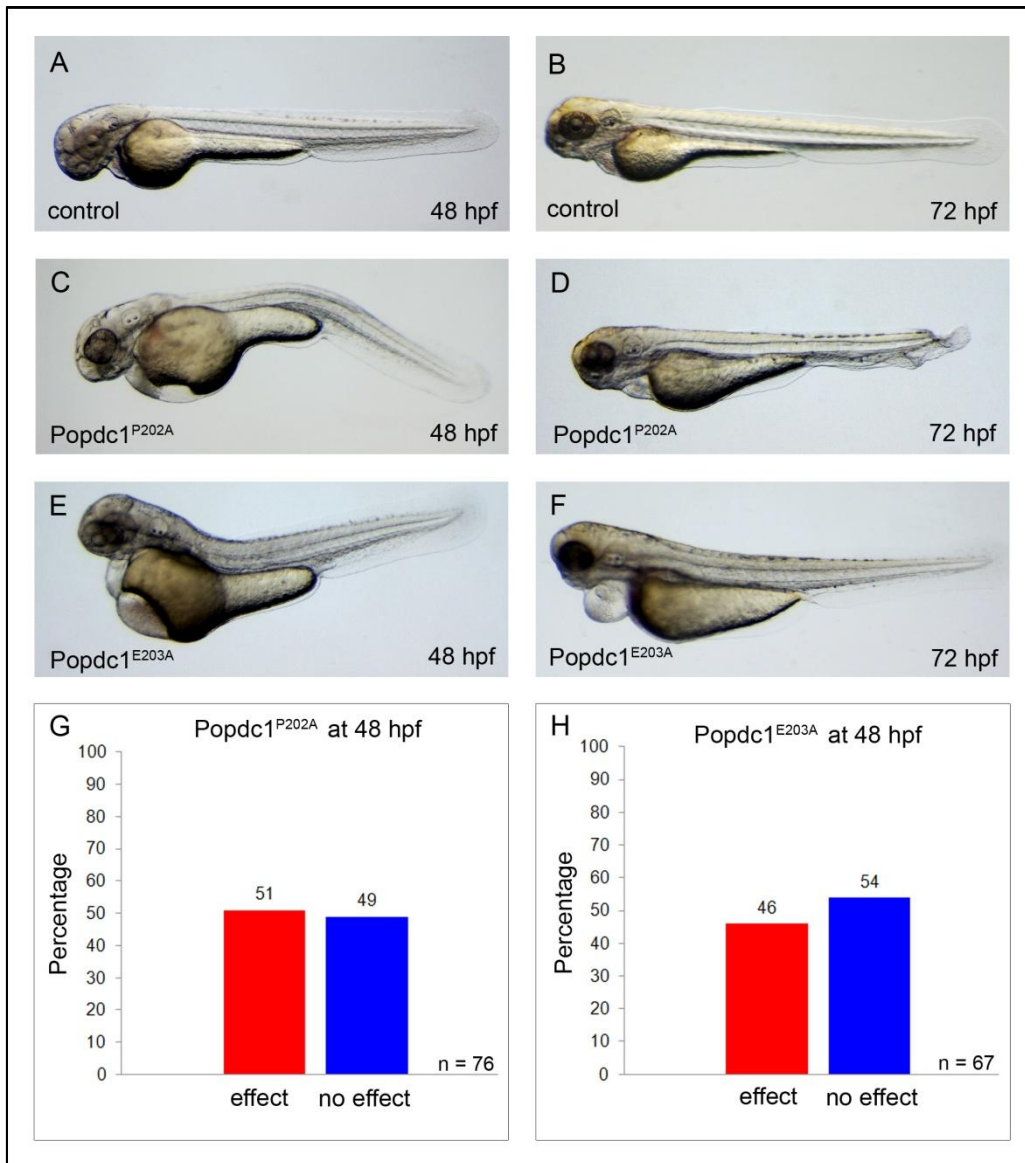


Figure 40: Injection of *Popdc1^{P202A}* and *Popdc1^{E203A}* resemble *Popdc1^{wt}* overexpression phenotype

Lateral views of (A, B) uninjected control embryos (These are the same as the one shown in Figure 38) (C, D) *Popdc1^{P202A}* and (E, F) *Popdc1^{E203A}* expressing embryos at 48 hpf and 72 hpf. *Popdc1^{P202A}* and *Popdc1^{E203A}* mutants displayed a clear cardiac phenotype with pericardial edema, blood retention and curved tail at 48 hpf resulting in pericardial edema and tail malformation at 72 hpf. Diagrams of phenotypically affected embryos showed that injection of the point mutation *Popdc1^{P202A}* resulted in a cardiac phenotype in 51 % of the embryos (G) while in *Popdc1^{E203A}* expressing embryos 46 % displayed a cardiac phenotype (H). Abbreviations: hpf = hours post fertilization.

Taken together, there is a strong correlation between cAMP binding ability and the number of zebrafish embryos with a pathological phenotype after injection of the particular cRNAs (Figure 41).

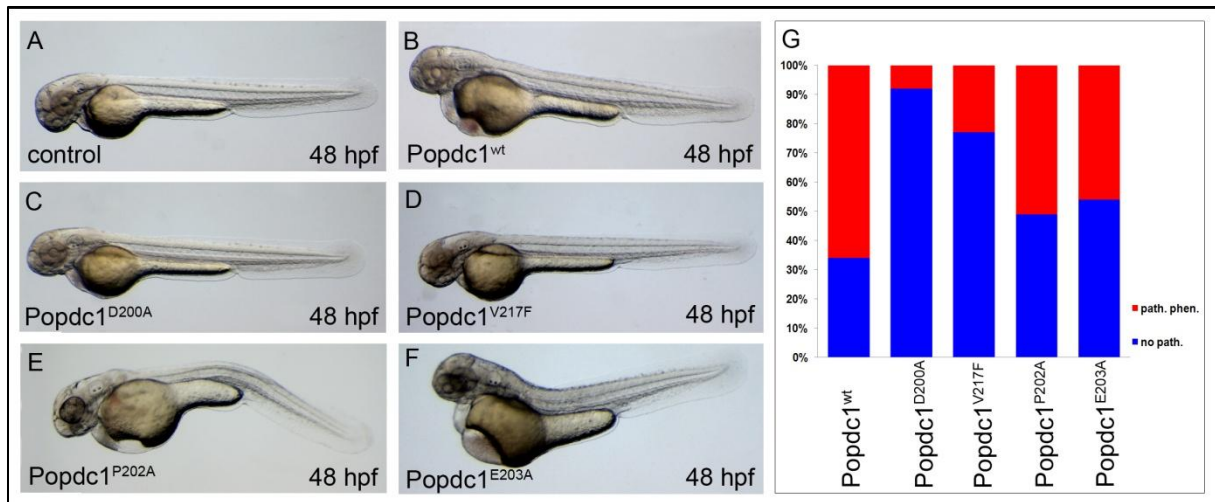


Figure 41: Overview of cardiovascular pathology after overexpression of Popdc1

(A-F) Bright field images of 48 hpf zebrafish embryos in lateral view from an uninjected embryo (A) or from embryos injected with (B) *Popdc1*^{wt}, (C) *Popdc1*^{D200A}, (D) *Popdc1*^{V217F}, (E) *Popdc1*^{P202A} and (F) *Popdc1*^{E203A}. (G) Diagram of embryos with normal (no pathological phenotype = no. path.; blue columns) or pathological phenotype (path. phen.; red column).

To get a deeper insight into the heart phenotypes of the *Popdc1* point mutations, I injected cRNA carrying point mutations into the transgenic zebrafish line *Tg(cmlc2:GFP)*. In contrast to the uninjected wild type embryos, which display a clear cardiac looping, the cardiac chambers of the *Popdc1* injected embryos appeared non-looped. This is probably caused by the pericardial edema which developed in these embryos due to cardiac malfunction and caused a lengthening of the whole heart. Although the heart chambers are not well looped, it is easy to distinguish the thick-walled ventricular and the thin-walled atrial chamber as well as the atrioventricular boundary of the *Popdc1* overexpressing zebrafish embryos (Figure 42).

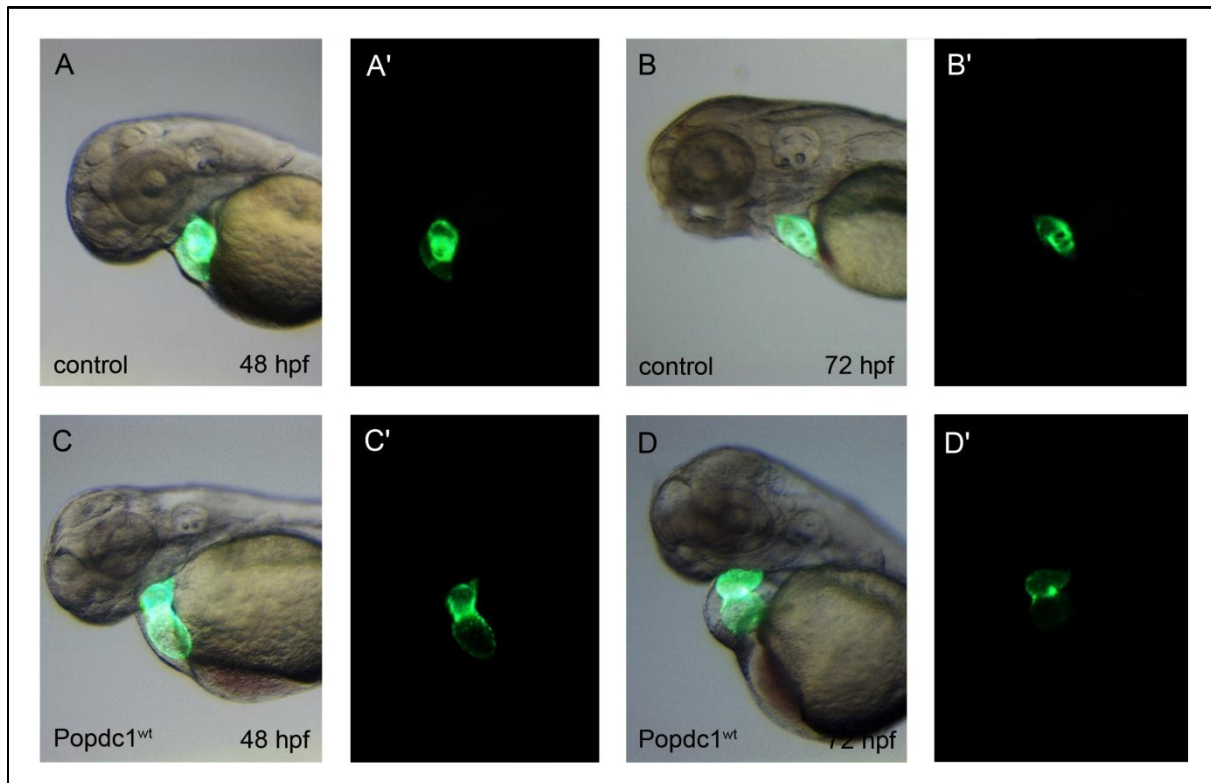


Figure 42: Overexpression of Popdc1 due to a lengthening of the heart chambers.

Overlays of brightfield pictures with the corresponding fluorescent images (A', B', C', D') of wild type embryos at (A) 48 hpf and (B) 72 hpf and the Popdc1 overexpressing embryos at (C) 48 hpf and (D) 72 hpf. The wild type embryo clearly showed the looped heart and the heart chambers (A- B'). Injection of Popdc1 capped RNA resulted in embryos with pericardial edema and blood retention (C-D'). Due to the edema the heart chambers are lengthened and cardiac looping was not observed. Abbreviations: hpf = hours post fertilization, wt = wild type.

As illustrated above, after injection of the point mutations Popdc1^{D200A} and Popdc1^{V217F} the overall phenotypes resembled the uninjected control. Upon closer examination no obvious change of the whole heart was discernible. No pericardial edema was observed, and the cardiac chambers were looped as expected. Furthermore, I could clearly distinguish the atrioventricular canal (Figure 43).

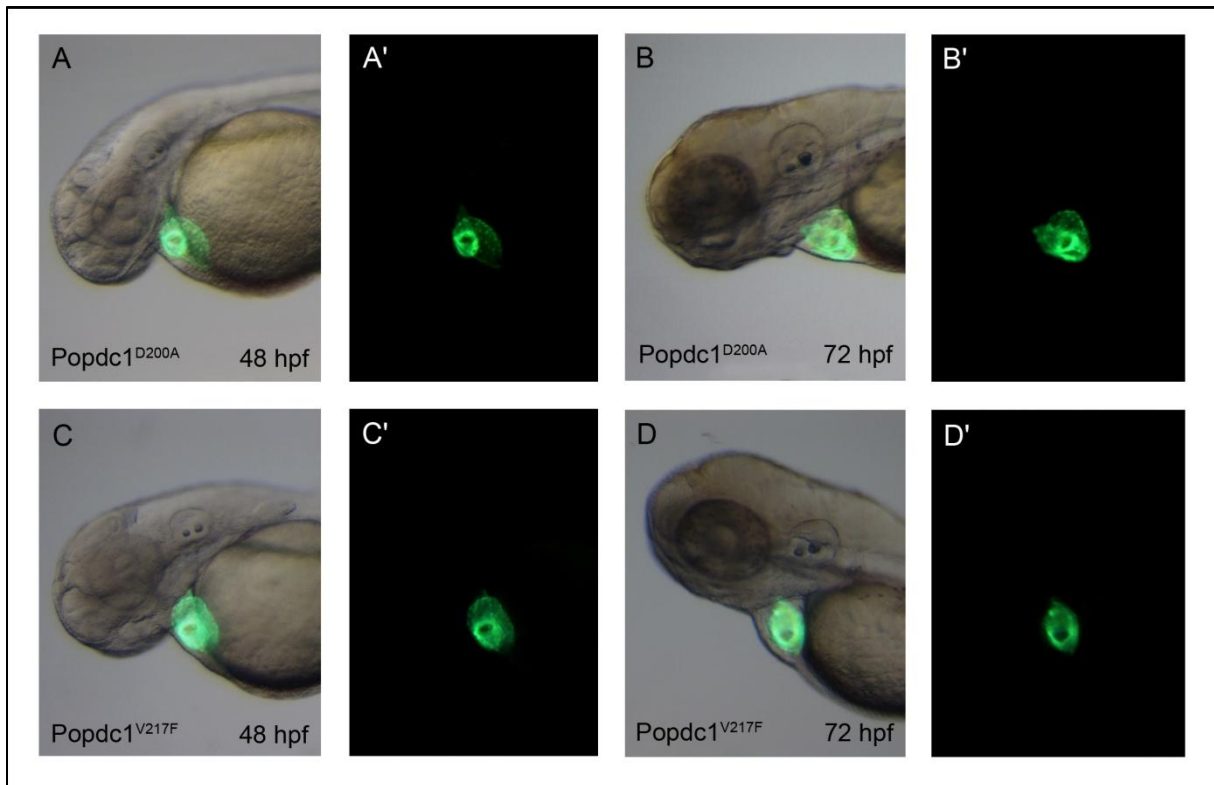


Figure 43: Point mutants *Popdc1^{D200A}* and *Popdc1^{V217F}* display no heart phenotype.

(A-D) Overlays of brightfield images with (A'-D') the fluorescent counterparts revealed that no gross morphological change of the heart could be observed in (A-B) *Popdc1^{D200A}* and (C-D') *Popdc1^{V217F}* expressing zebrafish embryos. Abbreviations: hpf = hours post fertilization.

Injection of *Popdc1^{P202A}* and *Popdc1^{E203A}* capped RNA into *Tg(cmlc2:GFP)* transgenic zebrafish eggs provided further evidence for the importance of cAMP binding of the Popdc1 Protein. *Popdc1^{P202A}* or *Popdc1^{E203A}* point mutants displayed pericardial edema, blood retention under the yolk and no heart looping at 48 hpf. Between 48 hpf and 72 hpf the pericardial edema increased and the ventricle collapsed, but the chambers were clearly distinguishable as well as the atrioventricular canal. Therefore, the ventricle seemed to be small and thickened at 72 hpf (Figure 44). Interestingly, the observed *Popdc1^{P202A}* point mutants were affected in the same extent as the *Popdc1^{wt}* expressing zebrafish embryos.

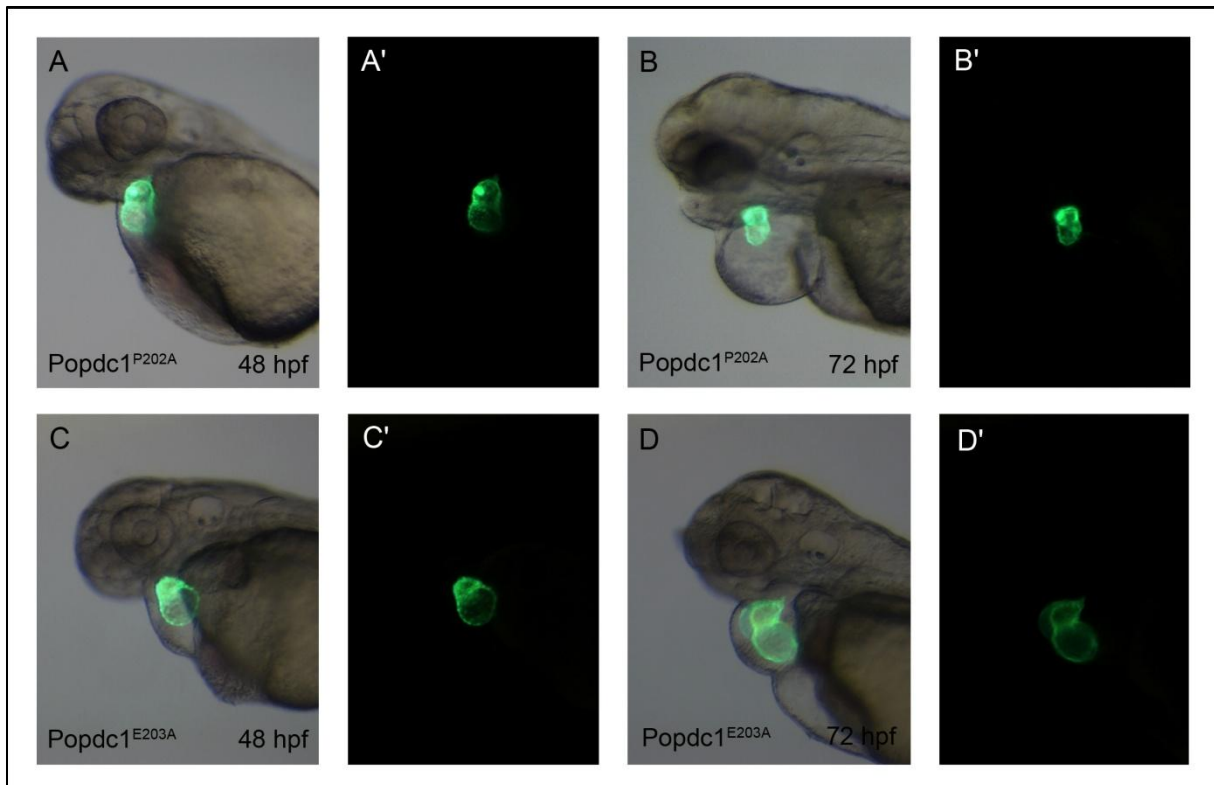


Figure 44: Point mutations Popdc1^{P202A} and Popdc1^{E203A} intensify the observed Popdc1 overexpression phenotype

(A, B, C, D) Overlay pictures of living zebrafish embryos presenting the merge of a brightfield and the corresponding fluorescence images (A', B', C', D'). Popdc1^{P202A} (A, A') and Popdc1^{E203A} (C, C') at 48 hpf displayed pericardial edema, blood retention and a non-looped heart. At 72 hpf Popdc1^{P202A} (B, B') and Popdc1^{E203A} (D, D') showed a collapsed ventricle and an increased edema. Abbreviations: hpf = hours post fertilization.

In order to further analyze the structural changes by histology, uninjected zebrafish embryos or zebrafish embryos expressing the point mutants Popdc1^{D200A}, Popdc1^{P202A}, or Popdc1^{wt} were embedded in plastic, sectioned and stained with hematoxylin/eosin. Transversal sections of uninjected embryos revealed the presence of a thin-walled atrium, an AV canal with cardiac cushions and a thick-walled ventricle. Because there was no pericardial edema, the heart is closer to the yolk. In contrast, Popdc1^{wt} injected embryos displayed pericardial edema and a lengthened heart. Despite the lengthened, nearly non-looped heart, the myocardium of atrium and ventricle resembled the wild type section and cardiac cushions could also be observed. The histological section of an embryo expressing the point mutation Popdc1^{D200A} was similar to the wild type section. The heart was looped, the myocardium of the atrium was thin-walled in contrast to the thick-walled ventricle and the cardiac cushion could be easily identified. However, the histology of the embryo expressing the point mutation Popdc1^{P202A} displayed a huge pericardial edema and a small heart. The thickness of the myocardium was not changed. Although the cushions could be detected, the heart itself was malformed (Figure 45).

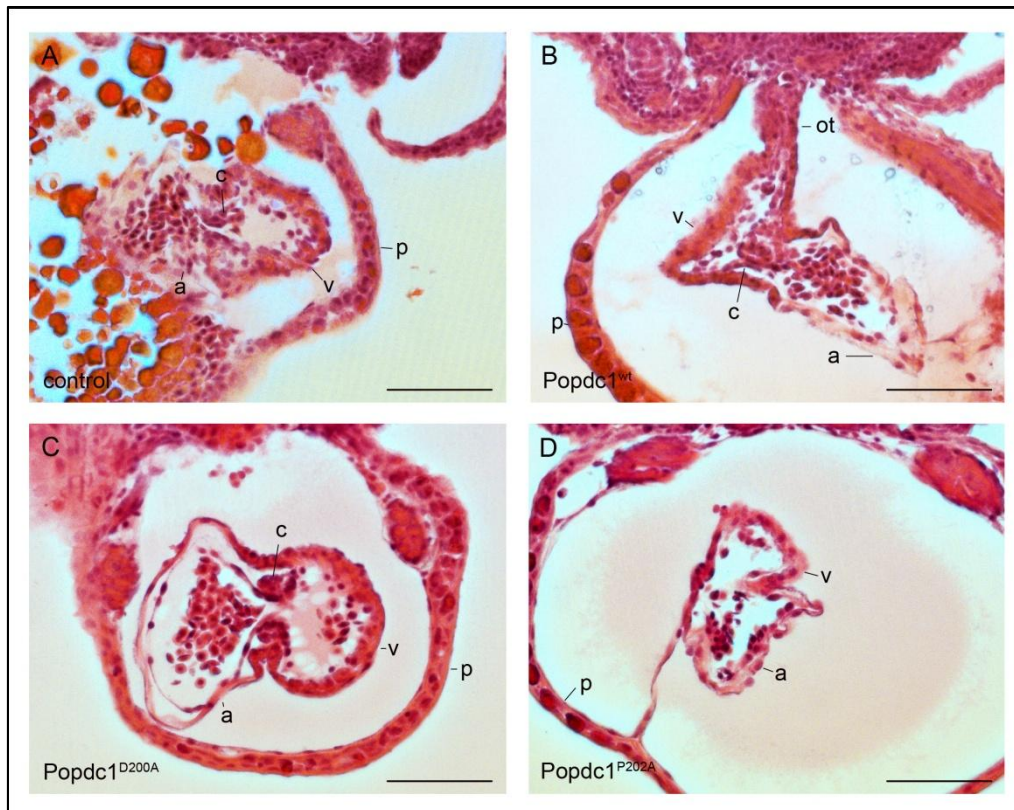


Figure 45: Histology of the embryonic zebrafish heart after overexpression of Popdc1^{wt}, Popdc1^{D200A} and Popdc1^{P202A}. (A-D) Transversal sections of the heart region of 48 hpf zebrafish hearts which were hematoxylin/eosin stained. (A) uninjected control, (B) Popdc1^{wt}, (C) Popdc1^{D200A} and (D) Popdc1^{P202A}. (B) Overexpression of wild type Popdc1 led to a non-looped lengthened heart, but the myocardium and the cardiac cushions were unchanged. (C) Zebrafish embryos expressing point mutation Popdc1^{D200A} resemble (A) control embryos. (D) Zebrafish embryos expressing point mutation Popdc1^{P202A} displayed a smaller, malformed heart. The myocardium seemed not to be affected and cardiac cushions could be detected. Abbreviations: a = atrium, c = cardiac cushions; p = pericard, v = ventricle, wt = wild type. Scale bar = 100 μ m.

To confirm that the cRNAs injected into the embryos were actually translated into protein, injected zebrafish embryos at different stages of development (shield stage, somite stage, 24 hpf, 48 hpf and 72 hpf) were used for detecting the recombinant proteins by Western blot analysis. However, this approach turned out to be difficult for different reasons. One major problem was the high proportion of yolk proteins in the early developing embryos. If the yolk was not removed, only 1 or 2 embryos (50 – 100 μ g) could be loaded per lane in order to avoid overloading effects which were due to the yolk protein. Moreover after loading protein of one embryo, I got major distortions in the molecular weight range of 80 to 100 kD caused by the dominant yolk protein vitellogenin which in turn diminished the chance to detect the expected Popdc1 protein at 50 kD. To increase the yield of non-yolk protein, I tried a deyolking method published by Link and colleagues (Link et al., 2006). Although this method reduced the yolk protein, our antibody directed against the myc-tag gave strong background bands. Furthermore, several other myc antibodies have been used and none gave satisfying results. Moreover, expression of Popdc1^{wt} as GFP fusion protein revealed that Popdc1 is really translated and is present in the plasma membrane (Franziska Guenther, unpublished observations).

6.4.2 Point mutations within the cyclic nucleotide binding domain of Popdc2 or overexpression of Popdc2 results in no obvious phenotype in zebrafish

Patrick Meister demonstrated in his diploma thesis that Popdc2^{D184A} and Popdc2^{V201F} displayed reduced binding to cAMP-agarose whereas Popdc2^{E187A} showed enhanced binding (Meister, 2008). For the *in vivo* analysis Popdc2^{wt}, Popdc2^{D184A} and Popdc2^{V201F} were subcloned into psGEM. cRNA transcripts of the various constructs were injected into 1-2 cell stage zebrafish embryos. Interestingly, in contrast to the results of Popdc1, injection of Popdc2^{wt} cRNA did not lead to an obvious overexpression phenotype. Only 10 percent of the 72 injected embryos displayed slight pericardial edema (Figure 46). Furthermore, an increase of the amount of cRNA that was injected had no significant effect on zebrafish development in general or cardiac development in particular.

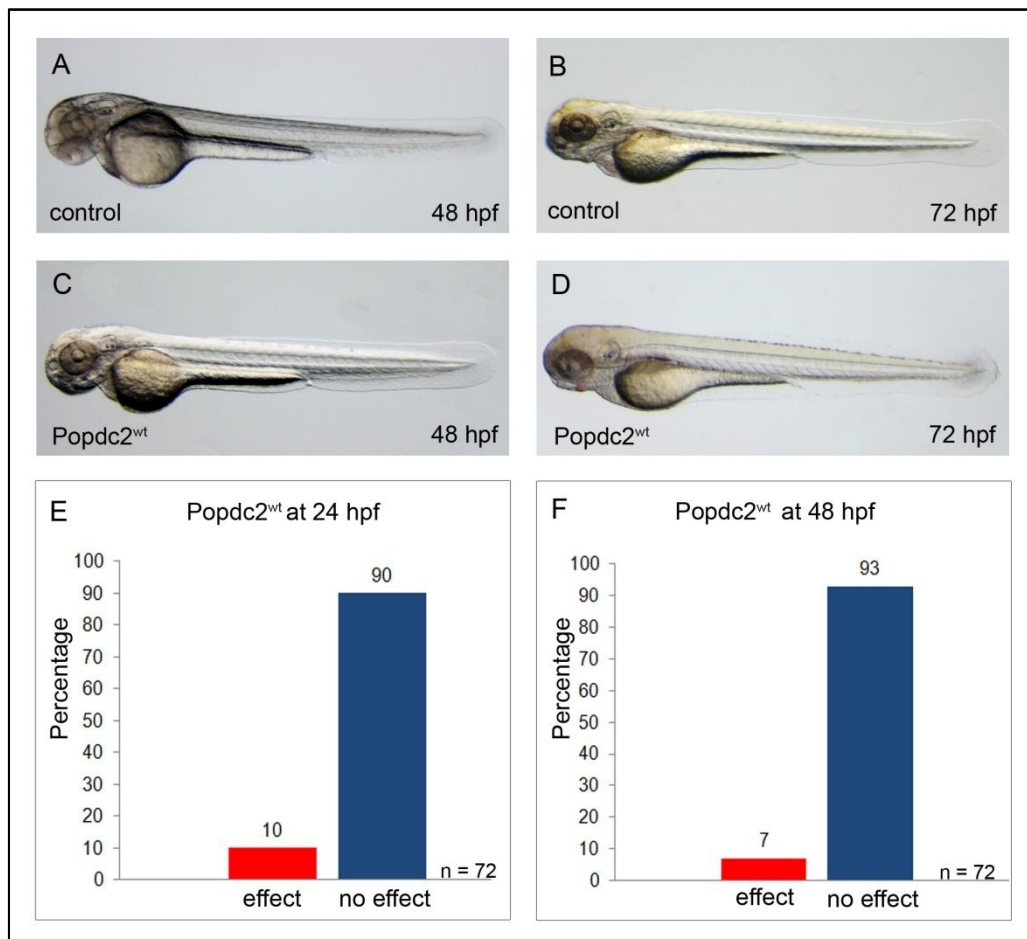


Figure 46: Popdc2 overexpression in zebrafish embryos resulted in no obvious phenotype.

(A, B) Lateral views of uninjected control and Popdc2 injected embryos at (C) 48 hpf and (D) 72 hpf. Overexpression of Popdc2 did not affect embryonic development. Diagrams of the number of embryos which were unaffected or showed signs of pathology at (E) 24 hpf and (F) 48 hpf. Only 10 % of the Popdc2 injected embryos at 24 hpf and 7% at 48 hpf displayed some form of pathology. Abbreviations: hpf = hours post fertilization.

Similarly, injection of the *Popdc2^{D184A}* and *Popdc2^{V201F}* cRNA in zebrafish embryos had no significant effect. The majority (83% in *Popdc2^{D184A}*, n = 66 and 88% in *Popdc2^{V201F}*, n = 17) of embryos developed no cardiovascular phenotype or any other defect (Figure 47).

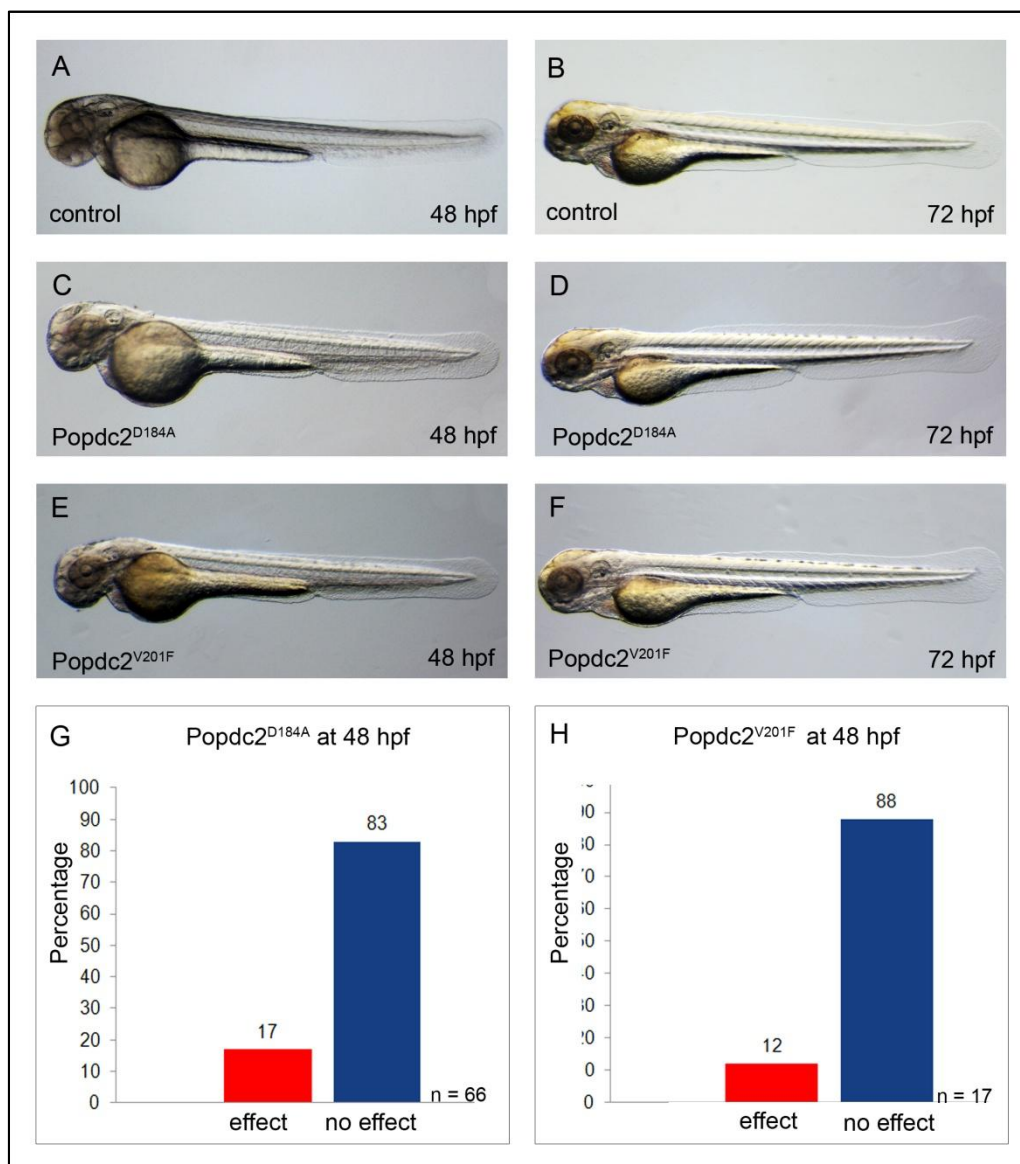


Figure 47: Overexpression of *Popdc2^{D184A}* or *Popdc2^{V201F}* have only marginal effects on zebrafish development. (A, B) Lateral view of uninjected control embryos. These are the same as the one shown in Figure 46. Pictures of representative zebrafish embryos injected with either (C, D) *Popdc2^{D184A}* or (E, F) *Popdc2^{V201F}* at 48 hpf and 72 hpf displayed no difference to wild type control embryos. The diagram of (G) *Popdc2^{D184A}* injected embryos or (H) *Popdc2^{V201F}* injected embryos demonstrates the faint effect on zebrafish heart function. Abbreviations: hpf = hours post fertilization.

6.5 Expression analyses of genes linked to arrhythmia

To date the zebrafish cardiac conduction system is rarely analyzed. Aside from cardiac action potential analysis and analysis of calcium release as a surrogate of the cardiac excitation pattern, little to nothing is known about the existence or absence of a sinoatrial node in zebrafish (Hu et al., 2000; Sedmera et al., 2003). Because of the observed cardiac arrhythmia phenotype in *popdc2* and *popdc3* morphants and particularly the distinct expression pattern of *popdc2* and *popdc3* in the zebrafish heart, it was worthwhile to search for marker genes which have been associated with development of the cardiac conduction system in other model systems. These marker genes should be further used to analyze the morphant's phenotype. Furthermore, I aimed to find marker genes for cardiac conduction system development in zebrafish.

6.5.1 *Shox2* is predominantly expressed in heart and brain in zebrafish development

The first candidate gene I focused on was *Shox2*. *Shox2* is a member of a small subfamily of paired, related homeodomain transcription factors (Blaschke et al., 1998). Due to its specific expression in the sinoatrial node in mice and the fact that *shox2* morpholino injected zebrafish embryos develop a severe sinus bradycardia as well as a sinus node exit block after 72 hpf (Blaschke et al., 2007), I decided to generate an *in situ* probe against zebrafish *shox2*. With the help of this probe I tried to identify the sinus node region in zebrafish, which until now has not yet been described.

At 24 hpf no *shox2* expression in the zebrafish heart tube could be detected, but strong *shox2* expression was observed in the diencephalon (Figure 48A-B). At 48 hpf, the expression in the brain increased. Thus, *shox2* expression was now found in the cranial ganglion, diencephalon, hindbrain, optic tectum and tegmentum (Figure 48C, D, F). Additionally, *shox2* was expressed in the ventral part and the apical ectodermal ridge of the pectoral fin. Although *shox2* expression was not found in the whole heart, 2 distinct but faint spots of *shox2* expression were detected right beneath the heart, which probably represents the bilateral inflow tract (Figure 48E).

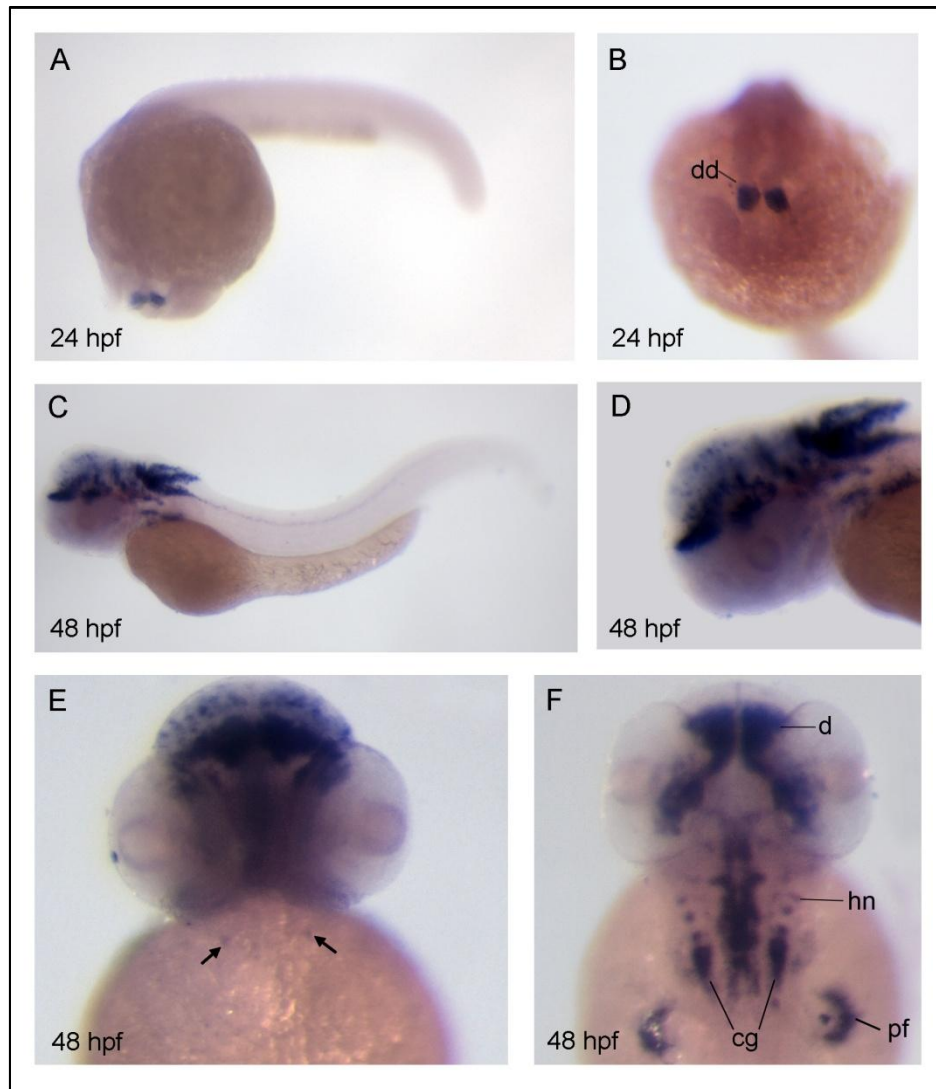


Figure 48: *Shox2* expression in the developing zebrafish embryo.

(A, C; D) Lateral, (F) dorsal and (B, E) ventral view of (A, B) 24 hpf and (C-F) 48 hpf embryos that were subjected to whole mount *in situ* hybridization analysis using a *shox2* probe. (A, B) At 24 hpf, *shox2* expression was observed in the dorsal diencephalon (dd). (C-F) At 48 hpf *shox2* was expressed in cranial ganglia (cg), diencephalon (d), hindbrain neurons (hn), optic tectum and pectoral fin (pf). At 48 hpf 2 distinct spot-like expression domains are present in the inflow tract region of the heart (E). Abbreviations: hpf = hours post fertilization.

6.5.2 The duplicated *hcn4* gene is expressed in distinct regions of the heart and in the diencephalon

As a second candidate gene to identify the pacemaker region of the zebrafish heart, I have chosen the *Hcn4* gene. *Hcn4* encodes for a voltage-gated channel, which is regulated by cyclic nucleotides (Kaupp et al., 2002; Biel et al., 2007). The channel produces a cation current that is slowly activated by membrane hyperpolarization (termed I_h , I_f , or I_q). I_h is known to control the heart rate and rhythm by acting as “pacemaker current” in the sinoatrial node, where *Hcn4* is predominantly expressed (Baruscotti et al., 2005). However, deletion of *Hcn4* in mice at adult stage only resulted in cardiac arrhythmia characterized by recurrent sinus pauses (Herrmann et al., 2007). Right now, nothing is known about the expression or role of *hcn4* in the zebrafish. Therefore, I used the blast algorithm of Ensembl (www.ensembl.org) to look for *hcn4*-related genes. I found two candidate genes,

which are located on chromosome 18 and 25, respectively. After cloning of a partial sequence by RT-PCR of the two candidates, I analyzed their expression pattern by whole mount *in situ* hybridization. I was interested if both *hcn4*-related genes are expressed in the heart, and if they have identical expression pattern or not. In both cases I found a nearly identical expression pattern (Figure 49). The strongest expression domain was observed in the brain. Cryosections through the brain revealed that the expression was mainly in the diencephalon (Fabai Wu, unpublished observations). At 48 hpf, when the cardiac chambers were already formed, I detected expression in the upper part of the heart which was divided into two spots (Figure 49B and D). Unfortunately, only with the whole mount *in situ* hybridization data in hand I was unable to determine whether the ventricle or the outflow tract expressed *hcn4*. In the future we have to identify the exact region of the two spots within the heart by double *in situ* hybridization analysis, furthermore, the stained embryos will need to be sectioned.

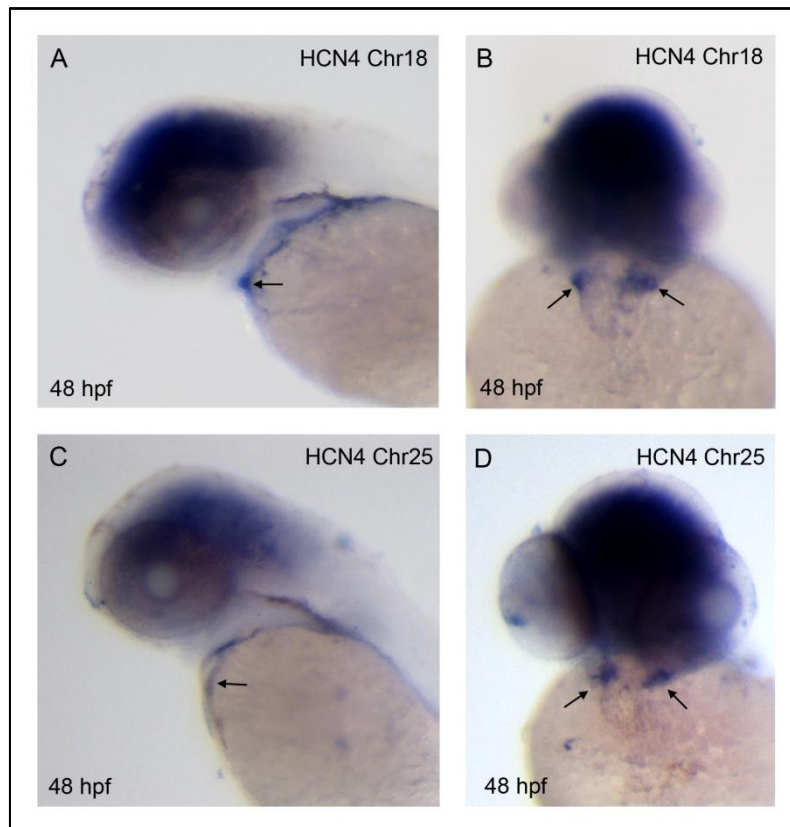


Figure 49: *Hcn4* expression is found in zebrafish brain and heart. (A-D) Whole mount *in situ* hybridization of *hcn4* related genes using 48 hpf zebrafish embryos. (A, B) Expression pattern of the *hcn4* related gene located on chromosome 18. (C, D) Expression pattern of the *hcn4* related gene located on chromosome 25 (C, D). Both genes are highly expressed in the brain and in two distinct spot-like expression domains in the heart (B, D). Abbreviations: hpf = hours post fertilization.

Unfortunately, neither of these two marker genes was expressed in the pacemaker region. Therefore, I did not perform expression analysis in the morphant's hearts. Moreover, since the cardiac conduction phenotype of *popdc2* and *popdc3* morphants primarily affect the atrioventricular canal and cause an AV block rather than affect the sinus node, other marker genes are probably more suitable.

7 DISCUSSION

7.1 Evolutionary conservation of *Popdc* gene family

7.1.1 Expression pattern

Previous data have suggested that in vertebrates such as frog (Hitz et al., 2002), chick, mouse and man (Andree et al., 2000; Breher et al., 2004; Froese and Brand, 2008; Torlopp et al., 2006) *Popdc* genes are expressed in heart and skeletal muscle. In this thesis I was able to confirm and extend this observation to the model system zebrafish. Furthermore, using whole mount *in situ* hybridization, I was able to show that *popdc2* is only expressed in the heart and skeletal muscles, whereas *popdc1* (Franziska Guentner, unpublished observations) and *popdc3* were also detected in the brain and other organs. The fact that *popdc2* expression during embryogenesis appears to be limited to muscle tissue, whereas *popdc1* and *popdc3* have a broader tissue distribution, was also observed in other model systems (Andree et al., 2000). Additionally, in mouse and chick hearts one *Popdc* gene was expressed transiently in subregions of the heart while another gene was expressed in the entire heart (Andree et al., 2000). In zebrafish, *popdc1* (Franziska Guentner, unpublished observations) and *popdc2* are both expressed throughout the heart with *popdc2* being stronger than *popdc1*, whereas *popdc3* is only expressed in distinct regions in the heart. This expression pattern of the heart and skeletal muscle is similar to the one, which was observed in the mouse and chick embryo. However, in the mouse, *Popdc2* expression was also detected in various smooth muscles-containing organs such as uterus, stomach, gut and even in the epithelium of the stomach (Froese and Brand, 2008). Thus, most likely, those expression patterns were not seen during the here utilized observation period or there is a fundamental difference between fish and terrestrial vertebrates. This is likely particularly with regard to the digestive system, which is known to be highly species specific.

Zebrafish *popdc2* expression started in the somites, whereas expression in the myocardium was first detected after fusion of the bilateral heart field and expression was maintained at least throughout the next three days. In *Popdc2^{-/-}* mice, strong *Popdc2-LacZ* labeling was found in the cardiac crescent and could be detected in the whole heart until adulthood. Furthermore, at E10.5, the myotomes within the somites and the putative facial muscle precursor cells were LacZ stained (Froese and Brand, 2008). Interestingly, at 72 hpf in zebrafish *popdc2* was also expressed in the facial muscles.

Alexander Froese revealed in his Ph.D. thesis that in adult heart tissue of transgenic *Popdc2^{-/-}* mice the cardiac conduction system like the sinoatrial node, the His bundle and the Purkinje fibers were strongly labeled by the *LacZ* transgene. This expression pattern was confirmed for the endogenous gene by whole mount *in situ* hybridization (Froese, 2008). However, in 72 hpf zebrafish embryos, no preferential expression in elements of the cardiac conduction system was detected by whole mount *in situ* hybridization nor observed on *in situ* sections of the heart. Possibly, 72 hpf zebrafish embryos are too young to detect differences between conduction tissue and working myocardium, although the zebrafish heart matures faster as the mouse one (Fishman and Chien, 1997; Stainier, 2001). Sections through an adult zebrafish heart and subsequent staining for *popdc2* expression could

solve the problem, however, to date the cardiac conduction system in zebrafish is not well delineated because of a lack of proper marker genes and of knowledge of its anatomic location. It is even not clear so far whether a sinoatrial node exists (Sedmera et al., 2003).

7.1.2 Function

Not only the overall expression pattern is conserved during evolution, but also the functional properties of the *Popdc* gene family are similar. Both, *Popdc1* and *Popdc2* null mutants in mice, and *popdc1*, *popdc2*, and *popdc3* zebrafish morphants develop cardiac conduction abnormalities (Froese et al., in preparation; Froese, 2008; Breher, 2009). In *popdc2* morphants, I observed irregular ventricular contractions with 2:1 and 3:1 atrioventricular (AV) block. Moreover, recordings of calcium transients using an indicator transgenic line *Tg(cmlc2:gCaMP)^{s878}* and SPIM confirmed the presence of an AV block in *popdc2* morphants. At later stages of cardiac maturation, also sinus pauses could be detected.

Consistent with these findings for *popdc2*, also in *popdc3* morphants an atrioventricular block was observed. In contrast to *popdc2* and *popdc3*, *popdc1* morphants did not develop an AV block but showed an overall reduced beating rate indicative of a sinus bradycardia and a weak contracting ventricle (Franziska Guenther, unpublished observation).

Different from the spontaneously developing phenotype in zebrafish larvae, *Popdc1^{-/-}* and *Popdc2^{-/-}* mice develop only stress-induced and age-dependent arrhythmia. At 3 months age, no arrhythmia could be detected in *Popdc2* null mutant mice, but between 3 and 8 months the stress-induced sinus pauses increased, and 8 month old *Popdc2^{-/-}* mice displayed an average of 542 ± 275 sinus pauses during 30 minutes compared to 2 ± 3 sinus pauses in wild type mice. This bradycardia phenotype is accompanied by degeneration of the inferior region of the sinus node (Froese et al., in preparation). Similar results were obtained for *Popdc1* null mutant mice (Breher, 2009). Interestingly, *popdc* morphants develop cardiac conduction abnormalities before adulthood. Probably, this is due to the rapid zebrafish development and life cycle, e.g. at 3 dpf zebrafish embryos are free-swimming larvae which already start to eat (Fishman and Chien, 1997; Kimmel et al., 1995). Moreover, zebrafish have a lower heart rate with 80 – 160 bpm (beats per minute), whereas mouse embryos display a heart rate of 300 – 600 bpm. These differences in heart rate also influences the heart cycle, especially the repolarization and the ion channel settings (Dahme et al., 2009) and might be one explanation for the obtained results. Additionally, although the three *popdc* genes in zebrafish apparently are all involved in the regulation of cardiac electrical activity, they play distinct roles. For example *popdc2* and *popdc3* are required for AV conduction, whereas *popdc1* is essential for primary pacemaker function in the sinus node activity. Possibly, knockdown of one *popdc* gene in zebrafish cannot be compensated by the others, thus leading to an embryonic arrhythmia phenotype. During evolution, mammals might have acquired a better functional redundancy, which could result in greater protection against heart failure, if one of the *Popdc* genes gets dysfunctional. Therefore, during murine embryogenesis, loss of one *Popdc* gene can probably be partially compensated by the remaining two *Popdc* genes. However, during aging, the sinus node overcomes several changes, the intrinsic heart rate, the expression of Connexin43 and ion channels decreases, the conduction time increases and fibrosis occurs (Dobrzynski et al., 2007; Jones et al.,

2004), and due to these changes the cardiac conduction system might no longer be able to compensate the loss of a single *Popdc* gene. The redundancy issue can only be tested, when a conditional triple knockout mouse has been generated or the different *popdc* morphants in zebrafish are coinjected.

Furthermore, we have to note that we used a knockdown to analyze *popdc* function in zebrafish. Regarding the interesting phenotype in mouse and zebrafish it is worthwhile to establish stable zebrafish mutant lines so that we can examine the function of *popdc* genes into adulthood. Furthermore, a stable mutant line will also reduce the variability and the side effects caused by morpholino injections. One method to establish stable *popdc* mutant zebrafish lines is the so-called TILLING (targeted induced local lesions in genomes) approach. To date, TILLING is the most established reverse genetics strategy in zebrafish. Therefore, the genomic DNA from a large library of ENU-mutagenized zebrafish has to be screened for mutations within the *popdc* gene by using Cel1 on pools of fish or by resequencing of single fish transcriptomes (Moens et al., 2008; Wienholds et al., 2002). Recently, alternatives to generate zebrafish mutant lines are arising such as insertional mutagenesis using pseudotyped retroviruses (Wang et al., 2007) or gene-specific deletions introduced by zinc-finger nucleases (Doyon et al., 2008; Meng et al., 2008). One advantage of the insertional mutagenesis is that retroviruses tend to integrate into the first introns or exons of genes and causes lots of mutagenic integrations as demonstrated by a strong reduction in RNA levels (Wang et al., 2007). In the zinc-finger approach, zinc-finger nucleases were designed to deliver frameshift mutations at defined target sites in the genome (Doyon et al., 2008; Meng et al., 2008). Both new methods circumvent the major drawback of TILLING that the identified mutation of interest might only be one of many heterozygous mutations in the genome of the mutant line (Moens et al., 2008). Once the *popdc* mutant zebrafish lines are established they can be crossed into different GFP-reporter lines such as those that have been utilized in this study in order to analyze cardiomyocyte shape or calcium signaling in the heart, respectively.

7.1.3 Alternative splicing

Unexpectedly, I detected by RT-PCR a 200 bp shorter transcript in the adult zebrafish ovary tissue. This variation could be due to a tissue-specific splice-variant of *popdc2* or it could also be a maternal transcript, but this has to be further analyzed by sequencing. Alternative splicing is a well-known phenomenon within the *Popdc* gene family and occurs in an evolutionary conserved pattern in all three members of the *Popdc* gene family. These splice products differ in the number of transmembrane domains and in the length of the carboxy-terminus (Andree et al., 2000; Breher et al., 2004; Parnes et al., 2007). Possibly, some splice variants have different functions or interaction partners and do not need the transmembrane domains and the complete carboxy-terminus. This hypothesis can be supported by the observation that *Popdc1* and *Popdc2* proteins do not only localize exclusively at plasma membranes, but were also detected in the nucleus (Breher, 2009; Schindler, 2009; Meister, 2009). Furthermore, splice products display tissue-specific patterns and even some of which are expressed differentially in an age-dependent manner. In rat for example, it was observed that the splice variant *Popdc2c* decreases from 20 % in the neonatal heart to 2.5 % or less in the adult heart (Parnes et al., 2007). To date, the functional role of the age-related redistribution of *Popdc2* splice variants is not further explored. Therefore, it would be of interest to focus also on the splice variants of *popdc2* in zebrafish and their expression in adult and embryonal tissue. After

careful analysis of the splice variants we could manipulate and modify the splice pattern with the help of splice-site morpholinos. This might unravel the functional importance of alternative splicing in the *Popdc* gene family.

7.2 *Popdc* gene family and its role in gastrulation

Popdc1 (*Bves*) is the only existing gene of the *Popdc* (gene) family in *Drosophila melanogaster* (Lin et al., 2007). In *X. laevis*, during early gastrulation only *popdc1* is expressed, while *popdc2* and *popdc3* are expressed later (Ripley et al., 2004). It has been proposed that in the frog *popdc1* is required during early embryogenesis for proper gastrulation movements (Ripley et al., 2006). In 10-20 % of the *Drosophila* embryos expressing antisense *DmBves*, Lin and colleagues observed abnormal epithelial movement which caused a failure of pole cell migration and embryonic lethality (Lin et al., 2007). Consistent with these findings, knockdown of *xbves* function using morpholinos injections leads to a developmental arrest at the stage of gastrulation induced by aberrant epithelial movements of epiboly and involution (Ripley et al., 2006). However, in zebrafish embryos *popdc1*, *popdc2* and *popdc3* are not expressed at shield stage, a point in time in gastrulation, where involution and epiboly have already started (Kimmel et al., 1995). In addition, we could never observe epithelial expression of *popdc* genes in zebrafish (Bettina Kirchmaier and Franziska Günthner, unpublished observations). Furthermore, *popdc1*, *popdc2*, and *popdc3* morphants did not display gastrulation defects. Moreover, *Popdc1*^{-/-} and *Popdc2*^{-/-} mice are viable and do not display embryonic lethality (Andree et al., 2002; Froese and Brand, 2008) and epithelial expression of *Popdc1* and *Popdc2* in developing mice and chick was only observed in stomach epithelium (Andree et al., 2002; Andree et al., 2000; Breher et al., 2004; Froese and Brand, 2008; Torlopp et al., 2006). Additionally, it has to be mentioned that morpholinos can cause non-specific site effects, and developmental retardation or gastrulation stops are not un-usual. Considering the small percentage of affected *Drosophila* embryos expressing antisense *DmBves* (Lin et al., 2007), the role of the *Popdc* gene family in epithelial rearrangements and movements is controversial and needs to be further carefully analyzed.

7.3 *Popdc* gene family and its role in muscle development and regeneration

7.3.1 Skeletal muscle development

Using whole mount *in situ* hybridization, I detected initial *popdc2* expression in the zebrafish during somitogenesis. Interestingly, *popdc2* expression was only observed in the adaxial cells in the myotomes in comparison to *myod* expression which shows a broader expression. However, at 24 hpf, *popdc2* was expressed throughout the entire myotome and not only in slow muscle fibers, suggesting that the early differential expression pattern reflects the state of differentiation. *Myod* is a myogenic regulatory factor and induces commitment to the myogenic fate (Coutelle et al., 2001; Weinberg et al., 1996). Adaxial cells, the precursors of slow muscle fibers, are the first to differentiate and elongate during myogenesis (Felsenfeld et al., 1991; Waterman, 1969). When myogenesis is initiated, *myod* is first detected in adaxial cells, which are clearly distinct from the presomitic mesoderm because of their epithelial-like cuboidal morphology. Later on, *myod* is also expressed in the lateral presomitic mesoderm and adaxial cells starting to differentiate and now possessing a

triangular morphology (Devoto et al., 1996). Comparing the expression pattern of *popdc2* and *myod*, at the start of *popdc2* expression, myogenesis has already progressed, and the labeled cells are in the stage of early differentiation. This view is also supported by the fact that the labeled cells had the typical adaxial cell shape, which is at the posterior end triangular and no longer cuboidal. Therefore, I conclude that *popdc2* expression in the zebrafish tail starts at the stage of early differentiation within slow and fast muscle fibers and is not expressed during determination of myogenic fate.

Knockdown of *popdc2* using the acceptor splice morpholino led to a disorganized tail musculature at 24 hpf and rhodamine-phalloidin staining revealed disorganized myofibrils within the somite borders. Additionally, at 72 hpf, the tail musculature appeared to be not as dense as in wild type controls. Combination of acceptor and donor splice morpholino enhanced the skeletal muscle defect and I could detect a remarkable deformation and compression of the myotomes altering its typical V-shape with an increasing effect on the more posterior segments in comparison to the wild type. Similar muscle defects were observed in *popdc1* morphants (Franziska Guenther, unpublished observations). Interestingly, a similar phenotype was observed in the case of *caveolin3* (Nixon et al., 2005) Moreover, to a large extent both genes share a similar expression pattern. Caveolae are small uncoated plasma membrane pits that function in signal transduction and *Caveolin3* is the only known isoform expressed in skeletal and cardiac muscle (Tang et al., 1996; Way and Parton, 1995). In zebrafish, *caveolin3* expression was first detected in the adaxial cells and later in the myotome, facial muscles and the pectoral fin muscles and *Caveolin3* protein is associated with t tubuli and the sarcolemma (Nixon et al., 2005). Electron micrographs of 48 hpf *caveolin3* morphant tails demonstrate that only small areas of organized filaments were build and that mitochondria scattered throughout the cells were interrupted from small areas of organized filaments rather than the organized arrangement of mitochondria surrounding the myofibrils observed in control-injected embryos (Nixon et al., 2005). These findings are consistent with the electron micrographs of 72 hpf *popdc2* morphants. Most recently, *Popdc1* was identified as a caveolae protein that associates with costameres and *Popdc1* co-sedimented with *Caveolin3* in sucrose density gradients (Alcalay et al., submitted). If *Popdc* proteins are interacting partners of *Caveolins* such as *Caveolin3*, it would be interesting to know if *Popdc2* in zebrafish is colocalized with *Caveolin3*, and if it is also involved in regulation of differentiation or fusion of muscle fibers like *Caveolin3* (Nixon et al., 2005). Therefore, it would be useful to have an antibody against *Popdc2* working in zebrafish that we can use together with the described *Caveolin* antibody (Nixon et al., 2005) to detect colocalization. Furthermore, we could isolate zebrafish muscle fibers to observe fiber organization as well as sarcomeric banding and we could utilize the fibers for further fusion studies with the help of slow muscle-specific and fast muscle-specific antibodies (Devoto et al., 1996).

The observed tail musculature phenotypes in *popdc1* and *popdc2* morphants are not surprising. Also in mouse, it is known that *Popdc1^{-/-}* and *Popdc2^{-/-}* mice display LacZ-expression in the hind limb and in the skeletal muscles (Andree et al., 2002; Froese and Brand, 2008). Furthermore, *Popdc1* null mutants exhibit a retarded ability to regenerate skeletal muscle, although isolated and cultured satellite cells display no obvious phenotype concerning myotube formation. Moreover, the cardiotoxin-induced skeletal muscle regeneration in *Popdc1* null

mutants leads to an upregulation of LacZ expression in activated satellite cells (Andree et al., 2002). *Popdc1* is furthermore involved in regulation of *Geft* (Smith et al., 2008) which is highly expressed in the adult skeletal muscle (Guo et al., 2003). Like *Popdc1*, *Geft* protein levels in mouse are highly modulated during the process of cardiotoxin-induced muscle injury and regeneration (Bryan et al., 2005).

With regard to the similar LacZ expression pattern of *Popdc1* and *Popdc2* null mutant mice in skeletal muscle, the observed skeletal muscle phenotype in *Popdc1* null mutant mice is likely to be present also in *Popdc2* null mutants, but this has to be further investigated. Unexpectedly, *Popdc1* and *Popdc2* null mutants display a typical whistling sound when getting disturbed and in both mouse mutants, older null mutant mice have a hunchback (Breher, 2009, Froese, 2008). Possibly, this is due to an unknown muscle defect affecting the muscles for breathing and for the back.

Another interesting relationship between *Popdc1* and skeletal muscle is shown by Barber et al. which propose *Popdc1* as a putative target gene of *Pax3* (Barber et al., 2002). *Pax3* is a transcription factor which plays an important role for neural, heart and skeletal muscle development. In the trunk, *Pax3* and later *Pax7* is expressed in self-renewing satellite cell-progenitors, which serve as adult muscle stem cells (Zammit et al., 2006).

7.3.2 Heart and craniofacial muscle development

At 72 hpf, *popdc2* expression in the zebrafish is restricted to the facial musculature and the heart. Moreover, *popdc2* morphants display in addition to the cardiac conduction abnormalities, also reduction in craniofacial muscle development. Interestingly, heart and craniofacial muscle developmental programs are tightly linked and were first described by Kirby et al., who identified the cardiac neural crest (Kirby et al., 1983). This relationship is further corroborated by numerous of known cardiac and craniofacial birth defects (Hutson and Kirby, 2003). Recently, also similarities between the second heart field and the second myogenic field in the head were discovered. Not only the second heart field, but also the second myogenic field contains *Isl1* positive cells which migrate into the arterial pole of the heart and into the distal myogenic core of the first branchial arch (Cai et al., 2003; Nathan et al., 2008).

In zebrafish, three different regulatory mechanisms of craniofacial myogenesis have been proposed where *Myf5* and *Myod* independently trigger the expression of muscle structural proteins and myofibril assembly (Lin et al., 2006). In pathway I, *myf5* can initiate myogenesis solely, but *myod* expression is necessary for further proceeding and enhancing of myogenesis, whereas in pathway II *myf5* and *myod* are both needed. In pathway III, *myod* modulates myogenesis directly. Unexpectedly, the observed reduction of the pharyngeal muscles e.g. adductor mandibulae, adductor operculi, dilator operculi, levator arcus palatini and the sternohyoideus in *popdc2* morphants are all regulated by pathway I only. The significance of this finding is, however, difficult to reconcile and requires further analysis.

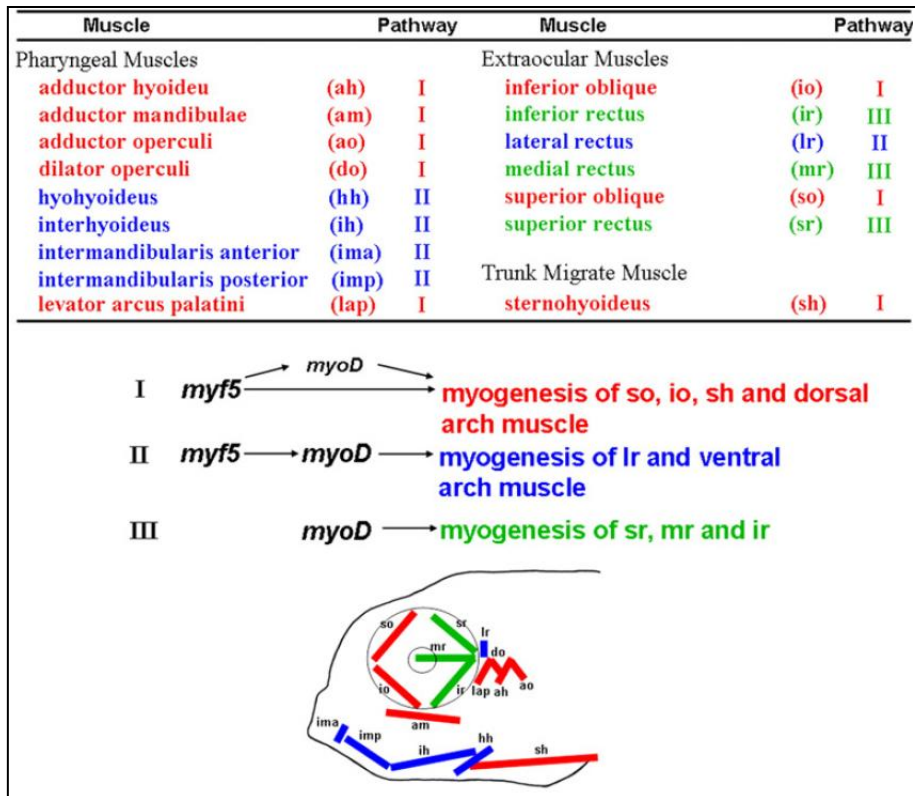


Figure 50: Model for the distinct modulation of *myf5* and *myoD* during craniofacial myogenesis of zebrafish. The schematic diagram represents all cranial muscles which are categorized into three groups representing the three different pathways. Pathway I, here depicted in red, demonstrates initiation of myogenesis at the basal level by *myf5*. Furthermore, *myf5* can trigger *myoD* expression to enhance myogenesis. In Pathway II, here depicted in blue, *myf5* specifies the muscle fate and *myoD* is the major factor of myogenesis. In Pathway III, here depicted in green, *myoD* modulates myogenesis directly. (Lin et al. (2006)).

7.4 *Popdc* gene family and its role in cell adhesion

Observations in cultured cardiomyocytes revealed that *Popdc1* accumulates at sites of cell-cell interactions (Breher, 2009). The same effect was seen by the Bader group during epithelialization where *Popdc1* was detected in cell-cell junctions and colocalizes with E-cadherin, ZO1 and Occludin (Osler et al., 2005; Osler et al., 2006). Furthermore, two other reports demonstrated that non-adherent L-cells lacking cadherin expression are able to adhere when they were transfected with wild type *Popdc1* (Kawaguchi et al., 2008; Wada et al., 2001), and *Popdc1* protein disruption decreases the tight junction integrity as well as the proper localization of junctional proteins (Osler et al., 2005). Moreover, *Popdc1* can build a complex with the tight junction component ZO1, and therefore it was proposed that *Popdc1* is able to induce cell-cell adhesion and might act as a novel recruiting or docking protein for junctional proteins. However, our group found no difference in cell culture, e.g. satellite cells derived from the *Popdc1* null mutant mouse and wild type sibling did not differ in the ability to undergo myotube formation (Andree et al., 2002). Recently, it has been shown that *Popdc1* interacts with the guanine nucleotide exchange factor-T (Geft) (Smith et al., 2008) and regulates the vesicular transport by interacting with Vamp3 (Hager et al., 2010), a SNARE protein that promotes the fusion of membranes during vesicular transport (McMahon et al., 1993). Disruption of *Popdc1* function leads to increased cell roundness accompanied with decreased activity of Rac1 and Cdc42, the downstream targets of Geft (Bryan et al., 2004; Bryan et al., 2006;

Guo et al., 2003). Interestingly, consistent with the above mentioned results, *popdc2* morphants display in contrast to control-injected zebrafish embryos single rounded cardiomyocytes within the ventricle. The observed roundness of the cardiomyocytes is a sign for a lack of adhesion (Benno Jungblut, personal communication) and resembles the cardiomyocyte changes in the zebrafish mutant *glass onion*. The *n-cadherin* expression in the zebrafish heart is mainly restricted to the myocard and individual cardiomyocytes in the *n-cadherin* zebrafish mutant *glass onion* are round shaped and loosely aggregated (Bagatto et al., 2006). This proves the important role of cell surface adhesion molecules in cardiovascular development. However, I cannot exclude that the observed roundness of cardiomyocytes in the *popdc2* morphant's heart is due to developmental retardation or aberrant maturation. The next step would include analysis of the distribution of junctional proteins in *popdc2* morphants and *in vivo* examination of *popdc2* morphant's cardiomyocytes over several days in development.

7.5 *Popdc* gene family, genetic modifier of cardiac arrhythmias

Loss of function analyses in mice, as well as morpholino-based knockdowns in zebrafish, revealed that *Popdc1*, *Popdc2*, and *Popdc3* cause cardiac arrhythmias (Froese, 2008; Breher, 2009; Froese et al., in preparation, Bettina Kirchmaier and Franziska Guenther, unpublished observations). Disease-causing genes for arrhythmias have been identified in humans and in studies of gene-targeted mice, as well as in zebrafish mutants. Based on their functions, these genes can be subdivided into ion channel genes e.g. *KvLQT1*, *Herg*, *Scn5a*, *Hcn4*, *Mink*, *MIRP1*, *Kir2.1* and *RyR2* (Splawski et al., 2000; Splawski et al., 1997), gap-junction-protein genes e.g. *Connexin40* and *Connexin43* (Gutstein et al., 2001; Hagendorff et al., 1999; Sidhu et al., 2005), and transcription factor genes like *HF-1b*, *Nkx2.5* and *Tbx5* (Nguyen-Tran et al., 2000). Recently, some new classes were found: a new class of cytoplasmic channel-interacting protein (KchiP2), a gene encoding the $\gamma 2$ subunit of the AMP-activated protein kinase (PRKAG2) (Arad et al., 2002), Ankyrin-B, an adaptor protein (Mohler et al., 2003), as well as $\alpha 1$ -Syntrophin (Ueda et al., 2008) and A-kinase-anchoring proteins (AKAPs) (Chen et al., 2007). AKAPs and $\alpha 1$ -Syntrophin are scaffolding proteins which interact with critical ion channel proteins (Chen et al., 2007; Ueda et al., 2008).

To date, the function of *Popdc* genes is not fully understood, but it is known that *Popdc* genes encode for transmembrane proteins (Knight et al., 2003). Based on the fact that loss of *Popdc* genes can trigger arrhythmia, and because of their subcellular protein distribution, *Popdc* genes might encode a novel class of channel proteins. To test this hypothesis, I generated three constructs with full-length coding sequence of murine *Popdc1*, murine *Popdc2* and murine *Popdc3*, respectively. These constructs were used to express *Popdc* proteins in *Xenopus* oocytes. To prove channel properties of the three *Popdc* proteins, voltage-clamp technique were utilized. However, no current was measured indicating that *Popdc* proteins do not have pore-forming activity (Breher, 2009).

7.5.1 *Popdc* genes, modulators of *Trek1*

After exclusion of the channel hypothesis in case of the *Popdc* gene family, we wondered whether *Popdc* proteins are able to modulate channels involved in heart rate control and rhythm. Therefore the *Hcn4* channel was tested, which is involved in generating the funny current also known as “pacemaker current” in the sinoatrial node (Baruscotti et al., 2005) and which after deletion in adult mice causes sinus pauses as observed in *Popdc1* and *Popdc2* null mutant mice (Stieber et al., 2003). However, *Hcn4* current from isolated *Popdc2* null mutant sinus node cells was not changed compared to the wild type control. Furthermore, Herrmann et al. demonstrated that *Hcn4* is not required for heart rate acceleration (Herrmann et al., 2007) suggesting that another channel might modulate the heart rate. Interestingly, *Popdc* proteins are able to modulate the channel *Trek1*, a two pore domain-containing potassium channel, (Breher, 2009). Although physiological evidence of the direct participation of *Trek1* current in stretch mediation has still to be proved, this channel has properties well suited to play a role in mediating background potassium conductance (Goldstein et al., 2005; Goldstein et al., 2001; Lesage and Lazdunski, 2000). Aside from its strong expression in the brain, *Trek1* is expressed in the heart (Aimond et al., 2000; Tan et al., 2004; Terrenoire et al., 2001) and confocal images detected *Trek1* channel proteins at the surface of cardiomyocytes in a pattern that appears suitable for sensing longitudinal stretch of the cells (Li et al., 2006). Further functional interaction studies between *Popdc1*, *Popdc2* or *Popdc3* and *Trek1* revealed a two-fold increase in *Trek1* current (Kuhntz, 2008; Breher, 2009). Moreover, direct interaction of *Popdc1* and *Trek1* was also demonstrated by FRET (fluorescence resonance energy transfer) analyses, GST-pulldowns and coimmunoprecipitation (Breher, 2009; Schindler, 2009). Furthermore, *Popdc1* and *Trek1* are colocalized in ventricular myocytes, the cardiac conduction system and in the working myocardium (Breher, 2009). Thus, *Trek1* is a hot candidate responsible for heart rate acceleration and *Popdc* proteins are modulating *Trek1* properties in a cAMP-dependent manner.

Next, it would be of high interest, if we could phenocopy *popdc1* and *popdc2* morphant phenotype by knockdown of *TREK-1* in zebrafish. To date, there are possibly two homologues of *Trek1*, also known as *Kcnk2*, in zebrafish, showing 74 % and 70 % similarity to murine *Trek1* protein, respectively. The first homologue lies on chromosome 17 and is an automated computational prediction displaying similarity to potassium channel, subfamily K, member 2 (NCBI Reference Sequence: XM_683094.2), the second one is a novel protein similar to vertebrate potassium channel subfamily K, member 2 (*Kcnk2*) on chromosome 3 (GenBank: CAI20606.1). It is not surprising, that in zebrafish two *trek1* genes might exist, because also *Hcn4* related genes are found three times in zebrafish due to the teleost genome duplication. This, however, might complicate the proposed phenocopy assay in zebrafish and we need first to check the expression pattern of the both *Trek1* homologues if it is similar or not. It is also possible, that like in the case of two zebrafish *Ncx1* homologues, they show different expression pattern, one predominantly expressed in the brain and one cardiac-specific but both expression pattern combined reflect the expression pattern observed in mouse and human (Langenbacher et al., 2005).

7.6 *Popdc* gene family – a novel class of cAMP binding proteins

Recently, we revealed that the *Popeye* domain resembles structurally a cyclic nucleotide binding domain and cAMP-binding might be mediated through direct interaction with the conserved DSPE and FQVT sequence motifs in this domain (Froese et al., in preparation; Breher, 2009; Kultz, 2008). The cAMP binding occurs in a binding domain which has structural, but almost no sequence similarities to other cAMP-binding cassettes of other cyclic nucleotide binding proteins. Specific interaction was demonstrated through binding of Popdc1, Popdc2 and Popdc3 with cAMP agarose (Froese et al., in preparation; Breher, 2009; Kultz, 2008; Meister, 2009). To perturb cyclic nucleotide binding, point mutations for the conserved residues in Popdc1 and Popdc2 were generated (Kultz, 2008; Meister, 2009). By using cAMP binding assays, the mutants Popdc1^{D200A}, Popdc1^{V217F}, Popdc2^{D184A} and Popdc2^{V201F} revealed strong impairment of cAMP binding whereas the mutants Popdc1^{E203A} and Popdc1^{P202A} displayed stronger binding affinity to cAMP agarose (Kultz, 2008; Meister, 2009).

I used the zebrafish to express the Popdc1 and Popdc2 cAMP mutations in a heterologous system. Interestingly, injection of Popdc1 cAMP point mutation resulted in phenotypes with a striking correlation to the cAMP binding assays (Kultz, 2008). Overexpression of wild type Popdc1 induced a cardiac phenotype displaying pericardial edema, blood retention and retarded blood circulation. In contrast, the Popdc1 point mutants Popdc1^{D200A} and Popdc1^{V217F}, which are characterized by low cAMP binding (Kultz, 2008), did not exhibit the Popdc1 overexpression phenotype and resembled that of uninjected control embryos. Moreover, Popdc1 point mutants Popdc1^{P202A} and Popdc1^{E203A}, which both are characterized by increased binding affinity to cAMP agarose *in vitro* (Kultz, 2008), displayed an intermediate phenotype or phenocopied that of wild type protein. Surprisingly, expression of Popdc2 cAMP point mutations in zebrafish did not show any significant effect on zebrafish development in general or cardiovascular development in particular. This unexpected outcome of Popdc2 overexpression might be explained by the aspect that *popdc2* is the predominantly expressed gene during cardiogenesis in zebrafish. Whereas *popdc1* displayed strongest expression at 24 hpf and declines between 24 hpf and 36 hpf (Guenther, 2008), *popdc2* expression remained strong between 24 hpf and 72 hpf. Therefore, Popdc2 overexpression might be compensated by the large amounts of intrinsic wild type protein, but Popdc1 overexpression could have stronger impact thinking of the low levels of intrinsic Popdc1 protein. Alternatively, however, the different results may also point to fundamental differences between Popdc2 and Popdc1, which still need to be further investigated. Unfortunately, protein detection of epitope-tagged Popdc1 or Popdc2 protein in the zebrafish was not possible due to strong background bands in western blot. However, based on the fact that the same constructs in *Xenopus* oocytes elicited the same phenotype suggests that the capped RNA is indeed translated into protein. To circumvent the western blot technique we could further generate Popdc1 and Popdc2 cAMP mutations fused to GFP. With these constructs we would not only prove proper translation by GFP fluorescence, but we could also further observe localization of the protein in zebrafish embryos. In the case of wild type Popdc1 this approach has already started revealing Popdc1 protein in the membrane (Franziska Guenther, unpublished observations).

Interestingly, Roland Schindler revealed in his Master thesis, using immunocytochemical assays and membrane protein biotinylation, that Popdc1^{D200A} and Popdc1^{P202A} are both membrane-localized thus indicating that the cAMP mutants are not simply misfolded, but it seems that in Cos cells possibly Popdc1^{D200A} and Popdc1^{P202A} might differ from wild type protein in the extent of membrane localization. In contrast, both, mutant and wild type protein are able to interact with Trek1 at the membrane as revealed by FRET-measurements using the bi-molecular sensor Popdc1-CFP/YFP-Trek1 (Schindler, 2009). Moreover, Popdc1^{D200A} coexpressed with Trek1 in frog oocytes is able to enhance Trek1 like wild type Popdc1 to 25 %, which suggests that this mutant does not essentially differ from wild type protein with regard to subcellular localization and protein interaction (Kuhntz, 2008; Breher, 2009).

7.7 *Popdc* gene family and its role in inherited diseases

7.7.1 *Popdc* gene family and the sick sinus node syndrome

I demonstrate in this work that *popdc2* morphants display AV block, sinoatrial block and reduced heart rate. It is furthermore known that *popdc1* morphants exhibit sinus bradycardia (Franziska Guenther, unpublished observations). Sinus bradycardia and sinoatrial blocks are signs for sinus node dysfunction. Interestingly, also *Popdc1* and *Popdc2* genes in mice play important roles in the ageing sinus node under stress (Froese, 2008; Breher, 2009). Sinus node dysfunction has also been reported for ion channels like *Hcn4* (Herrmann et al., 2007) and the cardiac sodium channel *Scn5a* (Tan et al., 2001). Deletion of *Hcn4* in adult mice results in cardiac arrhythmia characterized by recurrent sinus pauses, but morphology of the sinus node cells itself was unchanged and the knockout mice did not show a change in heart rate acceleration (Herrmann et al., 2007). Moreover, mutations in the human *HCN4* gene causing mutated or truncated channel proteins have been found to be associated with sinus bradycardia (Milanesi et al., 2006; Nof et al., 2007; Schulze-Bahr et al., 2003; Ueda et al., 2004). Tan et al. described the first functional characterization of an inherited mutation in the human *SCN5A* gene due to slowing of the myocardial conduction (Tan et al., 2001). However, not only deletion or mutation of ion channels causes sinus node dysfunction. Mohler and colleagues discovered in 2003 that loss-of-function mutation in the gene *Ankyrin-B* results in dominantly inherited type 4 LQT syndrome (Mohler et al., 2003). Ankyrin-B is a member of a family of versatile membrane adaptors und loss of *Ankyrin-B* influences its binding proteins like the sodium/calcium exchanger *Ncx1*, inositol-1,4,5-trisphosphate receptors and the Na/K ATPase which are reduced at t tubule sites (Mohler et al., 2003). Moreover, *Shox2*, a member of a small subfamily of paired, related homeodomain transcription factors, is implicated to cause sinus bradycardia and sinus exit block in *shox2* zebrafish morphants and *Shox2* null mutant mice display a hypoplastic sinoatrial region in contrast to wild type siblings (Blaschke et al., 2007). However, human phenotypes caused by *SHOX2* deficiency have not been identified so far, but *HCN4*, *SCN5A* and *ANKYRIN-B* have been implicated with familial cases of sinus node disease in human (Mohler et al., 2003; Schulze-Bahr et al., 2003; Tan et al., 2001). Possibly, *Popdc* gene mutations might also cause sinus node disease, and therefore I suggest to screen for possible POPDC gene alterations in aging patients with predisposition for the sick sinus node syndrome. The incidence of patients with sick sinus syndrome increases rapidly with age and impaired heart rate acceleration during exercise or stress as

well as severe sinus bradycardia, sinus pauses or arrest, sinus exit block, chronic atrial tachyarrhythmias, alternating periods of atrial bradyarrhythmias and tachyarrhythmias are signs for this disease (Dobrzynski et al., 2007).

Despite the sick sinus node syndrome, defects in *Popdc* genes might provide an insight into several cardiac arrhythmia phenotypes. *Popdc2* and *popdc3* morphants in zebrafish develop an atrioventricular block. Existence of an atrioventricular block is known in several zebrafish mutant lines like *ginger*, *breakdance* and *hiphop* where the atrial beats outnumber ventricular beats (Arnaout et al., 2007; Kopp et al., 2005; Stainier et al., 1996; Warren and Fishman, 1998). The observed aberrant electrical activity in the zebrafish mutant line *breakdance* is consistent with *popdc2* and *popdc3* morphants: the fluorescent waves representing calcium transients were visible spreading from the atrium to the atrioventricular junction, but no fluorescent changes were seen in the ventricle. *Breakdance* affects the *Kcnh2* channel and is described as a zebrafish model for human LQT syndrome (Arnaout et al., 2007). The LQT syndrome is a genetically heterogeneous disease affecting 1 in 5000 persons causing a disorder of ventricular repolarization. The LQT syndrome is identified via ECG tracings where the QT time is prolonged. The QT represents a summation of the time required for the ventricles to repolarize and is measured from the start of the QRS complex to the end of the T wave (Ackerman, 2004; Ackerman and Clapham, 1997). Therefore, I propose that mutations within the *Popdc* gene family might also correlate with LQT syndrome in humans.

7.7.1.1 Arrhythmia and cellular changes, a matter of correlation?

Interestingly, beneath the aforementioned mouse models, it exists an age-related disease model in mouse. *Klotho* null mutant mice express LacZ in the sinoatrial node region and display age- and stress-dependent sinus node dysfunction and sudden death consistent with the data obtained for *Popdc1* and *Popdc2* null mutant mice. Surprisingly, there was no sign of degenerative structural change in the sinus node region like observed in both *Popdc* null mutant mice (Takeshita et al., 2004).

Knockdown of *popdc2* in zebrafish using an antisense morpholino-based approach led to cardiac conduction abnormalities by developing primarily an atrioventricular (AV) block. In order to find a morphological substrate for the observed AV conduction defect, I studied the structure of the AV canal in *popdc2* morphants with and without arrhythmia using confocal microscopy. However, no evidence for morphological alterations of the pacemaker cardiomyocytes was obtained and I further excluded that the observed arrhythmia phenotype in the *popdc2* morphant is based on a defect in cardiac valve development. Regarding the literature, zebrafish arrhythmias are not necessarily caused by morphological alterations of cardiomyocytes or valves. Recently, Milan et al. revealed in his newest zebrafish screen for genetic regulators of myocardial repolarization that only about one half of the identified zebrafish mutants display morphological defects (Milan et al., 2009). Therefore, I conclude that the cardiac conduction phenotype in *popdc2* morphants in zebrafish is independent of cellular alterations, and is primarily caused by electrical activity changes of the heart. However, it would be interesting to observe the cellular shape of the pacemaker cardiomyocytes after several days of arrhythmia in the *popdc2* morphants. Possibly, morphological alterations of cardiomyocytes or valves develop secondarily due to the extreme exposure of the heart.

However, *Popdc2* null mutant mice display an age-dependent reduction of the sinus node tissue and sinus node cell extensions. Furthermore, Masson's Trichome Staining of the 8 month old SAN reveals a loss of extracellular matrix in the control sibling, whereas in the *Popdc2* null mutant the inferior domain of the sinus node shows an increase (Froese et al., in preparation). The reduction of the sinus node tissue was accompanied with stress-dependent sinus pauses. Interestingly, in 3 months old *Popdc2* null mutant mice neither loss of sinus node tissue nor stress-related arrhythmia was observed (Kreissl, 2009). To date, it is not fully clear, if structural alterations and developing arrhythmia in *Popdc2*^{-/-} mice are correlated. To elucidate the structural alterations within the sinus node over time and its correlation to arrhythmia, we could intercross transgenic reporter mice containing *Hcn4*-GFP and *Cx40*-GFP into the *Popdc2* mutant line. The *Hcn4* channel represents the predominantly expressed HCN channel isoform in SA node cells and is responsible for the "funny" current which plays a key role in the pacemaker potential of the sinus node (DiFrancesco, 1986). Therefore, *Hcn4* is a well-known marker for sinus node cells and *Popdc2* null mutant mice expressing additionally GFP in all sinus node cells could be used to image the whole sinus node without the need of cryosections and subsequent antibody staining which can lead to a structural loss of the sinus node tissue. Furthermore, we can isolate pure sinus node cells using FACS to determine the amount of remaining sinus node cells and we can observe the developmental change of single sinus node cells as well as utilize the purified cells for cell culture. Connexin40 is involved in the strong electric coupling at the periphery of the node by forming medium and large conductance channels (Boyett et al., 2006) and is expressed in the atrium, in the conducting bundle branches and Purkinje fibers. Introduction of GFP-tagged *Connexin40* in the *Popdc2* mutant mouse would help to analyze the fast conducting system and the direct periphery of the sinus node. Both transgenic mouse lines together might highlight the age-dependent anatomical alterations in the sinus node region of *Popdc2* null mutant mice and maybe reveals the mechanism behind.

In conclusion, the ability of *Popdc* gene family to modulate the cardiac conduction system is highly conserved throughout lower and higher vertebrates. However, the study in zebrafish reveals for the first time specific functions for different members of the *Popdc* gene family. Therefore, we propose that *popdc2* and *popdc3* are required for AV conduction, whereas *popdc1* is essential for primary pacemaker function in the sinus node. Interestingly, *popdc* morphants also develop a skeletal musculature phenotype which has to be further explored in zebrafish and mouse.

In the future, double and triple knockouts have to be investigated to circumvent redundancy and to specify all functions of *Popdc* gene family. Furthermore new protein interaction partners of *Popdc* have to be identified to in turn highlight the role of *Popdc* gene family in signaling pathways.

8 LITERATURE

- Ackerman, M. J., 2004. Cardiac channelopathies: it's in the genes. *Nat Med.* 10, 463-4.
- Ackerman, M. J., Clapham, D. E., 1997. Ion channels—basic science and clinical disease. *N Engl J Med.* 336, 1575-86.
- Ahmad, N., Long, S., Rebagliati, M., 2004. A Southpaw Joins the Roster: The Role of the Zebrafish nodal-related Gene Southpaw in Cardiac LR Asymmetry. *Trends in Cardiovascular Medicine.* 14, 43-49.
- Aimond, F., Rauzier, J. M., Bony, C., Vassort, G., 2000. Simultaneous activation of p38 MAPK and p42/44 MAPK by ATP stimulates the K⁺ current ITREK in cardiomyocytes. *J Biol Chem.* 275, 39110-6.
- Alexander, J., Rothenberg, M., Henry, G. L., Stainier, D. Y., 1999. casanova plays an early and essential role in endoderm formation in zebrafish. *Dev Biol.* 215, 343-57.
- Alcalay, Y., Hochhauser, E., Dick, J., Brand, T., Kessler-Icekson, G. Popdc1 is identified as a caveolae protein that associates with costameres and plays a role in the heart response to ischemia. submitted.
- Andree, B., Fleige, A., Arnold, H. H., Brand, T., 2002. Mouse Pop1 is required for muscle regeneration in adult skeletal muscle. *Mol Cell Biol.* 22, 1504-12.
- Andree, B., Hillemann, T., Kessler-Icekson, G., Schmitt-John, T., Jockusch, H., Arnold, H. H., Brand, T., 2000. Isolation and characterization of the novel popeye gene family expressed in skeletal muscle and heart. *Dev Biol.* 223, 371-82.
- Arad, M., Benson, D. W., Perez-Atayde, A. R., McKenna, W. J., Sparks, E. A., Kanter, R. J., McGarry, K., Seidman, J. G., Seidman, C. E., 2002. Constitutively active AMP kinase mutations cause glycogen storage disease mimicking hypertrophic cardiomyopathy. *J Clin Invest.* 109, 357-62.
- Armstrong, E. J., Bischoff, J., 2004. Heart valve development: endothelial cell signaling and differentiation. *Circ Res.* 95, 459-70.
- Arnaout, R., Ferrer, T., Huisken, J., Spitzer, K., Stainier, D. Y., Tristani-Firouzi, M., Chi, N. C., 2007. Zebrafish model for human long QT syndrome. *Proc Natl Acad Sci U S A.* 104, 11316-21.
- Bagatto, B., Francl, J., Liu, B., Liu, Q., 2006. Cadherin2 (N-cadherin) plays an essential role in zebrafish cardiovascular development. *BMC Dev Biol.* 6, 23.
- Baker, K., Warren, K. S., Yellen, G., Fishman, M. C., 1997. Defective "pacemaker" current (I_h) in a zebrafish mutant with a slow heart rate. *Proc Natl Acad Sci U S A.* 94, 4554-9.
- Barber, T. D., Barber, M. C., Tomescu, O., Barr, F. G., Ruben, S., Friedman, T. B., 2002. Identification of target genes regulated by PAX3 and PAX3-FKHR in embryogenesis and alveolar rhabdomyosarcoma. *Genomics.* 79, 278-84.
- Baruscotti, M., Bucchi, A., Difrancesco, D., 2005. Physiology and pharmacology of the cardiac pacemaker ("funny") current. *Pharmacol Ther.* 107, 59-79.
- Beis, D., Bartman, T., Jin, S. W., Scott, I. C., D'Amico, L. A., Ober, E. A., Verkade, H., Frantsve, J., Field, H. A., Wehman, A., Baier, H., Tallafuss, A., Bally-Cuif, L., Chen, J. N., Stainier, D. Y., Jungblut, B., 2005. Genetic and cellular analyses of zebrafish atrioventricular cushion and valve development. *Development.* 132, 4193-204.
- Biel, M., Schneider, A., Wahl, C., 2002. Cardiac HCN channels: structure, function, and modulation. *Trends Cardiovasc Med.* 12, 206-12.
- Biel, M., Michalakis, S., 2007. Function and dysfunction of CNG channels: insights from channelopathies and mouse models. *Mol Neurobiol.* 35, 266-77.
- Birboim, H. C., Doly, J., 1979. A rapid alkaline extraction procedure for screening recombinant plasmid DNA. *Nucleic Acids Res.* 7, 1513-23.
- Blaschke, R. d. J., Monaghan, A. P., Schiller, S., Schechinger, B., Rao, E., Padilla-Nash, H., Ried, T., Rappold, G. A., 1998. SHOT, a SHOX-related homeobox gene, is implicated in craniofacial, brain, heart, and limb development. *Proceedings of the National Academy of Sciences of the United States of America.* 95, 2406-2411.
- Blaschke, R. J., Hahurij, N. D., Kuijper, S., Just, S., Wisse, L. J., Deissler, K., Maxelon, T., Anastassiadis, K., Spitzer, J., Hardt, S. E., Scholer, H., Feitsma, H., Rottbauer, W., Blum, M., Meijlink, F., Rappold, G., Gittenberger-de Groot, A. C., 2007. Targeted mutation reveals essential functions of the homeodomain transcription factor Shox2 in sinoatrial and pacemaking development. *Circulation.* 115, 1830-8.
- Boogerd, C. J., Moorman, A. F., Barnett, P., 2009. Protein interactions at the heart of cardiac chamber formation. *Ann Anat.* 191, 505-17.
- Boyett, M. R., Dobrzynski, H., 2007. The sinoatrial node is still setting the pace 100 years after its discovery. *Circ Res.* 100, 1543-5.
- Boyett, M. R., Inada, S., Yoo, S., Li, J., Liu, J., Tellez, J., Greener, I. D., Honjo, H., Billeter, R., Lei, M., Zhang, H., Efimov, I. R., Dobrzynski, H., 2006. Connexins in the sinoatrial and atrioventricular nodes. *Adv Cardiol.* 42, 175-97.
- Brand, T., 2003. Heart development: molecular insights into cardiac specification and early morphogenesis. *Dev Biol.* 258, 1-19.
- Breher, S. S., Mavridou, E., Brenneis, C., Froese, A., Arnold, H. H., Brand, T., 2004. Popeye domain containing gene 2 (Popdc2) is a myocyte-specific differentiation marker during chick heart development. *Dev Dyn.* 229, 695-702.
- Breher, S. S. Die kardiale Funktion von Popdc1 in der Maus: Vom Gen zum Phän (Ph.D. thesis). University of Wuerzburg, Wuerzburg, Germany, 2009.
- Bruzzzone, R., White, T. W., Paul, D. L., 1996. Connections with connexins: the molecular basis of direct intercellular signaling. *Eur J Biochem.* 238, 1-27.
- Bryan, B., Kumar, V., Stafford, L. J., Cai, Y., Wu, G., Liu, M., 2004. GEFT, a Rho family guanine nucleotide exchange factor, regulates neurite outgrowth and dendritic spine formation. *J Biol Chem.* 279, 45824-32.
- Bryan, B. A., Cai, Y., Liu, M., 2006. The Rho-family guanine nucleotide exchange factor GEFT enhances retinoic acid- and cAMP-induced neurite outgrowth. *J Neurosci Res.* 83, 1151-9.
- Bryan, B. A., Mitchell, D. C., Zhao, L., Ma, W., Stafford, L. J., Teng, B. B., Liu, M., 2005. Modulation of muscle regeneration, myogenesis, and adipogenesis by the Rho family guanine nucleotide exchange factor GEFT. *Mol Cell Biol.* 25, 11089-101.
- Buckingham, M., Meilhac, S., Zaffran, S., 2005. Building the mammalian heart from two sources of myocardial cells. *Nat Rev Genet.* 6, 826-35.
- Cai, C. L., Liang, X., Shi, Y., Chu, P. H., Pfaff, S. L., Chen, J., Evans, S., 2003. Isl1 identifies a cardiac progenitor population that proliferates prior to differentiation and contributes a majority of cells to the heart. *Dev Cell.* 5, 877-89.

- Chen, J. N., Haffter, P., Odenthal, J., Vogelsang, E., Brand, M., van Eeden, F. J., Furutani-Seiki, M., Granato, M., Hammerschmidt, M., Heisenberg, C. P., Jiang, Y. J., Kane, D. A., Kelsh, R. N., Mullins, M. C., Nusslein-Volhard, C., 1996. Mutations affecting the cardiovascular system and other internal organs in zebrafish. *Development*. 123, 293-302.
- Chen, J. N., van Eeden, F. J., Warren, K. S., Chin, A., Nusslein-Volhard, C., Haffter, P., Fishman, M. C., 1997. Left-right pattern of cardiac BMP4 may drive asymmetry of the heart in zebrafish. *Development*. 124, 4373-82.
- Chen, L., Marquardt, M. L., Tester, D. J., Sampson, K. J., Ackerman, M. J., Kass, R. S., 2007. Mutation of an A-kinase-anchoring protein causes long-QT syndrome. *Proceedings of the National Academy of Sciences*. 104, 20990-20995.
- Cheng, C. F., Kuo, H. C., Chien, K. R., 2003. Genetic modifiers of cardiac arrhythmias. *Trends Mol Med*. 9, 59-66.
- Chi, N. C., Shaw, R. M., Jungblut, B., Huisken, J., Ferrer, T., Arnaout, R., Scott, I., Beis, D., Xiao, T., Baier, H., Jan, L. Y., Tristani-Firouzi, M., Stainier, D. Y., 2008. Genetic and physiologic dissection of the vertebrate cardiac conduction system. *PLoS Biol*. 6, e109.
- Christoffels, V. M., Habets, P. E., Franco, D., Campione, M., de Jong, F., Lamers, W. H., Bao, Z. Z., Palmer, S., Biben, C., Harvey, R. P., Moorman, A. F., 2000. Chamber formation and morphogenesis in the developing mammalian heart. *Dev Biol*. 223, 266-78.
- Christoffels, V. M., Smits, G. J., Kispert, A., Moorman, A. F., 2010. Development of the pacemaker tissues of the heart. *Circ Res*. 106, 240-54.
- Combs, M. D., Yutzey, K. E., 2009. Heart valve development: regulatory networks in development and disease. *Circ Res*. 105, 408-21.
- Coutelle, O., Blagden, C. S., Hampson, R., Halai, C., Rigby, P. W., Hughes, S. M., 2001. Hedgehog signalling is required for maintenance of myf5 and myoD expression and timely terminal differentiation in zebrafish adaxial myogenesis. *Dev Biol*. 236, 136-50.
- Dahme, T., Katus, H. A., Rottbauer, W., 2009. Fishing for the genetic basis of cardiovascular disease. *Dis Model Mech*. 2, 18-22.
- Davidson, B., Levine, M., 2003. Evolutionary origins of the vertebrate heart: Specification of the cardiac lineage in *Ciona intestinalis*. *Proc Natl Acad Sci U S A*. 100, 11469-73.
- Devoto, S. H., Melancon, E., Eisen, J. S., Westerfield, M., 1996. Identification of separate slow and fast muscle precursor cells in vivo, prior to somite formation. *Development*. 122, 3371-80.
- DiFrancesco, D., 1986. Characterization of single pacemaker channels in cardiac sino-atrial node cells. *Nature*. 324, 470-3.
- Dobrzynski, H., Boyett, M. R., Anderson, R. H., 2007. New insights into pacemaker activity: promoting understanding of sick sinus syndrome. *Circulation*. 115, 1921-32.
- Doyon, Y., McCammon, J. M., Miller, J. C., Faraji, F., Ngo, C., Katibah, G. E., Amora, R., Hocking, T. D., Zhang, L., Rebar, E. J., Gregory, P. D., Urnov, F. D., Amacher, S. L., 2008. Heritable targeted gene disruption in zebrafish using designed zinc-finger nucleases. *Nat Biotechnol*. 26, 702-8.
- Felsenfeld, A. L., Curry, M., Kimmel, C. B., 1991. The fub-1 mutation blocks initial myofibril formation in zebrafish muscle pioneer cells. *Dev Biol*. 148, 23-30.
- Fishman, M. C., Chien, K. R., 1997. Fashioning the vertebrate heart: earliest embryonic decisions. *Development*. 124, 2099-117.
- Fozzard, H. A., Hanck, D. A., 1996. Structure and function of voltage-dependent sodium channels: comparison of brain II and cardiac isoforms. *Physiol Rev*. 76, 887-926.
- Froese, A., Brand, T., 2008. Expression pattern of Popdc2 during mouse embryogenesis and in the adult. *Dev Dyn*. 237.
- Froese, A. The Popeye domain containing gene 2 (Popdc2): Generation and functional characterization of a null mutant in mice and promoter analysis (Ph.D. thesis). University of Wuerzburg, Wuerzburg, Germany, 2008.
- Froese, A., Breher, S. S., Schlueter, J., Waldeyer, C., Schindler R. F. R., Nikolaev, V., O., Kuhtz, J., Wischmeyer, E., Kirchmaier, B., C., Vauti, F., Müller, T., D., Torlopp, A., Stieber, J., Ludwig, A., Arnold, H., H., Kirchhof, P., Fabritz, L., Brand, T. The Popeye domain containing gene family encodes a novel class of cAMP binding proteins involved in cardiac pacemaking. In preparation.
- Gajewski, K., Fossett, N., Molkentin, J. D., Schulz, R. A., 1999. The zinc finger proteins Pannier and GATA4 function as cardiogenic factors in *Drosophila*. *Development*. 126, 5679-88.
- Goldstein, S. A., Bayliss, D. A., Kim, D., Lesage, F., Plant, L. D., Rajan, S., 2005. International Union of Pharmacology. LV. Nomenclature and molecular relationships of two-P potassium channels. *Pharmacol Rev*. 57, 527-40.
- Goldstein, S. A., Bockenhauer, D., O'Kelly, I., Zilberberg, N., 2001. Potassium leak channels and the KCNK family of two-P-domain subunits. *Nat Rev Neurosci*. 2, 175-84.
- Goodenough, D. A., Goliger, J. A., Paul, D. L., 1996. Connexins, connexons, and intercellular communication. *Annu Rev Biochem*. 65, 475-502.
- Grifone, R., Kelly, R. G., 2007. Heartening news for head muscle development. *Trends Genet*. 23, 365-9.
- Guenther, F. Analyse der Expression und Funktion des popdc1 Gens im Zebrafisch (Diploma thesis). University of Wuerzburg, Wuerzburg, Germany, 2008.
- Guo, X., Stafford, L. J., Bryan, B., Xia, C., Ma, W., Wu, X., Liu, D., Songyang, Z., Liu, M., 2003. A Rac/Cdc42-specific exchange factor, GEFT, induces cell proliferation, transformation, and migration. *J Biol Chem*. 278, 13207-15.
- Gurney, A., Manoury, B., 2009. Two-pore potassium channels in the cardiovascular system. *Eur Biophys J*. 38, 305-18.
- Gutstein, D. E., Morley, G. E., Tamaddon, H., Vaidya, R., Schneider, M. D., Chen, J., Chien, K. R., Stuhlmann, H., Fishman, G. I., 2001. Conduction Slowing and Sudden Arrhythmic Death in Mice With Cardiac-Restricted Inactivation of Connexin43. *Circ Res*. 88, 333-339.
- Hagendorff, A., Schumacher, B., Kirchhoff, S., Luderitz, B., Willecke, K., 1999. Conduction Disturbances and Increased Atrial Vulnerability in Connexin40-Deficient Mice Analyzed by Transesophageal Stimulation. *Circulation*. 99, 1508-1515.
- Hager, H. A., Roberts, R. J., Cross, E. E., Proux-Gillardeaux, V., Bader, D. M., 2010. Identification of a novel Bves function: regulation of vesicular transport. *EMBO J*.
- Harvey, R. P., 1996. NK-2 homeobox genes and heart development. *Dev Biol*. 178, 203-16.
- Harvey, R. P., 2002. Patterning the vertebrate heart. *Nat Rev Genet*. 3, 544-56.
- Hassel, D., Scholz, E. P., Trano, N., Friedrich, O., Just, S., Meder, B., Weiss, D. L., Zitron, E., Marquart, S., Vogel, B., Karle, C. A., Seemann, G., Fishman, M. C., Katus, H. A., Rottbauer, W., 2008. Deficient zebrafish ether-a-go-go-related gene channel gating causes short-QT syndrome in zebrafish reggae mutants. *Circulation*. 117, 866-75.
- Hedley, P. L., Jørgensen, P., Schlamowitz, S., Wangari, R., Moolman-Smook, J., Brink, P. A., Kanters, J. K., Corfield, V. A., Christiansen, M., 2009. The genetic basis of long QT and short QT syndromes: A mutation update. *Human Mutation*. 30, 1486-1511.
- Heikinheimo, M., Scandrett, J. M., Wilson, D. B., 1994. Localization of transcription factor GATA-4 to regions of the mouse embryo involved in cardiac development. *Dev Biol*. 164, 361-73.

- Herrmann, S., Stieber, J., Stockl, G., Hofmann, F., Ludwig, A., 2007. HCN4 provides a 'depolarization reserve' and is not required for heart rate acceleration in mice. *EMBO J.* 26, 4423-32.
- Hinton, R. B., Jr., Lincoln, J., Deutsch, G. H., Osinska, H., Manning, P. B., Benson, D. W., Yutzey, K. E., 2006. Extracellular matrix remodeling and organization in developing and diseased aortic valves. *Circ Res.* 98, 1431-8.
- Hirsinger, E., Stellabotte, F., Devoto, S. H., Westerfield, M., 2004. Hedgehog signaling is required for commitment but not initial induction of slow muscle precursors. *Dev Biol.* 275, 143-57.
- Hitz, M. P., Pandur, P., Brand, T., Kuhl, M., 2002. Cardiac specific expression of *Xenopus* Popeye-1. *Mech Dev.* 115, 123-6.
- Hsieh, D. J.-Y., Liao, C.-F., 2002. Zebrafish M muscarinic acetylcholine receptor: cloning, pharmacological characterization, expression patterns and roles in embryonic bradycardia. *British Journal of Pharmacology.* 137, 782-792.
- Hu, N., Sedmera, D., Yost, H. J., Clark, E. B., 2000. Structure and function of the developing zebrafish heart. *Anat Rec.* 260, 148-57.
- Huang, C. J., Tu, C. T., Hsiao, C. D., Hsieh, F. J., Tsai, H. J., 2003. Germ-line transmission of a myocardium-specific GFP transgene reveals critical regulatory elements in the cardiac myosin light chain 2 promoter of zebrafish. *Dev Dyn.* 228, 30-40.
- Huisken, J., Stainier, D. Y., 2009. Selective plane illumination microscopy techniques in developmental biology. *Development.* 136, 1963-75.
- Huisken, J., Swoger, J., Del Bene, F., Wittbrodt, J., Stelzer, E. H., 2004. Optical sectioning deep inside live embryos by selective plane illumination microscopy. *Science.* 305, 1007-9.
- Hutson, M. R., Kirby, M. L., 2003. Neural crest and cardiovascular development: a 20-year perspective. *Birth Defects Res C Embryo Today.* 69, 2-13.
- Jacobson, A. G., Sater, A. K., 1988. Features of embryonic induction. *Development.* 104, 341-59.
- Jin, S.-W., Beis, D., Mitchell, T., Chen, J.-N., Stainier, D. Y. R., 2005. Cellular and molecular analyses of vascular tube and lumen formation in zebrafish. *Development.* 132, 5199-5209.
- Jones, S. A., Lancaster, M. K., Boyett, M. R., 2004. Ageing-related changes of connexins and conduction within the sinoatrial node. *The Journal of Physiology.* 560, 429-437.
- Kaup, U. B., Seifert, R., 2002. Cyclic Nucleotide-Gated Ion Channels. *Physiol. Rev.* 82, 769-824.
- Kawaguchi, M., Hager, H. A., Wada, A., Koyama, T., Chang, M. S., Bader, D. M., 2008. Identification of a novel intracellular interaction domain essential for Bves function. *PLoS ONE.* 3, e2261.
- Keating, M. T., Sanguinetti, M. C., 2001. Molecular and cellular mechanisms of cardiac arrhythmias. *Cell.* 104, 569-80.
- Kelly, R. G., Brown, N. A., Buckingham, M. E., 2001. The arterial pole of the mouse heart forms from Fgf10-expressing cells in pharyngeal mesoderm. *Dev Cell.* 1, 435-40.
- Kelly, R. G., Buckingham, M. E., 2002. The anterior heart-forming field: voyage to the arterial pole of the heart. *Trends Genet.* 18, 210-6.
- Kikuchi, Y., Trinh, L. A., Reiter, J. F., Alexander, J., Yelon, D., Stainier, D. Y., 2000. The zebrafish bonnie and clyde gene encodes a Mix family homeodomain protein that regulates the generation of endodermal precursors. *Genes Dev.* 14, 1279-89.
- Kimmel, C. B., Ballard, W. W., Kimmel, S. R., Ullmann, B., Schilling, T. F., 1995. Stages of embryonic development of the zebrafish. *Dev Dyn.* 203, 253-310.
- Kirby, M. L., Gale, T. F., Stewart, D. E., 1983. Neural crest cells contribute to normal aorticopulmonary septation. *Science.* 220, 1059-61.
- Knight, R. F., Bader, D. M., Backstrom, J. R., 2003. Membrane topology of Bves/Pop1A, a cell adhesion molecule that displays dynamic changes in cellular distribution during development. *J Biol Chem.* 278, 32872-9.
- Kopp, R., Schwerte, T., Pelster, B., 2005. Cardiac performance in the zebrafish breakdance mutant. *J Exp Biol.* 208, 2123-34.
- Kreissl, S. Immunohistochemische Analysen zur Pathomorphologie des Reizleitungssystems der Popdc2-Nullmutante (Diploma thesis). University of Wuerzburg, Wuerzburg, Germany, 2009.
- Kuhtz, S. Struktur-Funktionsanalyse der Popeye-Domäne des Popdc1 Proteins der Maus: "site-directed" Mutagenese, cAMP-Bindung und phänotypische Charakterisierung (Diploma thesis). University of Wuerzburg, Wuerzburg, Germany, 2008.
- Kuo, C. T., Morrisey, E. E., Anandappa, R., Sigrist, K., Lu, M. M., Parmacek, M. S., Soudais, C., Leiden, J. M., 1997. GATA4 transcription factor is required for ventral morphogenesis and heart tube formation. *Genes Dev.* 11, 1048-60.
- Langenbacher, A. D., Dong, Y., Shu, X., Choi, J., Nicoll, D. A., Goldhaber, J. I., Philipson, K. D., Chen, J. N., 2005. Mutation in sodium-calcium exchanger 1 (NCX1) causes cardiac fibrillation in zebrafish. *Proc Natl Acad Sci U S A.* 102, 17699-704.
- Laugwitz, K. L., Moretti, A., Lam, J., Gruber, P., Chen, Y., Woodard, S., Lin, L. Z., Cai, C. L., Lu, M. M., Reth, M., Platoshyn, O., Yuan, J. X., Evans, S., Chien, K. R., 2005. Postnatal isl1+ cardioblasts enter fully differentiated cardiomyocyte lineages. *Nature.* 433, 647-53.
- Lee, R. K., Stainier, D. Y., Weinstein, B. M., Fishman, M. C., 1994. Cardiovascular development in the zebrafish. II. Endocardial progenitors are sequestered within the heart field. *Development.* 120, 3361-6.
- Lesage, F., 2003. Pharmacology of neuronal background potassium channels. *Neuropharmacology.* 44, 1-7.
- Lesage, F., Lazdunski, M., 2000. Molecular and functional properties of two-pore-domain potassium channels. *Am J Physiol Renal Physiol.* 279, F793-801.
- Li, Y., Um, S. Y., McDonald, T. V., 2006. Voltage-gated potassium channels: regulation by accessory subunits. *Neuroscientist.* 12, 199-210.
- Lin, C. Y., Yung, R. F., Lee, H. C., Chen, W. T., Chen, Y. H., Tsai, H. J., 2006. Myogenic regulatory factors Myf5 and Myod function distinctly during craniofacial myogenesis of zebrafish. *Dev Biol.* 299, 594-608.
- Lin, S., Zhao, D., Bownes, M., 2007. Blood vessel/epicardial substance (bves) expression, essential for embryonic development, is down regulated by Grk/EFGR signalling. *Int J Dev Biol.* 51, 37-44.
- Link, V., Shevchenko, A., Heisenberg, C. P., 2006. Proteomics of early zebrafish embryos. *BMC Dev Biol.* 6, 1.
- Lyons, I., Parsons, L. M., Hartley, L., Li, R., Andrews, J. E., Robb, L., Harvey, R. P., 1995. Myogenic and morphogenetic defects in the heart tubes of murine embryos lacking the homeo box gene Nkx2-5. *Genes Dev.* 9, 1654-66.
- McMahon, H. T., Ushkaryov, Y. A., Edelman, L., Link, E., Binz, T., Niemann, H., Jahn, R., Sudhof, T. C., 1993. Cellubrevin is a ubiquitous tetanus-toxin substrate homologous to a putative synaptic vesicle fusion protein. *Nature.* 364, 346-9.
- Meister, P. Mutagenese der Phosphat-Bindungskassette von Popdc2- Biochemische Charakterisierung und Herstellung eines Targetingkonstruktes (Diploma thesis). University of Wuerzburg, Wuerzburg, Germany, 2009.
- Meng, X., Noyes, M. B., Zhu, L. J., Lawson, N. D., Wolfe, S. A., 2008. Targeted gene inactivation in zebrafish using engineered zinc-finger nucleases. *Nat Biotechnol.* 26, 695-701.

- Mikawa, T., Hurtado, R., 2007. Development of the cardiac conduction system. *Semin Cell Dev Biol.* 18, 90-100.
- Milan, D. J., Giokas, A. C., Serluca, F. C., Peterson, R. T., MacRae, C. A., 2006. Notch1b and neuregulin are required for specification of central cardiac conduction tissue. *Development.* 133, 1125-32.
- Milan, D. J., Kim, A. M., Winterfield, J. R., Jones, I. L., Pfeufer, A., Sanna, S., Arking, D. E., Amsterdam, A. H., Sabeh, K. M., Mably, J. D., Rosenbaum, D. S., Peterson, R. T., Chakravarti, A., Kaab, S., Roden, D. M., MacRae, C. A., 2009. Drug-sensitized zebrafish screen identifies multiple genes, including GINS3, as regulators of myocardial repolarization. *Circulation.* 120, 553-9.
- Milan, D. J., MacRae, C. A., 2010. Zebrafish genetic models for arrhythmia. *Progress in Biophysics and Molecular Biology.* 98, 301-308.
- Milan, D. J., MacRae, C. A., 2005. Animal models for arrhythmias. *Cardiovasc Res.* 67, 426-437.
- Milan, D. J., Peterson, T. A., Ruskin, J. N., Peterson, R. T., MacRae, C. A., 2003. Drugs that induce repolarization abnormalities cause bradycardia in zebrafish. *Circulation.* 107, 1355-8.
- Milanesi, R., Baruscotti, M., Gnecci-Ruscone, T., DiFrancesco, D., 2006. Familial sinus bradycardia associated with a mutation in the cardiac pacemaker channel. *N Engl J Med.* 354, 151-7.
- Miquerol, L., Dupays, L., Theveniau-Ruissy, M., Alcolea, S., Jarry-Guichard, T., Abran, P., Gros, D., 2003. Gap junctional connexins in the developing mouse cardiac conduction system. *Novartis Found Symp.* 250, 80-98; discussion 98-109, 276-9.
- Moens, C. B., Donn, T. M., Wolf-Saxon, E. R., Ma, T. P., 2008. Reverse genetics in zebrafish by TILLING. *Brief Funct Genomic Proteomic.* 7, 454-9.
- Mohler, P. J., Schott, J. J., Gramolini, A. O., Dilly, K. W., Guatimosim, S., duBell, W. H., Song, L. S., Haurogne, K., Kyndt, F., Ali, M. E., Rogers, T. B., Lederer, W. J., Escande, D., Le Marec, H., Bennett, V., 2003. Ankyrin-B mutation causes type 4 long-QT cardiac arrhythmia and sudden cardiac death. *Nature.* 421, 634-9.
- Moorman, A. F., Christoffels, V. M., 2003a. Cardiac chamber formation: development, genes, and evolution. *Physiol Rev.* 83, 1223-67.
- Moorman, A. F., Christoffels, V. M., 2003b. Development of the cardiac conduction system: a matter of chamber development. *Novartis Found Symp.* 250, 25-34; discussion 34-43, 276-9.
- Moorman, A. F., Christoffels, V. M., Anderson, R. H., 2005. Anatomic substrates for cardiac conduction. *Heart Rhythm.* 2, 875-86.
- Morrissey, E. E., Ip, H. S., Lu, M. M., Parmacek, M. S., 1996. GATA-6: a zinc finger transcription factor that is expressed in multiple cell lineages derived from lateral mesoderm. *Dev Biol.* 177, 309-22.
- Nakai, J., Ohkura, M., Imoto, K., 2001. A high signal-to-noise Ca(2+) probe composed of a single green fluorescent protein. *Nat Biotechnol.* 19, 137-41.
- Nathan, E., Monovich, A., Tirosh-Finkel, L., Harrelson, Z., Rousso, T., Rinon, A., Harel, I., Evans, S. M., Tzahor, E., 2008. The contribution of Islet1-expressing splanchnic mesoderm cells to distinct branchiomic muscles reveals significant heterogeneity in head muscle development. *Development.* 135, 647-57.
- Nerbonne, J. M., Kass, R. S., 2005. Molecular physiology of cardiac repolarization. *Physiol Rev.* 85, 1205-53.
- Nguyen-Tran, V. T., Kubalak, S. W., Minamisawa, S., Fiset, C., Wollert, K. C., Brown, A. B., Ruiz-Lozano, P., Barrere-Lemaire, S., Kondo, R., Norman, L. W., Gourdie, R. G., Rahme, M. M., Feld, G. K., Clark, R. B., Giles, W. R., Chien, K. R., 2000. A novel genetic pathway for sudden cardiac death via defects in the transition between ventricular and conduction system cell lineages. *Cell.* 102, 671-82.
- Nixon, S. J., Wegner, J., Ferguson, C., Mery, P. F., Hancock, J. F., Currie, P. D., Key, B., Westerfield, M., Parton, R. G., 2005. Zebrafish as a model for caveolin-associated muscle disease; caveolin-3 is required for myofibril organization and muscle cell patterning. *Hum Mol Genet.* 14, 1727-43.
- Nof, E., Luria, D., Brass, D., Marek, D., Lahat, H., Reznik-Wolf, H., Pras, E., Dascal, N., Eldar, M., Glikson, M., 2007. Point mutation in the HCN4 cardiac ion channel pore affecting synthesis, trafficking, and functional expression is associated with familial asymptomatic sinus bradycardia. *Circulation.* 116, 463-70.
- O'Brien, T. X., Lee, K. J., Chien, K. R., 1993. Positional specification of ventricular myosin light chain 2 expression in the primitive murine heart tube. *Proceedings of the National Academy of Sciences of the United States of America.* 90, 5157-5161.
- Olson, E. N., 2006. Gene regulatory networks in the evolution and development of the heart. *Science.* 313, 1922-7.
- Osler, M. E., Chang, M. S., Bader, D. M., 2005. Bves modulates epithelial integrity through an interaction at the tight junction. *J Cell Sci.* 118, 4667-78.
- Osler, M. E., Smith, T. K., Bader, D. M., 2006. Bves, a member of the Popeye domain-containing gene family. *Dev Dyn.* 235, 586-93.
- Parnes, D., Jacoby, V., Sharabi, A., Schlesinger, H., Brand, T., Kessler-Icekson, G., 2007. The Popdc gene family in the rat: molecular cloning, characterization and expression analysis in the heart and cultured cardiomyocytes. *Biochim Biophys Acta.* 1769, 586-92.
- Pelster, B., Burggren, W. W., 1996. Disruption of Hemoglobin Oxygen Transport Does Not Impact Oxygen-Dependent Physiological Processes in Developing Embryos of Zebra Fish (*Danio rerio*). *Circ Res.* 79, 358-362.
- Pogwizd, S. M., Bers, D. M., 2004. Cellular basis of triggered arrhythmias in heart failure. *Trends Cardiovasc Med.* 14, 61-6.
- Priori, S. G., Aliot, E., Blomstrom-Lundqvist, C., Bossaert, L., Breithardt, G., Brugada, P., Camm, A. J., Cappato, R., Cobbe, S. M., Di Mario, C., Maron, B. J., McKenna, W. J., Pedersen, A. K., Ravens, U., Schwartz, P. J., Trusz-Gluza, M., Vardas, P., Wellens, H. J. J., Zipes, D. P., 2001. Task Force on Sudden Cardiac Death of the European Society of Cardiology. *Eur Heart J.* 22, 1374-1450.
- Reese, D. E., Zavaljevski, M., Streiff, N. L., Bader, D., 1999. bves: A novel gene expressed during coronary blood vessel development. *Dev Biol.* 209, 159-71.
- Reiter, J. F., Alexander, J., Rodaway, A., Yelon, D., Patient, R., Holder, N., Stainier, D. Y., 1999. Gata5 is required for the development of the heart and endoderm in zebrafish. *Genes Dev.* 13, 2983-95.
- Ripley, A. N., Chang, M. S., Bader, D. M., 2004. Bves is expressed in the epithelial components of the retina, lens, and cornea. *Invest Ophthalmol Vis Sci.* 45, 2475-83.
- Ripley, A. N., Osler, M. E., Wright, C. V., Bader, D., 2006. Xbves is a regulator of epithelial movement during early *Xenopus laevis* development. *Proc Natl Acad Sci U S A.* 103, 614-9.
- Roden, D. M., Balsler, J. R., George, A. L., Jr., Anderson, M. E., 2002. Cardiac ion channels. *Annu Rev Physiol.* 64, 431-75.
- Rones, M. S., McLaughlin, K. A., Raffin, M., Mercola, M., 2000. Serrate and Notch specify cell fates in the heart field by suppressing cardiomyogenesis. *Development.* 127, 3865-76.

- Scherz, P. J., Huisken, J., Sahai-Hernandez, P., Stainier, D. Y., 2008. High-speed imaging of developing heart valves reveals interplay of morphogenesis and function. *Development*. 135, 1179-87.
- Schindler, R. Proteinbiochemische Untersuchungen zur Funktionsweise der Popeye domain containing Proteinfamilie (Masterthesis). University of Wuerzburg, Wuerzburg, 2009.
- Schulze-Bahr, E., Neu, A., Friederich, P., Kaupp, U. B., Breithardt, G. n., Pongs, O., Isbrandt, D., 2003. Pacemaker channel dysfunction in a patient with sinus node disease. *The Journal of Clinical Investigation*. 111, 1537-1545.
- Schwerte, T., Fritsche, R., 2003. Understanding cardiovascular physiology in zebrafish and *Xenopus* larvae: the use of microtechniques. *Comp Biochem Physiol A Mol Integr Physiol*. 135, 131-45.
- Schwerte, T., Pelster, B., 2000. Digital motion analysis as a tool for analysing the shape and performance of the circulatory system in transparent animals. *J Exp Biol*. 203, 1659-1669.
- Sedmera, D., Reckova, M., deAlmeida, A., Sedmerova, M., Biermann, M., Volejnik, J., Sarre, A., Raddatz, E., McCarthy, R. A., Gourdie, R. G., Thompson, R. P., 2003. Functional and morphological evidence for a ventricular conduction system in zebrafish and *Xenopus* hearts. *Am J Physiol Heart Circ Physiol*. 284, H1152-60.
- Sidhu, J. S., Rajawat, Y. S., Rami, T. G., Gollob, M. H., Wang, Z., Yuan, R., Marian, A. J., DeMayo, F. J., Weilbacher, D., Taffet, G. E., Davies, J. K., Carling, D., Khoury, D. S., Roberts, R., 2005. Transgenic Mouse Model of Ventricular Preexcitation and Atrioventricular Reentrant Tachycardia Induced by an AMP-Activated Protein Kinase Loss-of-Function Mutation Responsible for Wolff-Parkinson-White Syndrome. *Circulation*. 111, 21-29.
- Smith, T. K., Hager, H. A., Francis, R., Kilkenny, D. M., Lo, C. W., Bader, D. M., 2008. Bves directly interacts with GEFT, and controls cell shape and movement through regulation of Rac1/Cdc42 activity. *Proc Natl Acad Sci U S A*. 105, 8298-303.
- Smyth, J. W., Hong, T. T., Gao, D., Vogan, J. M., Jensen, B. C., Fong, T. S., Simpson, P. C., Stainier, D. Y., Chi, N. C., Shaw, R. M., 2010. Limited forward trafficking of connexin 43 reduces cell-cell coupling in stressed human and mouse myocardium. *J Clin Invest*. 120, 266-79.
- Splawski, I., Shen, J., Timothy, K. W., Lehmann, M. H., Priori, S., Robinson, J. L., Moss, A. J., Schwartz, P. J., Towbin, J. A., Vincent, G. M., Keating, M. T., 2000. Spectrum of mutations in long-QT syndrome genes. KVLQT1, HERG, SCN5A, KCNE1, and KCNE2. *Circulation*. 102, 1178-85.
- Splawski, I., Tristani-Firouzi, M., Lehmann, M. H., Sanguinetti, M. C., Keating, M. T., 1997. Mutations in the hminK gene cause long QT syndrome and suppress IKs function. *Nat Genet*. 17, 338-40.
- Stainier, D. Y., 2001. Zebrafish genetics and vertebrate heart formation. *Nat Rev Genet*. 2, 39-48.
- Stainier, D. Y., Fouquet, B., Chen, J. N., Warren, K. S., Weinstein, B. M., Meiler, S. E., Mohideen, M. A., Neuhaus, S. C., Solnica-Krezel, L., Schier, A. F., Zwartkruis, F., Stemple, D. L., Malicki, J., Driever, W., Fishman, M. C., 1996. Mutations affecting the formation and function of the cardiovascular system in the zebrafish embryo. *Development*. 123, 285-92.
- Stainier, D. Y., Lee, R. K., Fishman, M. C., 1993. Cardiovascular development in the zebrafish. I. Myocardial fate map and heart tube formation. *Development*. 119, 31-40.
- Stainier, D. Y., Weinstein, B. M., Detrich, H. W., 3rd, Zon, L. I., Fishman, M. C., 1995. Cloche, an early acting zebrafish gene, is required by both the endothelial and hematopoietic lineages. *Development*. 121, 3141-50.
- Stickney, H. L., Barresi, M. J., Devoto, S. H., 2000. Somite development in zebrafish. *Dev Dyn*. 219, 287-303.
- Stieber, J., Herrmann, S., Feil, S., Loster, J., Feil, R., Biel, M., Hofmann, F., Ludwig, A., 2003. The hyperpolarization-activated channel HCN4 is required for the generation of pacemaker action potentials in the embryonic heart. *Proc Natl Acad Sci U S A*. 100, 15235-40.
- Takeshita, K., Fujimori, T., Kurotaki, Y., Honjo, H., Tsujikawa, H., Yasui, K., Lee, J.-K., Kamiya, K., Kitaichi, K., Yamamoto, K., Ito, M., Kondo, T., Iino, S., Inden, Y., Hirai, M., Murohara, T., Kodama, I., Nabeshima, Y.-i., 2004. Sinoatrial Node Dysfunction and Early Unexpected Death of Mice With a Defect of klotho Gene Expression. *Circulation*. 109, 1776-1782.
- Tan, H. L., Bink-Boelkens, M. T. E., Bezzina, C. R., Viswanathan, P. C., Beaufort-Krol, G. C. M., van Tintelen, P. J., van den Berg, M. P., Wilde, A. A. M., Balsev, J. R., 2001. A sodium-channel mutation causes isolated cardiac conduction disease. *Nature*. 409, 1043-1047.
- Tan, J. H., Liu, W., Saint, D. A., 2004. Differential expression of the mechanosensitive potassium channel TREK-1 in epicardial and endocardial myocytes in rat ventricle. *Exp Physiol*. 89, 237-42.
- Tang, Z., Scherer, P. E., Okamoto, T., Song, K., Chu, C., Kohtz, D. S., Nishimoto, I., Lodish, H. F., Lisanti, M. P., 1996. Molecular cloning of caveolin-3, a novel member of the caveolin gene family expressed predominantly in muscle. *J Biol Chem*. 271, 2255-61.
- Terrenoire, C., Lauritzen, I., Lesage, F., Romey, G., Lazdunski, M., 2001. A TREK-1-like potassium channel in atrial cells inhibited by beta-adrenergic stimulation and activated by volatile anesthetics. *Circ Res*. 89, 336-42.
- Thompson, J. D., Higgins, D. G., Gibson, T. J., 1994. CLUSTAL W: improving the sensitivity of progressive multiple sequence alignment through sequence weighting, position-specific gap penalties and weight matrix choice. *Nucleic Acids Res*. 22, 4673-80.
- Thompson, R. P., Reckova, M., deAlmeida, A., Bigelow, M. R., Stanley, C. P., Spruill, J. B., Trusk, T. T., Sedmera, D., 2003. The oldest, toughest cells in the heart. *Novartis Found Symp*. 250, 157-74; discussion 174-6, 276-9.
- Tirosh-Finkel, L., Elhanany, H., Rinon, A., Tzahor, E., 2006. Mesoderm progenitor cells of common origin contribute to the head musculature and the cardiac outflow tract. *Development*. 133, 1943-53.
- Torlopp, A., Breher, S. S., Schluter, J., Brand, T., 2006. Comparative analysis of mRNA and protein expression of Popdc1 (Bves) during early development in the chick embryo. *Dev Dyn*. 235, 691-700.
- Traver, D., Paw, B. H., Poss, K. D., Penberthy, W. T., Lin, S., Zon, L. I., 2003. Transplantation and in vivo imaging of multilineage engraftment in zebrafish bloodless mutants. *Nat Immunol*. 4, 1238-46.
- Tzahor, E., 2009. Heart and craniofacial muscle development: a new developmental theme of distinct myogenic fields. *Dev Biol*. 327, 273-9.
- Ueda, K., Nakamura, K., Hayashi, T., Inagaki, N., Takahashi, M., Arimura, T., Morita, H., Higashiuesato, Y., Hirano, Y., Yasunami, M., Takishita, S., Yamashina, A., Ohe, T., Sunamori, M., Hiraoka, M., Kimura, A., 2004. Functional characterization of a trafficking-defective HCN4 mutation, D553N, associated with cardiac arrhythmia. *J Biol Chem*. 279, 27194-8.
- Ueda, K., Valdivia, C., Medeiros-Domingo, A., Tester, D. J., Vatta, M., Farrugia, G., Ackerman, M. J., Makielski, J. C., 2008. Syntrophin mutation associated with long QT syndrome through activation of the nNOS-SCN5A macromolecular complex. *Proceedings of the National Academy of Sciences*. 105, 9355-9360.

- Unger, V. M., Kumar, N. M., Gilula, N. B., Yeager, M., 1999. Three-dimensional structure of a recombinant gap junction membrane channel. *Science*. 283, 1176-80.
- Vasavada, T. K., DiAngelo, J. R., Duncan, M. K., 2004. Developmental expression of Pop1/Bves. *J Histochem Cytochem*. 52, 371-7.
- Wada, A. M., Reese, D. E., Bader, D. M., 2001. Bves: prototype of a new class of cell adhesion molecules expressed during coronary artery development. *Development*. 128, 2085-93.
- Wang, D., Jao, L. E., Zheng, N., Dolan, K., Ivey, J., Zonies, S., Wu, X., Wu, K., Yang, H., Meng, Q., Zhu, Z., Zhang, B., Lin, S., Burgess, S. M., 2007. Efficient genome-wide mutagenesis of zebrafish genes by retroviral insertions. *Proc Natl Acad Sci U S A*. 104, 12428-33.
- Warga, R. M., Kane, D. A., Ho, R. K., 2009. Fate Mapping Embryonic Blood in Zebrafish: Multi- and Unipotential Lineages Are Segregated at Gastrulation. *Developmental Cell*. 16, 744-755.
- Warren, K. S., Baker, K., Fishman, M. C., 2001. The slow mo mutation reduces pacemaker current and heart rate in adult zebrafish. *Am J Physiol Heart Circ Physiol*. 281, H1711-9.
- Warren, K. S., Fishman, M. C., 1998. "Physiological genomics": mutant screens in zebrafish. *Am J Physiol*. 275, H1-7.
- Waterman, R. E., 1969. Development of the lateral musculature in the teleost, *Brachydanio rerio*: a fine structural study. *Am J Anat*. 125, 457-93.
- Way, M., Parton, R. G., 1995. M-caveolin, a muscle-specific caveolin-related protein. *FEBS Lett*. 376, 108-12.
- Weinberg, E. S., Allende, M. L., Kelly, C. S., Abdelhamid, A., Murakami, T., Andermann, P., Doerre, O. G., Grunwald, D. J., Riggleman, B., 1996. Developmental regulation of zebrafish MyoD in wild-type, no tail and spadetail embryos. *Development*. 122, 271-80.
- Wienholds, E., Schulte-Merker, S., Walderich, B., Plasterk, R. H., 2002. Target-selected inactivation of the zebrafish rag1 gene. *Science*. 297, 99-102.
- Yelon, D., Home, S. A., Stainier, D. Y. R., 1999. Restricted Expression of Cardiac Myosin Genes Reveals Regulated Aspects of Heart Tube Assembly in Zebrafish. *Developmental Biology*. 214, 23-37.
- Yutzey, K. E., Rhee, J. T., Bader, D., 1994. Expression of the atrial-specific myosin heavy chain AMHC1 and the establishment of anteroposterior polarity in the developing chicken heart. *Development*. 120, 871-83.
- Zammit, P. S., Relaix, F., Nagata, Y., Ruiz, A. P., Collins, C. A., Partridge, T. A., Beauchamp, J. R., 2006. Pax7 and myogenic progression in skeletal muscle satellite cells. *J Cell Sci*. 119, 1824-32.

9 APPENDIX

9.1 Abbreviations

ah	adductor hyoideu
am	adductor mandibulae
Amhc	atrial myosin heavy chain
Anf	atrial natriuretic factor
ao	adductor operculi
APS	ammonium persulphate
ATP	adenosine triphosphatase
AV	atrioventricular
AVB	atrioventricular bundle
AVC	atrioventricular canal
AVN	atrioventricular node
BCIP	5-bromo-4-chloro-3-indolyl-phosphate
2,3 BDM	2,3-Butanedione monoxime
Bmp	bone morphogenetic protein
Bves	blood vessel epicardial substance
BSA	bovine serum albumin
bvz	brain ventricular zone
c	cardiac cushions
cc	cardiac cone
cDNA	copy DNA
cg	cranial ganglia
cRNA	capped mRNA
Cx	connexin
d	diencephalon
DAB	diaminobenzidine
dd	dorsal diencephalon
dH ₂ O	distilled water
ddH ₂ O	double distilled water
DEPC	diethyl pyrocarbonate
DMSO	dimethyl sulphoxide
DNA	deoxyribonucleic acid
do	dilator operculi
dpf	days post fertilization
E3	embryonic medium
ECG	electrocardiogramm
EDTA	ethylenediaminetetraacetic acid
EM	electron microscopy
EMT	epithelial-mesenchymal transformation
ENU	N-ethyl-N-nitrosourea
ET-1	endothelin-1
fb	fin bud
Fgf	fibroblast growth factor
FITC	fluorescein isothiocyanate
Flk1	fetal liver kinase 1
Gata	GATA-binding protein
Geft	guanine nucleotide exchange factor T
GFP	green fluorescent protein
Hand	heart and neural crest derivatives expressed transcript
hb	hindbrain
Hcn4	hyperpolarization-activated cyclic nucleotide-gated cation channel 4

HH	hamburger hamilton
hh	hyohyoideus
hm	hypaxial muscles
hn	hindbrain neurons
hpf	hours post fertilization
HRP	horseradish peroxidase
ht	heart tube
ih	interhyoideus
ima	intermandibularis anterior
imp	intermandibularis posterior
io	inferior oblique
IPTG	isopropyl- β -D-thiogalactopyranoside
ir	interior rectus
irx	iroquois homeobox protein
isl 1	insulin gene enhancer protein, a LIM homeodomain transcription factor
lap	levator arcus palatine
LB medium	Luria-Bertani medium
lhb	lateral hindbrain
LQT	long QT
lr	lateral rectus
MESAB/Tricaine	ethyl-m-aminobenzoate methanesulphonate
Mesp-1 (2)	mesoderm posterior 1 (2)
mhb	midbrain-hindbrain boundary
mr	medial rectus
NBT	4-nitroblue tetrazolium chloride
NCBI	National Center of Biotechnology Information
NCX1	sodium-calcium exchanger 1
Nkx2.5	Nk2 transcription factor
ov	otic vesicles
p	pericard
PBS	phosphate-buffered saline
PCR	polymerase chain reaction
pf	pectoral fin bud
PFA	paraformaldehyde
PKA	cAMP dependent protein kinase
Popdc	Popeye domain containing
PTU	1-phenyl-2-thiourea
RNA	ribonucleic acid
RT-PCR	reverse transcriptase polymerase chain reaction
SAN	sinus node/sinoatrial node
Scn5a	sodium channel, voltage-gated, type V, alpha subunit
SDS	sodium dodecyl sulphate
sh	sternohyoideus
Shh	sonic hedgehog
SNARE	soluble N-ethylmaleimide-sensitive-factor attachment receptor
so	superior oblique
SPIM	selective plane illumination microscopy
SQT	short QT
sr	superior rectus
SSC	saline sodium citrate
SSS	sick sinus syndrome
TBS	Tris buffered saline
Tbx	t-box transcription factor
TL	Tupfel long fin
TRITC	tetramethylrhodamine isothiocyanate
TU	Tuebingen

Vamp3	vesicle-associated membrane protein 3
vd	ventral diencephalon
Vegf	vascular endothelial growth factor
vm	ventral mesencephalon
Vmlc2	ventricular myosin light chain 2
Wnt	wingless-type MMTV integration site family
wt	wild type
ZO1	zona occludens 1

9.2 Genetic nomenclature

The used genetic nomenclature is in accordance with the established conventions for each species for naming genes, proteins, and mutant phenotypes. In this thesis, I followed the established conventions when referring to a gene in a particular species (see table below). When I referred to a gene or gene family generically, without intending restriction to a particular species, I used the same convention as for the mouse.

Organism	Gene	Protein
Mouse	<i>Hoxa4</i>	Hoxa4
Human	<i>HOXA4</i>	HOXA4
Zebrafish	<i>cyclops, cyc</i>	Cyclops, Cyc
Drosophila	<i>sevenless, sev</i> (named after recessive mutant phenotype)	Sevenless, SEV
	<i>Deformed, Dfd</i> (named after dominant mutant phenotype, or named by homology with another species)	Deformed, DFD
Chick	<i>HOXA4</i>	HOXA4
Xenopus	<i>hoxa4</i>	hoxa4

9.3 Supplemental videos

- S1: 6 dpf wild type zebrafish heart recorded by high speed video microscopy.
- S2: 6 dpf arrhythmic *popdc2* morphant heart recorded by high speed video microscopy.
- S3: Calcium transients of a 5 dpf control injected zebrafish heart recorded by SPIM (video to Figure 25A).
- S4: Calcium transients of a 5 dpf *popdc2* morphant heart exhibiting a second grade AV block recorded by SPIM (video to Figure 25B).
- S5: Calcium transients of a 5 dpf *popdc2* morphant heart exhibiting a third grade AV block recorded by SPIM (video to Figure 25C).
- S6: Calcium transients of a 6 dpf *popdc2* morphant heart exhibiting a second grade AV block recorded by SPIM (video to Figure 26B).
- S7: Calcium transients of a 6 dpf *popdc2* morphant heart exhibiting a sinoatrial block recorded by SPIM (video to Figure 26C).
- S8: Heart of a 7 dpf control injected zebrafish (*Tg(flk1:GFP x gata1:DsRed)*) displaying normal heart beat.
- S9: Heart of a 7 dpf *popdc2* morphant (*Tg(flk1: GFP x gata1:DsRed)*) displaying complete heart block.
- S10: Calcium transients of a 3 dpf control injected zebrafish heart recorded by SPIM (video to Figure 36A).
- S11: Calcium transients of a 3 dpf *popdc3* morphant heart exhibiting no pathological alteration recorded by SPIM (video to Figure 36B)
- S12: Calcium transients of a 4 dpf control injected zebrafish heart recorded by SPIM (video to Figure 37A).
- S13: Calcium transients of a 4 dpf *popdc3* morphant heart exhibiting a complete heart block recorded by SPIM (video to Figure 37B).

9.4 Eidesstattliche Erklärung

Hiermit erkläre ich an Eides statt, dass ich die vorliegende Arbeit selbstständig und nur unter Verwendung der angegebenen Hilfsmittel und Literatur angefertigt habe.

Ich erkläre weiterhin, dass ich diese Dissertation weder in gleicher noch in ähnlicher Form in anderen Prüfungsverfahren vorgelegt habe.

Ich habe außer den mit dem Zulassungsbescheid urkundlich vorgelegten Graden keine weiteren akademischen Grade erworben oder zu erwerben versucht.

.....
Würzburg, den 10.05.2010

.....
Bettina Carmen Kirchmaier

9.5 Curriculum vitae

Persönliche Daten

Name: Bettina Carmen Kirchmaier
Geburtsdatum: 31.07.1979
Geburtsort: Frankfurt am Main
Staatsangehörigkeit: deutsch

Schulischer Werdegang

08/86 bis 06/90 Textor Grundschule, Frankfurt am Main
08/90 bis 06/99 Schiller-Gymnasium, Frankfurt am Main
Juni 1999 Allgemeine Hochschulreife

Studium

08/99 bis 09/99 Sommerschulstudent an der Stritch School of Medicine der Loyola Universität in Chicago.
10/99 bis 09/01 Technische Universität Darmstadt, Diplomstudium der Biologie
05/04 bis 01/05 Ruprechts-Karl Universität Heidelberg
Externe Diplomarbeit in der Medizinischen Klinik III
Thema: „Regulation von Herzwachstum im Zebrafisch“
Januar 2005 Diplom und Prüfung in den Fächern Biochemie, Pflanzenphysiologie und Zell- und Entwicklungsbiologie

Berufstätigkeit

06/05 bis 11/05 Wissenschaftlicher Mitarbeiter am Leibniz Institut für Arterioskleroseforschung in Münster

Promotionsstudium

Seit Dezember 2005 Promotion mit dem Thema „Functional characterization of the *Popeye domain containing* gene family in zebrafish“ bei Prof. Dr. Thomas Brand, Lehrstuhl für Zell- und Entwicklungsbiologie, Universität Würzburg

Universitäre Aktivitäten

01/07 bis 12/08 Graduiertenkolleg sprecherin vom GK 1048: Organogenesis, Universität Würzburg
Oktober 2007 Mitorganisation des dritten internationalen Symposiums „Drilling into Life's Depths“ an der Universität Würzburg
März 2009 Mitorganisation des vierten internationalen Symposiums „Revolution Research“ an der Universität Würzburg

Fortbildung

30. Juni 2006	Teilnahme am Workshop für deskriptive Statistik „Forschendes Lernen“, Würzburg
10. Mai 2006	Teilnahme am Charles River Laboratories Seminar „Research Models in Cardiovascular Research“, Frankfurt am Main
26. Juli 2007	Teilnahme am ENSEMBL Genome Analysis Workshop, Würzburg
08. August 2008	Teilnahme am Workshop „Academic English – Basics“, Würzburg
01.-02. Oktober 2008	Teilnahme am Workshop „Presenting Professionally“, Würzburg
19. – 20. Januar 2010	Teilnahme am Workshop „Scientific Writing“, Würzburg

Stipendien

Reisestipendium von der Company of Biologists im Jahr 2006

EMBO Short Term Fellowship ASTF-96-2007

Reisestipendium 2008 von der ESC Working Group on Developmental Anatomy and Pathology

Stipendium für ein individuelles Trainingsprogramm im Jahr 2009 von FP6 Projekt LSHM-CT-2005-018630 “Heart Repair”

Wissenschaftliche Forschungsaufenthalte

Herbst 2006 und Herbst 2007	Zweiwöchiger Aufenthalt in Innsbruck bei Dr. Thorsten Schwerte zur Erlernung einer noninvasiven Methode zur Auswertung des Herzrhythmus.
Frühjahr 2009	Sechswöchiger Aufenthalt in San Francisco bei Prof. Didier Stainier zur Erlernung einer Methode zur Auswertung des Erregungsleitungssystems im Zebrafisch mittels selective plane illuminating microscopy (SPIM)

9.6 Eigene Publikationen

Kirchmaier, B. C., Schwerte, T., Huisken J., Winkler, C., Jungblut B., Stainier D. Y. R., Brand, T.: The Popeye domain containing gene 2 (*popdc2*) in zebrafish is required for cardiac conduction. (Eingereicht).

Fiedler J., Jazbutyte V., **Kirchmaier B.**, Galuppo P., Kneitz S., Pena J. T. R., Soutschek, J., Brand T., Tuschl T., Engelhardt S., Ertl G., Bauersachs J. and Thum T.: Targeting endothelial microRNA-24 improves angiogenesis and preserves cardiac function after myocardial infarction. (In Vorbereitung).

Froese A., Breher S. S., Schlueter J., Waldeyer C., Schindler, R. F. R., Nikolaev, V., O., Kuhtz, J., Wischmeyer, E., **Kirchmaier B. C.**, Vauti F., Müller T. D., Torlopp A., Stieber, J., Ludwig, A., Arnold H.-H., Kirchhof P., Fabritz L., Brand T.: The popeye domain containing gene family encodes a novel class of cAMP binding proteins involved in cardiac pacemaking. (In Vorbereitung).

9.7 Teilnahme an wissenschaftlichen Tagungen

September 2006	6. GfE School “Cell Polarity in Development and Disease” in Güzburg, Deutschland. Posterpräsentation: “Essential functions of <i>popdc2</i> for cardiac and skeletal muscle development in zebrafish”.
Februar 2007	5 th Dutch-German Joint Meeting of Molecular Cardiology Groups in Würzburg, Deutschland.
März 2007	17. Wissenschaftliche Tagung der Gesellschaft für Entwicklungsbiologie in Marburg, Deutschland. Posterpräsentation: “Essential functions of <i>popdc2</i> for cardiac and skeletal muscle development in zebrafish”.
Oktober 2007	Third international student symposium „Drilling into Life’s Depths“ in Würzburg, Deutschland.
März 2008	Bi-annual meeting of the working group on developmental anatomy and pathology in Alberobello, Italien. Posterpräsentation: “Essential functions of <i>popdc2</i> for cardiac and skeletal muscle development in zebrafish”.
September 2008	First international symposium “Image Mining” in Obergurgl, Österreich. Posterpräsentation: “Essential functions of <i>popdc1</i> and <i>popdc2</i> for cardiac and skeletal muscle development in zebrafish”
July 2009	6 th European zebrafish genetics and development meeting in Rom, Italien. Posterpräsentation: “Function of the <i>popdc</i> gene family in cardiac conduction system development”

9.8 Acknowledgements

Ich möchte mich als erstes bei meinem Doktorvater Prof. Dr. Thomas Brand bedanken für das interessante Promotionsthema, die vielen anregenden Diskussionen und die Hilfestellung bei der Antragstellung für die Forschungsaufenthalte während meiner Promotion.

Desweiteren bedanke ich mich bei Prof. Dr. Christoph Winkler für das Interesse an meinem Doktorthema und die Übernahme des Zweitgutachtens.

Ferner bedanke ich mich bei allen ehemaligen und jetzigen Mitgliedern der Arbeitsgruppe Brand (Sascha, Stephe, Franzi, Roland, Patrick, Juliane, Sonja, Jan, Angela, Uschi, Reinhild, Anneliese, Elisabeth, Johanna) für die gute Arbeitsatmosphäre, die gewährten Hilfestellungen und die methodischen Anregungen.

Für die freundliche Aufnahme in ihr Labor und für die tolle Zusammenarbeit bedanke ich mich ganz herzlich bei Dr. Thorsten Schwerte, Prof. Didier Stainier, Dr. Jan Huisken und Dr. Benno Jungblut.

Beim GK 1048, besonders Herrn Prof. Scharl und Frau Gabi Heilmann, bedanke ich mich für die Bereitschaft unkompliziert neue Seminare einzuführen und die Forschung mit erheblichem Einsatz zu unterstützen.

Für die finanzielle Unterstützung in Form von Reisestipendien danke ich EMBO, Development, der ESC Working Group on Developmental Anatomy and Pathology und EU „HeartRepair“, sowie in Form einer Promotions Abschlußförderung der Frauenförderung der Uni Würzburg.

Ich bedanke mich bei allen Mitgliedern des Lehrstuhls Zell- und Entwicklungsbiologie für anregende Gespräche und Hilfestellungen, sowie besonders bei Dr. Norbert Wilken für die Rettung der Promotionsdaten aus meinem maroden Computer.

Ein herzlicher Dank geht weiterhin an meine fleißigen Korrekturleser Roland Schindler, Juliane Kutzt, Franziska Günthner, Claudia Wollny, Roswitha Ehnes, Holger Dill (bitte Beschwerden direkt an die betreffenden Personen richten..) und an meinen Onkel Manfred, der sich um Layout und Druck gekümmert hat.

Holger, ich danke Dir für Deine Unterstützung in allen Bereichen und daß Du diese lange, stressige Zeit mit mir in einer viel zu kleinen Wohnung durchgestanden hast.